Univerzita Karlova v Praze
Přírodovědecká fakulta
a
Ústav makromolekulární chemie
Akademie věd České republiky, v.v.i.

Studijní program: Makromolekulární chemie
Studijní obor: Makromolekulární chemie

Ing. Michal Babič

Superparamagnetické nano- a mikročástice s hydrofilními povrchy

Superparamagnetic nano- and microparticles with hydrophilic surfaces

Dizertační práce

Vedoucí závěrečné práce/Školitel: Ing. Daniel Horák, CSc.

Praha, 2012

Prohlášení

Prohlašuji, že tuto dizertační práci jsem vypracoval samostatně, na Ústavu makromolekulární chemie AV ČR, v.v.i. pod vedením školitele Ing. Daniela Horáka, CSc. Tuto práci ani její podstatnou část jsem nepředložil k získání jiného nebo stejného akademického titulu. Veškerou použitou literaturu jsem řádně citoval.

V Praze dne ..... **podpis: .....**

Poděkování

Úvodem bych chtěl poděkovat svému školiteli a vedoucímu Oddělení polymerních částic ÚMCH AV ČR, v.v.i., Ing. Danielu Horákovi, CSc. za trpělivé odborné vedení. Osobní poděkování patří kolegům Ing. Zdeňku Plichtovi a paní Heleně Solařové za pomoc a sdílení zkušeností při osvojování laboratorních technik pro přípravu koloidních systémů. Doc. RNDr. Miroslavě Trchové, DSc. děkuji za cenné poznatky v oboru FTIR na komplikovaných vzorcích nanočástic, paní Jiřině Hromádkové za pořízení snímků z elektronových mikroskopů a paní Miloslavě Plichtové za prvkové analýzy.

Zvláštní poděkování pak patří kolektivu Mgr. Pavly Jendelové, Ph.D. (ÚEM AV ČR, v.v.i., Laboratoř tkáňových kultur a kmenových buněk a Centrum buněčné terapie a tkáňových náhrad 2. LF UK) za práci na buněčných kulturách a Mgr. Vítu Herynkovi Ph.D. (IKEM, Pracoviště klinické a experimentální spektroskopie) za experimenty v oboru MRI. Oběma navíc patří dík i za cenné konzultace z biologických oborů.

Doc. Ing. Emilu Pollertovi, DrSc. (FZÚ AV ČR, v.v.i., Oddělení magnetik a supravodičů) děkuji za konzultace a fyzikální měření v oboru magnetických materiálů a také za cenný osobní vklad.

Souhrn

PhD. práce „Superparamagnetické nano- a mikročástice s hydrofilními povrchy“ se zabývá přípravou a charakterizací magneticky aktivních částicových materiálů pro značení buněk a jejich následné zobrazení magnetickou rezonancí a přípravou částicových materiálů s výhledem použití v magnetických separacích biologických materiálů. Práce je rozdělena do tří částí podle typu experimentálně řešené problematiky.

První část popisuje výběr a optimalizaci syntézy superparamagnetických nanočástic oxidů železa s vhodnými toxikologickými, morfologickými a fyzikálně-chemickými vlastnostmi. Pro výrobu nano- a mikročásticových materiálů zamýšlených pro diagnostiku i separace byly jako výchozí materiál zvoleny částice maghemitu (γ-Fe_2O_3) připravované následnou postsyntézní oxidací částic magnetitu (Fe_3O_4). Konvenční technika přípravy magnetitu zásaditou koprecipitací Fe(II) a Fe(III) solí byla modifikována tak, že bylo dosaženo rutinní produkce nanočástic se zúženou distribucí velikostí částic bez nutnosti použití povrchově aktivních činidel v průběhu syntézy. Připravené nanočástice maghemitu o velikosti cca. 6 nm vykazovaly v porovnání s literárními údaji vysokou hodnotu saturační magnetizace $M_s \sim 70$ A·m^2·kg^{-1}. Tím bylo experimentálně vyvráceno tvrzení, že saturační magnetizace nanočásticových materiálů závisí pouze na velikosti krystalitu a nezávisí na způsobu jejich přípravy. Morfologie nanočástic byla vyhodnocena obrazovou analýzou snímků z rastrovacího (SEM) a transmisního elektronového mikroskopu (TEM), pomocí dynamického rozptylu světla (DLS) byla změřena hydrodynamická velikost a zeta-potenciál. Struktura maghemitu byla potvrzena práškovou rentgenovou difrakcí (XRD). Saturační magnetizace byla změřena pomocí SQUID magnetometru.

Ve druhé části jsou popsány metody povrchových modifikací maghemitových nanočástic pomocí D-manózy, poly(L-lysinu) a poly(*N*,*N*-dimethylakrylamidu) za účelem značení kultur kmenových buněk a jejich následného zobrazování pomocí magnetické rezonance (MRI). Díky takto upraveným nanočásticím bylo dosaženo homogenního „proznačení“ vysokého podílu buněk v kulturách s minimálními negativními vlivy na jejich viabilitu. Experimentálně bylo prokázáno zvýšení kontrastu buněčných kultur kmenových buněk při zobrazování MRI jak na želatinových modelech, tak na buněčných kulturách *in vitro* i *in vivo* po implantaci. Povrchové úpravy byly analyzovány pomocí TEM, DLS, prvkové analýzy, ATR-FTIR a rozměrově vylučovací chromatografií (SEC).

Třetí část práce se zabývá přípravou hydrofilních mikročástic na bázi poly(*N*,*N*-dimethylakrylamidu) plněných nanočásticemi maghemitu. Na základě experimentálního hodnocení možností přípravy neplněných poly(*N*,*N*-dimethylakryl-amidových) mikročástic pomocí suspenzní, inverzní emulzní a disperzní polymerizace byla jako vhodná metoda pro přípravu částic se superparamagnetickým plnivem zvolena inverzní emulzní polymerizace s použitím nekonvečního stabilizátoru. Byly tak připraveny mikročástice s vysokým obsahem magnetického nanoplniva (až 70 hm.%) a s jeho náhodnou distribucí v matrici. Byl popsán vliv objemu a koncentrace koloidu obsahujícího maghemitové nanočástice na morfologii a výtěžek připravovaných mikročástic. Morfologie mikročástic byla vyhodnocena pomocí obrazové analýzy SEM, TEM a snímků ze světelného mikroskopu; složení částic bylo staveno pomocí prvkové analýzy a analýzy obsahu Fe.

Summary

The PhD. thesis "Superparamagnetic nano- and microparticles with hydrophilic surfaces" deals with a preparation and characterization of superparamagnetic nano- and microparticles with hydrophilic surfaces for cell labeling and magnetic separations of biological materials. The wok is divided into three parts according to the experimentally solved problem.

First part describes an optimization of synthesis of iron oxide nanoparticles with suitable toxicological, morphological and physico-chemical properties for aplications in biological systems. Maghemite (γ-Fe_2O_3) particles were prepared by controlled oxidation of magnetite (Fe_3O_4). Magnetite was obtained by modification of a conventional alkaline coprecipitation of Fe(II) and Fe(III) salts in order to produce nanoparticles with a rather narrow size distribution in the absence of a surfactant during the synthesis. Prepared maghemite nanoparticles were *ca*. 6 nm in diameter and their saturation magnetization was $M_s \sim 70$ A·m^2·kg^{-1}. Such value is much higher in comparison with literature data. Generally accepted proposition that the M_s depends not on the preparation method, but only on the nanoparticle size, was thus questioned. Morphology of maghemite nanoparticles was determined by image analysis of SEM and TEM micrographs, hydrodynamic size and zeta-potential was measured by DLS. The structure of the maghemite was confirmed by X-ray diffraction (XRD) and saturation magnetization was measured using a SQUID magnetometer.

Second part describes surface modifications of maghemite nanoparticles with D-manose, poly(L-lysine) and poly(*N*,*N*-dimethylacrylamide) with the aim to label stem cells in order to enable their post implantation tracking using magnetic resonance imaging (MRI). High efficiency of the cell labeling was achieved with such modified nanoparticles; viability of the cells was not affected. Contrast enhancement of the stem cells on MRI scan was proved both in gelatin models and in cell cultures *in vitro* before implantation and *in vivo* after the implantation. The surface modifications were analyzed using TEM, DLS, elemental analysis, ATR-FTIR and SEC.

Third part of the thesis deals with a preparation of hydrophilic microparticles based on poly(*N*,*N*-dimethylacrylamide) filled with maghemite nanoparticles. First, a preparation of neat poly(*N*,*N*-dimethylacrylamide) microparticles was described. From three investigated methods, suspension, dispersion and inverse emulsion polymerization, the last one was chosen as a suitable technique for the preparation of magnetic composite microparticles. Resulting composite microparticles contained high amounts of magnetic nanofillers (up to 70 wt.%) randomly distributed in the polymer matrix. Effects of volume and concentration of maghemite colloid added into the polymerization feed on the microparticle`s morphology and yield were described. Morphology was investigated using SEM, TEM and light micrographs. Composition of the microparticles was determined using elemental analysis and analysis of Fe content.

OBSAH

Seznam zkratek a symbolů

IMAC afinitní chromatografie na imobilizovaných iontech kovů
MRI zobrazovací magnetická rezonance
M magnetizace ($A \cdot m^2 \cdot kg^{-1}$)
H intenzita vnějšího magnetického pole
χ_m magnetická susceptibilita ($m^3 \cdot kg^{-1}$)
T teplota (K)
C Curiova konstanta
T_C Curiova teplota (K)
T_N Neelova teplota
M_S saturační magnetizace ($A \cdot m^2 \cdot kg^{-1}$)
M_r remanentní magnetizace ($A \cdot m^2 \cdot kg^{-1}$)
H_c koercivní pole
SPIONssuperparamagnetické nanočástice oxidů železa
Me atom přechodového kovu
PVA polyvinylalkohol
PEO poly(oxyethylen)
V objem
R elektrický odpor
TEM transmisní elektronová mikroskopie
f frekvence
B_0 intenzita vnějšího longitudiálního magnetického pole
PD protonová hustota
T_1 longitudiální relaxační čas
T_2 transverzální relaxační čas
RF radiofrekvenční puls
FID signál spontánní relaxace spinových momentů po excitaci RF
T_E čas detekce spinového echa, echo čas
T_R čas opakování excitačního pulsu, repetiční čas
RI inverzní zotavení
T_I čas aplikace 90° RF pulsu následujícího po 180° RF pulsu při technice RI
r_1, r_2 relaxivity ($s^{-1} \cdot mol^{-1}$)
DOTA 1,4,7,10-tetraazacyklododekan-*N*,*N'*,*N''*,*N'''*-tetraoctová kyselina
DTPA diethylentriaminpentaoctová kyselina
M_w hmotnostně vážený průměr molekulové hmotnosti
RES retikuloendoteliální systém
XRD rozptyl Roentgenova záření
CLRs lektinové receptory typu C
CRDs sacharid rozeznávající domény
DMEM kultivační médium Dulbecco`s Modified Eagle Medium
FBS fetální hovězí sérum
ATR zeslabená úplná reflektance
FTIR infračervená spektroskopie s Fourierovou transformací
PLL poly(L-lysin)
PDMAAm poly(*N*,*N*-dimethylakrylamid)
ACVA 4,4´- azobis(4-kyanovalerová kyselina)
HPLC vysokoúčinná kapalinová chromatografie
DLS dynamický rozptyl světla
PETPTA pentaerytritolpropoxylát-triakrylát
CAB acetát butyrát celulózy

1. ÚVOD

Bouřlivý rozvoj biologických, biochemických a biomedicínských odvětví v posledních dvaceti letech odhalil potřebu nových částicových materiálů, které by usnadnily, zefektivnily a v mnoha případech vůbec umožnily řadu speciálních i rutinních úkonů jak v laboratorním, tak i průmyslovém měřítku. Kombinace vlastností polymerů, přírodních i syntetických, s vlastnostmi superparamagnetických nanočástic do formy kompozitních nano- a mikročástic pak otevírá paletu materiálových řešení, kterými lze na tyto potřeby odpovědět. Rychlá a velmi levná separace magnetických nosičů z reakčních směsí bez nutnosti použití filtračních nebo centrifugačních zařízení je přínosem nejen v laboratorní, ale i výrobní praxi. Podobně jako u chromatografických separací, lze i pomocí magnetických částic realizovat celou řadu řízených interakcí částicových médií s analytem: od interakcí nespecifických (iontové, hydrofobní, vodíkovými můstky) přes interakce zprostředkované funkčními skupinami (tvorba chelátů a komplexů, afinitní chromatografie na imobilizovaných iontech kovů - IMAC) až po vysoce specifické interakce (antigen-protilátka, avidin-biotin, enzym-substrát, enzym-inhibitor).

Možnost kontroly pohybu magnetických částic pomocí vnějšího magnetického pole lze využít nejen k odstranění (vyzvednutí) částic z často kompozičně i fázově složitých systémů, ale i k dopravě či zavedení chemického, biologického, nebo fyzikálního motivu na místo zamýšleného působení. Pomocí magnetických nosičů lze zavádět katalytické nebo enzymatické systémy na přesně definovaná místa a také je v průběhu procesů přemísťovat uvnitř reakčních prostředí, nebo mezi nimi, např. mezi jednotlivými fázemi reakční směsi. Magnetické částice také představují prostředek k destrukci nádorových buněk cíleným dopravením, nebo zadržením, chemoterapeutických a biologicky aktivních látek. K záměru zničení živé nádorové tkáně, nebo patogenního mikroorganismu, lze však navíc využít i schopnosti samotných magnetických částic produkovat teplo ve střídavém magnetickém poli, tzv. hyperthermie. Další možnost k využití superparamagnetických částic v biomedicínských disciplínách se nabízí ve schopnostech těchto částic ovlivňovat ve vodných prostředích relaxační časy excitovaných spinů atomů vodíku. Tyto částice lze díky této vlastnosti velmi výhodně použít jako kontrastní látky

v zobrazovacích technikách magnetické rezonance (MRI – magnetic resonance imaging).

Na předchozím výčtu možných bioaplikací superparamagnetických částic, který zdaleka není úplný, protože nezahrnuje technické aplikace, jako je stínění elektromagnetického záření, těsnící prvky, hydraulické tlumící systémy atd., lze snadno ukázat, že o úspěšnosti použití těchto částic budou ve velké míře rozhodovat, vedle vlastností objemových, vlastnosti jejich povrchů. A právě v této oblasti se nachází ideální prostor pro uplatnění poznatků z oboru makromolekulární chemie.

Z morfologického hlediska lze problematiku kompozitních superparamagnetických částic rozdělit do tří úrovní: a) superparamagnetické anorganické nanočástice jako základní materiál jader kompozitních částic, b) superparamagnetické nanočástice s upraveným povrchem, kde hlavním nositelem objemových vlastností částic zůstává anorganický krystalit, avšak jeho povrchové vlastnosti jsou upraveny pro potřeby konkrétní aplikace polymery nebo jinými organickými látkami a c) magnetické polymerní mikročástice, kde polymerní materiál tvoří hlavní objemový podíl kompozitu, v němž jsou uloženy superparamagnetické nanočástice; polymerní materiál tak určuje morfologii mikročástic.

2. CÍLE DIZERTAČNÍ PRÁCE

- Metodické zvládnutí přípravy superparamagnetických nanočástic oxidů železa.
- Optimalizace přípravy nanočástic oxidů železa s ohledem na reprodukovatelnou morfologii produktu v množství převyšujícím 1 g na jednu syntézu a možnosti následné povrchové modifikace.
- Návrh a realizace povrchových úprav superparamagnetických oxidů železa s ohledem na reprodukovatelnost a nízkou procesní náročnost za účelem značení kmenových buněk pro jejich následné zobrazování MRI.
- Prověření možnosti přípravy mikročástic na bázi poly(*N*,*N*-dimethylakrylamidu) metodami heterogenních polymerizací.
- Prověření možnosti přípravy kompozitních mikročástic na bázi poly(*N*,*N*-dimethylakrylamidu) se superparamagnetickým nanočásticovým plnivem metodami heterogenních polymerizací.

3A. SUPERPARAMAGNETICKÉ NANOČÁSTICE

K popisu magnetických vlastností daného materiálu je třeba znát vztah mezi magnetizací *M* (magnetickou polarizací) a magnetickým polem *H*, které tuto magnetizaci vyvolalo. Na základě chování materiálů v magnetickém poli je lze (s výjimkou supravodičů) rozdělit do dvou skupin. První skupinou jsou materiály magneticky slabé, jejichž magnetizace dosahuje pouze malých hodnot (např. $M_{H2O} = -0{,}9 \cdot 10^{-8}$ A·m^2·kg^{-1})[a]. Magneticky silné materiály naproti tomu dosahují vysokých hodnot magnetizace (např. $M_{magnetit} = \sim 90$ A m^2 kg^{-1}). Látky magneticky slabé rozdělujeme na látky paramagnetické a diamagnetické. Obě skupiny látek vykazují lineární závislost magnetizace na vnějším magnetickém poli a jejich magnetizace můžeme vyjádřit vztahem (1)

$$M(r) = \chi_m H(r) M(r) \qquad (1)$$

kde χ_m je magnetická susceptibilita. Pro diamagnetika nabývá malých záporných hodnot (typicky $-1 \cdot 10^{-6}$ až $-1 \cdot 10^{-3}$ m^3·kg^{-1}), u paramagnetik pak malých kladných hodnot (typicky 10^{-6} až 10^{-3} m^3·kg^{-1}). Magnetická susceptibilita závisí na teplotě a tato závislost je vyjádřena Curieovým zákonem (2)

$$\chi_m = C/T \qquad (2)$$

kde *T* (K) je absolutní teplota a *C* je Curieova konstanta charakteristická pro daný materiál. Látky ze skupiny para- a diamagnetik díky jejich slabé odezvě na vnější magnetické pole nejsou vhodnými materiály pro přípravu kompozitních částic, kterými zamýšlíme pomocí vnějšího magnetického pole manipulovat.

Látky se silným magnetickým chováním, které je způsobeno samovolným uspořádáváním nevykompenzovaných magnetických momentů atomů do magnetických domén, klasifikujeme jako feromagnetika, ferimagnetika, antiferomagnetika, aj. Liší se od para- a diamagnetik nejen vyššími hodnotami magnetizací a magnetických susceptibilit (0.01–10^6 m^3·kg^{-1}), ale také složitou závislostí magnetizace na intenzitě vnějšího magnetického pole, kterou popisuje tzv. hysterezní křivka magnetizace (obr. 1a).

---

[a] Ačkoliv je soustavou SI jasně definována jednotka specifické magnetizace jako *M* (A·m^2·kg^{-1}), v praxi se více používá vyjádření v systému CGS pomocí *M* (emu/g). Převodní vztah mezi jednotkami je pak 1 A·m^2·kg^{-1} = 1 emu/g (emu = electromagnetic unit).

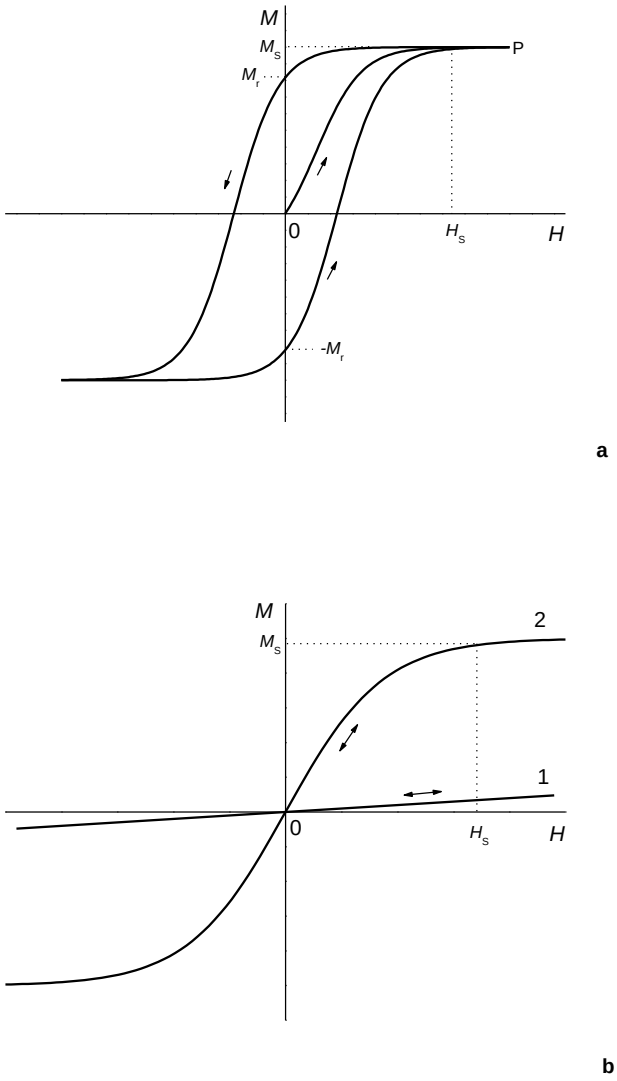

Obr. 1. Schematické znázornění chování feromagnetika (a), paramagnetika (b, křivka 1) a superparamagnetika (b, křivka 2) ve vnějším magnetickém poli.

Magnetické momenty se uspořádávají do domén jen při teplotách pod kritickou hodnotou, tzv. Currieovou teplotou T_C pro feromagnetika a Neelovou teplotou T_N pro ferimagnetika a antiferomagnetika. Pod touto kritickou teplotou narůstá hodnota magnetizace s narůstající hodnotou intenzity magnetického pole až do dosažení tzv. saturační magnetizace M_S (obr. 1a). Hodnota M_S je významnou charakteristikou každého magnetického materiálu a je závislá na teplotě. Pod T_C (T_N) hodnota M_S klesá s rostoucí teplotou. Další významnou charakteristikou magnetického materiálu je hodnota magnetizace odpovídající nulové intenzitě vnějšího pole, tzv. remanentní magnetizace, též remanen-

ce (M_r) (obr. 1a). Nulové hodnoty (M_r) lze dosáhnout buď působením vnějšího pole s opačnou orientací (koercivní pole H_c), nebo zvýšením teploty nad T_C (T_N). Materiál se stává nad T_C (T_N) paramagnetikem, ztrácí své vnitřní magnetické vlastnosti a i svou magnetickou historii, která obecně také podmiňuje celkové magnetické chování materiálu. Teplota T_C (T_N) je proto velmi důležitou materiálovou charakteristikou.[1]

Závislost vnitřní magnetizace superparamagnetik na vnějším magnetickém poli lze popsat jako chování látek magneticky silných a je kombinací chování paramagnetik (obr. 1b, křivka 1) a feromagnetik (obr 1a). Superparamagnetické látky vykazují monotónní závislost magnetizace na intenzitě vnějšího pole pod T_C (T_N) podobně jako paramagnetika, ale magnetizace zůstává téměř konstantní po dosažení saturace M_s (obr 1b, křivka 2). V porovnání s feromagnetickými látkami, superparamagnetika nevykazují hysterezi a mají nulovou remanenci M_r. Hodnoty magnetických susceptibilit superparamagnetik se nacházejí mezi hodnotami pro paramagnetika a feromagnetika. Superparamagnetické chování vykazují malé krystality (typicky 1–30 nm) materiálů, které ve stavu bloku vykazují chování feromagnetické. Jinými slovy, řezáním objemného kusu feromagnetického materiálu se lze dopracovat určité kritické velikosti, pod kterou se již původně feromagnetický materiál chová za dané teploty superparamagneticky. Takovéto chování bylo pozorováno pro různé materiály, jako jsou oxidy železa, ferity, slitiny (Fe-C, Fe-Co), kovy, aj. Komplexní chování superparamagnetik však nezávisí jen na teplotě, materiálovém složení a rozměru krystalitů, ale je ovlivněno i charakterem povrchu a přiléhajícími částicemi. Díky rozměru částic v řádu jednotek nanometrů, každá superparamagnetická částice ovlivňuje magnetické chování přiléhající (nebo sousedící) částice magnetickým polem, které sama generuje. Charakter a složení jejich povrchu pak hraje významnou roli v chování částicových materiálů v porovnání s chováním stejných materiálů ve stavu objemového bloku[2, 3]. Zbytkové sloučeniny z procesu přípravy nanočástic a povrchově aktivní látky proto mají významný vliv na magnetické vlastnosti reálného souboru částic.

Superparamagnetické anorganické nanočástice jako základní materiál jader kompozitních částic (s majoritním i minoritním zastoupením magneticky „neaktivního“ polymeru) tedy mohou nabídnout prakticky využitelné vlastnosti, předurčující do značné míry jejich aplikační možnosti. Jsou to:

- Silná odpověď na vnější magnetické pole – čím silnější je odpověď, tím nižší může být intenzita aplikovaného vnějšího pole, nebo je dosažena lepší dynamika procesu.
- Velmi nízká remanentní magnetizace – čím nižší je remanence, tím lepší je následná dispergovatelnost částic po vypnutí vnějšího magnetického pole. Nulová remanence pak nezpůsobuje žádné interakce magnetického charakteru mezi jednotlivými částicemi po vypnutí magnetického pole, které by vedly k nežádoucí agregaci částic v systému.
- Malý rozměr (průměr) funkční jednotky; povrchové úpravy, stejně jako většina separačních a transportních procesů jsou procesy heterogenní, tedy čím menší jsou částice, tím větší specifický povrch je k dispozici pro následné interakce.
- Odpovídající chemická stabilita při různých pH a redoxních podmínkách.
- Přiměřená cena a snadný proces přípravy (v některých případech).

Superparamagnetické částice jsou často připravovány ve formě koloidních disperzí magnetických částic ve vodě nebo nepolárních rozpouštědlech. Tyto koloidy, nazývané „magnetické kapaliny“, nebo „ferofluidy“, byly v poslední době předmětem souborných prací[4, 5] a monografií[6, 7].

3A.1 Magnetit a maghemit

Ve skupině látek pojmenované jako „oxidy železa“, kterou lze obecně popsat vzorcem $Fe_xO_yH_z$ (ve většině případů $z = 0$), vynikají svými vlastnostmi magnetit a maghemit. Dosahují totiž nejvyšších hodnot saturační magnetizace M_s = 80-100 $A \cdot m^2 \cdot kg^{-1}$, což je o dva řády výše, než hodnoty M_s zbývajících oxidů železa[8]. Superparamagnetické chování bylo objeveno u krystalitů těchto látek s průměrem menším než 30 nm. Tyto krystality jsou často označovány jako SPIONs – superparamagnetic iron oxide nanoparticles. Saturační magnetizace SPIONs je obvykle o 20-50 % nižší, než pro oxidy železa ve formě objemového bloku. Dalším výrazným rysem SPIONs je jejich biokompatibilita[9]. Magnetit a maghemit v superparamagnetickém stavu lze navíc snadno a levně připravit, což jejich praktickou použitelnost dále umocňuje. Ferofluidy oxidů železa často obsahují směs maghemitu a magnetitu.

Magnetit, Fe_3O_4 ($FeO \cdot Fe_2O_3$), je černý, ferimagnetický podvojný oxid se strukturou inverzního spinelu obsahující Fe(II) a Fe(III) ionty[8]. Je speciálním případem ferritových materiálů, jejichž složení lze vyjádřit jako $MeO \cdot Fe_2O_3$, kde Me je atom přechodového kovu. Mikrometrové krystality magnetitu (s nenulovou remanencí) se používaly k výrobě magnetofonových pásek a v jiných průmyslových aplikacích kvůli jeho vysoké hodnotě M_s.

Maghemit, γ-Fe_2O_3, je tmavý červenohnědý ferimagnetický materiál, s krystalovou strukturou podobnou magnetitu, avšak s kationtově deficitními místy. Je to významný magnetický pigment s podobnými vlastnostmi jako má magnetit[8]. Díky jeho podobnosti s magnetitem je často zařazován mezi ferity, i když nemá složení podvojného oxidu. Obvykle se připravuje oxidací magnetitu. Jako oxidační činidlo se používá peroxid vodíku[10], dusičnan železnatý[11], chlornan sodný nebo vzduch[12].

3A.1.1 Příprava a vlastnosti superparamagnetických nanočástic magnetitu a maghemitu

V současnosti je již k dispozici mnoho metod přípravy SPIONs, kdy úpravou reakčních a procesních podmínek lze vyrábět nanočástice s požadovanými parametry, jako je morfologie, velikost, distribuce velikostí částic a magnetické vlastnosti. Realita je ovšem taková, že postupy poskytující monodisperzní částice s vynikajícími magnetickými (i krystalovými) vlastnostmi velmi často neumožňují, díky nutnosti užití povrchově aktivních látek a stabilizátorů, následnou chemickou modifikaci (funkcionalizaci) jejich povrchů. Proto musí být vždy pečlivě zvolen kompromis s ohledem na zamýšlené použití nanočástic a dostupné (realizovatelné) podmínky přípravy.

Historicky první metodou přípravy superparamagnetického magnetitu bylo mechanické mletí 4 obj.% magnetitové rudy v kulovém mlýně spolu s 10-20 obj.% kyseliny olejové v organickém rozpouštědle, typicky v kerosenu[13]. Tato metoda však byla díky své nákladnosti a polydisperzitě produktu nahrazena metodami chemickými, které lze rozdělit na tři skupiny: tepelné rozklady organometalických prekurzorů, hydrotermální procesy a koprecipitace zásadami.

Tepelné rozklady organometalických sloučenin železa poskytují zpravidla dokonale sférické monodisperzní nanočástice o průměru 10-25 nm, s dobrými magnetickými

vlastnostmi. Jedná se zejména o rozklad pentakarbonylu železa[14, 15], acetylacetonátu železitého[16] a *N*-nitrosofenylhydroxylaminu železitého[17]. Všem dosud popsaným metodám tepelných rozkladů je však společný jeden rys, a to nutnost použití povrchově aktivních činidel, např. kyseliny olejové, či funkcionalizovaného poly(oxyethylenu), které brání další následné modifikaci povrchů nanočástic.

Hydrotermální procesy jsou založeny na reakcích směsí oxidů[18] nebo hydroxidů[19] železa ve vodném prostředí (alternativně v prostředí 1,2-ethandiolu[20]) za superkritických podmínek, zahrnujících teploty nad 200 °C a tlaky nad 14 MPa. Výsledné vlastnosti produktů však (dle názoru autora) dostatečně nevyvažují vysoké procesní nároky metody.

Koprecipitace zásadami je metoda nejvíce rozšířená, snadno realizovatelná a nabízí mnoho způsobů, jak ovlivnit výsledné vlastnosti produktu. Poskytuje krystality nejčastěji s průměrem do 10 nm a s distribucí velikosti výrazně užší, než metoda mechanického mletí. Z hlediska morfologie a úzké distribuce velikostí nanočástic však kvalit dvou předchozích procesů, zejména tepelných rozkladů, nedosahuje. Nabízí však možnost výroby nanočástic, jejichž povrch je snadno dostupný pro další modifikace. Proces tvorby magnetitu (oxidu železito-železnatého) vyjadřuje následující rovnice (3):

$$2\ Fe^{3+} + Fe^{2+} + 8\ OH^- \rightarrow Fe_3O_4 + 4\ H_2O \qquad (3)$$

Popis typické přípravy je následující[21]: vodný roztok amoniaku se za neustálého míchání přidává k roztoku železité a železnaté soli v molárním poměru Fe(III)/Fe(II) blízkému 2. Metodika závisí na typu a koncentraci solí (chloridy převažují) a báze, dále na přídavku chelatačních činidel, povrchově aktivních látek, teplotě, rychlosti přidávání báze, poměru k roztoku solí a na procesu zrání. Vznikající sraženina je ponechána růst a poté promývána opakovaně destilovanou vodou pomocí magnetické separace až do tvorby koloidu; tento proces se nazývá peptizace.

Utváření produktu a morfologie částic se dá ovlivnit různými parametry koprecipitačního procesu. Rychlý růst pH do rozmezí 8,5-10 je nezbytný[22]. Pomalé přidávání báze vede k tvorbě hnědé nemagnetické sraženiny, pravděpodobně hydroxidů železa. Rychlé přidání zásady k roztoku solí za intenzivního míchání umožňuje současnou tvorbu hydroxidů železnatého a železitého, které spontánně následně reagují za vzniku

černé sraženiny magnetitu. Proces lze vést i obráceně, tedy pomalým přidáváním roztoku solí do roztoku báze. Pokud jsou v procesu použity silné báze, jako NaOH, KOH a LiOH, může vznikat, částečně nebo úplně, nemagnetický produkt. Hydroxid amonný je preferován, protože při jeho použití tento efekt tvorby nemagnetického produktu pozorován nebyl. Srážení a zrání precipitátu také závisí na teplotě, částice menší než 10 nm lze obdržet v teplotním rozmezí 25-80 °C[22]. Proces zrání sraženiny ovlivňuje výsledné magnetické vlastnosti produktu.

Hlavní výhodou koprecipitační techniky je možnost přípravy vodných koloidů SPIONs bez použití povrchově aktivních látek[21, 23]. V tomto případě je stabilizace dosaženo elektrostatickými náboji na povrchu nanočástic, např. chloristanovými, citrátovými a dusičnanovými anionty, nebo tetramethylamoniovými kationty; produktem je pak kyselý, nebo zásaditý ferofluid[21, 24]. Stabilita koloidu je tak dosažena odpudivými elektrostatickými interakcemi mezi souhlasnými náboji na površích nanočástic. Takto dosažená stabilita je však velmi citlivá na přítomnost dalších elektrolytů v supernatantu, proto je třeba udržet pH v určitých úzkých rozmezích a zároveň použít malou iontovou sílu koloidního roztoku. Částice koloidního roztoku se shlukují do agregátů (aglomerátů) čítajících obvykle 5-100 nanočástic v závislosti na jejich náboji a iontové síle koloidu. Vysrážené nanočástice mohou být znovu stabilizovány (peptizovány) v polárních i nepolárních prostředích přídavkem povrchově aktivního činidla s odpovídajícím HLB[b]. Jako povrchově aktivní látky se používají různé nízkomolekulární sloučeniny, např. vyšší mastné kyseliny[25] a sacharidy[26, 27] a tyto pak ovlivňují výsledné rozměry a magnetické vlastnosti SPIONs[28]. Ferofluidy mohou být také stabilizovány polymery, a to polysacharidy[29], mezi nimiž nejvýznamnější postavení lze připsat dextranu[30-33], polyvinylalkoholem (PVA)[34-40], poly(oxyethylenem) (PEO)[41], poly(oxyethylen-*co*-propen) disfosfonátem[42], kyselinou polymethakrylovou, substituovanými polyakrylamidy, aj. Stabilizace polymery je dosahováno dvojím způsobem: buď *in situ*, kdy jsou železitá a železnatá sůl koprecipitovány v alkalickém roztoku polymeru, nebo post-syntézní modifikací, kdy je roztok polymeru přidáván k předem připravenému magnetickému koloidu.

[b] HLB (hydrophilic-lipophilic balance) je bezrozměrné číslo používané k charakterizaci povrchově aktivních látek; nabývá hodnot od 0 do 20. Vyjadřuje poměr mezi hydrofilní a lipofilní částí molekuly povrchově aktivní látky. Hodnota 0 je přiřazena kompletně hydrofobní molekule, hodnota 20 pak molekule zcela hydrofilní. Metody stanovení HLB byly definovány W.C. Griffinem[1949, 1945] a J. T. Daviesem [1957].

Přítomnost rozpuštěného polymeru v průběhu vzniku nanočástic výrazně ovlivňuje proces srážení, nukleaci a stabilitu vznikajících koloidních částic. Polymerní stabilizátory však kromě stability mohou mít i další význam. Tím, že výrazně mění charakter povrchu nanočástic, přispívají k jejich chemické odolnosti a biokompatibilitě.

Pro potřeby této dizertační práce bylo nutno přistoupit k dílčím úpravám výše popsaného základního koprecipitačního procesu přípravy magnetitu. Výchozími vodnými roztoky solí železa byly experimentálně nalezeny jako ideální 0,1 mol·dm^{-3} $FeCl_3 \cdot 6\ H_2O$ a 0,1 mol·dm^{-3} $FeCl_2 \cdot 4\ H_2O$ v objemovém zastoupení V_{FeCl3}/V_{FeCl2} = 2/1. Jako bázický roztok, do jehož přebytku jsou soli sráženy, byl zvolen 0,5 mol·dm^{-3} vodný roztok NH_3. Dále byla zohledněna skutečnost, že magnetit ve skutečnosti vzniká kvantitativní reakcí $Fe(OH)_3$ a $Fe(OH)_2$ (vznikajících v zásaditém prostředí z železitých a železnatých solí) v molárním poměru 2/1 a nutnou podmínkou[22] pro průběh reakce je udržení pH v rozmezí 8,5-10. Pokud tento molární poměr dodržen není a zejména dojde-li k přebytku $Fe(OH)_3$, je výsledkem souběžně se vznikem magnetitu i vznik nemagnetických oxidů železa, které jsou okludovány na povrchu magnetitových částic a zhoršují jak morfologické a magnetické vlastnosti připravovaného produktu, tak i jeho koloidní stabilitu. S koprecipitační reakcí ovšem souběžně probíhá i oxidace $Fe(OH)_2$ na $Fe(OH)_3$. Tento proces prakticky soutěží s koprecipitační reakcí a výsledkem může být nestechiometrický přebytek $Fe(OH)_3$ se stejnými negativními důsledky na kvalitu produktu. Tomuto jevu se dá předejít (vedle zamezení přístupu atmosférického kyslíku do reakčního prostředí) použitím 1,1-1,2 násobku stechiometrického množství železnaté soli, jejíž okamžitý reakční přebytek průběžně oxiduje na $Fe(OH)_3$ a ten reaguje s dosud neoxidovaným $Fe(OH)_2$ za vzniku magnetitu[7]. Výsledný produkt vykazuje, v porovnání s reakcí ve stechiometrickém poměru, lepší magnetické vlastnosti, ale také nepříliš žádoucí širší distribuci velikostí částic. Toto rozšíření distribuce velikostí částic lze připsat opožděnému vzniku krystalitových zárodků z oxidačních produktů přebytkové železnaté soli. Později vznikající zárodky mají ovšem díky celkovému snížení koncentrace reagujících komponent vzhledem k předchozímu vyloučení majoritního podílu částic jiné podmínky k růstu a zrání. Z důvodu potlačení rozšíření distribuce velikostí nanočástic a zároveň kvůli udržení hodnot M_s blízkých blokovému stavu bylo přikročeno k rozdělení syntézy magnetitových částic bazickou koprecipitací do dvou kroků. V prvním kroku byl roztok 0,1 mol dm^{-3} $FeCl_3 \cdot 6\ H_2O$ převeden 0,9 násobkem stechiometrického množ-

ství amoniaku na $Fe(OH)_3$ za intenzivní sonikace. V druhém kroku byl ke vzniklému koloidnímu roztoku přidán 0,1 mol·dm^{-3} $FeCl_2 \cdot 4\ H_2O$ ve výše zmíněném objemovém zastoupení V_{FeCl3}/V_{FeCl2} = 2/1 a tato směs byla jednorázově vlita do objemového přebytku 0,5 mol·dm^{-3} vodného roztoku NH_3 za míchání a probublávání dusíkem při laboratorní teplotě. Za stejných podmínek byl precipitát podroben zrání v trvání 45 min. Vzniklý magnetit byl promýván demineralizovanou vodou (R = 18,2 MΩ) za použití magnetické separace až do dosažení spontánní peptizace. Následně byl vzniklý a peptizovaný magnetit podroben za sonikace oxidaci na maghemit použitím NaClO. Oxidací na maghemit tak bylo zohledněno zamýšlené použití v biologických systémech, protože magnetit díky přítomnosti Fe^{3+} a Fe^{2+} je klasickým oxidoredukčním katalytickým systémem, který představuje potenciální riziko pro biochemické pochody v živých buňkách, např. katalýzou rozkladu organoperoxidických metabolitů na volné kyslíkové radikály. Teoretickou oporu pro tento krok lze odvodit i ze skutečnosti, že v obou depotních lidských bílkovinách pro železo, feritinu a hemosiderinu (viz. níže), se vyskytují pouze kationty Fe^{3+}. Po oxidaci byly nanočástice maghemitu promývány až do peptizace výše popsaným způsobem a konečně sonikovány.

Připravené nanočástice γ-Fe_2O_3 používané v této disertační práci jako výchozí materiál vykazovaly na TEM snímku (obr. 2a) kulovitou morfologii s číselným průměrem průměrů částic D_n = 6,3 nm a indexem polydiperzity PDI = 1,33. Struktura maghemitu byla potvrzena práškovou RTG difraktometrií (obr. 2b). Magnetizačním měřením pomocí SQUID magnetometru byla stanovena saturační magnetizace maghemitových nanočástic za laboratorní teploty M_s ~ 70 emu/g (obr. 3), což představuje asi 90 % hodnoty uváděné pro blokový maghemit (78 emu/g)[8]. Tato skutečnost je tak v příkrém rozporu s tvrzením, že saturační magnetizace nanočásticových materiálů závisí pouze na velikosti krystalitu a nezávisí na způsobu jejich přípravy[43]. Z publikovaných údajů vyplývá, že hodnoty M_s činí cca 65, 55, 50 a 30 emu/g pro 12, 9, 8 a 4 nm částice maghemitu[43]. Interpolací těchto hodnot se dá hodnota M_s pro 6 nm částice odhadnout na M_s ~ 40 emu/g, což představuje asi 57 % námi reálně zjištěné hodnoty. Lze tedy vyvrátit tvrzení, že hodnota M_s nezávisí na způsobu přípravy nanočástic.

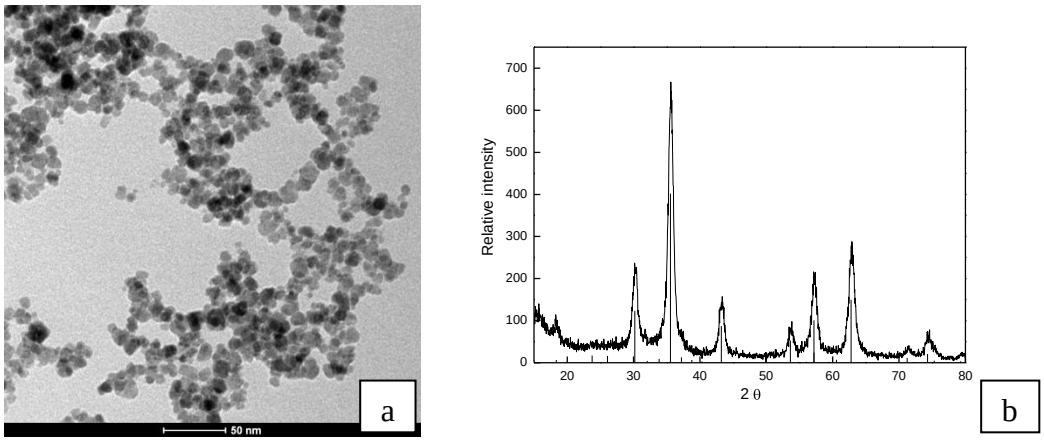

Obr. 2. a) TEM fotografie nanočástic maghemitu, D_n = 6,3 nm, PDI = 1,33. b) práškový RTG difraktogram připravených nanočástic γ-Fe_2O_3. Svislé čáry odpovídají standardu γ-Fe_2O_3.[44]

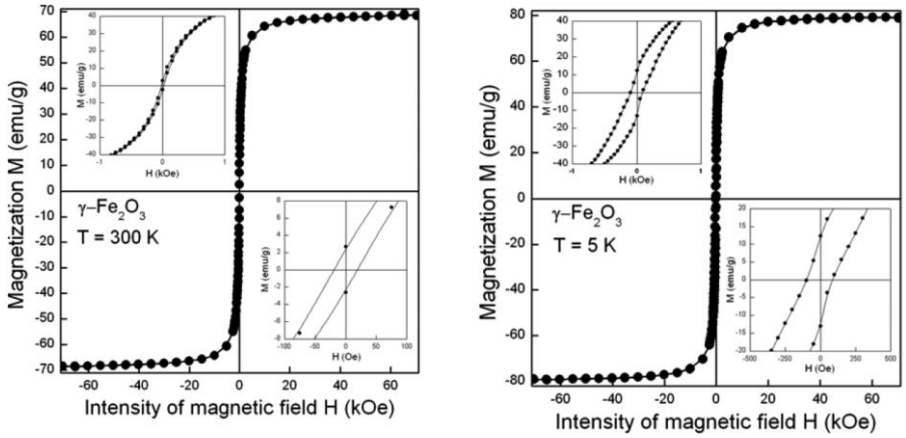

Obr. 3. Hysterezní křivky magnetizace nanočástic γ-Fe_2O_3 měřené pomocí SQUID magnetometru při teplotách 300 K a 5 K[45].

3B. SUPERPARAMAGNETICKÉ NANOČÁSTICE S UPRAVENÝM POVRCHEM PRO ZNAČENÍ KMENOVÝCH BUNĚK

S rozvojem lékařských technik směrem od transplantací celých orgánů k transplantacím jejich částí, či buněk, a v souvislosti s pokroky v oblasti manipulací s kmenovými buňkami, vyvstává velmi silná potřeba neinvazivní detekce těchto implantovaných buněk či jejich souborů v kompartmentech[c] příjemce. Monitorování buněk vnášených do organismu příjemce s terapeutickým záměrem by tak umožnilo topologické zhodnocení úspěšnosti jejich vnesení po operaci a další sledování jejich osudu v čase po implantaci[46]. Pro účely regenerativní medicíny je velmi důležité vědět, zda implantované buňky zůstávají na místě zamýšleného vnesení, zda přežívají a případně dělí-li se. Tyto dosud velmi těžko dostupné informace by výrazně přispěly k rozvoji technik buněčných a tkáňových terapií.

Nejpokročilejší metodou, vhodnou pro relativně rychlé, neinvazivní, prostorové zobrazování měkkých tkání s vysokým rozlišením, je bezesporu zobrazovací magnetická rezonance (MRI). Použitím vhodné kontrastní látky, která by dokázala v časovém horizontu několika týdnů až měsíců zůstat fyzicky ztotožněna s konkrétními buňkami a jejíž signál by se z hlediska intenzity v čase neměnil (nebo se měnil jen nevýrazně), by bylo možné výše zmíněné potřeby regenerativní a transplantační medicíny a buněčné terapie uspokojit. Při výběru a vývoji takovéto kontrastní látky pak musí být zohledněny fyzikálně-chemické principy tvorby kontrastu při MRI zobrazení spolu s chováním látky v biologických prostředích, zejména její toxicita a biodistribuce.

[c]Kompartment je morfologicky definovaná část celku, částečně nebo úplně oddělená, zpravidla se zřetelnou vnější hranicí, která selektivně ovlivňuje výměnu látek mezi vnějším a vnitřním prostorem. Ve farmakologii je pak význam kompartmentu rozšířen pro oblast, která má z hlediska kinetiky léčiva a jeho distribuce jednotné vlastnosti.

3B.1 Princip MRI

MRI je neinvazivní zobrazovací lékařská technika, která využívá interakcí radiofrekvenčních pulsů s tkáněmi umístěnými v silném magnetickém poli. Jejím výsledkem jsou obrazy řezů (rovin) tkáňového prostředí (vnitřních orgánů těla). Zobrazovaným objektem jsou prakticky vodíková jádra (protony) molekul vody, která tvoří většinu objemu tkání a jejíž molekuly mají v závislosti na typu tkáně různou pohyblivost. Jenom malá část těchto protonů přispívá k měřitelnému signálu, který je dán rozdílným uspořádáním (paralelním, nebo antiparalelním) vzhledem k vektoru intenzity vnějšího magnetického pole. Protony jsou schopny absorbovat energii krátkého radiofrekvenčního pulsu při jejich rezonanční frekvenci f_0 (při intenzitě vnějšího magnetického pole B_0 = 1,5 T je f_0 = 63,86 MHz). Po absorbování energie radiofrekvenčního pulsu vodíková jádra tuto energii uvolňují a vracejí se tak zpět do stavu původní rovnováhy s vnějším magnetickým polem. Transmise této energie vodíkovými jádry při návratu do jejich původního stavu je následně pozorována jako MRI signál. Rozdíly v pohyblivosti molekul vody v závislosti na výskytu v konkrétním typu tkáně pak způsobují jemné rozdíly v MRI signálech a tyto rozdíly pak vedou k rozlišení jednotlivých typů tkání. Intenzita měřeného signálu úzce závisí na hustotě spinů (PD – proton density) a na relaxačních časech (T_1 a T_2), záleží pak na konkrétní zobrazovací technice a výběru mezipulsového intervalu. Zjednodušeně lze provedení MRI metody popsat takto: sledovaný objekt je vystaven vnějšímu podélnému magnetickému poli, což vyvolá paralelní i antiparalelní uspořádání jednotlivých spinů vodíkových jader s výslednou tkáňovou magnetizací M_0 se směrem totožným s B_0. Zároveň začnou magnetické momenty vodíkových jader vytvářet precesní pohyb určený Larmorovou frekvencí. Larmorova frekvence závisí jednak na intenzitě vnějšího magnetického pole a jednak na typu atomového jádra (pro lékařské účely mají největší význam jádra vodíková ^{1}H, pro speciální případy se však využívají i jádra fosforu ^{31}P a uhlíku ^{13}C). Kolmo na toto pole je vyslán radiofrekveční puls RF s frekvencí totožnou s Larmorovou frekvencí, který vychyluje precesující vektory z orientace podle vnějšího longitudiálního pole o 90°. Více protonů je pak orientováno antiparalelně (větší energetická náročnost), čímž dochází k narušení rovnováhy ustavené v objemu tkáně vnějším magnetickým polem. Dochází tak ke změně velikosti podélné složky tkáňové magnetizace M_0 (ve směru osy pulsu). Zároveň puls sjednocuje

fáze precesních kmitů (precesující vektory jsou přivedeny do stavu koherence), čímž vzniká příčná složka vektoru tkáňové magnetizace, který byl dosud nulový. Po vypnutí kolmého pulsu pak spiny uvolňují přijatou energii z pulsu do okolí a vracejí se tak k původní orientaci dle podélného pole a do výchozích energetických stavů. Vyzařovaná energie je snímána cívkami v ose RF pulsu. Takto získaný signál se označuje zkratkou FID (free induction decay) a má tvar harmonického průběhu s exponenciálně klesající amplitudou. Návraty k výchozím hodnotám mají určitá časová zpoždění, nazývaná relaxační časy. Rozlišovány jsou dva typy těchto relaxačních časů, zmíněné T_1 a T_2.

- T_1 (spin-mřížková relaxace, longitudiální relaxační čas) je pro diagnostické účely do značné míry chápán jako biologický parametr, neboť je využíván k rozlišení mezi jednotlivými typy tkání. Tyto tkáňově specifické časy vystihují dobu potřebnou k přeuspořádání orientace spinů vychýlených kolmým pulsem zpět do výchozí orientace podle podélného pole. T_1 relaxační čas (řádově v milisekundách) též vystihuje, jak rychle nabude vektor podélné magnetizace 63 % své původní hodnoty. Tato emitovaná energie tak poskytuje informaci o okolí relaxujících jader, např. tuková tkáň absorbuje uvolňovanou energii protonů rychleji než tkáň s vyšším podílem vody.
- T_2 (též spin-spin relaxační čas, transverzální relaxační čas) vyjadřuje čas potřebný k postupné ztrátě fázové jednotnosti (koherence způsobené radiofrekvenčním pulsem) vlivem magnetických polí jednotlivých částic způsobujících drobné lokální nehomogenity magnetického pole. T_2 pak udává čas, za který dojde k poklesu velikosti magnetizace kolmé složky na 37 % svého maxima. V praxi je pak pokles příčné složky tkáňové magnetizace ovlivněn ještě drobnými změnami v nehomogenitě vnějšího magnetického pole. Pokles je tak podstatně strmější; příslušnou relaxační konstantu označujeme jako T_2^*. I když u klasického MR zobrazování je tento jev většinou nežádoucím a je snaha jej potlačit, přesto lze i T_2^* využít ke zlepšení kontrastu MR obrazu.

Hlavním cílem MR zobrazování je vytvořit snímek s kontrastem mezi jednotlivými typy tkání. Jas v obrázku ovlivňuje mnoho faktorů. Mezi základní tři patří již zmiňované relaxace T_1 a T_2, resp. T_2^* a *PD*. Vhodným uspořádáním pulsní sekvence lze dosáhnout požadovaného kontrastu (T_1-, T_2- a *PD*-vážený obrázek). Kontrasty snímků, vycházející z odlišnosti relaxačních časů různých typů tkání, se realizují změnou způsobu,

kterým jsou spiny excitovány a jejichž relaxační signál je následně pozorován. Prakticky se tedy kontrasty snímků vytvářejí změnami parametrů pulsní sekvence. Základní měřící sekvencí pro T_2-vážený obraz je sekvence spinového echa (spin echo SE), která se skládá z jednoho 90° excitačního pulsu a jednoho, nebo více, refokusačních 180° pulsů. Excitační 90° puls sklopí spiny do transverzální roviny. Vzájemnou spin-spinovou interakcí a v důsledku nehomogenit magnetického pole se spiny postupně rozfázovávají. V čase $T_E/2$ (T_E – time echo) se aplikuje 180° refokusační excitační puls a tento otočí spiny zrcadlovým způsobem. Po uplynutí dalšího intervalu $T_E/2$ se spiny sfázují a nastává maximum spinového echa. Amplituda spinového echa je vždy menší, než původní amplituda signálu FID v okamžiku po ukončení 90° RF pulsu. Smyslem tvorby spinového echa je potlačit pokles signálu způsobený nehomogenitami magnetického pole. Je třeba zmínit tři hlavní parametry pulsní sekvence, které ovlivňují kontrast. Prvním je energie použitá na radiofrekvenční excitační puls, která se vyjadřuje jako sklápěcí úhel (sklopení vektoru tkáňové magnetizace). Čím více energie vyzáříme do vzorku tkáně, tím více času je třeba pro plnou relaxaci. Druhý parametr je čas T_R, který udává dobu, po níž opakovaně aplikujeme jednotlivé excitační pulsy. S kratším časem T_R je i méně času k T_1 relaxaci. Posledním parametrem je čas spinového echa T_E. Při delším času T_E budou jádra s kratším časem T_2 přispívat k měřenému signálu méně. Základní měřící sekvencí pro T_1-vážený obraz je sekvence inverzního zotavení (inversion recovery RI) tvořená sekvencí 180° a 90° RF impulsů. První 180° RF puls překlopí vektor magnetizace o 180°, ten změní směr, nezmění však velikost. Poté se začne uplatňovat relaxace T_1 a magnetizace se vrací do rovnovážného stavu, což se projeví exponenciálním růstem vektoru tkáňové magnetizace ze záporných do kladných hodnot. V čase T_I (inversion time) následuje 90° RF impuls, který překlopí vektor magnetizace do roviny kolmé na vnější magnetické pole. V přijímací cívce je detekován FID signál, jehož amplituda závisí na T_1 relaxačním čase zobrazované tkáně. Lékařská i badatelská praxe se však stále častěji setkává s potřebami zviditelnit i takové patologické či fyziologické změny a jevy, jejichž kontrast se nastavováním výše zmíněných přístrojových parametrů nelepší. Vyvstává tak jediná možnost, jak dosáhnout zlepšení tkáňového kontrastu, a to změnou vnitřních (tkáňových) parametrů použitím kontrastní látky v zobrazovaném kompartmentu[47, 48].

3B.2 Kontrastní látky pro MRI

Kontrastní látka je chemická substance zavedená do anatomicky, nebo funkčně, definované oblasti za účelem jejího zobrazení. Způsobuje zvýšení rozdílu mezi různými tkáněmi, nebo mezi tkání normální a abnormální, pozměněním jejich relaxačních časů. Kontrastní látky pro MRI jsou tradičně klasifikovány podle vlivu na konkrétní relaxační čas jako T_1 kontrastní a T_2 kontrastní. V současnosti si velmi dynamický vývoj nových kontrastních látek pro MRI vyžádal jemnější klasifikaci, zohledňující např. chemickou či morfologickou strukturu látek, nebo typ fyzikálního působení v kompartmentu. Kontrastní látky je možno klasifikovat i podle kompartmentu, v němž jsou použity. Klasifikace kontrastních látek tak ze zjevných důvodů není zatím sjednocena, často dochází k prolínání jednotlivých klasifikačních kritérií a úplné postihnutí aktuálního stavu by překračovalo rámec této práce. Proto je nutné zmínit, že způsoby klasifikací, použité níže, byly vzhledem k aktuálnímu stavu účelově zúženy se záměrem vykreslit pozadí problému řešeného v této práci.

- T_1 kontrastní látky (též pozitivní kontrastní látky) způsobují zkrácení T_1 relaxačního času (zvýšení intenzity signálu u T_1-váženého zobrazení). Na MRI skenu se projevují ve vztahu k okolí jako relativně světlá pole (či body). Mezi typické zástupce patří nízkomolekulární sloučeniny a komplexy gadolinia, manganu nebo železa.
- T_2 kontrastní látky (též negativní kontrastní látky) se projevují na MRI skenu jako relativně tmavá pole (či body) ve vztahu k okolí. Tyto látky způsobují lokální nehomogenity magnetického pole, což ovlivňuje především spin-spin relaxační efekt projevující se zkrácením T_1 a T_2 relaxačních časů. Mezi typické zástupce patří fero- a superparamagnetické částice oxidů železa (a feritů) o velikostech do cca. 300 nm.

Jak již však bylo naznačeno výše, toto tradiční dělení MRI kontrastních látek na T_1 a T_2 kontrastní látky není vždy přesné, protože T_1 kontrastní látka snižující čas T_1 zároveň zmenšuje stejnou měrou i T_2. Naopak, T_2 kontrastní látka nutně také zmenšuje T_1 , ale efekt zkrácení T_1 je výrazně menší, než efekt zkrácení T_2. Klasifikaci dále komplikuje fakt, že projevy jak T_1, tak T_2 kontrastních látek závisejí na použité zobrazovací pulsní

sekvenci, intenzitě vnějšího pole, velikosti molekuly kontrastní látky a způsobu kompartmentalizace látky v konkrétním typu tkáně. Přesnější zařazení kontrastních látek pak nabízejí následující klasifikace podle typu chování látek v magnetickém poli:

- Paramagnetické kontrastní látky obsahují ionty přechodových kovů s jedním nebo více nepárovými elektrony, které proto vykazují permanentní magnetický moment. Ve vodných roztocích těchto látek pak dochází k interakci mezi elektronovým magnetickým momentem paramagnetického atomu a slabšími magnetickými momenty protonů blízkých molekul vody. Molekulární pohyby způsobují náhodné fluktuace těchto dipólových interakcí a snižují T_1 a T_2 relaxační časy protonů vody. Typickými zástupci[49, 50] jsou ionty Gd^{3+} a Mn^{2+}, které velmi efektivně redukují T_1 a T_2. Tyto paramagnetické ionty však nemohou být použity samostatně v jejich disociované formě, protože vykazují vysokou toxicitu a navíc i nežádoucí biodistribuci (kumulují se v kostech, játrech a slezině). Gadoliniové soli při fyziologickém pH rychle hydrolyzují za vzniku nerozpustného $Gd(OH)_3$. Proto byly (a stále jsou) studovány jejich organické cheláty s vysokou termodynamickou a kinetickou stabilitou snižující toxicitu a zajišťující odpovídající biodistribuci. Gd^{3+} cheláty snižují T_1 a T_2 relaxační časy protonových jader cílové tkáně a proto v závislosti na relativní míře těchto snížení jsou klasifikovány jako T_1 i T_2 látky. Efektivitu MRI kontrastních látek vyjadřují hodnoty relaxivit r_1 a r_2, které popisují schopnost snížení T_1 a T_2 relaxačních časů protonů vody vztažené na jednotku koncentrace (zpravidla mmol) iontů kovu. Zlepšeného kontrastu na MRI skenu je dosaženo tehdy, má-li daný typ chelátu zvýšenou afinitu ke konkrétnímu typu tkáně, nebo je-li sledovaný orgán více vaskularizován ve srovnání s jeho okolím. Patologické tkáně (nádorové, zánětlivé) jsou metabolicky i morfologicky odlišné od tkání ve fyziologickém stavu a mají zpravidla vyšší zádrž kontrastní látky. Pozitivita (zesvětlení) nebo negativita (ztmavení) signálu kontrastní látky je pak dána typem vážení zobrazení.
- Superparamagnetické kontrastní látky představují koloidy krystalitů superparamagnetických částic, zpravidla oxidů železa, viz. kapitola 3A. „Superparamagnetické nanočástice“. Omezeně lze nalézt i práce využívající ferity, které mají z hlediska kontrastu pro MRI sice lepší fyzikální vlastnosti, ale komplikací je toxicita feritových heteroatomů, jako je Co, Ni, Cu a Mn. Pro účely MRI je třeba

superparamagnetické částice povrchově upravit tak, aby se zabránilo jejich shlukování. Nežádoucí agregace by jednak způsobovala negativní změny v mobilitě tělními tekutinami, opsonizaci a následné pohlcení makrofágy a zároveň by zvyšovala riziko ucpání cévních kapilár (embolizaci). Superparamagnetická kontrastní látka pro MRI se tedy skládá z jednoho nebo i více superparamagnetických jadérek obalených do další vrstvy, např. dextranu nebo siliky. Relaxace indukovaná spuperparamagnetickými částicemi se vysvětluje pomocí klasické teorie spinové relaxace ve vnější elektronové sféře, doplněné Curiovou relaxační teorií[51]. Tato teorie bere do úvahy ovlivnění rychlosti relaxace protonů vody difundující do blízkosti nepárových elektronů zodpovědných za magnetické vlastnosti materiálu částice. Tyto částice vykazují silný T_1 relaxační efekt, a protože zároveň díky vlastní magnetické susceptibilitě mění homogenitu aplikovaného vnějšího pole, také zlepšují T_2 relaxaci. Významným závěrem teorie relaxace ve vnější sféře je pak tvrzení, že poměr relaxivit r_2/r_1 stoupá s rostoucí velikostí superparamagnetických jader, proto menší částice vykazují vyšší redukci T_1 než částice větší[52-54]. Původně byly superparamagnetické částice vyvíjeny hlavně jako T_2 kontrastní látky s negativním efektem v MRI zobrazování[55]. Další pokusy se superparamagnetickými částicemi menšími než 10 nm však ukázaly[53, 54, 56, 57] jejich výrazný vliv také na snížení T_1. Často lze v odborné literatuře nalézt zobecňující tvrzení, že celkový rozměr částice (zahrnující obal a jádro) podmiňuje farmakokinetiku kontrastní látky, rozměr jádra pak relaxivitu částice.

- Susceptibilitní kontrastní látky. Z makroskopického pohledu mohou interakce dlouhého dosahu převládat nad výše popsanými vlivy na T_2 nebo T_2^* relaxační časy u všech typů kontrastních látek. Tento mechanizmus, známý jako susceptibilitou indukovaná relaxace[58], se vztahuje k vektoru vnitřní magnetizace kontrastní látky. Jednotlivé vektory vnitřních magnetizací individuálních nanočástic se uspořádávají (u superparamagnetických se generují *in situ*) podle směru vnějšího magnetického pole. Pokud se superparamagnetická kontrastní látka nachází v zobrazovaném kompartmentu, pak se může celý kompartment projevovat na MRI skenu jako sekundární kontrastní látka. Protony vody na vzdálenější straně kompartmentu (mimo bezprostřední blízkost částice) jsou ovlivněny celkovou magnetizací superparamagnetického podílu v kompartmentu a proto relaxují

mechanizmem spinové relaxace ve vnější elektronové sféře. Kontrastní efekt závisí na magnetickém momentu, lokální koncentraci a prostorové distribuci kontrastní látky, rozměrech a geometrii kompartmentu, difusní konstantě vody v daném prostředí, apod.

Kontrastní látky v současnosti používané v klinickém a experimentálním režimu lze rozdělit z hlediska chemického složení do dvou hlavních skupin:

- Komplexy Gd^{3+} (minoritně i Dy^{3+}, Cr^{3+}, Fe^{2+}, Mn^{2+}), kde jako organické ligandy dominují zejména nízkomolekulární sloučeniny na bázi různě substituované DOTA (1,4,7,10-tetraazacyklododekan-*N*,*N'*,*N''*,*N'''*-tetraoctová kyselina) a DTPA (diethylentriaminopentaoctová kyselina)[59] – viz obr 4.

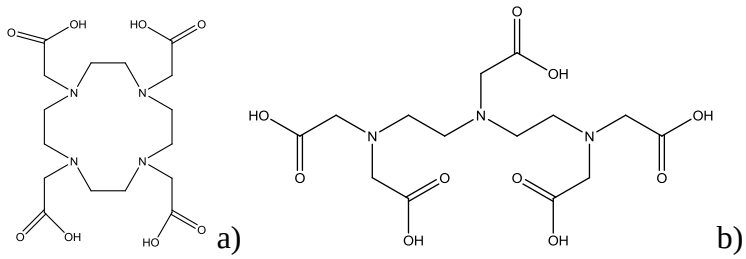

Obr.4. a) DOTA, b) DTPA.

- Superparamagnetické částice, u nichž je třeba hledat individuální odlišnosti z hlediska chemické stavby hlavně v jejich povrchové úpravě. Konvenčními částicemi, které byly v době začátku řešení dizertační práce schváleny pro klinickou praxi (nebo alespoň dostupné na trhu jako experimentální materiál)[d], jsou částice oxidů železa (často označované jako nestechiometrické oxidy) s povrchem upra-

[d] Od cca. r. 2004 prochází vývoj a výroba superparamagnetických kontrastních látek v komerční sféře útlumem. Patrně prvním preparátem, jehož vývoj byl přerušen po převzetí firmy Amersham Health firmou GE Healthcare, byl Clariscan®. Od roku 2007 pokračuje stahování registrací jednotlivých přípravků (Sinerem™) na žádost samotných výrobců z ekonomických a licenčních důvodů. Odhadovaný počet klinických aplikací superparamagnetických částic se nejeví v současnosti farmaceutickým společnostem jako rentabilní. V pozadí zastavování vývoje (zejména v USA) stojí patrně i rozhodnutí administrativy (9.8.2001) presidenta G.W. Bushe o omezení podpory výzkumu kmenových buněk v USA, čímž se aplikační prostor pro superparamagnetické kontrastní látky zúžil. Ke konci roku 2008 francouzská společnost Guerbet ukončila výrobu preparátu Endorem™, umožnila však doprodej vyrobených přípravků. V r. 2009 požádala společnost Bayer Shering DE o stažení registrace preparátu Resovist®. Další komplikace patrně vyvstanou i díky rozhodnutí Evropského soudního dvora ze dne 18.10.2011 ohledně zrušení platnosti patentových a licenčních práv ke kulturám embryonálních kmenových buněk, po kterém se tak pro evropské výzkumné instituce zhoršuje výhled návratnosti investic do výzkumu.

veným dextranem. Pod obchodním názvem Endorem™ (Feridex®) nebo Sinerem™ jsou vyráběny firmou Guerbet; Ferrumoxtran (syn. Combidex) je pak produktem firmy Amag Pharmaceuticals. Karboxydextranem povlečený oxid železa je na trhu pod názvem Resovist® od Bayer Schering Pharma, poly(oxyethylenem) modifikovaný koloid Clariscan® (syn. PEG-FERRON) pak dodává GE Healthcare. Velikost paramagnetického jadérka, jak již bylo uvedeno výše, určuje převládající vliv na vznik kontrastu, tedy zda se jedná o mechanizmus relaxace ve vnější sféře, nebo spíše o susceptibilitní efekt.

Při volbě vhodného typu MRI kontrastní látky pro značení kmenových buněk je nutné zohlednit i chování látky v biologickém prostředí, zejména její biodistribuci a toxicitu. Doposud dostupné MRI kontrastní látky (tedy schválené, nebo pro použití v experimentálním režimu) byly vyvíjeny s cílem jejich systemického podání (aplikace do krevního oběhu). Od takto podaných kontrastních látek je pak primárně požadováno zlepšení kontrastu buď intravaskulárního prostoru, nebo extracelulární tekutiny. Pro kontrastování extracelulárních tekutin je třeba, aby kontrastní látka prosákla co nejdříve po injekčním podání přes cévní výstelku do intersticia (za fyziologického stavu by takováto látka neměla procházet hematoencefalickou bariérou[e]) a zároveň, aby rychlost jejího vylučování ledvinami umožnila časově zvládnout zobrazení požadovaných oblastí. Tyto požadavky dostatečně naplňují nízkomolekulární Gd^{3+} komplexy s deriváty DTPA a DOTA ligand, které mají poločas prosáknutí z krevního řečiště asi 5 min. a poločas renální eliminace asi 80 min. Nicméně, vlastnosti těchto komplexů, které jsou velmi výhodné pro kontrastování intersticia, je zároveň diskvalifikují pro záměr kontrastování kultivovaných buněk. Tyto látky vykazují v prostředí biologických tekutin velmi vysokou difuzivitu. Proto by bylo velmi obtížné vytvořit koncentrační rozdíl mezi buňkou a jejím okolím, který by zajistil dostatečný kontrast, zejména pak v delším časovém intervalu. Proti

[e]Hematoencefalická bariéra je rozhraní oddělující krevní prostor od prostoru centrálního nervového systému (CNS) a zabezpečující tak omezený transport látek z krevního řečiště. Je tvořena především těsným uspořádáním buněk cévního endotelu a její primární funkcí je ochrana CNS před poškozením xenobiotiky. Při některých patologických stavech se prostupnost této bariéry zvyšuje a proto je možné tyto patologie identifikovat díky kumulaci MRI kontrastní látky v mezibuněčném prostoru CNS.

Gd^{3+} chelátům stojí i jejich toxicita, která je sice z hlediska systemického podání přijatelná, avšak při použití do jednotlivých buněk představuje vážnou překážku. Pro kontrastování intravaskulárního prostoru je však třeba, aby kontrastní látka přes cévní výstelku prosakovala co nejméně a v krevním řečišti setrvala v potřebné koncentraci zajišťující kontrast déle, než látky pro kontrastování extracelulární tekutiny. Výrazného omezení prosakování do intersticia se dá dosáhnout zvýšením molekulové hmotnosti kontrastní látky nad hodnotu $M_w > 20\,000$. Podle způsobu dosažení tohoto parametru se dají látky pro kontrastování krevního řečiště rozdělit do tří skupin: a) nízkomolekulární Gd^{3+} komplexy nekovalentně se navazující na lidský sérový albumin (nejčastěji deriváty DOTA a DTPA komplexů) b) polymerní Gd^{3+} komplexy tvořené buď modifikací nízkomolekulárního komplexu vodorozpustným polymerem, nebo hydrofilním dendrimerem se skupinami chelatujícími Gd^{3+} a c) částicové systémy. V případě použití polymerních a albuminových Gd^{3+} komplexů pro značení buněk zůstává výhrada toxicity jako u látek pro kontrastování extracelulárních tekutin. Současně přetrvává i problém s dosažením dostatečného rozdílu kontrastu v konkrétní buňce v delším časovém úseku. Částicové systémy založené na oxidech železa vykazují z hlediska biodistribuce značně odlišné chování v porovnání s nízkomolekulárními Gd^{3+} komplexy. Pohyb nízkomolekulárních komplexů v biologických tekutinách je přednostně určován difůzí a omezován převážně exkluzními limity jednotlivých tkáňových rozhraní. Vylučovacímu mechanizmu dominuje ledvinová filtrace (renální exkrece). Naproti tomu biodistribuce nanočástic je ve stejném prostředí většinově ovlivňována sorpcí bílkovin na povrch částic, tzv. opsonizací[60]. Vzhledem k rozměrům bílkovinných struktur a nanočástic je třeba uvažovat též sorpci částic na molekulu bílkoviny; hlavní vylučovací cesta je pak určena aktivitou retikuloendoteliálního systému (RES). Cizorodý povrch nanočástic (jedná se o obecný jev neomezující se pouze na nanočástice) je bezprostředně po depozici do krevního oběhu obsazován (opsonizován) protilátkami a je takto „označen“ pro pohlcení a zneškodnění cirkulujícími nebo fixnímy fagocytujícími buňkami. V závislosti na typu fagocytující buňky jsou pak nanočástice vylučovány z krevního oběhu játry, slezinou a mízními uzlinami[61], kde dochází k přechodné akumulaci částic. Proces vyloučení částic z těla je tak výrazně delší, než renální exkrece. Jak už bylo zmíněno dříve, superparamagnetické částice byly vyvíjeny před-

nostně se záměrem systemického podání za účelem kontrastování prostoru krevního kompartmentu[f]. Plazmový poločas nanočástic je určován především aktivitou RES; po intravenózním podání koloidního nosiče dochází k jeho eliminaci z krevního kompartmentu v řádu minut a typická finální biodistribuce částic je pak 80-90 % v játrech, 5-8 % ve slezině a 1-2 % v kostní dřeni[62]. Aby bylo možno dosáhnout experimentálně realizovatelného kontrastu krevního řečiště v čase, bylo potřeba upravit povrch nanočástic tak, aby se opsonizace omezila a eliminace částic z krevního oběhu fagocytujícími buňkami snížila[63, 64]. K takovéto povrchové úpravě se používají už zmiňované vodorozpustné polymery jako dextran[65], karboxydextran[66], heparin[67], poly(oxyethylen)[64, 68] a poly(*N*-vinylpyrolidon)[69]. Pro požadovanou aplikaci je třeba nalézt optimální kompromis mezi hustotou polymerního obalu a jeho tloušťkou (celkovou hydrodynamickou velikostí částic)[70]. V současnosti je u komerčně dostupných preparátů používán k pokrytí povrchu superparamagnetických oxidů železa pro systemické podání lineární polymer dextran, který zvyšuje plazmový poločas i nad 2 hod.[71].

3B.2.1 Povrchové úpravy nanočástic pro značení kmenových buněk

Spolupracující medicínská pracoviště se racionálně snažila nejprve využít při experimentech s kulturami mezenchymových kmenových buněk (MSC) dostupný materiál, konkrétně preparát Endorem™ firmy *Guerbet,* což jsou částice oxidů železa o průměru 5,5 nm s povrchem pokrytým dextranem a celkovým hydrodynamickým průměrem asi 100 nm. Superparamagnetické částice oxidu železa představují vhodný zdroj MRI kontrastu vzhledem k tvorbě relativně velké nehomogenity magnetického pole. Jejich endocytováním by došlo ke ztotožnění signálu s konkrétní buňkou, který by byl stálý v relativně dlouhém časovém úseku (v řádu dnů až týdnů). Zároveň se u částice oxidů železa předpokládal jen malý toxický účinek částic na endocytující buňku. Přirozenou součástí některých typů měkkých tkání je totiž

[f] Systemické podání superparamagnetických nanočástic se postupně vyvinulo také v cílené kontrastování mízních uzlin a jater díky aktivitě RES, a také plic, v nichž dochází k přechodné kumulaci částic v krevních kapilárách díky jejich specifické anatomii.

bílkovino-anorganická kompozitní struktura zvaná feritin, což je superparamagnetický fosfatovaný krystalit ferihydritu ($FeOOH \cdot 0{,}4\ H_2O$, starší způsob zápisu $5\ Fe_2O_3 \cdot 9\ H_2O$) s průměrem cca. 5-10 nm obalený kulovitou vrstvou proteinových řetězců apoferitinu, který velikost navýší na 13 nm[g8]. Při kultivaci mezenchymových kmenových buněk za účelem vytvoření experimentální terapeutické kultury tak byl do kultivačního média přidáván kvůli kontrastování buněk výše zmíněný preparát Endorem™ s částečně uspokojivými výsledky. Spolupracující pracoviště požadovala oproti komerčnímu preparátu, sloužícímu dále jako referenční vzorek, změny v těchto sledovaných parametrech:

- zvýšení procenta označených buněk *in vitro*,
- „rovnoměrné proznačení" buněčné kultury,
- zvýšení množství částic internalizovaných buňkou, tzn. zlepšení kontrastu kultury po implantaci,
- snížení množství nanočástic adherovaných k vnější straně buněčné membrány a
- stejnou, nebo vyšší viabilitu označených buněk, než poskytuje Endorem™.

Jako hlavní strategie naplnění výše uvedených byla zvolena cesta vytvoření nového způsobu pokrytí povrchu SPIONs. Stávající dextranová obálka nanočástic totiž byla vyvíjena s ohledem na potlačení opsonizace jejich povrchu. Tím se snížila nejen schopnost adhezní vazby mezi částicemi a cirkulujícími proteiny, ale i vazby mezi částicemi a proteiny fixními, např. receptory buněčných membrán indukujícími adhezi nebo endocytózu. Tato snížená adheze k bílkovinným strukturám buněčných membrán pak s největší pravděpodobností způsobovala malý podíl částicemi označených buněk v kultuře, spolu s malým počtem částic internalizovaných jednot-

[g] Vedle feritinu, který slouží jako zásobní bílkovina pro železo s oboustranným transferem Fe iontů, lze v lidském organizmu nalézt ještě hemosiderin. Ten je v organizmu ukládán výhradně intracelulárně odpověď na přehlcení železem. Hemosiderin vzniká ve formě nerozpustných granulek s tvrdým jádrem a bílkovinnou slupkou. Pomocí XRD byla potvrzena existence hemosiderinu ve dvou formách: (i) primární hemosiderin (s ferihydritovým jádrem) vznikající jako odpověď na přehlcení organizmu železem ze stravy a (ii) sekundární hemosiderin (s jádrem goethitu) jako následek opakovaných transfuzí při léčení thallasemie. Hemosiderin vzniká také následkem krvácení do měkkých tkání.

livými buňkami. Možnost chemické modifikace dextranového povrchu komerčních částic nebyla rozvíjena v této práci na základě předpokladu, že zvětšováním celkového hydrodynamického rozměru by se pravděpodobnost endocytózy snižovala ze sterických důvodů.

Vhodným přístupem ke zlepšení kvantitativních parametrů internalizace, tj. zvýšení počtu částic pohlcených buňkou a podílu označených buněk v kultuře, se ukázala být přímá modifikace povrchů SPIONs látkami, u kterých existoval teoreticky či prakticky podložený předpoklad specifické, či nespecifické, indukce endocytózy (transportu buněčnou membránou). K zajištění kvalitativních parametrů internalizace, tj. zlepšení rovnoměrnosti proznačení kultury a minimálnímu snížení viability buněk, bylo nutné zohlednit toxický vliv použitých látek na buněčnou kulturu. Důležitou roli hrál i vliv modifikace povrchů SPIONs na potlačení tvorby náhodných shluků (agregátů) částic v časovém intervalu od kontaktu částic s kultivačním médiem do okamžiku úspěšné internalizace buňkou.

3B.2.1.1 D-manóza

D-manóza byla zvolena k povlékání nanočástic pro svou schopnost zprostředkovat vysoce specifický kontakt SPIONs s buňkami prostřednictvím vazby ke konkrétním receptorům buněčných membrán. Záměrem bylo využít interakce typu oligosacharid-lektin[h] s manózovými receptory buňky, jejichž přítomnost, prvotně přisuzovaná pouze buňkám imunitního systému (makrofágům a dendritickým buňkám) byla potvrzena i u endotelových buněk. Myší a lidské lektiny s vazebnou aktivitou pro manózu zahrnují transmembránové proteiny makrofágů, lymfatického a jaterního endotelu (MMR skupiny IV); Endol 180 fibroblastů, makrofágů a endotelových buněk; dendritickou neintegrinovou buněčně specifickou intercelulární adhezní molekulu-3 (DC-SIGN) dendritických buněk, alveolárních a peritoneálních makrofágů; jí příbuzný L-SIGN (skupiny II, receptory typu 2), nebo jejich myší homologa (SIGNR), Langerin Langerhansových buněk a povrchové proteiny A a D (skupiny III)[72-77]. Všechny tyto receptory jsou označovány souhrnně jako lektinové receptory

[h] Lektiny jsou cukry vázající proteiny, které jsou velmi specifické díky motivům podobným sacharidovým strukturám. Hrají důležitou biologickou roli v rozeznávání buněk a proteinů. Výskyt určitých typů lektinů podmiňuje například typ krevní skupiny jedince.

typu C (CLRs) se schopností vázat cukry prostřednictvím jedné, nebo více, sacharid rozeznávající domény (CRD) v procesu řízeném koncentrací vápníku[75-77]. Specifická vazba k manóze je zprostředkována sekvencí aminokyselin tvořící CRD. Navíc, jejich trojrozměrná konformace a multimerizující uspořádání umožňují i vazbu ke složitějším strukturám nesoucím manózové motivy. Lineární uspořádání tří CRDs v jednom polypeptidu manózového receptoru je vhodné pro rozeznání jednotlivých koncových manózových motivů. CRDs jsou tak schopny vazby i s povrchy s vysokou hustotou koncových manózových jednotek[78]. Transmembránový manózový receptor zprostředkovává endocytózu a funguje tak jako antigen-pohlcující receptor[79-82]. MMR-IV receptory takto rozeznávají patogeny jako *Pneumocystis carinii, Candida albicans, Leishmania donovani, Trypanosome cruzi* a příslušníky rodu *Mycobacterium.* DC-SIGN pak rozeznává virové patogeny jako HIV, virus hepatitidy typu C, cytomegalovirus, Dengue, nebo Ebola. Další podrobné informace o současném stavu terapeutického cílového směrování pomocí manózy lze nalézt v literatuře[83].

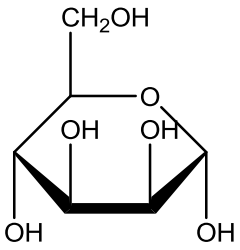

Obr. 5. Vzorec D-manózy; α-D-Manopyranóza

Lze předpokládat, že manóza se k povrchu maghemitu váže díky synperiplanárnímu uspořádání hydroxylových skupin v poloze 2 a 3 ve své molekule. Navíc je známo, že aromatické 1,2-di- a 1,2,3-trihydroxylové sloučeniny (např. dopamin a kyselina gallová) poskytují s železitými ionty barevné komplexy. Tento předpoklad se potvrdil, neboť po modifikaci nanočástic D-manózou a následném opakovaném promytí produktu demineralizovanou vodou a odstředění byl vypočten obsah manózy z výsledků elementární analýzy ve vysušeném vzorku 19 hm.%. Tento výsledek byl potvrzen opakovaně i po elučním testu 0,15 mol·dm^{-3} NaCl. Z takto vysokého obsahu manózy v konjugátu lze odvodit, že manóza pokrývá povrch maghemitových částic v podobě složitějšího útvaru, než je monomolekulární vrstva. Byl proto navržen model pokrytí, který zahrnuje tvorbu vodíkových vazeb mezi *ortho-*

dihydroxylovými skupinami D-manózy v polohách 2 a 3 s hydroxylovými skupinami v poloze 1 a 4 (obr. 6). Obr. 7 popisuje adsorpci D-manózy na povrch částic. Při nízkých poměrech D-manóza/γ-Fe_2O_3 se většina D-manózy sorbovala na povrch částic; s rostoucím poměrem podíl adsorbované manózy postupně klesal až do dosažení konstantní hodnoty. Z obr. 7 tak lze usuzovat, že množství adsorbované D-manózy na povrchu nanočástic je do dosažení hmotnostního poměru D-manóza/γ-Fe_2O_3 ~ 1 nezávislé na celkové koncentraci D-manózy v roztoku a je výsledkem chemisorpce. Přítomnost D-manózy na povrchu nanočástic maghemitu potvrzuje i ATR-FTIR analýza suchého promytého vzorku (obr. 8).

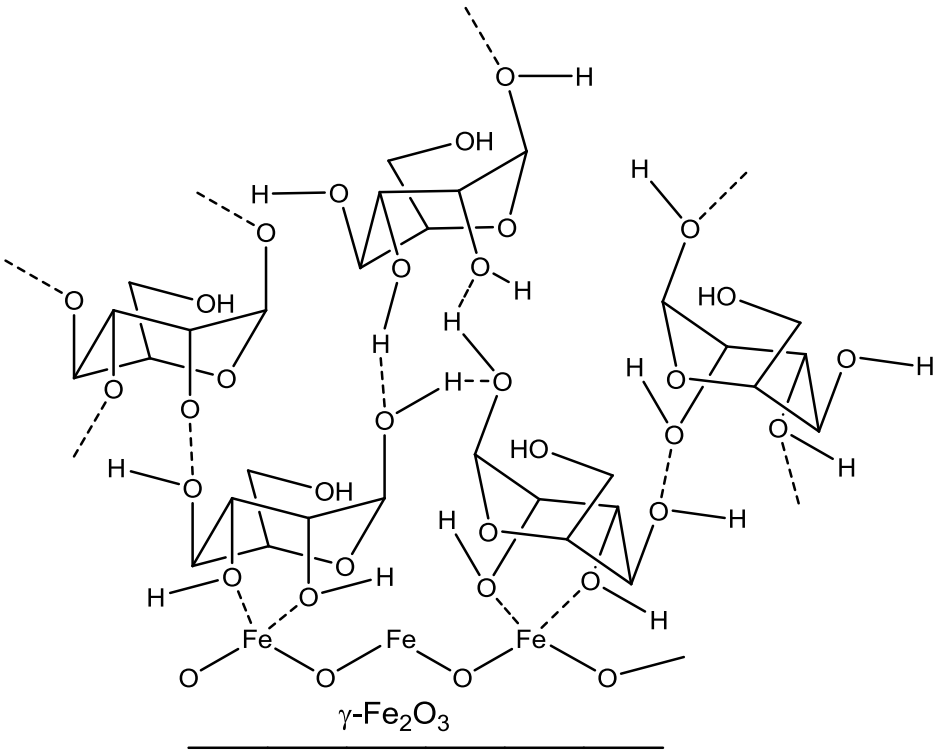

Obr. 6. Schématický návrh uspořádání molekul D-manózy na povrchu nanočástice γ-Fe_2O_3.

D-manózou modifikované částice vykazovaly odolnost vůči agregaci v kultivačním DMEM médiu obohaceném 10 hm.% FBS (fetal bovine serum). Se zvyšujícím se obsahem D-manózy vzhledem k maghemitu se množství adherovaných FBS bílkovin na povrch částic snižovalo (obr. 9). Byl nalezen optimální hmotnostní poměr D-manóza/γ-Fe_2O_3 = 2,6 z hlediska internalizace částic buňkami (tab. 1). Při vyšším poměru již docházelo vedle internalizace i k nežádoucí adhezi nanočástic na vnější stěnu buněčné membrány, což se zároveň projevilo zhoršením viabi-

lity MSC patrně z důvodu omezení transportních funkcí buněčné membrány. Při optimálním poměru byla pozorována (obr. 10) vyšší internalizace částic potkaními (57±6 %) a lidskými (84±5 %) mezenchymovými kmenovými buňkami[84] než u komerčního Endoremu™ (37±6 % pro potkaní a 62±5 % pro lidské buňky). Viabilita buněčné kultury[84] dosahovala 80-95 %.

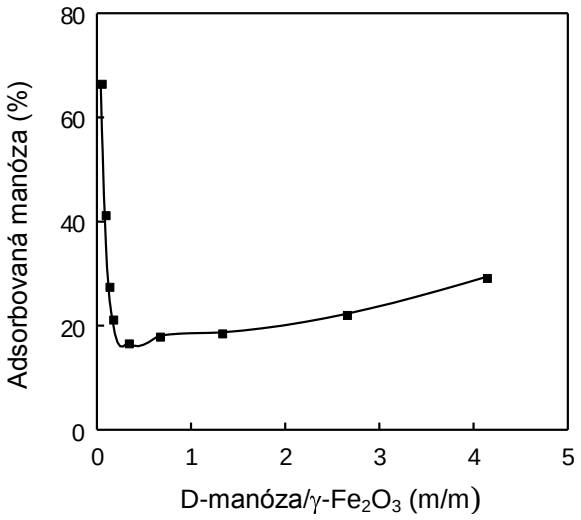

Obr. 7. Závislost množství adsorbované D-manózy na povrch nanočástic z roztoku na poměru D-manóza/γ-Fe_2O_3.

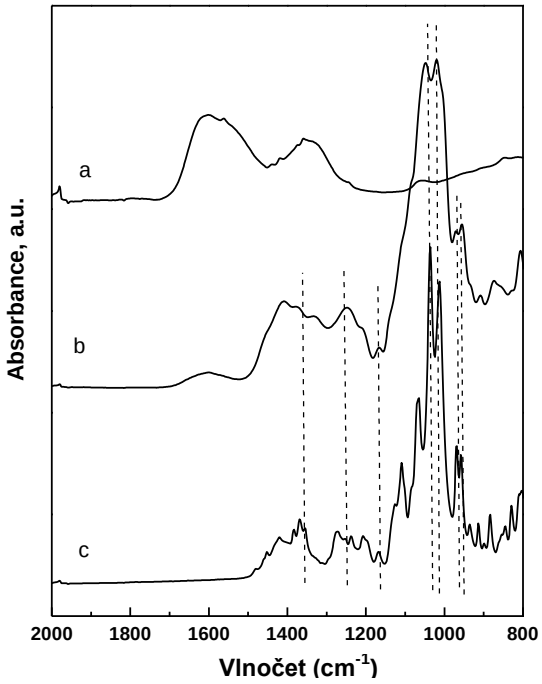

Obr. 8. ATR FTIR spektrum maghemitových nanočástic (a) před a (b) po modifikaci povrchu D-manózou (vzorek č. 4, tab. 1); (c) spektrum čisté D-manózy.

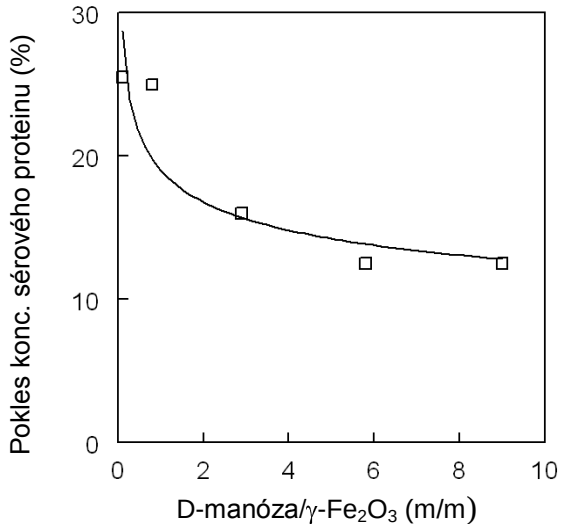

Obr. 9. Vliv poměru D-manóza/γ-Fe_2O_3 na pokles koncentrace sérového proteinu v kultivačním médiu, vztaženému k standardu (výchozí DMEM médium zředěno vodou v obj. poměru 1/1) po sorpci proteinu D-manózou modifikovanými nanočásticemi. Stanoveno UV spektrofotometrií při 274 nm.

Tab. 1. Značení buněk nemodifikovanými a D-manózou modifikovanými nanočásticemi a jejich charakteristiky.

Vzorek č.	D-manóza/γ-Fe_2O_3 (w/w)	D_n (nm)[a]	PDI[b]	Podíl označených buněk[c] (%)
Endorem™	-	5,6	1,45	58,6
2	0	6,05	1,46	27,9
3	1,3	5,9	1,39	49,1
4	2,6	6,6	1,33	80,6
5	4,1	6,4	1,26	51,3

[a] D_n – číselný průměr velikostí částic stanovený obrazovou analýzou TEM fotografií; [b] PDI – index polydisperzity; [c] půměr z 10 měření;

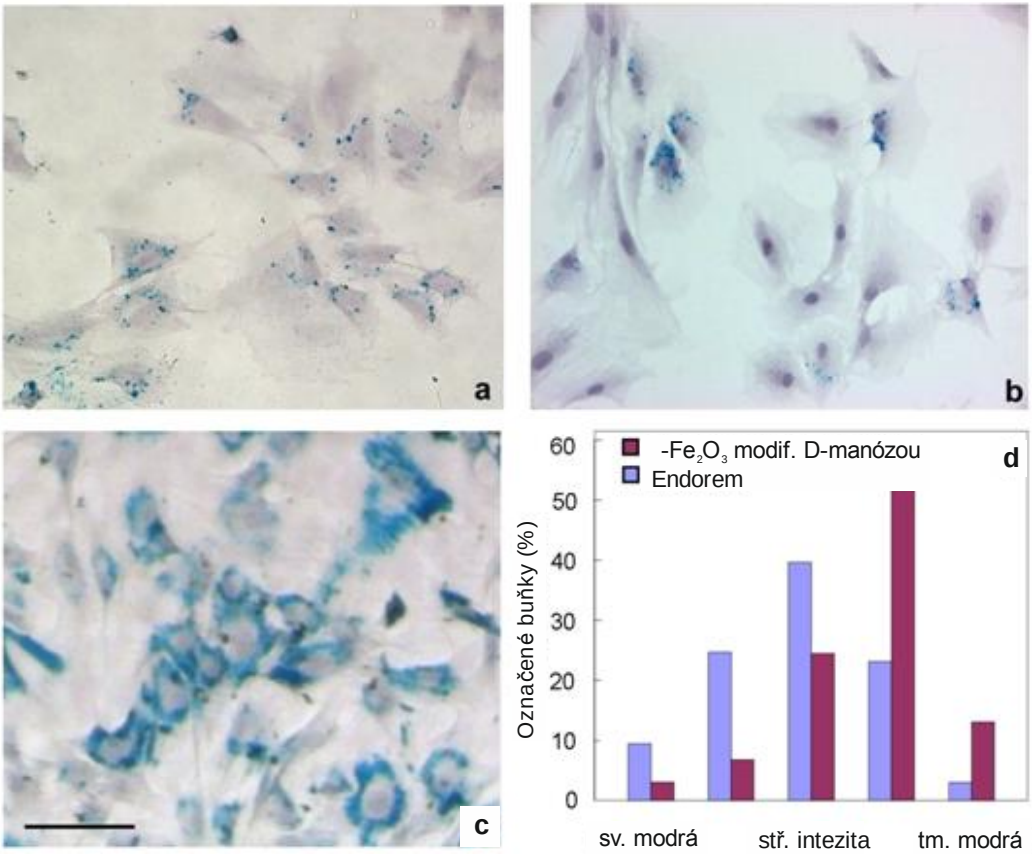

Obr. 10. Mikroskopické snímky mezenchymových kmenových buněk kostní dřeně potkana značených (a) Endoremem™ (kontrolní experiment), (b) primárními nemodifikovanými nanočásticemi maghemitu a (c) D-manózou modifikovanými maghemitovými nanočásticemi (vzorek č. 4, tab 1). Měřítko 50 μm. (f) Histogram znázorňující distribuci intenzity obarvení nanočástic Berlínskou modří v potkaních stromálních buňkách značených Endoremem™ nebo D-manózou modifikovanými maghemitovými nanočásticemi.

Podrobnosti lze nalézt v příloze č. 1 a 4 této práce[84, 85].

3B.2.1.2 Poly(L-lysin)

Poly(L-lysin) (PLL) má jako polykation schopnost indukovat endocytózu nespecificky prostřednictvím elektrostatických interakcí se záporně nabitým povrchem buněčných membrán (klidový potenciál savčích buněčných membrán dosahuje dle typu buňky -50 až -100 mV)[86]. PLL je také využíván v mikrobiologii jako činidlo zajišťující adhezi buněčných kultur ke stěnám kultivačních nádob. Dále je používán i jako transfekční činidlo v genovém inženýrství a genové terapii[87].

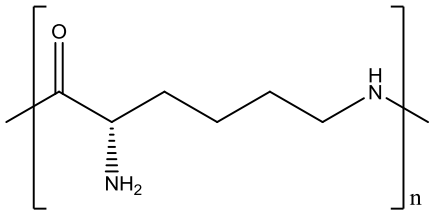

Obr. 11. Vzorec poly(L-lysinu).

K modifikaci povrchu záporně nabitých nanočástic γ-Fe_2O_3 jsme zamýšleli využít především elektrostatických interakcí s kladně nabitým PLL v kombinaci s minoritní komplexací koncových karboxylových skupin PLL s elektrondeficitními povrchovými atomy Fe. Sledováním závislosti zeta potenciálu na hmotnostním poměru PLL/γ-Fe_2O_3 jsme dle očekávání zjistili, že s rostoucím poměrem zeta potenciál roste (obr. 12). Při poměru vyšším než 0,009 zeta potenciál již nabýval takových hodnot ($\geq$ -42 mV), že nebyl schopen zajistit dostatečnou elektrostatickou repulsi částic a tyto agregovaly.

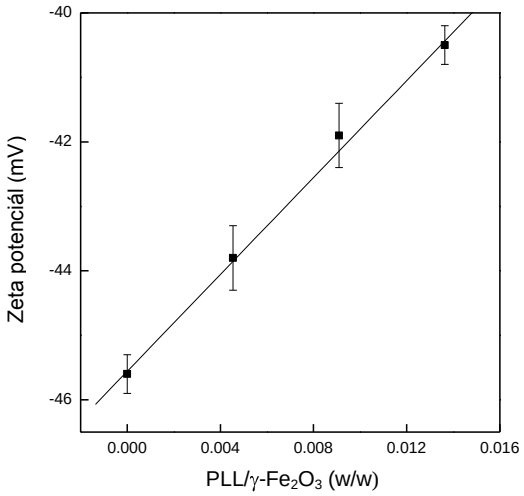

Obr. 12. Závislost zeta potenciálu na poměru PLL/γ-Fe_2O_3.

Pomocí DLS byl popsán vliv poměru PLL/γ-Fe_2O_3 na hydrodynamickou velikost modifikovaných nanočástic a jejich polydisperzitu v časovém rozsahu do 152 dnů od přípravy materiálu (obr. 13). Zjistili jsme, že od poměru PLL/γ-Fe_2O_3 = 0,02 w/w dochází s dalším zvýšením množství PLL (M_w = 93 800) k výraznému nárůstu jak hydrodynamického průměru, tak i polydisperzity, což nás vedlo k závěru, že nad poměrem > 0,02 w/w dochází k vzájemnému spojování nanočástic pomocí řetězců PLL (tzv. bridging). Efekt spojování částic řetězci PLL narůstá s časem, proto byla doba použitelnosti vzorků ke značení buněčných kultur stanovena na 90 dnů od přípravy materiálu.

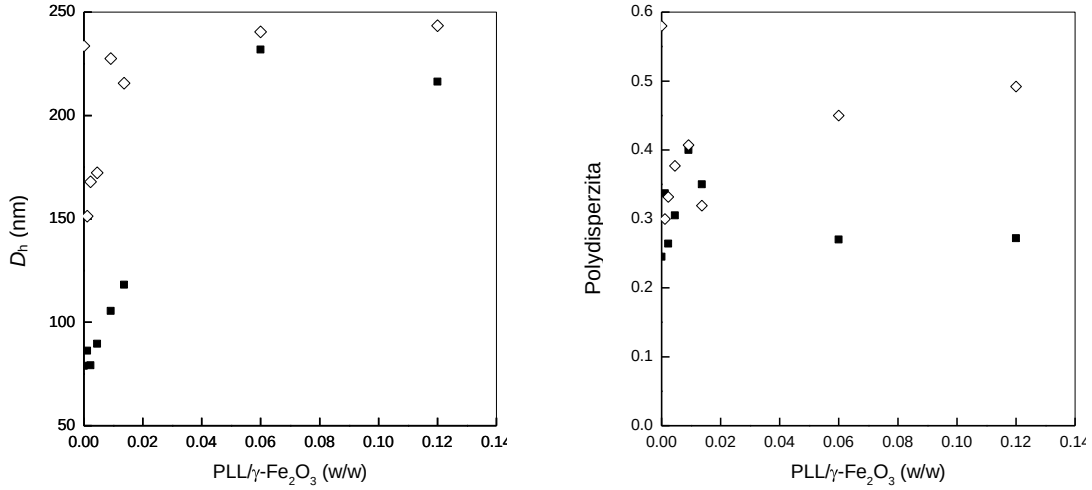

(a) (b)

Obr. 13. Závislost (a) hydrodynamického průměru částic D_h a (b) polydisperzity, měřených pomocí DLS, na poměru PLL/γ-Fe_2O_3 (■) 1 den a (◊) 152 dnů po přípravě.

Testem na buněčných kulturách (obr. 14) bylo zjištěno, že již při nízkých poměrech PLL/γ-Fe_2O_3, konkrétně 0,002 w/w, došlo k cca. zdvojnásobení procenta potkaních mezenchymových kmenových buněk označených nanočásticemi v porovnání s použitím nemodifikovaných částic. Jako optimální byl stanoven poměr PLL/ γ-Fe_2O_3 = 0,009 w/w, kdy bylo dosaženo 92 % proznačení buněčné kultury, v porovnání s 28 % pro nemodifikované částice. Komerční preparát za identických podmínek proznačil 60 % buněk v populaci (tab. 2).

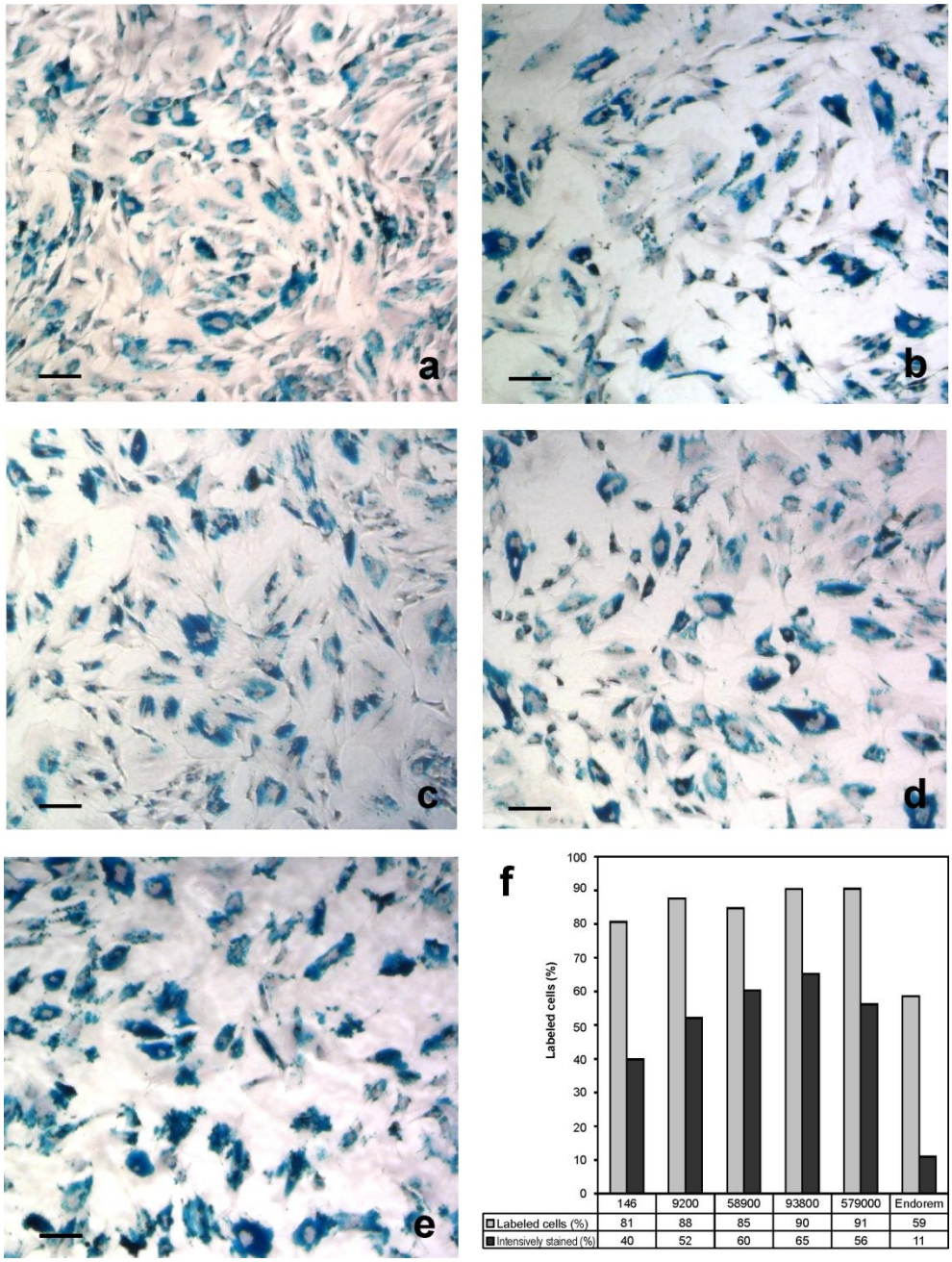

Obr. 14. Mikroskopické snímky rMSCs značených maghemitovými nanočásticemi modifikovanými PLL – vliv molekulové hmotnosti PLL. M_w = (a) 146, (b) 9 200, (c) 58 900, (d) 93 800 a (e) 579 000. Měřítko 50 μm. (f) Histogram ukazuje závislost intenzity vybarvení nanočástic modifikovaných PLL a standardu Endorem™ Berlínskou modří - molekulové hmotnosti PLL. Šedé sloupce reprezentují podíl označených buněk částicemi v kultuře a černé sloupce pak podíl intenzivně označených buněk v kultuře.

Tab. 2. *In vitro* značení mezenchymových buněk kostní dřeně (MSC) nanočásticemi maghemitu s povrchem upraveným PLL

Vzorek	Modifikace	Koncentrace		PLL/γ-Fe_2O_3 (w/w)	D_n[a] (nm)	PDI[b]	Označené buňky[c] (%)	
		PLL (mg/ml)	γ-Fe_2O_3 (mg/ml)				MSC (potkaní)	MSC (lidské)
1	0	-	2.2	0	6.05	1.46	27.9	-
2	PLL[d]	0.005	2.2	0.002	6.2	1.32	48.6	-
3	PLL[d]	0.01	2.2	0.005	6.2	1.37	65.5	-
4	**PLL[d]**	**0.02**	**2.2**	**0.009**	**5.5**	**1.30**	**92.2**	**87.5**
Endorem™	Dextran		11.2[e]	-	5.4	1.43	60.0	65.2

[a] D_n – číselný průměr velikostí částic stanovený obrazovou analýzou TEM fotografií; [b] PDI –index polydisperzity; [c] půměr z 10 měření; [d] M_w = 388 100; [e] mg Fe/ml.

Dále bylo k modifikaci povrchu nanočástic použito šest různých molekulových hmotností PLL, konkrétně 9 200; 58 900; 93 800; 388 100; 579 000 a 146 (samotný L-lysin). Při M_w = 579000 bylo pozorováno označení 90 % buněčné populace (tab. 3), avšak na vnějších stranách buněčných membrán byly přítomny i neodmývatelné shluky okludovaných částic. Jako optimální z hlediska procenta označených buněk v kultuře byl stanoven rozsah molekulových hmotností PLL 90 000–400 000. Při ověřování výsledků na kultuře lidských stromálních buněk bylo dosaženo prakticky stejných výsledků.

Tab. 3. Vliv molekulové hmotnosti PLL na procento označení potkaních MSCs modifikovanými maghemitovými nanočásticemi[a].

M_w	Endorem™[b]	146	9,200	58,900	93,800	388,100	579,000
Označené buňky[c] (%)	58.6	80.6	87.6	84.7	90.4	92.2	90.5

[a] vzorek č.3 z předchozí tabulky; [b] kontrolní vzorek; [c] průměr 15 měření.

S rostoucím poměrem PLL/γ-Fe_2O_3 se mírně zvyšovala adsorbce proteinů z živného DMEM média obohaceného 10 % FBS na povrch PLL modifikovaných částic (obr. 13). Lze tak předpokládat synergické působení PLL a adsorbovaných proteinů FBS na internalizaci částic buňkami. Množství adsorbovaných proteinů

FBS však nezáviselo na molekulové hmotnosti PLL použitého k pokrytí nanočástic (obr. 14).

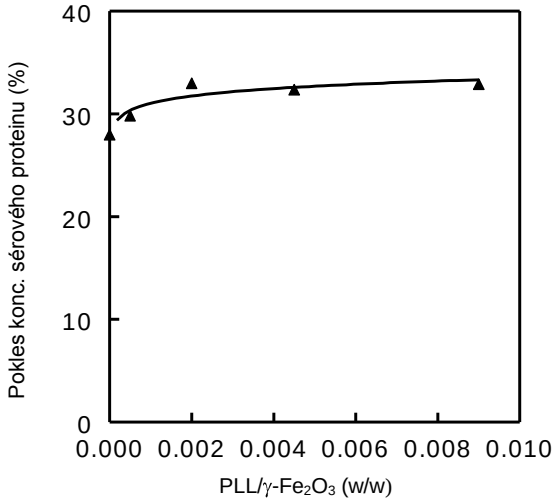

Obr. 15. Vliv hmotnostního poměru PLL/γ-Fe_2O_3 na koncentraci sérového proteinu v kultivačním médiu vztažené k výchozí koncentraci (DMEM/voda = 1/1 v/v) po adsorpci na PLL-modifikovaných maghemitových nanočásticích. Koncentrace sérového proteinu byla stanovena UV spektrofotometrií při 274 nm.

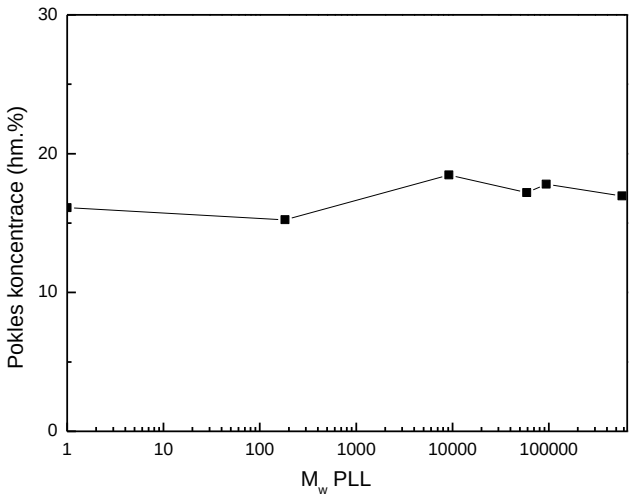

Obr. 16. Vliv molekulové hmotnosti PLL na koncentraci sérového proteinu v kultivačním médiu vztažené k výchozí koncentraci (DMEM/voda = 1/1 v/v) po adsorpci na PLL-modifikovaných maghemitových nanočásticích. Koncentrace sérového proteinu byla stanovena UV spektrofotometrií při 274 nm; PLL/γ-Fe_2O_3 = 0,009 w/w - vzorek č. 4, tab. 2.

Aminokyselinová analýza hydrolyzátu živného média po separaci přidaných PLL modifikovaných částic neprokázala nárůst koncentrace L-lysinu (tab. 4), z čehož lze usuzovat, že ve styku s živným médiem k desorpci PLL z povrchu nanočástic nedocházelo, což ostatně potvrzuje i korelace procenta označených buněk s PLL/γ-Fe_2O_3 poměrem (tab. 2).

Tab. 4. Koncentrace L-lysinu v hydrolyzovaném supernatantu po odstranění modifikovaných a nemodifikovaných nanočástic maghemitu z média[a]

Vzorek	modifikace	médium	LL[b] (mg/ml)
1	PLL	NaCl	0.015
2	-	DMEM/FBS	0.419
3	PLL	DMEM/FBS	0.281
4[c]	-	DMEM/FBS	0.613

[a] 0,64 ml koloidu (34,7 mg γ-Fe_2O_3/ml); [b] L-lysin po hydrolýze; [c] kontrola (médium bez přídavku nanočástic).

Přítomnost PLL na povrchu maghemitových částic byla prokázána ATR FTIR spektroskopií (obr. 16).

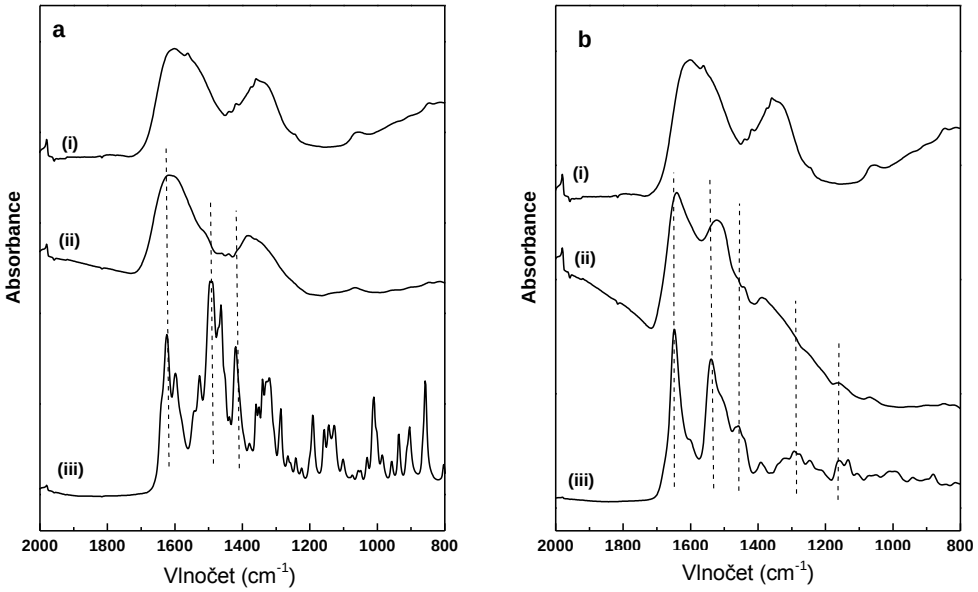

Obr. 17. ATR FTIR spektra γ-Fe_2O_3 nanočástic před a po modifikaci povrchu pomocí (a) LL a (b) PLL; (i) maghemit před modifikací, (ii) po modifikaci a (iii) spektrum čistého LL (a) a PLL (b).

Schopnost poskytovat kontrast při MR zobrazování PLL modifikovaných maghemitových nanočástic jako značícího činidla mezenchymových kmenových buněk byla úspěšně potvrzena při testech *in vitro* i *in vivo* na krysím modelu (obr. 18)

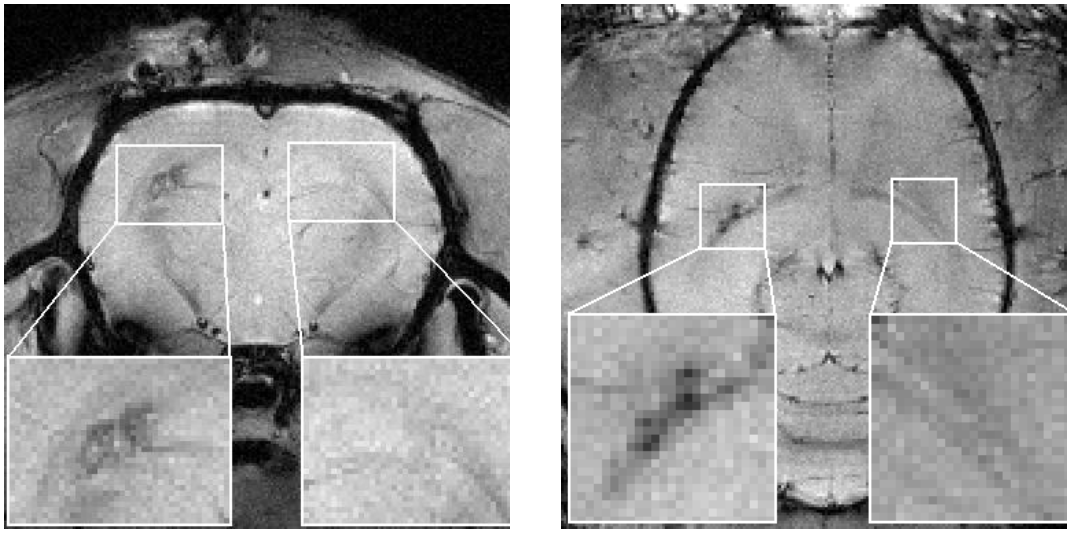

(a) (b)

Obr. 18. (a) Axiální a (b) radiální MR zobrazení mozku potkana s 1 000 buňkami označenými maghemitovými nanočásticemi modifikovanými PLL implantovanými do levé hemisféry a 1 000 buňkami značenými Endoremem^{TM} implantovanými do pravé hemisféry. MR obrazy byly pořízeny tři dny po implantaci. Zvětšená pole dobře ukazující zlepšení signálu v levé hemisféře oproti signálu v pravé hemisféře.

Více podrobností lze nalézt v přílohách č. 2 a 4 této práce[84, 88].

3B.2.1.3 Poly(*N*,*N*-dimethylakrylamid)

Poly(*N*,*N*-dimethylakrylamid) (PDMAAm) byl zvolen k povlékání γ-Fe_2O_3 jako neutrální hydrofilní polymerní materiál. PDMAAm velmi snadno polymerizuje ve vodných i organických prostředích do velmi vysokých konverzí, dobře kopolymerizuje s mnoha funkčními komonomery a též snadno vytváří pravidelné sítě, zejména se síťovadly akrylátového typu[89].

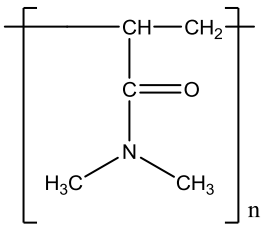

Obr. 19. Vzorec poly(*N*,*N*-dimethylakrylamidu)

Použití PDMAAm k úpravě povrchů γ-Fe_2O_3 tak nabízelo několik výhod: a) sterickou stabilizaci prostřednictvím řetězců vodorozpustného, netoxického a inertního

polymeru[90, 91], b) omezení interakcí povrchů γ-Fe_2O_3 se sérovými bílkovinami, které vedou k tvorbě velkých a relativně kompaktních shluků částic a sérových proteinů a c) relativně snadné zavedení funkčních skupin kopolymerizací s vhodnými komonomery, které umožňují následné kovalentní navázání vysoce specifických biomolekul, jako jsou protilátky, enzymy, peptidy, cukry, apod. Navázání biospecifických molekul k povrchu γ-Fe_2O_3 prostřednictvím funkcionalizovaného PDMAAm tak bylo prvotním záměrem tohoto přístupu.

Při počátečním experimentálním ověřování toxicity PDMAAm modifikovaných SPIONs na buněčnou kulturu mezenchymových kmenových buněk však byl pozorován výrazný efekt zvýšení internalizace nanočástic buňkami. V porovnání s nepovlečeným γ-Fe_2O_3 a Endorememᵀᴹ, částice s povrchem upraveným PDMAAm označily výrazně více potkaních i lidských stromálních buněk v kultuře (tab. 5). Buňky označené částicemi s povrchem upraveným PDMAAm vykazovaly rovněž vyšší viabilitu v porovnání s částicemi nepovlečeného γ-Fe_2O_3 a Endorememᵀᴹ.

Tab. 5. Efektivita značení mezenchymových kmenových buněk nemodifikovanými maghemitovými nanočásticemi, částicemi s povrchem upraveným PDMAAm a kontrolním Endorememᴿ.

	Procento označených buněk	
	rMSC	hMSC
Endoremᴿ	39 ± 6	68 ± 5
Nemodifikovaný γ-Fe_2O_3	46 ± 5	70 ± 5
PDMAAm-modifikovaný γ-Fe_2O_3	59 ± 5	82 ± 5

K povrchové modifikaci částic byla použita roztoková polymerizace DMAAm ve vodném koloidu γ-Fe_2O_3 iniciovaná 4,4´-azobis(4-kyanovalerovou kyselinou) (ACVA). Byla zjištěna přímá úměra mezi množstvím ACVA v násadě a množstvím PDMAAm na povrchu promytých částic. Při množství ACVA ≥ 15 mg na 500 mg γ-Fe_2O_3 částic v násadě byla po polymerizaci pozorována nežádoucí agregace částic.

Tab. 6. Povrchová úprava maghemitových nanočástic roztokovou polymerizací DMA-Am.

Vzorek č.	Polymerizační násada			Stabilita koloidu	D_h[c] (nm)	Vázaný PDMAAm[d] (hm.%)
	γ-Fe_2O_3 (g)	DMAAm (g)	ACVA (mg)			
1[a]	0,5	0	0	-	127 ± 3	0
2[b]	0,5	0,5	0	-	161 ± 3	0,21
3	0,5	0,375	3,8	agr.	n.a.	
4	0,5	0,5	5	++	81,4 ± 0,6	0,7
5	0,5	1	10	++	56,9 ± 0,3	1,2
6	0,5	1,5	15	+	171 ± 5	1,95
7	**0,5**	**1**	**5**	**++**	**77,8 ± 0,3**	**1,52**
8	0,5	1	15	+	172 ± 22	1,7
9	0,5	1	20	agr.	n.a.	2,74
10	0,5	1	30	agr.	n.a.	4,95
11	0,5	0,375	10	++	55 ± 5	1,03
12	0,5	0,5	10	++	67±3	1,1
13	**0,5**	**1,5**	**10**	**agr.**	**328 ± 4**	**1,06**
14	0,5	2	10	agr.	614 ± 12	1,6
15	1	1	10	++	76,6±0,5	2,1
16	1,5	1	10	++	83,5 ± 0,2	0,88
17	2	1	10	++	75,1 ± 0,1	0,96
18	**2,5**	**1**	**10**	**++**	**76 ± 0,5**	**0,74**

[a] Primární nemodifikovaný γ-Fe_2O_3 (kontrola);[b] roztok PDMAAm byl přidán k nemodifikovaným γ-Fe_2O_3 částicím; [c] D_h, hydrodynamický průměr částic stanovený pomocí DLS; [d] výpočet z analýzy prvků.
- slabá stabilita (agregace pozorována do týdne); + vysoká stabilita (do 3 měsíců od přípravy se nevyskytl sediment); ++ velmi vysoká stabilita (sediment se nevyskytl do 6 měsíců od přípravy).

Vliv ACVA na fyzikálně-chemické vlastnosti koloidu maghemitu byl detailně vyšetřen měřením pH, D_h a zeta-potenciálu v závislosti na měnícím se hmotnostním

poměru ACVA/γ-Fe_2O_3. Obr. 20 ukazuje, že při hmotnostním poměru ACVA/γ-Fe_2O_3 vyšším než 0,02 dochází ke skokovému nárůstu hydrodynamické velikosti částic a částečnému výskytu agregátů, který se s rostoucím poměrem dále prohlubuje. Vysvětlení lze nalézt v růstu zeta-potenciálu nad hodnotu -30 mV při překročení poměru 0,02. Nárůst zeta-potenciálu je indukován snižováním pH s rostoucím množstvím ACVA v koloidu, (obr. 20). Možnou cestou, jak zvýšit množství PDMAAm vázaného k povrchu nanočástic γ-Fe_2O_3 a zároveň potlačit vznik agregátů by tak mohlo být použití ACVA ve formě draselné či sodné soli, tato možnost však dále z časových důvodů rozvíjena nebyla.

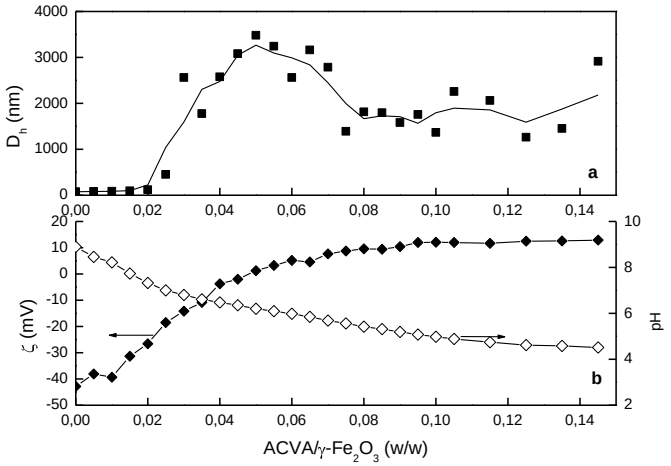

Obr. 20. Závislost (■) hydrodynamického průměru D_h (a), (♦) ζ-potenciálu a (◊) pH (b) na hmotnostním poměru ACVA/γ-Fe_2O_3.

Přítomnost PDMAAm na povrchu γ-Fe_2O_3 částic po polymerizaci a jejich důkladném promytí byla potvrzena ATR FTIR spektroskopií (obr. 20)a prvkovou analýzou (tab. 6). Molekulové hmotnosti PDMAAm na povrchu nanočástic, které byly stanoveny pomocí HPLC-DLS po rozpuštení γ-Fe_2O_3 v kyselině a odsolení ve vodném roztoku, činily M_w ~ 1000 000 (obr. 21).

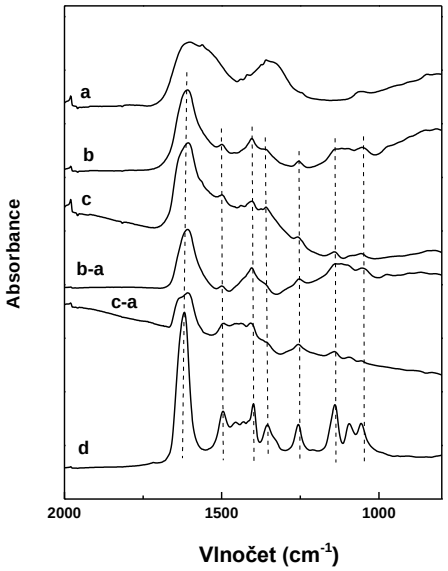

Obr. 20. ATR FTIR spektra nanočástic γ-Fe_2O_3 před a po úpravě povrchu pomocí PDMAAm. (a) Před úpravou, (b) úprava roztokovou polymerizací v přítomnosti nanočástic γ-Fe_2O_3 (č. 3, tab. 6), (c) úprava enkapsulací nanočástic γ-Fe_2O_3 předem připraveným PDMAAm – (č. 2, tab. 6), (b-a) a (c-a) rozdílová spektra příslušných modifikovaných nanočástic a výchozího γ-Fe_2O_3, a (d) čistý PDMAAm.

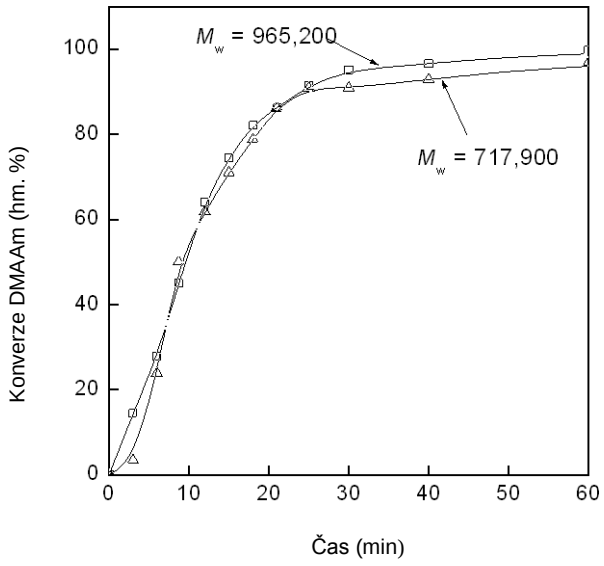

Obr 21. Konverzní křivky roztokové polymerizace DMAAm v (Δ) přítomnosti a (□) nepřítomnosti nanočástic γ-Fe_2O_3 v polymerizační násadě.

Koloidní stabilita nanočástic γ-Fe_2O_3 s povrchem upraveným polymerizací DMAAm byla sledována měřením D_h a PDI pomocí DLS v rozsahu 120 dní od přípravy (obr. 22). Z obrázku je dobře patrné zvýšení dlouhodobé stability koloidu polymerizací DMAAm při použití poměru ACVA/γ-Fe_2O_3 > 0,02 w/w v porovnání s nemodifikovanými maghemitovými částicemi.

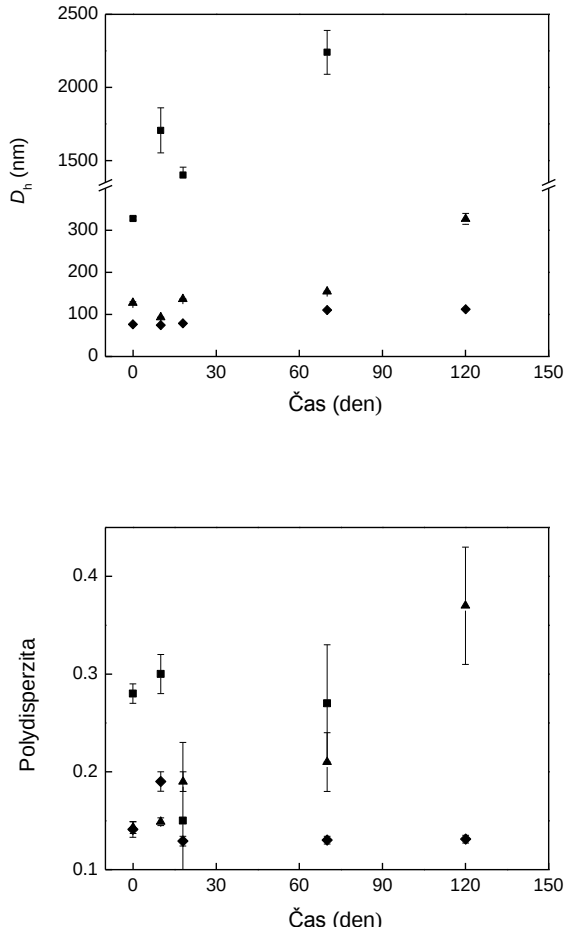

Obr. 22. Závislost (a) hydrodynamického průměru částic D_h a (b) polydisperzity v čase od přípravy, měřeno pomocí DLS; (▲) nemodifikovaný γ-Fe_2O_3 č. 1, PDMAAm-modifikovaný γ-Fe_2O_3 (♦) č. 18 (ACVA/γ-Fe_2O_3 = 0,004 w/w) a (■) č. 13 (ACVA/γ-Fe_2O_3 = 0,02 w/w) (tab. 6).

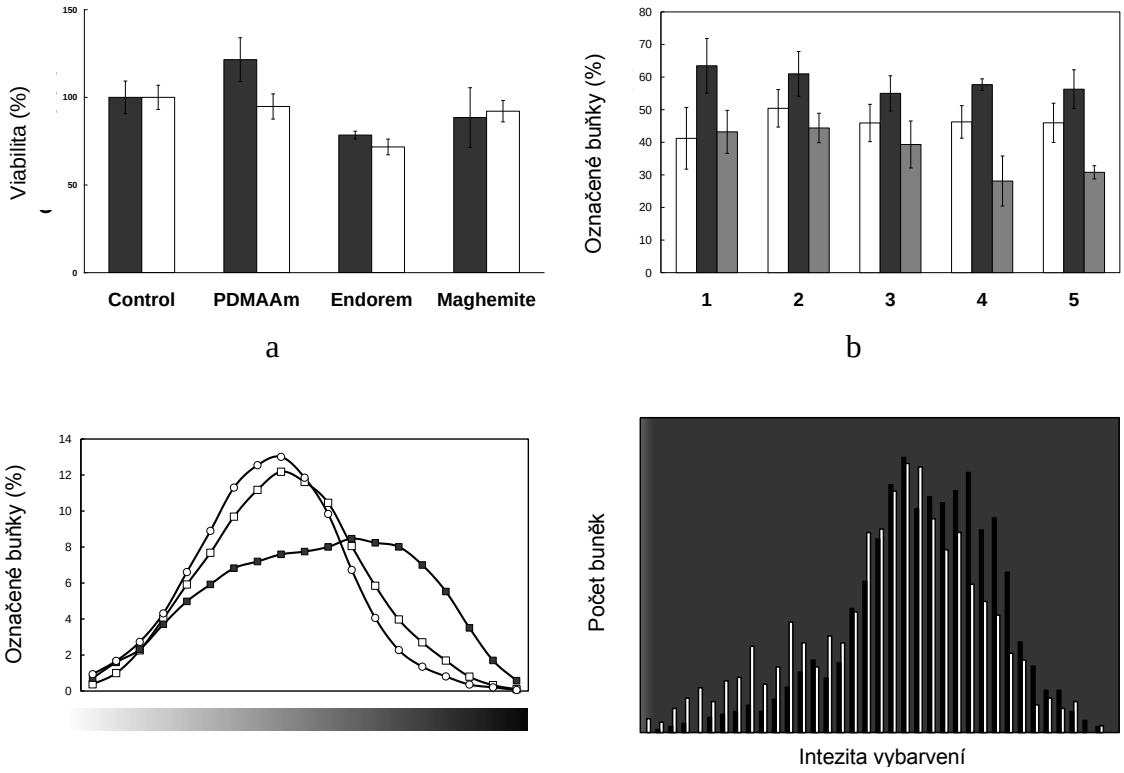

Obr. 23. (a) Viabilita potkaních (■) a lidských MSCs (□) značených nanočásticemi oxidů železa. Jako PDMAAm-modifikované částice byl použit vzorek (tab. 6, č. 7). (b) Účinnost značení kultury vyjádřená jako procento potkaních MSCs (pro 1.-5. pasáž; sloupce 1-5) značených nemodifikovanými γ-Fe_2O_3 (□) a PDMAAm-modifikovanými γ-Fe_2O_3 nanočásticemi (tab. 6, č. 7) (■) a Endorememᵀᴹ (■). (c) Distribuce intenzity vybarvení Berlínskou modří rMSCs buněk s pohlcenými nemodifikovanými γ-Fe_2O_3 (□), PDMAAm-modifikovanými γ-Fe_2O_3 nanočásticemi (■) a Endorememᵀᴹ (o) (osa x). (d) Histogramy intenzity vybarvení potkaních a lidských mezenchymových kmenových buněk; je zřetelná výrazně vyšší intenzita značení lidských mezenchymových buněk (■) v porovnání s potkaními (□).

Obr. 24. T_2-vážené MR zobrazení mozku potkana s 5 000 rMSCs značenými PD-MAAm-modifikovanými maghemitovými nanočásticemi (tab. 6, č. 7) implantovanými do levé hemisféry a značenými Endoremem^{TM} a implantovanými do pravé hemisféry. Bílé šipky ukazují místo implantace buněk do potkaní hlavy, černé šipky ukazují místo výskytu nanočástic maghemitu. Obrázek tak znázorňuje nejen lepší kontrast v porovnání s komerčním preparátem, ale i postimplantační migraci kmenových buněk mozkovou tkání.

Podrobnosti lze nalézt v přílohách 3 a 4 této práce[84, 92].

3C. MAGNETICKÉ POLYMERNÍ MIKROČÁSTICE

Jak již bylo naznačeno výše, magnetické polymerní mikročástice jsou kompozitní materiály, kde polymer tvoří zpravidla hlavní objemový podíl - matrici, v níž jsou uloženy superparamagnetické nanočástice (magnetické plnivo); polymer tak dominantně určuje morfologii mikročástic. Velikosti mikročástic se nacházejí nejčastěji v intervalu 0,3–100 μm. Z aplikačního hlediska se magnetické polymerní mikročástice uplatňují nejčastěji jako separační a transportní média; velkou pozornost v posledních letech pak přitahují diagnostické nástroje v podobě mikročásticových imunoesejí.

Užitná hodnota magnetických polymerních mikročástic pro danou aplikaci závisí na mnoha vlastnostech, zejména hodnotě nasycené magnetizace, morfologii, tvaru, velikosti a její distribuci. Mezi mnoha možnými tvary (tyčinky, trubky, prstence, disky, nepravidelné útvary, atd.) zaujímá výjimečné postavení tvar koule a to díky jejím hydrodynamickým vlastnostem. V porovnáním s ostatními tvary, soubory pravidelných koulí trpí nejmenším vzájemným mechanickým oděrem a vykazují nejmenší sklony k fragmentaci působením mechanických a hydrodynamických sil v průběhu manipulace. Spolu s pravidelným kulovitým tvarem pak hraje důležitou roli i distribuce velikostí částic, protože monodisperzní částice (nebo alespoň s úzkou distribucí velikostí; index polydisperzity PDI[i]= 1,0-1,3) vykazují jednotné fyzikální a fyzikálně-chemické vlastnosti a jejich soubory v kapalinách jsou odolnější vůči shlukování, než soubory částic polydisperzních. Pro biologické aplikace v kapalných prostředích jsou pak nejvhodnější částice o velikostech v intervalu 0,5-5 μm. Větší částice totiž nabízejí menší specifický povrch dostupný pro navazování funkčních skupin, nebo pro imobilizace biologicky aktivních látek. U menších částic pak hrozí zhoršení jejich „manipulovatelnosti“ vnějším magnetickým polem, protože takové částice mohou vykazovat nízkou magnetickou susceptibilitu a při pokusu o záchyt pomocí vnějšího magnetického pole může dojít k převaze hydrodynamických sil nad silami magnetickými.

Komerčně dostupné mikročástice pro magnetické separace mají matrice vyrobené ze syntetických nebo přírodních polymerů. Polystyrenové (PS) a poly(methyl-

[i] PDI = D_w/D_n; $D_w = \Sigma n_i D_i^4/\Sigma n_i D_i^3$; $D_n = \Sigma n_i D_i/\Sigma n_i$

methakrylátové) (PMMA) matrice pak patří k těm nejčastějším. Jejich výhodou je relativně levná, snadná a průmyslově dobře zvládnutá výroba heterogenními, převážně *o*/*w*, polymerizačními technikami. V bioaplikacích však poměrně velkou nevýhodu představuje relativně vysoká hydrofobicita polystyrenových povrchů, která způsobuje nežádoucí nespecifické adsorpce proteinů k separačnímu médiu. Tato nespecifická adsorpce prostřednictvím hydrofobních interakcí snižuje u imunoesejí účinnost imunospecifické reakce s antigenem díky převrstvení navázané protilátky adherujícími proteiny. Současně zhoršuje také selektivitu, protože vedle specificky vázaných antigenů k protilátce mohou jiné antigeny adherovat nespecificky. Zmíněné vlivy vedly ke snaze zvýšit hydrofilitu povrchů částic, a to buď prostřednictvím modifikací hydrofobních povrchů hydrofilními látkami, jako je kyselina polyakrylová, poly(oxyethylen), dextran, apod., nebo použitím hydrofilních polymerů přímo k výrobě matrice částic. K přípravě hydrofilní matrice magnetických mikročástic jsou nejčastěji používány přírodní polymery dextran a celulóza, ze syntetických se nejdříve do popředí zájmu dostal poly(2-hydroxyethylmethakrylát) (PHEMA) jakožto biokompatibilní, netoxický, mechanicky odolný materiál s nízkou nespecifickou adsorpcí proteinů[93].

3C.1 Příprava magnetických polymerních mikročástic

Příprava magnetických polymerních mikročástic zahrnuje různé postupy "zabalení" magnetických plniv do polymerní hmoty; vznikají tak různé morfologie kompozitních částic. Podle distribuce magnetických částic v polymerní matrici lze kompozitní částice zařadit do jedné ze tří základních morfologických skupin kompozitních částic (obr. 25): a) typ slupka–magnetické jádro („core-shell"), b) částice s homogenní (náhodnou) distribucí plniva v mikročásticové matrici („homogeneous multicore") a c) částice s povrchovou (podpovrchovou) vrstvou magnetického plniva na polymerním těle („strawberry" morfologie).

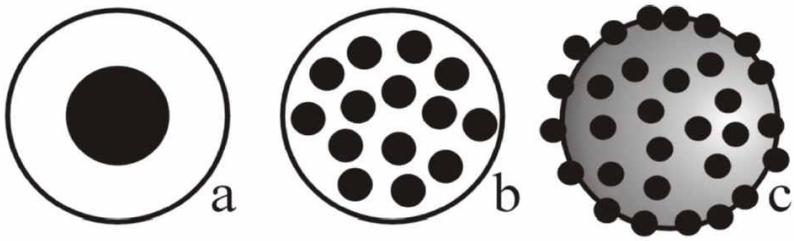

Obr. 25. Morfologie polymerních mikročástic s magnetickými plnivy: a) typ slupka – magnetické jádro, b) homogenní (náhodná) distribuce plniva v mikročásticové matrici a c) povrchová (podpovrchová) vrstva magnetického plniva na polymerním těle.

Nanokompozitní mikročástice lze připravit třemi základními přístupy, jimiž jsou:

- Enkapsulace odděleně připravených magnetických plniv hotovými polymery. Sem patří separace fází, metoda odpařování rozpouštědla, proces „vrstva za vrstvou“, „sol-gel“ metody.
- *In situ* příprava magnetických částic uvnitř pórů předem připravených porézních polymerních mikročástic[94].
- Heterogenní polymerizační techniky vedené v přítomnosti magnetických částic v reakčním prostředí. Do této skupiny patří suspenzní, disperzní, emulzní, miniemulzní a mikroemulzní polymerizace.

Enkapsulace odděleně připravených magnetických plniv hotovými polymery a *in situ* příprava magnetických částic uvnitř pórů částic nebyly předmětem této práce, proto nejsou v dalším textu rozvedeny. Jejich podrobnější přehled však lze nalézt v příloze č. 5 této práce[95].

3C.1.1 Heterogenní polymerizační techniky vedené v přítomnosti magnetických částic

Magnetické polymerní mikročástice jsou připravovány polymerizací různých typů monomerů v přítomnosti disperzí magnetických nanočástic. V heterogenních polymerizačních systémech hraje důležitou roli typ, rozměr a polydisperzita nanočástic, dále pak jejich dispergovatelnost a agregační stabilita v polymerizačním médiu. Přestože jsou heterogenní polymerizační techniky v literatuře poměrně ostře rozděleny na suspenzní, disperzní, emulzní, miniemulzní a mikroemulzní polymerizace, v praxi někdy nelze daný funkční heterogenní systém přesně zařadit do konkrétní kategorie. Dalším kompli-

kujícím faktorem, jak z hlediska klasifikace, tak samotného provádění polymerizace, je přítomnost nanočástic v polymerizační násadě. Tyto nanočástice často ovlivňují kinetiku polymerizace, srážení vznikající polymerní fáze a celkovou stabilitu systému. Z těchto důvodů by mělo mít magnetické plnivo vyšší afinitu k monomerům, a z nich vznikajícím polymerům, v porovnání s afinitou k jiným složkám polymerizačního systému, zejména ke stabilizátorům a emulgátorům. Vyšší afinita ke stabilizátorům a emulgátorům, v porovnání s afinitou k monomerům a jejich polymerům, výrazně ovlivňuje morfologii připravovaných kompozitních mikročástic. Dochází k transportu nanoplniva z monomerní fáze na fázové rozhraní formující se mikročástice (obr. 26-28, *pořízeno na vzorcích připravených Ing Hanou Mackovou, PhD.*), nebo dokonce k úplnému přechodu (vypírání) plniva z monomerní do kontinuální (často vodné) fáze.

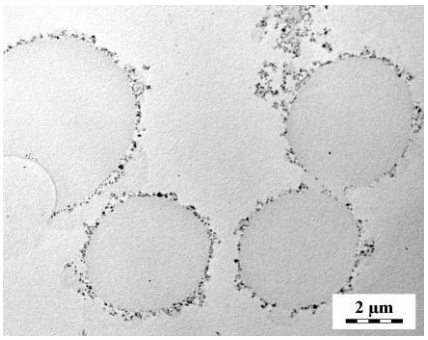

Obr. 26. Transmisní elektronová mikrofotografie řezu mikročásticemi připravenými inverzní emulzní polymerizací *N*-isopropylakrylamidu v přítomnosti magnetických nanočástic; emulgátorem byl sorbitolmonooleát (Span 80).

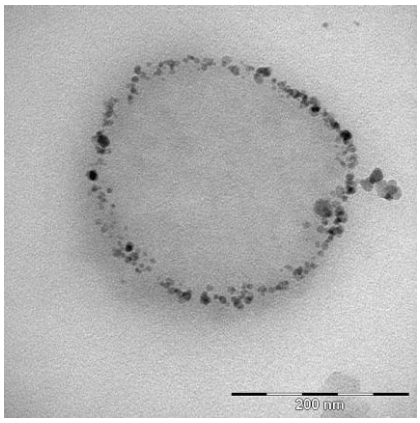

Obr. 27. Transmisní elektronová mikrofotografie řezu mikročásticí připravenou srážecí polymerizací *N*-propargylakrylamidu v toluenu v přítomnosti magnetických nanočástic modifikovaných kyselinou olejovou.

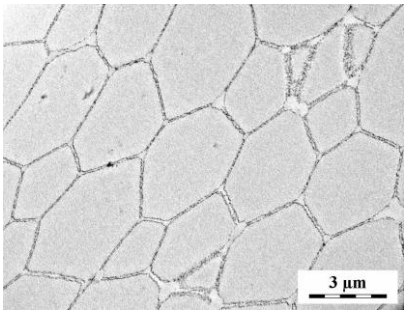

Obr. 28. Transmisní elektronová mikrofotografie řezu poly(2-hydroxyethyl-methakrylát-*co*-glycidyl-methakrylátovými) mikročásticemi připravenými disperzní polymerizací ve směsi toluen/2-methylpropan-1-ol stabilizované acetátem butyrátem celulózy (CAB 381-20) v přítomnosti magnetických nanočástic modifikovaných kyselinou olejovou.

3C.1.1.1 Suspenzní polymerizace

Suspenzní polymerizace je nejstarší heterogenní polymerizační technika. Poskytuje kulové částice o široké distribuci velikostí (vysoké polydisperzitě) v rozsahu velikostí od mikrometrů po milimetry. Monomer(y), magnetické plnivo a iniciátor tvoří monomerní fázi ve formě kapek dispergovaných v kontinuální (typicky vodné) fázi, ve které je rozpuštěn stabilizátor. Stabilizátory jsou nejčastěji přírodní, modifikované přírodní, nebo čistě syntetické lineární či blokové a roubované polymery.

Názorná je příprava hydrofobních polymerních částic. Dispergovanou (monomerní) fázi tvoří směs styrenu, divinylbenzenu (síťovadlo), glycidyl-methakrylátu a 2,2´-

azobis(isobutyronitrilu) (AIBN; iniciátor), dále může být přítomen porogen (např. směs toluen/heptan) a magnetické plnivo. Tato fáze je dispergována do vodného kontinuálního prostředí a celá násada je míchána po celou dobu polymerizace. V závislosti na reakčních podmínkách lze obdržet mikročástice o velikosti 65-300 μm s obsahem magnetické složky 2-7 hm.%. Takto připravené částice jsou například používány po reakci s ethylendiaminem a reaktivní modří 2 (Cibachrom Blue F3GA) jako ligand pro afinitní adsorpci proteinů[96].

Protože hydrofilní polymerní mikročástice většinou nelze připravit ve vodných kontinuálních fázích, byla vyvinuta inverzí suspenzní polymerizace. Jako příklad lze uvést přípravu magnetických poly(4-vinylpyridin-*co*-ethylen-dimethakrylátových) částic s molekulárním otiskem 2,4-dichlorofenoxyoctové kyseliny, popř. částic s povrchem modifikovaným [3-(methakryloxy)propyl]trimethoxysilanem v silikonovém oleji jako kontinuální fázi. Vysoká viskozita kontinuální fáze pomáhala potlačit koalescenci dispergovaných monomerních kapek. Vzhledem ke svému nepolárnímu charakteru se silikonový olej nemísil s monomery. Jako iniciátor byl v dispergované fázi použit redoxní systém benzoylperoxid/dimethylanilin, reakce byla vedena při 10 °C a výsledné částice[97] měly 20 μm velikost s obsahem magnetické složky 1,1 hm.%.

3C.1.1.2 Emulzní polymerizace

Emulzní polymerizace je proces, v průběhu kterého se kapalný monomer emulgovaný ve vodné kontinuální fázi mění na stabilní systém pevných polymerních mikročástic, tzv. latex. Rozměry vzniklých částic jsou zpravidla v rozmezí stovek nanometrů až jednoho mikrometru. Mikročástice (na začátku kapénky monomeru) jsou stabilizovány emulgátorem či ochranným koloidem (syntetický nebo přírodní polymer, popř. anorganický koloid při tzv. Pickeringově stabilizaci[98, 99]) adsorbovaným na jejich povrchu; iniciátor je vždy rozpuštěný v kontinuální fázi. Při tzv. očkovacích emulzních polymerizacích je nutnou podmínkou, aby koncentrace emulgátoru byla pod kritickou micelární koncentrací. Tato nízká koncentrace brání vzniku nových micel emulgátoru a tím i malých částic bez magnetického plniva. Bylo navrženo několik modelů pro popis mechanizmu emulzní polymerizace. Nejčastěji jsou přijímány micelární mechanizmus a mechanizmus homogenní nukleace[100].

Pro přípravu magnetických částic emulzní polymerizací existují dva koncepty. První zahrnuje dispergaci magnetického plniva v monomerní fázi s možným přídavkem organického rozpouštědla. Druhý je naopak založen na dispergaci plniva ve fázi kontinuální (typicky vodné) stabilizované přídavkem hydrofilních polymerů. Zatímco první koncept nachází uplatnění pro polymerizaci hydrofobních monomerů, druhý je typický spíše pro hydrofilní monomery.

Typickým příkladem polymerizace hydrofobního monomeru je očkovací emulzní kopolymerizace styrenu a divinylbenzenu iniciovaná AIBN nebo persíranem draselným. Nanočástice maghemitu (7 nm) stabilizované kyselinou olejovou v oktanu byly emulgovány do vodné fáze obsahující neionogenní povrchově aktivní činidlo Triton X-405 (poly(oxyethylen)isooktylcyklohexyl ether). Disperze byla smíchána se směsí styrenu a divinylbenzenu, byl přidán AIBN a směs byla míchána za laboratorní teploty, aby se monomerní kapky s iniciátorem adsorbovaly na kapénky emulgovaného ferrofluidu. Polymerizace byla zahájena zahřátím reakční směsi. Byla-li polymerizace iniciována persíranem draselným, byl jeho vodný roztok přidán do směsi až po zbotnání maghemitové emulze monomery. Zatímco ve vodě nerozpustný iniciátor AIBN poskytoval latexové částice hemisférického tvaru, polymerizace iniciovaná persíranem draselným produkovala homogenní kulovité částice[101].

Méně obvyklý přístup zahrnuje dispergaci magnetických plniv do vodné kontinuální fáze. Přitom se využívá homogenního nukleačního mechanizmu založeného na omezené rozpustnosti monomeru v kontinuální fázi. Iniciace je zahájena v kontinuální fázi, následuje růst oligomerních řetězců, které se po dosažení kritické délky vysrážejí do nukleí; polymerizace pak pokračuje a výsledkem jsou latexové částice. Příkladem tohoto typu je polymerizace glycidyl-methakrylátu (GMA) dispergovaného ve vodné fázi obsahující magnetit stabilizovaný dextranem, nebo karboxymethyldextranem či [2-(diethylamino)ethyl]dextranem[102]. Jako emulgátor byl použit Disponil AES 60 (poly(oxyethylen)alkylaryl ethersulfát sodný) a jako iniciátor 4,4´-azobis(4-kyanopentanová kyselina) nebo persíran draselný. V závislosti na podmínkách byly připraveny částice o velikostech v rozmezí 70-400 nm.

3C.1.1.3 Mikroemulzní polymerizace

Mikroemulze je popisována jako stabilní isotropní a opticky transparentní disperze dvou nemísitelných kapalin připravená za použití stabilizačního systému, kterým může být povrchově aktivní látka, směs takových sloučenin, nebo směs povrchově aktivní látky a kosurfaktantu[103]. Aby bylo možné připravit termodynamicky stabilní mikroemulzi, je třeba použít velké množství povrchově aktivní látky (cca. 10-15 hm.%); současně podíl dispergované fáze nesmí překročit 10-15 hm.% z celé polymerizační násady. Mikroemulzní polymerizace produkuje velmi malé částice, typicky v rozmezí 12-30 nm; specifický povrch částic je tudíž velký (~ 450 m^2/g). Příkladem je příprava magnetických hydrofilních částic inverzní mikroemulzní kopolymerizací akrylamidu a *N,N´*-methylenbisakrylamidu iniciovaná AIBN, který spolu s vodnou disperzí magnetitu stabilizovaného citrátem sodným tvořil vodnou fázi. Tato fáze pak byla dispergována v toluenu za použití emulgátoru Aerosol OT (bis(2-ethylhexyl)sulfojantaran sodný). Výsledná velikost částic byla regulována v rozmezí 80-180 nm koncentrací síťovadla a emulgátoru ve vodě. Obsah magnetického plniva v částicích činil 5-23 hm.% a odpovídal poměru složek v systému před zahájením polymerizace. Na tomto základě pak byla předpokládána úplná inkorporace magnetického plniva do polymerní matrice[104].

Naopak překvapivě velké částice (1-5 μm) poskytl systém, ve kterém byly magnetitové nanočástice (10 nm) stabilizované kyselinou olejovou dispergovány ve styrenu, divinylbenzenu, kyselině methakrylové a akrylamidu. Monomerní fáze s magnetickým plnivem pak byla dispergována ve vodné fázi obsahující dodecylsulfát sodný (SDS; emulgátor), cetylalkohol (kosurfaktant) a persíran draselný (iniciátor)[105].

3C.1.1.4 Miniemulzní polymerizace

Miniemulze vyznačují se vysokou stabilitou jsou připravovány za vysokých střihových (smykových) sil pomocí ultrazvuku nebo v komorových a průtokových dispergátorech. Jsou tvořeny monodisperzními monomerními kapénkami o velikostech v rozmezí 30-500 nm, které jsou kostabilizovány nízkomolekulárním pomocným stabi-

lizátorem. Tento kostabilizátor musí být rozpustný v dispergované (monomerní) fázi, zatímco v kontinuální (vodné) fázi musí být naopak nerozpustný. Typickým pomocným stabilizátorem miniemulzí je hexadekan, který potlačuje splývání drobných monomerních kapének do větších kapek (tzv. Ostwaldovo zrání) a zajišťuje dlouhodobě stabilitu. Aniontové, kationtové, nebo neionogenní povrchově aktivní činidlo přítomné v kontinuální fázi pak brání koalescenci částic vzájemnými srážkami, ke kterým dochází v průběhu polymerizace[103]. Jako příklad lze uvést miniemulzní polymerizaci styrenu, kdy směs styrenu a pomocného stabilizátoru (hexadekanu) byla dispergována ve vodném roztoku SDS za použití intenzivní sonikace. K takto připravené styrenové miniemulzi pak byla za použití ultrazvuku přimíchána disperze magnetitu (10 nm) stabilizovaná taktéž pomocí SDS; iniciace byla provedena persulfátem draselným a zvýšením teploty. Vzniklé magnetické částice[106] měly velikost kolem 60 nm a obsah magnetitu 20-35 hm.%.

Příkladem použití inverzní (w/o) miniemulzní techniky je příprava magnetických polyakrylamidových částic (60-160 nm). Akrylamid, *N,N´*-methylenbisakrylamid a magnetické částice stabilizované polyakrylovou kyselinou byly smíseny ve zředěném vodném roztoku amoniaku a tato suspenze byla dispergována sonikací v roztoku Span 80 (sorbitol monooleát) v cyklohexanu. Vzniklé kompozitní částice obsahovaly 13 hm.% magnetitu[107].

3C.1.1.5 Disperzní polymerizace

Objev disperzní polymerizace, která je mechanizmem blízká srážecí polymerizaci, spadá do období vývoje nevodných disperzních nátěrových hmot firmou ICI[j108]. Výhoda této techniky spočívá v jednoduchosti jejího provedení. Probíhá-li polymerizace v alkoholickém prostředí, vznikají částice o velikosti v řádu jednotek mikrometrů a s velmi úzkou distribucí velikostí. Metoda vyžaduje maximální pozornost při výběru reakčního média, které musí být dobrým rozpouštědlem pro monomer(y), ale pro vznikající polymer rozpouštědlem termodynamicky špatným. Mezi heterogenními polyme-

[j] Imperial Chemical Industries, původně britská společnost, dnes patří do nizozemského konsorcia Akzo Nobel.

rizacemi zaujímá disperzní technika zvláštní postavení tím, že na jejím počátku tvoří polymerizační násada roztok a polymerní fáze vzniká teprve v průběhu propagace. Mechanizmus disperzní polymerizace lze popsat následujícím způsobem. Zahřátím roztoku monomeru, iniciátoru a stabilizátoru dochází k rozpadu iniciátoru za vzniku oligomerních radikálových růstových center. Oligomerní řetězce se po dosažení kritické délky vylučují z roztoku a vzájemně precipitují do nukleí. Tato nuklea agregují do primárních částic za současné adheze molekul stabilizátoru na jejich povrch. Je-li dosaženo stádia, kdy již další nová nuklea nevznikají (ustala tvorba primárních radikálů), vzniklé primární částice dále narůstají díky pokračující propagaci a dosahují víceméně uniformních rozměrů. Růstové mechanizmy primárních částic jsou v zásadě dva. První spočívá v polymerizaci uvnitř částic zbotnalých molekulami monomeru a oligomerními řetězci. Druhý mechanizmus pak zahrnuje růst částic akumulací polymerních řetězců z roztoku na povrch primárních částic[10, 109]. Určitou nevýhodou disperzní techniky je nutnost použití jen omezeného množství síťovadla (typicky do 2 hm.%), protože větší množství síťovadla ovlivňuje vznik nukleí a primárních částic a často dochází k vyloučení polymerní hmoty ve formě nepravidelného bloku. Zavedení magnetických nanočástic do disperzní polymerizace také představuje poměrně velký zásah do přirozeného mechanizmu této polymerizace. Nanočástice totiž mohou reakci ovlivňovat například tím, že slouží jako očka pro vznik nukleí a primárních částic a také tím, že v blízkosti jejich povrchu může být koncentrace monomerů zvýšena oproti celkové koncentraci v systému. V případě, že vznikající polymer má nízkou afinitu k povrchu nanočástic, nebo pokud je nosná kapalina velmi dobrým srážedlem pro vznikající polymer a tudíž srážení oligomerních řetězců probíhá rychleji než jejich adsorpce na povrch nanočástic, lze dosáhnout nežádoucího stavu, kdy vedle magnetických nanočástic vznikají nemagnetické polymerní mikročástice, nebo jsou magnetické nanočástice jen adsorbovány na povrchu polymerní mikročástice.

Jako příklad použití disperzní techniky lze uvést polymerizaci 2-hydroxyethylmethakrylátu ve směsi toluen/2-methylpropan-1-ol iniciovanou benzoylperoxidem a stabilizovanou acetátem butyrátem celulózy v přítomnosti krychliček nebo jehliček oxidů železa (cca. 100 × 500 nm) za vzniku 1-2 μm mikročástic[110]. Síťované částice pak byly připraveny pomocí dodatečného přídavku síťovadla (ethylen-dimethakrylát) 2 hod. po začátku polymerizace. Podobné mikročástice byly připraveny disperzní polymerizací

GMA iniciovanou AIBN a stabilizovanou pomocí poly(*N*-vinylpyrolidonu) ve směsi ethanol/voda za přítomnosti jehliček oxidů železa. Obsah magnetického plniva[111] byl typicky 12-15 hm.%.

3C.1.1.6 Inverzní heterogenní polymerizační techniky

S výjimkou disperzních polymerizací, kde je důležitá citlivá volba rozpustnostních parametrů nosného média ve vztahu k monomerům a jejich polymerům, ostatní výše popsané heterogenní polymerizační techniky většinou spočívají v dispergování monomerní organické fáze ve vodě (tzv. *o/w* systém). Toto provedení však k přípravě mikročástic z hydrofilních polymerů nelze použít, protože ve vodném prostředí se vznikající částice rozpouštějí, popř. koaleskují. V literatuře lze často nalézt zjednodušené tvrzení, že k provedení heterogenních polymerizací založených na dispergování monomerní vodné fáze v organickém rozpouštědle (tzv. *w/o* systém) postačuje pouze zaměnit vodnou a nepolární fázi za současné úpravy jejich vzájemného objemového zastoupení a vybrat vhodný emulgátor s vyšším podílem nepolární vzhledem k polární části. Provedení heterogenních technik typu w/o však výrazně komplikují dvě hlavní skutečnosti: a) nízké dielektrické konstanty nepolárních nosných kapalin znemožňující využít výhod elektrostatické stabilizace částic a b) vyšší hustota dispergované vodné monomerní fáze (typicky ρ = 1000 kg·m^{-3}) v porovnání s nižší hustotou nepolárního nosného média (typicky ρ = 800-900 kg·m^{-3}). což klade zvýšené nároky na stabilizaci a míchání polymerizačního systému vzhledem k nežádoucímu působení tíhového zrychlení na dispergovanou fázi. Konstrukce úspěšného *w/o* heterogenního polymerizačního systému tak bohužel zůstává prozatím v čistě empirické rovině a značně závisí na zkušenostech experimentátora.

3C.1.2 Magnetické poly(*N*,*N*-dimethylakrylamidové) mikročástice

K přípravě hydrofilních magnetických částic byl vybrán jako monomer *N*,*N*-dimethylakrylamid (DMAAm). Poly(*N*,*N*-dimethylakrylamid (PDMAAm) je velmi dobře rozpustný ve vodě i při vysokých molekulových hmotnostech (M_n ~ 10^6) a sou-

časně je termoresponzivní[112, 113]. Jak už bylo zmíněno v kapitole 3B.2.1.3., DMAAm snadno polymerizuje ve vodných i organických prostředích do vysokých konverzí. Rovněž dobře kopolymerizuje s mnoha funkčními komonomery a snadno tvoří pravidelné sítě, zejména se síťovadly akrylátového typu[89]. PDMAAm a jeho kopolymery byly použity při regeneraci olejů[114], PDMAAm zakotvený na pevné fázi je pak užitečný jako bezrozpouštědlový systém v organických reakcích[115] a při katalýze kovy[116]. V porovnání s akrylamidem, DMAAm nevykazuje silné vodíkové interakce. Poly(*N*-mono- a *N*,*N*′-disubstituované) akrylamidy a methakrylamidy jsou inertní, netoxické a biokompatibilní[90, 91], takže představují dobrou náhradu za polyakrylamid. Kopolymerizace DMAAm s komonomery akrylátového a methakrylátového typu umožňuje nastavit hydrofilní/hydrofobní charakter výsledného produktu. DMAAm byl použit[117] například ke zvýšení dolní kritické rozpouštěcí teploty (LCST) poly(*N*-isopropylakrylamidu) z 32 °C na 37 °C. Pokud by se tedy podařilo připravit magnetické PDMAAm částice, představovaly by vítanou alternativu k magnetickým hydrofobním nosičům, které by byly vhodné pro různé aplikace v biologických prostředích.

3C.1.2.1 Příprava neplněných PDMAAm částic

PDMAAm mikročástice nebyly v odborné literatuře na začátku řešení dizertační práce popsány. Bylo tedy nejdříve třeba experimentálně prověřit možnosti jejich přípravy různými polymerizačními technikami.

Inverzní suspenzní polymerizace DMAAm

Dispergovaná fáze byla tvořena vodným roztokem DMAAm a *N*,*N*′-methylenbisakrylamidu (MBAAm; síťovadlo) spolu s persulfátem amonným (iniciátor). Roztok byl dispergován ve směsi toluen/trichlorethylen s přídavkem acetátu butyrátu celulosy (CAB; stabilizátor). Trichlorethylen byl použit jako součást kontinuální fáze pro jeho vysokou hustotu (ρ = 1460 kg·m^{-3}), která kompenzovala jinak obvyklý nežádoucí rozdíl hustot mezi kontinuální a monomerní fází. Skutečnost, že kapénka dispergované monomerní fáze suspenzní polymerizace představuje prakticky kompletní polymerizační systém izolovaný fázovým rozhraním od kontinuální fáze, marginalizuje vliv trichlorethylenu na polymerizaci jakožto přenosového činidla. Použití vody jako

součásti dispergované fáze bylo nezbytné, protože samotná směs monomerů ji nemohla vytvořit, jelikož monomery byly rozpustné také v organických rozpouštědlech. Produktem série polymerizací, lišících se zastoupením síťovadla v monomerech, byly pravidelné kulovité hydrogelové částice se širokou distribucí velikostí a číselným průměrem velikostí částic kolem 60 μm. Čím byly částice zesítěnější, tím méně však botnaly ve vodě.

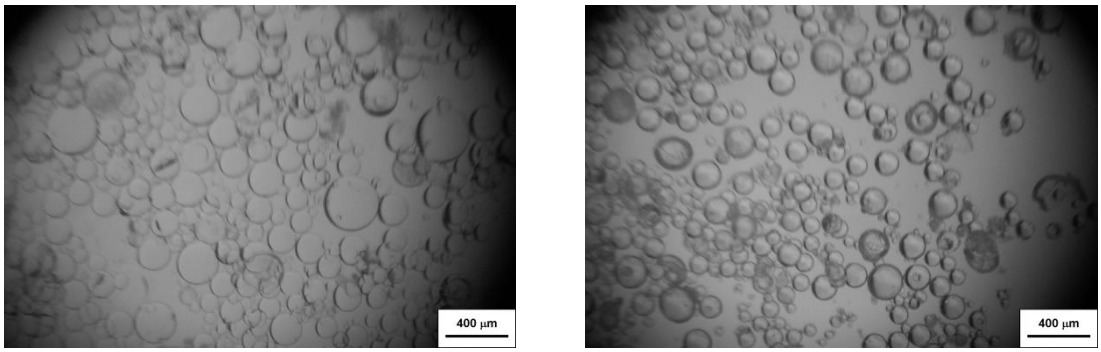

a b

Obr. 29. Světelná mikrofotografie (a) ve vodě zbotnalých a (b) suchých mikročástic P(DMAAm-*co*-5%MBAAm) připravených inverzní suspenzní polymerizací ve směsi toluen/trichlorethylen.

Inverzní emulzní polymerizace DMAAm

Inverzní emulzní polymerizační systém byl velmi podobný inverznímu suspenznímu uspořádání. Odlišoval se použitím iniciátoru (AIBN) rozpuštěným v kontinuální fázi. Monomerní fáze byla dispergována v kontinuální pomocí intenzivní sonikace za současného chlazení směsí voda/led. Experimentálně byl zjišťován vliv koncentrací povrchově aktivního činidla, síťovadla a iniciátoru na velikost a polydisperzitu částic. V závislosti na reakčních podmínkách byly velikosti částic v rozmezí 130 nm – 1 μm a distribuce velikostí částic charakterizovaná PDI nabývala hodnot od velmi uspokojivých (PDI = 1,13) až po nepřijatelné (PDI = 3,86). Použité povrchově aktivní činidlo (CAB) není typickým příkladem amfifilního emulgátoru pro tvorbu emulzních polymerizačních systémů, byl však prověřován pro tuto techniku jako jeden z možných přístupů k řešení problému nežádoucí migrace magnetických nanočástic k fázovému rozhraní, jsou-li přítomny konvenční emulgátory.

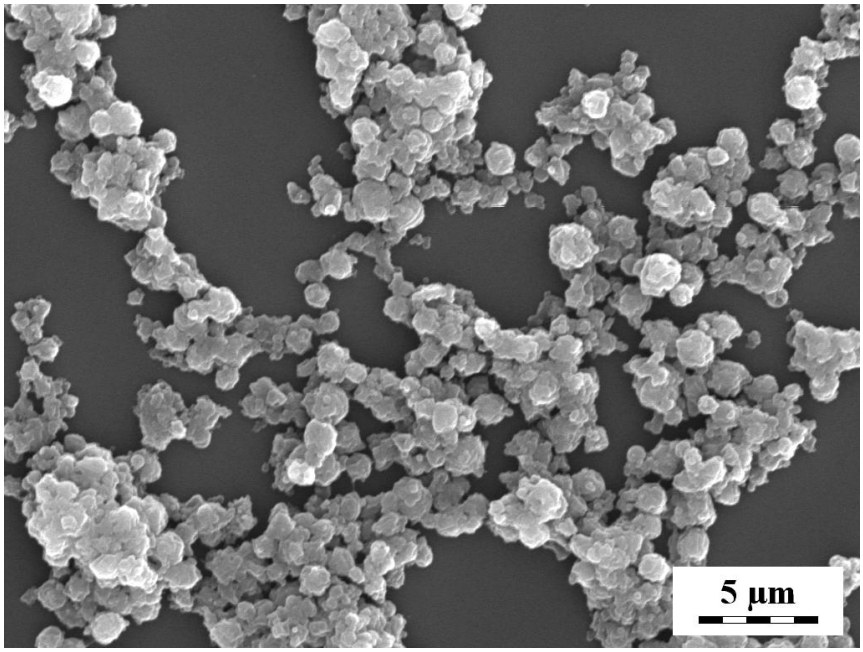

Obr. 30. SEM mikrofotografie P(DMAAm-*co*-5%MBAAm) mikročástic připravených inverzní emulzní polymerizací ve směsi toluen/trichlorethylen.

Disperzní polymerizace DMAAm

Jak už bylo uvedeno, disperzní polymerizace nabízí v porovnání s oběma předchozími technikami výhodu snadné přípravy monodisperzních mikročástic. Nevýhodu naopak představuje možnost použití jen velmi malého množství síťovadla, což vznikající hydrofilní částice znevýhodňuje v aplikacích ve vodných prostředích. Oba předpoklady se prakticky naplnily, neboť v závislosti na reakčních podmínkách se podařilo připravit pravidelné monodisperzní částice o velikostech 1-2 µm, ale již velmi malý přídavek (0,25 hm.%) síťovadla vedl k vysrážení polymerní hmoty do nepravidelného bloku.

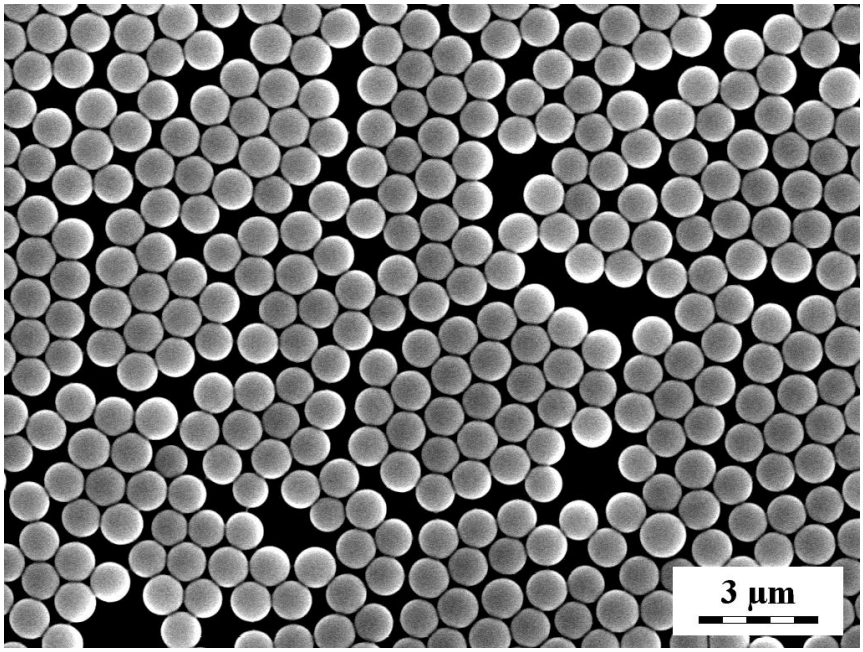

Obr. 31. SEM mikrofotografie PDMAAm mikročástic připravených disperzní polymerizací. Polymerizační podmínky: toluen/heptan 9,5/17,5 w/w; 3.6 hm.% monomerů a 1 hm.% Kratonu G 1650 [poly(styren-*block*-ethylenbutylen-*block*-styren)] v násadě, 1 hm.% AIBN v monomeru.

Oblasti velikostí a distribucí velikostí PDMAAm částic dosažených jednotlivými technikami shrnuje diagram na obr. 32. Podrobnosti pak lze nalézt v příloze č. 6 této práce[118].

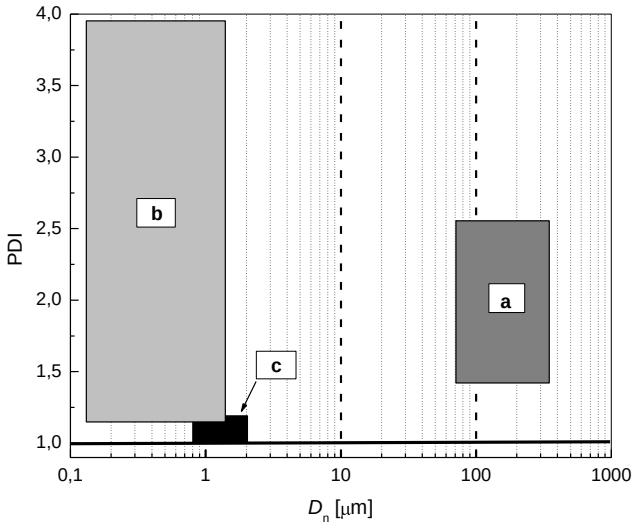

Obr. 32. Velikosti a distribuce velikostí PDMAAm mikročástic připravených a) suspenzní, b) inverzní emulzní a c) disperzní polymerizací DMAAm.

3C.1.2.2 Příprava magnetických PDMAAm mikročástic

Na základě poznatků z předchozí kapitoly byla vybrána k přípravě magnetických PDMAAm mikročástic technika inverzní emulzní polymerizace. Při přípravě nemagnetických PDMAAm mikročástic síťovaných MBAAmbylo pozorováno, že tyto částice jsou velmi měkké a vykazují tak nedostatečnou mechanickou odolnost při manipulaci v mokrém (zbotnalém) stavu. Přistoupili jsme proto k záměně bifunkčního síťovadla MBAAm za trifunkční pentaerythritolpropoxylát-triakrylát (PETPTA) (obr. 33).

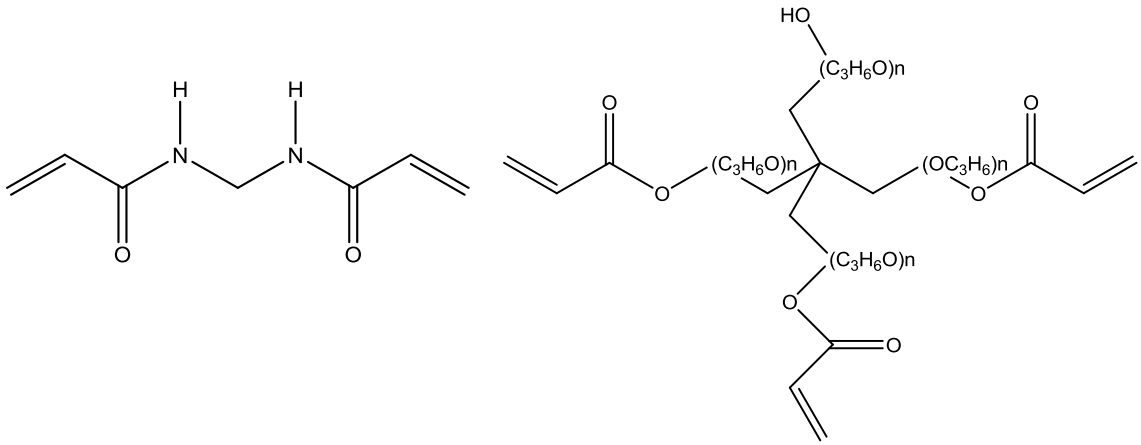

a b

Obr 33. Vzorce síťovadel a) MBAAm a b) PETPTA.

Poměrně dobrou mechanickou odolnost ve zbotnalém stavu vykazovaly částice PDMAAm síťované 40 hm.% PETPTA. Ke zdokumentování vlivu přítomnosti vodných koloidů magnetických nanočástic na výslednou velikost a morfologii kompozitních magnetických mikročástic byly provedeny inverzní emulzní polymerizace v následujícím experimentálním uspořádání:

Různé objemy vodných koloidů maghemitu o třech různých koncentracích γ-Fe_2O_3 spolu s 1,2 g DMAAm a 0,8 g PEPTA byly dispergovány použitím ultrazvukového dispergátoru za chlazení ledem ve směsi toluen/trichlorethylen (48/20 w/w) obsahující 3 g stabilizátoru CAB 381-20 a 0,02 g iniciátoru AIBN. Polymerizační systém byl probubláván dusíkem po dobu 10 min. a následně polymerizován při 70 °C po dobu 8 hod. za míchání kotvovým míchadlem rychlostí 700 ot.·min.$^{-1}$. Po polymerizaci byly vzniklé

částice opakovaně promyty ethylacetátem za použití magnetické separace. Promyté částice byly analyzovány pomocí SEM a obrazovou analýzou byl stanoven průměr částic D_n a index polydispersity PDI. Obsah maghemitu v mikročásticích byl vypočten z výsledků elementární analýzy.

Inverzní emulzní kopolymerizací DMAAm a PETPTA v přítomnosti koloidních maghemitových nanočástic vznikaly polydisperzní (PDI = 1,2–3,3) magnetické polymerní mikročástice v intervalu velikostí 120–300 nm. Data v obr. 34 ukazují, že objem a především koncentrace maghemitového koloidu v polymerizační násadě zásadně ovlivňují morfologické vlastnosti vznikajících mikročástic. Velikost mikročástic při použití koloidu s koncentrací nanočástic 43 mg/ml se v závislosti na jeho objemu výrazně měnila, avšak tyto změny nevykazovaly žádný trend. Naproti tomu při použití koloidu o koncentraci maghemitu 141 mg/ml se velikost vznikajících kompozitních mikročástic v závislosti na objemu koloidu v polymerizační násadě prakticky neměnila (obr. 34).

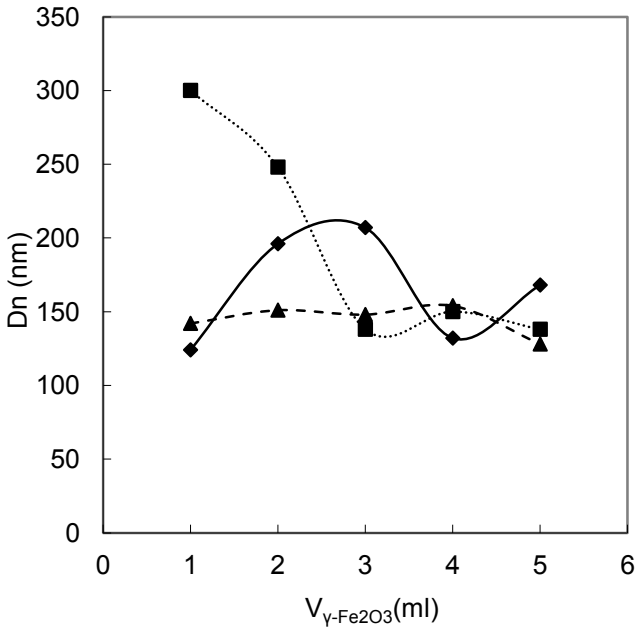

Obr. 34. Vliv koncentrace a objemu ($V_{\gamma\text{-}Fe2O3}$) přidaného vodného koloidu γ-Fe_2O_3 na velikost magnetických P(DMAAm-*co*-40% PETPTA) částic**.** Koncentrace koloidu (♦) 43 mg/ml, (■) 89 mg/ml a (▲) 141 mg/ml.

Při všech třech použitých koncentracích koloidu se obsah maghemitu ve vznikajících mikročásticích se zvyšujícím se objemem koloidu v polymerizační násadě zvyšoval

lineárně, byl však nalezen velký rozdíl mezi teoreticky vypočteným a stanoveným obsahem maghemitu v mikročásticovém kompozitu (obr. 35).

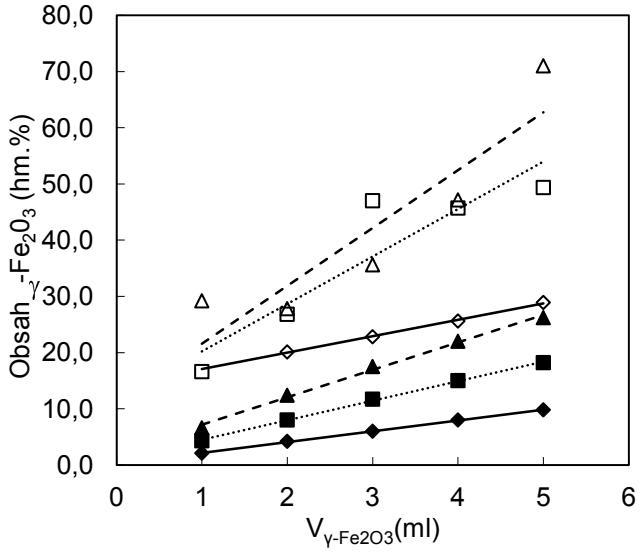

Obr. 35. Vliv koncentrace a objemu přidaného vodného koloidu γ-Fe_2O_3 na obsah maghemitu v magnetických P(DMAAm-*co*-40% PETPTA) $V_{\gamma\text{-}Fe2O3}$ mikročásticích. (♦, ◊) 44 mg/ml, (■, □) 89 mg/ml a (▲, Δ) 141 mg/ml; (♦, ■, ▲) teoretický a (◊, □, Δ) nalezený obsah γ-Fe_2O_3.

S rozdílnou koncentrací koloidu použitého v polymerizaci se výrazně měnila i morfologie produktu. U nižší koncentrace koloidu byl pozorován vznik částic nepravidelného tvaru s vysokou polydisperzitou (obr. 36, a) a vznikající částice jevily nízkou odolnost vůči agregaci. S použitím vyšších koncentrací koloidů došlo k potlačení agregace vznikajících mikročástic, které nabývaly kulovitých tvarů a užší distribuce velikostí (obr. 36 b, c).

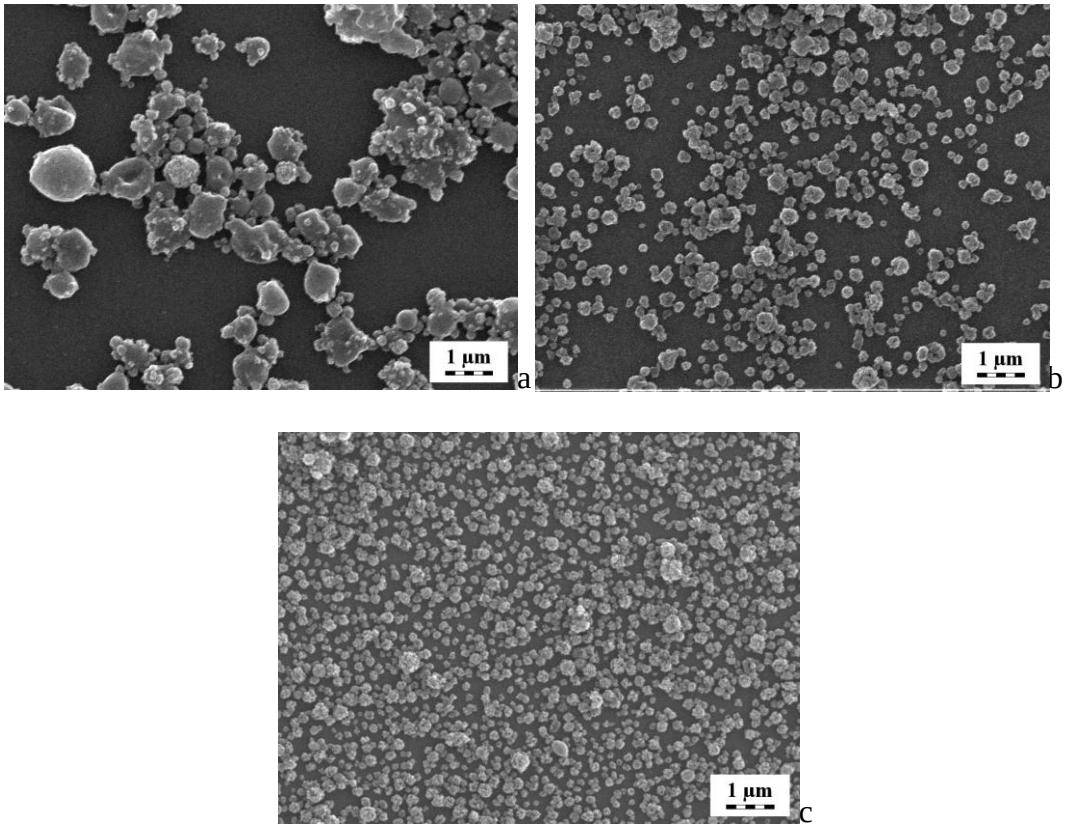

Obr. 36. SEM mikrofotografie magnetických P(DMAAm-*co*-40%PETPTA mikročástic. Polymerizační podmínky: 2 g monomerů, 48/20 (g/g) toluen/trichlorethylen, 1 hm.% AIBN v monomerech, 4.3 hm.% CAB v násadě, 5 ml vodného koloidu maghemitu o koncentraci γ-Fe_2O_3 (a) 43,6 mg/ml, D_n = 196 nm, PDI = 3,3, (b) 89 mg/ml, D_n = 138 nm, PDI = 1,19 a (c) 141 mg γ-Fe_2O_3/ml, D_n = 128 nm, PDI = 1,31.

Výtěžek přípravy mikročástic závisel přímo úměrně na objemu přidaného maghemitového koloidu (obr. 37).

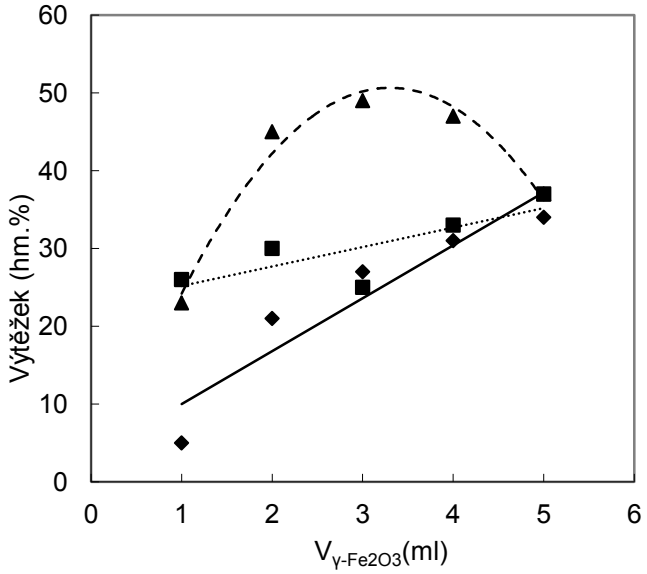

Obr. 37. Vliv koncentrace a objemu přidaného vodného koloidu γ-Fe_2O_3 na výtěžek magnetickýh P(DMAAm-*co*-40% PETPTA) mikročástic**.** Koncentrace koloidu (♦) 43, (■) 89 a (▲) 141 mg/ml.

K vysvětlení výše popsaných jevů lze nabídnout dvě možnosti:

- a) Maghemitové nanočástice rozptýlené v monomerní fázi inverzního emulzního systému fungují jako stabilizátor nebo pomocný stabilizátor (kostabilizátor) monomerní kapky[99]. V jejich působení tak lze nalézt analogii s působením klasických emulgátorů v emulzních polymerizacích v koncentracích nad a pod kritickou micelární koncentrací. Slabinou této hypotézy je však pozorovaná náhodná distribuce nanoplniva v mikročásticové matrici (obr. 38), která je však z hlediska požadovaných vlastností cílového produktu žádaným výsledkem. Lze totiž vyslovit předpoklad, že při působení nanočástic jako stabilizátoru kapky, jsou maghemitové nanočástice přednostně zastoupeny na povrchu polymerní mikročástice v porovnání s jejím středem. Na druhou stranu nelze opomenout fakt, že se zvyšující se koncentrací nanočástic se zároveň zvyšuje i viskozita monomerní fáze, což samo o sobě přispívá ke stabilizaci.
- b) Pouze monomery adsorbované na povrchu nanočástic se účastní tvorby polymerní mikročástice. Zbývající neadsorbované monomery jsou rozpuštěny v kontinuální fázi, nebo z nich vzniklé polymery jsou posléze vymyty v průběhu promývání a magnetické separace. Na tuto možnost

ukazuje rozdíl mezi teoretickým a nalezeným množstvím maghemitu v kompozitu a zmíněná závislost výtěžku polymerizace na množství maghemitových nanočástic přidaných do násady.

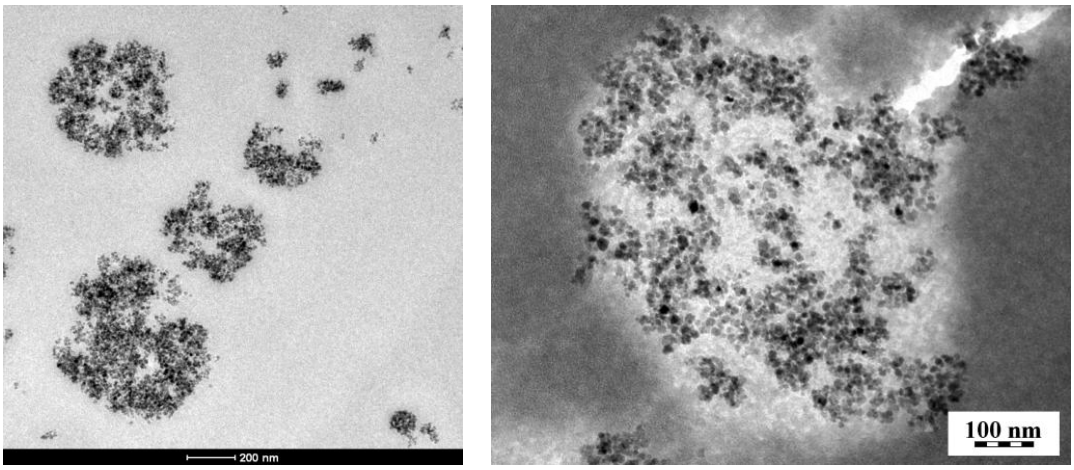

a b

Obr. 38. TEM mikrofotografie ultratenkých řezů P(DMAAm-*co*-40% PETPTA) mikročástic obsahujících γ-Fe_2O_3. (a) Zalito v epoxidové pryskyřici a (b) po kontrastování polymerní matrice pomocí RuO_4.

Lze tak vyslovit závěr, že pomocí inverzní emulzní kopolymerizace DMAAm a PETPTA v přítomnosti koloidních maghemitových nanočástic lze připravit kompozitní částice s obsahem magnetického plniva od ~ 20 do ~ 70 hm.%, které je náhodně rozptýleno v polymerní matrici. Morfologie, velikost, obsah plniva a výtěžek kompozitních mikročástic závisí na koncentraci a objemu přidaného koloidu.

4. ZÁVĚR

- Byla vyvinuta syntéza superparamagnetických γ-Fe_2O_3 nanočástic modifikací techniky koprecipitace Fe(II) a Fe(III) solí v zásaditém prostředí. Metoda poskytuje nanočástice ve formě stabilního vodného koloidu. Povrch γ-Fe_2O_3 nanočástic je dobře dostupný pro následné povrchové modifikace
- Byly navrženy tři typy povrchových úprav γ-Fe_2O_3 nanočástic za účelem značení kultur kmenových buněk a jejich zobrazování pomocí MRI. Nanočásticemi s povrchy upravenými D-manózou, poly(L-lysinem) a poly(*N*,*N*-dimethylakrylamidem) bylo dosaženo homogenního „proznačení" vysokého podílu buněk v kulturách s minimálními negativními vlivy na jejich viabilitu. Experimentálně bylo úspěšně ověřeno splnění záměru zvýšit kontrast buněčné kultury při zobrazování MRI jak na želatinových modelech, tak na buněčných kulturách *in vitro* před, i *in vivo* po implantaci.
- Byla popsána příprava poly(*N*,*N*-dimethylakrylamidových) mikročástic suspenzní, inverzní emulzní a disperzní polymerizací. Současně byly popsány vlivy reakčních parametrů na morfologii, velikost a šířku distribuce velikostí mikročástic.
- Byla popsána příprava kompozitních magnetických poly(*N*,*N*-dimethylakrylamidových) mikročástic inverzní emulzní polymerizací. Současně byl popsán vliv přítomnosti nanočástic v polymerizačním systému na morfologii, velikost a polydisperzitu mikročástic. Na řezech kompozitních mikročástic byla prokázána náhodná distribuce nanoplniva v polymerní matrici. Nově vyvinuté magnetické polymerní mikročástice jsou slibné pro separace biomolekul ze složitých směsí.

5. SEZNAM LITERATURY.

1. Sedlák, B.; Štoll, I., *Elektřina a magnetismus*. 2nd. ed.; Academia: Praha, **2002**.
2. Zeng, H.; Zheng, M.; Skomski, R.; Sellmyer, D. J.; Liu, Y.; Menon, L.; Bandyopadhyay, S. *J. Appl. Phys.* **2000,** 87, (9 II), 4718-4720.
3. Burke, N. A. D.; Stöver, H. D. H.; Dawson, F. P. *Chem. Mater.* **2002,** 14, (11), 4752-4761.
4. Willard, M. A.; Kurihara, L. K.; Carpenter, E. E.; Calvin, S.; Harris, V. G. *Int. Mater. Rev.* **2004,** 49, (3-4), 125-170.
5. Jeong, U.; Teng, X.; Wang, Y.; Yang, H.; Xia, Y. *Adv. Mater.* **2007,** 19, (1), 33-60.
6. Berkovsky, B. M.; Medvedev, V. F.; Krakov, M. S. *Magnetic Fluids: Engineering Applications*, Begell House inc., New York, **1993**.
7. Blums, E.; Cebers, A.; Maiorov, M. M. *Magnetic Fluids*, Walter de Gruyter & co., Berlin, **1997**.
8. Cornell, R. M.; Schwertmann, U., *The Iron Oxides*. 2nd ed.; Wiley-VCH, Weinheim, **2003**.
9. Mornet, S.; Vasseur, S.; Grasset, F.; Duguet, E. *J. Mater. Chem.* **2004,** 14, (14), 2161-2175.
10. Richard, J.; Vaslin, S.; US Patent 5,976,426, **1999**.
11. Bee, A.; Massart, R.; Neveu, S. *J. Magn. Magn. Mater.* **1995,** 149, (1-2), 6-9.
12. Carpenter, E. E.; Long, J. W.; Rolison, D. R.; Logan, M. S. *J. Appl. Phys* **2006,** 99.
13. Papell, S. S.; US Patent 3,215,572, **1965**.
14. Gonzales, M.; Krishnan, K. M. *J. Magn. Magn. Mater.* **2005,** 293, (1), 265-270.
15. Pei, W.; Kumada, H.; Natusme, T.; Saito, H.; Ishio, S. *J. Magn. Magn. Mater.* **2007,** 310, (2nd Supll. Part 3), 2375-2377.
16. Dixit, S.; Jeevanandam, P., *Advanced Materials Research*. **2009**, 67, 221-226.
17. Rockenberger, J.; Scher, E. C.; Alivisatos, A. P. *J. Am. Chem. Soc.* **1999,** 121, (49), 11595-11596.
18. Makovec, D.; Drofenik, M.; Znidarsic, A. *J. Am. Ceram. Soc.* **1999,** 82, (5), 1113-1120.
19. Rozman, M.; Drofenik, M. *J. Am. Ceram. Soc.* **1995,** 78, (9), 2449-2455.
20. Inoue, M.; Nishikawa, T.; Inui, T. *J. Mater. Res.* **1998,** 13, (4), 856-860.
21. Massart, R. *IEEE Trans. Magn.* **1981,** MAG-17, (2), 1247-1248.
22. Zaitsev, V. N.; Shliomis, M. I. *Dokl. Akad. Nauk (SSSR)* **1969,** 188, 1621-1624.
23. Jolivet, J. P.; Massart, R.; Fruchart, J. M. *Nouv. J. Chim.* **1983,** 7, (5), 325-331.
24. Bacri, J. C.; Perzynski, R.; Salin, D.; Cabuil, V.; Massart, R. *J. Magn. Magn. Mater.* **1986,** 62, (1), 36-46.
25. Rocchiccioli-Deltcheff, C.; Franck, R.; Cabuil, V.; Massart, R. *J. Chem. Res.* **1987,** 5, 126-127.
26. Groman, E. V.; Josephson, L.;US Patent 5,248,492, **1993**.
27. Palmacci, S., Josephson, L., Groman, L. V. WO 9,505,669A1, **1995**.
28. Shafi, K. V. P. M.; Ulman, A.; Yan, X.; Yang, N. L.; Estournès, C.; White, H.; Rafailovich, M. *Langmuir* **2001,** 17, (16), 5093-5097.
29. De Cuyper, M.; Müller, P.; Lueken, H.; Hodenius, M; DE Patent 19,624,426A1, **1988**.

30. Jiang, W.; Yang, H. C.; Yang, S. Y.; Horng, H. E.; Hung, J. C.; Chen, Y. C.; Hong, C. Y. *J. Magn. Magn. Mater.* **2004,** 283, (2-3), 210-214.
31. Kawaguchi, T.; Hasegawa, M. *J. Mater. Sci.: Mater. Med.* **2000,** 11, (1), 31-35.
32. Liberti, P. A., Rao, G. C., Chiarappa, J. N., US Patent 5,698,271, **1997**.
33. Molday, R. S.; U.S. Patent 4,452,773, **1984**..
34. Pardoe, H.; Chua-anusorn, W.; St. Pierre, T. G.; Dobson, J. *J. Magn. Magn. Mater.* **2001,** 225, (1-2), 41-46.
35. Chastellain, M.; Petri, A.; Hofmann, H. *J. Colloid Interface Sci.* **2004,** 278, (2), 353-360.
36. Qiu, X. P.; Winnik, F. *Chin. J. Polym. Sci. (English Edition)* **2000,** 18, (6), 535-539.
37. Lin, H.; Watanabe, Y.; Kimura, M.; Hanabusa, K.; Shirai, H. *J. Appl. Polym. Sci.* **2003,** 87, (8), 1239-1247.
38. Xue, B.; Tong, X. D.; Sun, Y. *Sep. Sci. Technol.* **2001,** 36, (11), 2449-2461.
39. Hofmann, H.; Petri-Fink, A.; Steitz, B.; von Rechenberg, B. *NSTI Nanotech Technical Proceedings* **2005,** 152-155.
40. Kumar, R. V.; Koltypin, Y.; Cohen, Y. S.; Cohen, Y.; Aurbach, D.; Palchik, O.; Felner, I.; Gedanken, A. *J. Mater. Chem.* **2000,** 10, (5), 1125-1129.
41. Zhang, Y.; Kohler, N.; Zhang, M. *Biomaterials* **2002,** 23, (7), 1553-1561.
42. Dumazet-Bonnamour, I.; Le Perchec, P. *Colloids Sur. A.* **2000,** 173, (1-3), 61-71.
43. Buschow, K. H. J., *Handbook of Magnetic Materials*. 1st ed.; Elsevier B.V.: Amsterdam, 2006; Vol. 16, p 534.
44. Babic, M.; Horak, D.; Jendelova, P.; Glogarova, K.; Herynek, V.; Trchova, M.; Likavcanova, K.; Lesny, P.; Pollert, E.; Hajek, M.; Sykova, E. *Bioconjugate Chem.* **2009,** 20, (2), 283-294.
45. Tocchio, A.; Horák, D.; Babic, M.; Trchová, M.; Veverka, M.; Beneš, M. J.; Šlouf, M.; Fojtík, A. *Journal of Polymer Science, Part A: Polymer Chemistry* **2009,** 47, (19), 4982-4994.
46. Bulte, J. W. M.; Kraitchman, D. L. *NMR Biomed.* **2004,** 17, (7), 484-499.
47. Weis, J.; Bořuta, P., *Úvod do magnetickej rezonancie*. GOEN, s.r.o.: Bratislava, **1998**; p 108.
48. Partain, C. L.; Ronald, R. P.; Patton, J. A.; Kulkarni, M. V.; James, A. E. J., *Magnetic Resonance Imaging* Vol. II - *Physical Principles and Instrumentation*. 2nd ed.; W. B. Saunders Company: Philadelphia, **1988**.
49. Koenig, S. H.; Brown Iii, R. D. *Prog. Nucl. Magn. Reson. Spectrosc.* **1990,** 22, (6), 487-567.
50. Banci, L.; Bertini, I.; Luchinat, C. *Nuclear and Electron Relaxation*; Wiley - VCH, Weinheim, **1991**.
51. Gueron, M. *J. Magn. Reson.* **1975,** 19, (1), 58-66.
52. Freed, J. H. *The Journal of Chemical Physics* **1978,** 68, (9), 4034-4037.
53. Koenig, S. H.; Kellar, K. E. *Magn. Reson. Med.* **1995,** 34, (2), 227-233.
54. Roch, A.; Muller, R. N.; Gillis, P. *J. Chem. Phys.* **1999,** 110, (11), 5403-5411.
55. Vogl, T. J.; Hammerstingl, R.; Schwarz, W.; Mack, M. G.; Müller, P. K.; Pegios, W.; Keck, H.; Eibl-Eibesfeldt, A.; Hoelzl, J.; Woessmer, B.; Bergman, C.; Felix, R. *Radiology* **1996,** 198, (3), 881-887.
56. Kellar, K. E.; Fujii, D. K.; Gunther, W. H. H.; Briley-Sæbø, K.; Bjørnerud, A.; Spiller, M.; Koenig, S. H. *J. Magn. Reson. Imaging* **2000,** 11, (5), 488-494.

57. Ahlström, K. H.; Johansson, L. O.; Rodenburg, J. B.; Ragnarsson, A. S.; Åkeson, P.; Börseth, A. *Radiology* **1999,** 211, (3), 865-869.
58. Yablonskiy, D. A.; Haacke, E. M. *Magn. Reson. Med.* **1994,** 32, (6), 749-763.
59. Geraldes, C.; Laurent, S. *Contrast Media Mol. Imaging* **2009,** 4, (1), 1-23.
60. Moghimi, S. M.; Patel, H. M. *Adv. Drug Delivery Rev.* **1998,** 32, (1-2), 45-60.
61. Weissleder, R.; Heautot, J. F.; Schaffer, B. K.; Nossiff, N.; Papisov, M. I.; Bogdanov Jr, A.; Brady, T. J. *Radiology* **1994,** 191, (1), 225-230.
62. Monfardini, C.; Veronese, F. M. *Bioconjugate Chem.* **1998,** 9, (4), 418-450.
63. Moghimi, S. M.; Szebeni, J. *Prog. Lipid Res.* **2003,** 42, (6), 463-478.
64. Moghimi, S. M.; Hunter, A. C.; Murray, J. C. *Pharmacol. Rev.* **2001,** 53, (2), 283-318.
65. Molday, R. S.; U.S. Patent 4,452,773, **1984**.
66. Reimer, P.; Balzer, T. *Eur. Radiol.* **2003,** 13, (6), 1266-1276.
67. Sjögren, C. E.; Johansson, C.; NÆvestad, A.; Sontum, P. C.; Briley-SÆbØ, K.; Fahlvik, A. K. *Magn. Reson. Imaging* **1997,** 15, (1), 55-67.
68. Peracchia, M. T. *S.T.P. Pharma Sci.* **2003,** 13, (3), 155-161.
69. Ghosh, P. K. *Indian J. Biochem. Biophys.* **2000,** 37, (5), 273-282.
70. Moghimi, S. M.; Hunter, A. C. *Trends Biotechnol.* **2000,** 18, (10), 412-420.
71. Bonnemain, B. *J. Drug Target.* **1998,** 6, (3), 167-174.
72. Figdor, C. G.; Van Kooyk, Y.; Adema, G. J. *Nat. Rev. Immunol.* **2002,** 2, (2), 77-84.
73. McGreal, E. P.; Martinez-Pomares, L.; Gordon, S. *Mol. Immunol.* **2004,** 41, (11 SPEC. ISS.), 1109-1121.
74. Keler, T.; Ramakrishna, V.; Fanger, M. W. *Expert Opin. Biol. Ther.* **2004,** 4, (12), 1953-1962.
75. Gijzen, K.; Cambi, A.; Torensma, R.; Figdor, C. G. *Curr. Protein Pept. Sci.* **2006,** 7, (4), 283-294.
76. In *A genomics resource for animal lectins. C-type lectin-like domain*. http://www.imperial.ac.uk/research/animallectins/, last update 03 October **2006**
77. McGreal, E. P.; Miller, J. L.; Gordon, S. *Curr. Opin. Immunol.* **2005,** 17, (1), 18-24.
78. Frisont, N.; Taylor, M. E.; Soilleux, E.; Bousser, M. T.; Mayer, R.; Monsigny, M.; Drickamer, K.; Roche, A. C. *J. Biol. Chem.* **2003,** 278, (26), 23922-23929.
79. Engering, A.; Geijtenbeek, T. B. H.; Van Vliet, S. J.; Wijers, M.; Van Liempt, E.; Demaurex, N.; Lanzavecchia, A.; Fransen, J.; Figdor, C. G.; Piguet, V.; Van Kooyk, Y. *J. Immunol.* **2002,** 168, (5), 2118-2126.
80. Engering, A. J.; Cella, M.; Fluitsma, D.; Brockhaus, M.; Hoefsmit, E. C. M.; Lanzavecchia, A.; Pieters, J. *Eur. J. Immunol.* **1997,** 27, (9), 2417-2425.
81. Engering, A. J.; Cella, M.; Fluitsma, D. M.; Hoefsmit, E. C. M.; Lanzavecchia, A.; Pieters, J. *Adv. Exp. Med. Biol.* **1997,** 417, 183-187.
82. Taylor, P. R.; Gordon, S.; Martinez-Pomares, L. *Trends Immunol.* **2005,** 26, (2), 104-110.
83. Irache, J. M.; Salman, H. H.; Gamazo, C.; Espuelas, S. *Expert Opin. Drug Delivery* **2008,** 5, (6), 703-724.
84. Horák, D.; Babič, M.; Jendelová, P.; Herynek, V.; Trchová, M.; Likavčanová, K.; Kapcalová, M.; Hájek, M.; Syková, E. *J. Magn. Magn. Mater.* **2009,** 321, (10), 1539-1547.

85. Horák, D.; Babič, M.; Jendelová, P.; Herynek, V.; Trchová, M.; Pientka, Z.; Pollert, E.; Hájek, M.; Syková, E. *Bioconjugate Chem.* **2007,** 18, (3), 635-644.
86. Vodrážka, Z., *Biochemie*. 2.nd ed.; Academia: Prague, 1999.
87. Laga, R.; Koňák, Č.; Šubr, V.; Ulbrich, K. *Colloid. Polym. Sci.* **2007,** 285, (13), 1509-1514.
88. Babič, M.; Horák, D.; Trchová, M.; Jendelová, P.; Glogarová, K.; Lesný, P.; Herynek, V.; Hájek, M.; Syková, E. *Bioconjugate Chem.* **2008,** 19, (3), 740-750.
89. Orakdogen, N.; Okay, O. *Polymer* **2006,** 47, (2), 561-568.
90. Kopecek, J.; Sprincl, L.; Bazilova, H.; Vacik, J. *J. Biomed. Mater. Res.* **1973,** 7, (1), 111-121.
91. Šprincl, L.; Vacík, J.; Kopeček, J.; Lím, D. *J. Biomed. Mater. Res.* **1971,** 5, (3), 197-205.
92. Babič, M.; Horák, D.; Jendelová, P.; Glogarová, K.; Herynek, V.; Trchová, M.; Likavčanová, K.; Lesný, P.; Pollert, E.; Hájek, M.; Syková, E. *Bioconjugate Chem.* **2009,** 20, (2), 283-294.
93. Wichterle, O.; Lím, D. *Nature* **1960,** 185, (4706), 117-118.
94. Ugelstad, J.; Berge, A.; Ellingsen, T.; Schmid, R.; Nilsen, T. N.; Mørk, P. C.; Sienstad, P.; Hornes, E.; Olsvik, Ø. *Prog. Polym. Sci.* **1992,** 17, (1), 87-161.
95. Horák, D.; Babič, M.; Macková, H.; Beneš, M. J. *J. Sep. Sci.* **2007,** 30, (11), 1751-1772.
96. Ma, Z. Y.; Guan, Y. P.; Liu, H. Z. *React. Funct. Polym.* **2006,** 66, (6), 618-624.
97. Wang, X.; Ding, X.; Zheng, Z.; Hu, X.; Cheng, X.; Peng, Y. *Macromol. Rapid Commun.* **2006,** 27, (14), 1180-1184.
98. Vignati, E.; Piazza, R.; Lockhart, T. P. *Langmuir* **2003,** 19, (17), 6650-6656.
99. Pickering, S. U. *J. Chem. Soc., Trans.* **1907,** 91, 2001-2021.
100. Fitch, R. M. *Br. Polym. J.* **1973,** 5, (6), 467-483.
101. Montagne, F.; Mondain-Monval, O.; Pichot, C.; Elaïssari, A. *J. Pol. Sci., Part A: Polym. Chem.* **2006,** 44, (8), 2642-2656.
102. Horák, D.; Chekina, N. *J. Appl. Polym. Sci.* **2006,** 102, (5), 4348-4357.
103. Elaissari, A.; Sauzedde, F.; Montagne, F.; Pichot, C. *Colloidal Polymers: Synthesis and Characterization*, Marcel Dekker, New York **2003**.
104. Deng, Y.; Wang, L.; Yang, W.; Fu, S.; Elaïssari, A. *J. Magn. Magn. Mater.* **2003,** 257, (1), 69-78.
105. Liu, Z. L.; Yang, X. B.; Yao, K. L.; Du, G. H.; Liu, Z. S. *J. Magn. Magn. Mater.* **2006,** 302, (2), 529-535.
106. Ramírez, L. P.; Landfester, K. *Macromol. Chem. Phys.* **2003,** 204, (1), 22-31.
107. Xu, Z. Z.; Wang, C. C.; Yang, W. L.; Deng, Y. H.; Fu, S. K. *J. Magn. Magn. Mater.* **2004,** 277, (1-2), 136-143.
108. Barrett, K. E. J. *Dispersion Polymerization in Organic Media*, John Wiley & Sons inc., New York, **1975**.
109. Li, X.; Sun, Z. *J. Appl. Polym. Sci.* **1995,** 58, (11), 1991-1997.
110. Horák, D.; Boháček, J.; Šubrt, M. *J. Pol. Sci., Part A: Polym. Chem.* **2000,** 38, (7), 1161-1171.
111. Horák, D. *Journal of Polymer Science, Part A: Polymer Chemistry* **2001,** 39, (21), 3707-3713.
112. Katayama, S.; Hirokawa, Y.; Tanaka, T. *Macromolecules* **1984,** 17, (12), 2641-2643.

113. Shibanuma, T.; Aoki, T.; Sanui, K.; Ogata, N.; Kikuchi, A.; Sakurai, Y.; Okano, T. *Macromolecules* **2000,** 33, (2), 444-450.
114. McCormick, C. L.; Elliott, D. L. *Macromolecules* **1986,** 19, (3), 542-547.
115. Yamamoto, S. I.; Hayashi, S.; Morita, H.; Moriya, O. *J. Polym. Sci., Part A: Polym. Chem.* **2004,** 42, (19), 5021-5025.
116. Kralik, M.; Hronec, M.; Lora, S.; Palma, G.; Zecca, M.; Biffis, A.; Corain, B. *J. Mol. Catal. A-Chem.* **1995,** 97, (3), 145-155.
117. Chaw, C. S.; Chooi, K. W.; Liu, X. M.; Tan, C. W.; Wang, L.; Yang, Y. Y. *Biomaterials* **2004,** 25, (18), 4297-4308.
118. Babic, M.; Horak, D. *Macromol. React. Eng.* **2007,** 1, (1), 86-94.

6. SEZNAM PUBLIKOVANÝCH PRACÍ

Publikace zahrnuté jako součást dizertační práce:

1) Horák D., Babič M., Jendelová P., Herynek V., Trchová M., Pientka Z., Hájek M., Syková E. D-mannose-modified iron oxide nanoparticles for stem cell labeling, *Bioconjugate Chem*., 18, 635-644 (2007).
2) Babič M., Horák D., Trchová M., Jendelová P., Glogarová K., Lesný P., Herynek V., Hájek M., Syková E. Poly(L-lysine)-modified iron oxide nanoparticles for stem cell labeling, *Bioconjugate Chem.*, 19, 740–750 (2008).
3) Babič M., Horák D., Jendelová P., Glogarová K., Herynek V., Trchová M., Likavčanová K., Hájek M., Syková E.: Poly(N,N-dimethylacrylamide)-coated maghemite nanoparticles for stem cell labeling, *Bioconjugate Chem.*, 20, 283-294 (2009).
4) Horák D., Babič M., Jendelová P., Herynek V., Trchová M., Likavčanová K., Kapcalová M., Hájek M., Syková E.: Effect of different magnetic nanoparticle coatings on the efficiency of stem cell labeling, *J. Magn. Magn. Mater*, 321,. 1539-1547. (2009).
5) Horák D., Babič M., Macková H., Beneš M.J. Preparation and properties of magnetic nano- and microsized particles for biological and environmental separations, *J. Sep. Sci.* 30, 1751-1772 (2007).
6) Babič M., Horák D. Poly(*N,N*-dimethylacrylamide)-based microspheres prepared by heterogeneous polymerizations, *Macromol. Reac. Eng.* 1, 86-94, (2007).
7) Horák D., Syková P., Babič M., Jendelová P., Hájek M. Method of preparation of superparamagnetic nanoparticles based on iron oxides with modified surface and superparamagnetic nanoparticles obtained by such a method. *EP 1 991 503 81*, (2010).

Publikace ostatní:

8) Hradil J., Pisarev A., Babič M., Horák D. Dextran-modified iron oxide nanoparticles, *China Particuology* 5, 162-168 (2007)
9) Hrubý M., Kučka J., Lebeda O., Macková H., Babič M., Koňák Č, Studenovský M., Sikora A., Kozempel J., Ulbrich K. New bioerodable thermoresponsive polymers for possible radiotherapeutic applications, *J. Controlled Rel.*, 119, 25-33 (2007)
10) Pollert E., Knížek K., Maryško M., Závěta K., Lančok A., Boháček J., Horák D., Babič M. Magnetic poly(glycidyl methacrylate) microspheres containing maghemite prepared by emulsion polymerization, *J. Magn. Magn. Mater.* 306, 241-247 (2006)
11) Tocchio A., Horák D., Babič M., Trchová M., Veverka M., Beneš M.J., Fojtík A. Magnetic poly(glycidyl methacrylate) particles prepared in the presence of surface-modified γ-Fe_2O_3, *J. Polym. Sci., Polym. Chem*, 47, 4982-4994 (2009).
12) Horák, D.,Shagotova, T.,Mitina, N.,Trchová, M.,Boiko, N.,Babič, M.,Stoika, R.,Kovářová, J.,Hevus, O.,Beneš, M.,Klyuchivska, O.,Holler, P.,Zaichenko, A. Surface-initiated polymerization of 2-hydroxyethyl methacrylate from heterotelechelic oligoperoxide-coated y-Fe_2O_3 nanoparticles and their engulfment by mammalian cells, *Journal of Materials Science - Materials in Medicine*, 23, 2637-2649 (2011).
13) Altanerova V., Cihova M., Babic M., Rychly B., Ondicova K., Mravec B., Altaner C. Human adipose tissue-derived mesenchymal stem cells expressing yeast cytosinedeaminase:Uracil phosphoribosyltransferase inhibit intracerebral rat glioblastoma, *Int. J. Cancer, in press*.

7. PŘÍLOHY

Příloha č. 1:
Horák D., Babič M., Jendelová P., Herynek V., Trchová M., Pientka Z., Hájek M., Syková E. D-mannose-modified iron oxide nanoparticles for stem cell labeling, *Bioconjugate Chem.*, 18, 635-644 (2007)

Příloha č. 2:
Babič M., Horák D., Trchová M., Jendelová P., Glogarová K., Lesný P., Herynek V., Hájek M., Syková E. Poly(L-lysine)-modified iron oxide nanoparticles for stem cell labeling, *Bioconjugate Chem.*, 19, 740–750 (2008)

Příloha č. 3:
Babič M., Horák D., Jendelová P., Glogarová K., Herynek V., Trchová M., Likavčanová K., Hájek M., Syková E.: Poly(N,N-dimethylacrylamide)-coated maghemite nanoparticles for stem cell labeling, *Bioconjugate Chem.*, 20, 283-294 (2009).

Příloha č. 4:
Horák D., Babič M., Jendelová P., Herynek V., Trchová M., Likavčanová K., Kapcalová M., Hájek M., Syková E.: Effect of different magnetic nanoparticle coatings on the efficiency of stem cell labeling, *J. Magn. Magn. Mater*, 321,. 1539-1547. (2009)

Příloha č. 5:
Horák D., Babič M., Macková H., Beneš M.J. Preparation and properties of magnetic nano- and microsized particles for biological and environmental separations, *J. Sep. Sci.* 30, 1751-1772 (2007)

Příloha č. 6:
Babič M., Horák D. Poly(*N*,*N*-dimethylacrylamide)-based microspheres prepared by heterogeneous polymerizations, *Macromol. Reac. Eng.* 1, 86-94,(2007)

Příloha č. 7:
Horák D., Syková P., Babič M., Jendelová P., Hájek M. Method of preparation of superparamagnetic nanoparticles based on iron oxides with modified surface and superparamagnetic nanoparticles obtained by such a method. *EP 1 991 503 81*, (2010)

Příloha č. 1

D-Mannose-Modified Iron Oxide Nanoparticles for Stem Cell Labeling

Daniel Horák,*[,†,‡] Michal Babič,[†,‡] Pavla Jendelová,[‡,§] Vít Herynek,[‡,||] Miroslava Trchová,[†] Zbyněk Pientka,[†] Emil Pollert,[⊥] Milan Hájek,[‡,||] and Eva Syková[‡,§]

Institute of Macromolecular Chemistry AS CR, Heyrovský Sq. 2, 162 06 Prague 6, Czech Republic, Center for Cell Therapy and Tissue Repair, Charles University, V Úvalu 84, 150 06 Prague 5, Czech Republic, Institute of Experimental Medicine AS CR, Víděnská 1083, 142 20 Prague 4, Czech Republic, Institute of Clinical and Experimental Medicine, Víděnská 1958/9, 140 21 Prague 4, Czech Republic, and Institute of Physics AS CR, Cukrovarnická 10, 162 53 Prague 6, Czech Republic
Received June 28, 2006; Revised Manuscript Received December 12, 2006

New surface-modified iron oxide nanoparticles were developed by precipitation of Fe(II) and Fe(III) salts with ammonium hydroxide according to two methods. In the first method, precipitation was done in the presence of D-mannose solution (in situ coating); the second method involved oxidation of precipitated magnetite with sodium hypochlorite followed by addition of D-mannose solution (postsynthesis coating). Selected nanoparticles were characterized by transmission electron microscopy (TEM), atomic force microscopy (AFM), elemental analysis, dynamic light scattering, infrared (IR), X-ray powder analysis, and ultrasonic spectrometry. While the first preparation method produced very fine nanoparticles ca. 2 nm in diameter, the second one yielded ca. 6 nm particles. Addition of D-mannose after synthesis did not affect the iron oxide particle size. UV−vis spectroscopy suggested that D-mannose suppresses the nonspecific sorption of serum proteins from DMEM culture medium on magnetic nanoparticles. Rat bone marrow stromal cells (rMSCs) were labeled with uncoated and D-mannose-modified iron oxide nanoparticles and with Endorem (Guerbet, France; control). Optical and transmission electron microscopy confirmed the presence of D-mannose-modified iron oxide nanoparticles inside the cells. D-Mannose-modified nanoparticles crossed the cell membranes and were internalized well by the cells. Relaxivity measurements of labeled cells in gelatin revealed very high relaxivities only for postsynthesis D-mannose-coated iron oxide nanoparticles.

INTRODUCTION

Regenerative medicine is a new field in which new treatment strategies are employed. One of the most promising approaches in preclinical research into brain or spinal cord injuries involves the use of cell therapies. After transplantation, the cells integrate into the host environment and respond to intrinsic signals (*1*). Stem cells administered via intravenous infusion migrate to the site of the injury and enter the nervous tissue through a more permeable or opened blood−brain barrier (*2*, *3*).

In the majority of experiments the donor cells are labeled before transplantation (retroviral labeling, bromodeoxyuridine, red fluorescent "cell tracker" PKH 26, green fluorescent protein [GFP]). After a certain time the host organism is sacrificed and evaluation of the position of the transplanted cells is carried out by microscopic analysis. This method, however, does not give data about the dynamics of the process or the movements of the transplanted stem cells in the host organism and requires sacrificing the host organism.

Initial findings confirmed that nanoparticles based on microcrystals of iron oxides could be observed by magnetic resonance imaging (MRI) in brain cells. The first reports (*4*, *5*) of imaging cell transplants labeled by superparamagnetic contrast agents in rat brains appeared in 1992. Different iron oxide nanoparticles coated by dextran were tested, and it was shown that MRI could be used for the dynamic in vivo tracking of labeled cells (*6*, *7*). The greatest progress was achieved with dextran-coated monocrystalline iron oxide nanoparticles (MION) (*8*, *9*), and the migration of MION-labeled oligodendrocyte progenitors was shown (*10*). Dendrimer-encapsulated superparamagnetic iron oxides were used for labeling and in vivo tracking of stem cells (*11*). Recently, immortalized cells from the MHP36 hippocampal cell line labeled in vitro with gadolinium rhodamine dextran were tracked in ischemia-damaged rat hippocampus in perfused brains ex vivo (*12*). Study of embryonic stem cells labeled in vitro with the magnetic resonance (MR) contrast agent Sinerem using a lipofection procedure successfully showed migration of labeled cells into focal cerebral ischemic lesions evoked by middle cerebral artery occlusion (*13*). Another suitable contrast agent for mesenchymal and embryonic stem cells is a commercially available contrast agent based on dextran-coated iron oxide nanoparticles, Endorem (Guerbet, France), which has also been approved as a blood pool agent for human use. Endorem-labeled cells migrated to a cortical photochemical lesion or a spinal cord compression lesion in rats (*14*−*16*).

Our aim is to design new iron oxide nanoparticles for stem cell labeling and investigate and control their surface and morphological characteristics. Surface modification of iron oxide is a key issue for enhancing its permeability through the cell membrane. Biocompatible polymers and targeting agents are therefore attached to the nanoparticle surface to prevent the nanoparticles from agglomeration, make them more biocompatible, and increase their nonspecific intracellular uptake (*17*). Our preliminary experiments with cationic (perchloric acid-stabilized) or anionic (tetramethylammonium hydroxide-stabilized) iron oxides showed that the colloids were unstable in the medium required for cell cultivation and that the particles aggregated. Similarly, dextran-coated iron oxide tended to adhere on the cell surface, while (diethylaminoethyl)dextran-

* To whom correspondence should be addressed. Phone: +420-296-809-260. Fax: +420-296-809-410. E-mail: horak@imc.cas.cz.
† Institute of Macromolecular Chemistry AS CR.
‡ Charles University.
§ Institute of Experimental Medicine AS CR.
|| Institute of Clinical and Experimental Medicine.
⊥ Institute of Physics AS CR.

10.1021/bc060186c CCC: $37.00
Published on Web 03/20/2007

coated particles hindered cell proliferation. Uptake of (carboxymethyl)dextran-coated ferrofluid by endocytosing cells was too low. In a continuation of the search for a suitable surface modification to enhance nanoparticle transport into the cells, D-mannose was selected as the cell surface is known to possess receptors for this molecule (*18*). Moreover, D-mannose-bound poly(2-hydroxyethyl methacrylate) hydrogels were found to support adhesion of keratinocytes (epidermal cells) and their subsequent cultivation without the presence of feeder cells (*19*).

EXPERIMENTAL SECTION

Materials. $FeCl_2 \cdot 4H_2O$, $FeCl_3 \cdot 6H_2O$, and D-mannose were purchased from Fluka (Buchs, Switzerland), sodium hypochlorite solution (NaClO) from Bochemie (Bohumín, Czech Republic), and sodium citrate dihydrate from Lachema (Brno, Czech Republic). All other reagent-grade chemicals were purchased from Aldrich (Milwaukee, WI) and used as received. The commercial contrast agent Endorem was provided by Guerbet (Roissy, France). Ultrapure Q water ultrafiltered on a Milli-Q Gradient A10 system (Millipore, Molsheim, France) was used for preparation of solutions.

In Situ Precipitation of Iron Oxide in D-Mannose Solution. Molday's procedure (*20*) for coating iron oxide nanoparticles with dextran was modified to prepare iron oxide nanoparticles in D-mannose solution. Briefly, 10 mL of 50 wt % D-mannose aqueous solution was mixed under stirring with 10 mL of a water solution containing 1.51 g of $FeCl_3 \cdot 6\ H_2O$ and 0.64 g of $FeCl_2 \cdot 4\ H_2O$; 15 mL of 7.5% NH_4OH solution was slowly added until pH 12 was reached, and the mixture was heated to 60 °C for 15 min. Large aggregates were destroyed by sonication (Ultrasonic Homogenizer 4710 Series, Cole-Palmer Instruments, at 40% output) for 5 min. To remove unreacted water-soluble salts and excessive D-mannose, particles were washed by dialysis using a Visking membrane (molecular weight cutoff 14 000; Carl Roth GmbH, Karlsruhe, Germany) against 2 L of water for 24 h at room temperature (the water was changed 5 times, 2 L each time) until pH 6 was reached. The volume of water was reduced by evaporation—dry residue: 80 mg of iron oxide/mL of colloid.

Preparation of Iron Oxide Nanoparticles and Postsynthesis Coating with D-Mannose. A solution of $FeCl_2$ (0.2 mol/L) and $FeCl_3$ (0.2 mol/L) in a 1:2 molar ratio was coprecipitated in an excess of 0.5 mol/L NH_4OH. After 15 min, the product was repeatedly separated in a magnetic field and washed with Q-water to reach peptization. The colloid was subsequently sonicated for 5 min (Ultrasonic Homogenizer 4710 Series, Cole-Palmer Instruments, 40% output) and oxidized with 5 wt % NaClO aqueous solution in the presence of 0.1 M sodium citrate solution. Washing and sonication procedures were then repeated. Finally, 20 wt % aqueous D-mannose solution was added to colloidal iron oxide (maghemite, γ-Fe_2O_3). The resulting product was washed three times with 10 mL of water after centrifugation at 14 000 rpm for 3 min (the colloid was so stable that it did not permit magnetic separation).

Characterization. The particle morphology and particle size distribution were examined by transmission electron microscopy (TEM; JEOL JEM 200 CX). An iron oxide nanoparticle dispersion in water was sprayed onto a grid with a carbon membrane. The number-average diameter was determined by measurement of at least 500 particles for each batch from microphotographs using the Atlas program (Tescan, Digital Microscopy Imaging, Brno, Czech Republic). The number-average (D_n) particle diameter was calculated as $D_n = \Sigma N_i D_i / \Sigma N_i$, where N_i is the number of particles with diameter D_i. Polydispersity PDI $= D_w/D_n$, where D_w is the weight-average particle diameter, $D_w = \Sigma N_i D_i^4 / \Sigma N_i D_i^3$. A multimode AFM Nanoscope IIIa (Digital Instruments, Santa Barbara, CA) was used to observe the nanoparticles in situ in tapping mode using OTESPA silicon cantilevers (Veeco Instruments, Dourdan, France) with a radius of 5 nm and oscillating at 245 kHz.

D-Mannose and iron oxide content was calculated from elemental analysis (Perkin-Elmer 2400 CHN) and from the iron content analyzed by atomic adsorption spectrometry (AAS Perkin-Elmer 3110) of an extract from a sample obtained with dilute HCl (1:1) at 80 °C for 1 h.

The hydrodynamic diameter (*z* average) and polydispersity as a measure of the distribution width were obtained by dynamic light scattering (DLS) with an Autosizer Lo-C (Malvern Instruments Ltd., Malvern, Great Britain).

The coating of D-mannose on the surface of the magnetic nanoparticles was investigated using a Fourier transformation infrared (FTIR) spectrometer (NICOLET IMPACT 400) in an H_2O-purged environment with a doped triglycine sulfate (DTGS) detector. The Golden Gate single attenuated total reflection (ATR) system (Specac Ltd., Orpington, Great Britain) was used to measure the spectra of powdered samples by an ATR spectroscopic technique over a wavelength range of 400−4000 cm^{-1}. Typical parameters used were as follows: 256 sample scans, resolution 4 cm^{-1}, Happ-Genzel apodization, KBr beamsplitter.

Differences in ultrasonic velocity between reference (water) and iron oxide colloid were monitored under the slow addition of various concentrations of D-mannose using an Ultrasound Spectrometer HR-US 102 (Ultrasonic Scientific, Dublin, Ireland). In a typical experiment, 1 mL of iron oxide colloid (18 mg of γ-Fe_2O_3/mL) was in the first cell and 1 mL of Q-water in the second cell. D-Mannose solution (1 mg of D-mannose/mL) was then simultaneously added in 10 μL aliquots to both cells with a Hamilton syringe.

X-ray powder diffraction using a Bruker D8 diffractometer (Cu Kα, Sol-X energy-dispersive detector) was used to determine the magnetite phase composition.

In protein adsorption experiments, 1 mL of the colloid with a concentration of 22 mg of iron oxide/mL was mixed with 1 mL of DMEM (Dulbecco's modified Eagle's medium)/10% FBS (fetal bovine serum) medium on a Vortex-T Genie-2 (Scientific Industries, Bohemia, USA) for 1 h; the liquid was separated from the solid by centrifugation and measured on a Perkin-Elmer Lambda 20 UV/vis spectrophotometer. An aqueous solution of DMEM/10% FBS medium (1/1 v/v) served as a standard.

Cell Cultures. To isolate rat bone marrow stromal cells (rMSCs), femurs were dissected from 4-week-old Wistar rats. The ends of the bones were cut, and the marrow was extruded with 5 mL of DMEM with L-glutamine (PAA, Pasching, Austria) using a needle and syringe. Marrow cells were plated in 80 cm^2 tissue culture flasks in DMEM/10% FBS with 100 U/mL penicillin and 100 U/mL streptomycin. After 24 h, the nonadherent cells were removed by replacing the medium. The medium was changed every 2−3 days as the cells grew to confluence. The cells were lifted by incubation with 0.25 wt % trypsin.

Transmission Electron Microscopy of Labeled Cells. For electron microscopic examination, rMSCs were fixed at 4 °C in 2.5% buffered glutaraldehyde for 1 h followed by 1% osmium tetroxide for 2 h. The cells were dehydrated in ascending concentrations of ethanol, immersed in propylene oxide, and embedded in Epon 812 resin (Agar Scientific Ltd., Standsted, England). The samples were cut in ultrathin sections (~60 nm), contrasted with 4% uranyl acetate and Reynold's lead citrate, and examined in a Philips Morgagni 268 electron microscope.

Quantitative Analysis of Labeled Cells. rMSCs were plated in duplicate on uncoated 6-well culture plates at a density of 10^5 cells/mm^2. Endorem or D-mannose-modified nanoparticles

Table 1. Cell Labeling with Surface-Modified and Unmodified Iron Oxide Nanoparticles and Their Characterization

run	D-mannose/γ-Fe_2O_3	D_n (nm)	PDI	percentage of labeled cells[a] (%)
Endorem				58.6
1[b]	7.3[d]	1.6	1.07	51.2[e]/82.3[f]
2	0	6.05	1.46	27.9
3[c]	1.3	5.9	1.39	49.1
4[c]	2.6	6.6	1.33	80.6
5[c]	4.1	6.4	1.26	51.3

[a] Average of 10 measurements. [b] In situ coating. [c] Postsynthesis coating. [d] D-Mannose/Fe_3O_4. [e] Diluted (0.02 mg of iron oxide/mL). [f] Undiluted (0.2 mg of iron oxide/mL) colloid.

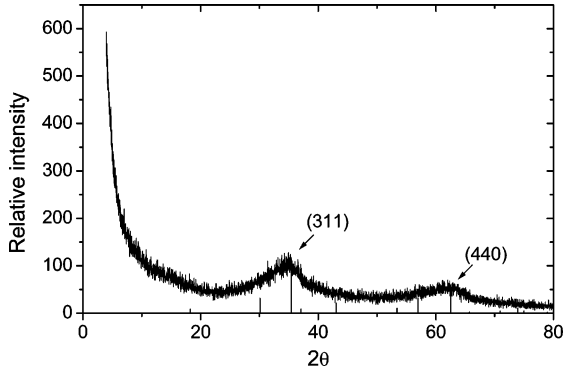

Figure 1. X-ray powder analysis of in situ D-mannose-coated magnetite nanoparticles No. 1. Vertical bars: Fe_3O_4 standard.

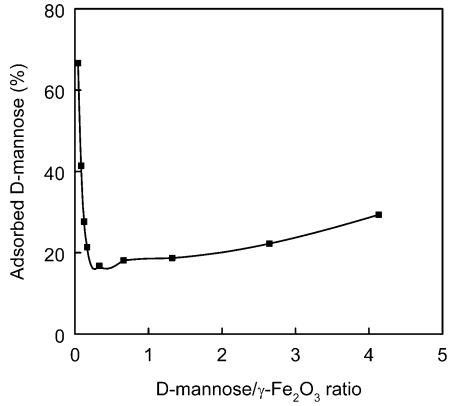

Figure 2. Dependence of the amount of D-mannose adsorbed from solution on the D-mannose/γ-Fe_2O_3 ratio.

were added to the culture medium (10 μL/mL) for 72 h. After the Endorem was washed out of the culture medium, the cells were fixed with 4% paraformaldehyde in 0.1 M PBS (phosphate-buffered saline) and stained for iron to produce ferric ferrocyanide (Prussian blue). Labeled and unlabeled cells were quantified using an inverted light microscope (Axiovert 200, Zeiss, Jena, Germany) by counting randomly five fields per well and two wells per each run. The cells captured on each image were manually labeled as Prussian blue positive or negative; the labeled cells were then counted, and the staining intensity of Prussian blue positive cells was evaluated using the Image analysis toolbox in Matlab 6.1 (The MathWorks, Natick, USA). Histograms of the intensity of the cytoplasmic staining were constructed.

MR Relaxometry and MR Imaging. Suspensions of contrast agents were prepared together with suspensions of cells labeled by Endorem or D-mannose-modified nanoparticles in 4% gelatin (Sigma, Czech Republic) and subjected to MR relaxometry. T_1 and T_2 relaxation times (which are responsible for contrast in T_1- and T_2-weighted MR images) were measured on a 0.5 T Bruker Minispec relaxometer. Relaxation time values were

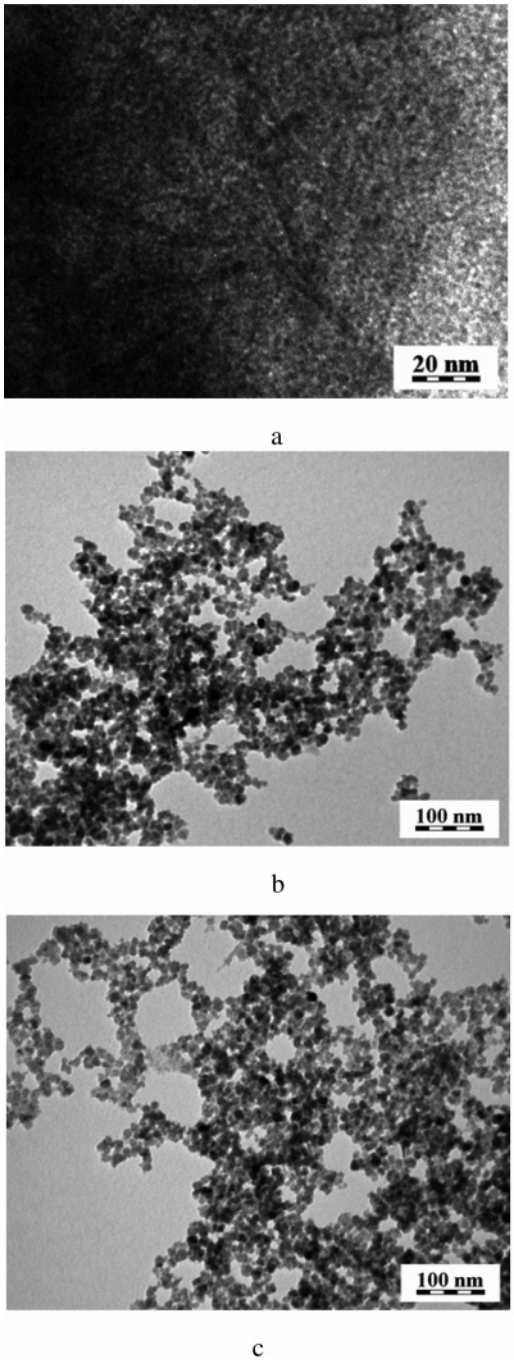

Figure 3. TEM images of in situ D-mannose-coated Fe_3O_4 particles (a; No. 1) and γ-Fe_2O_3 particles before (b; No. 2) and after modification with D-mannose (c; No. 3).

converted to relaxivities and, after deducting the contribution of pure gelatin, related to the actual iron concentration c, i.e., $r_1 = (1/T_1 - 1/T_{1gel})/c$ or $r_2 = (1/T_2 - 1/T_{2gel})/c$ in the case of contrast agent suspensions. In the case of samples containing labeled cells, the relaxivity was related, after deducting the contribution of unlabeled cells, to 10^6 cells in 1 mL.

Samples containing labeled cells (31 100 or 62 200 cells suspended in 0.5 mL of 4% gelatin) underwent MR imaging using a standard T_2-weighted turbospin echo sequence (effective echo time $T_E = 62.7$ ms, repetition time $T_R = 3000$ ms, matrix 256×256, slice thickness 1 mm, FOV = 35 mm). As a control, 62 000 unlabeled cells were suspended in 0.5 mL of 4% gelatin.

Iron Analysis. The amount of iron in the cells after mineralization was determined by spectrophotometry. Cell-containing samples were mineralized by addition of 5 mL of

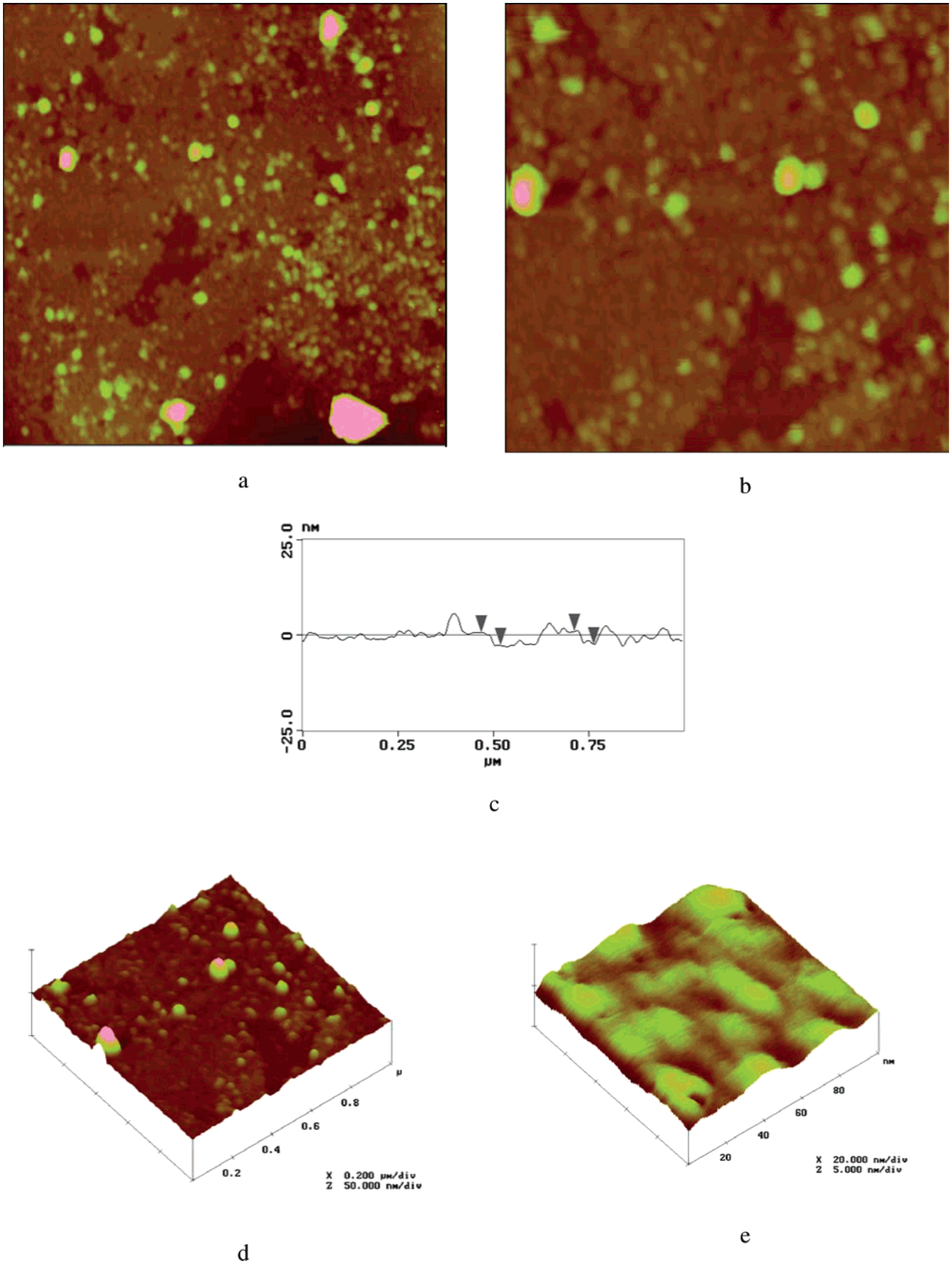

Figure 4. AFM images of D-mannose-stabilized magnetite particles No. 1: (a) overview and (b) detailed micrograph of the layer of magnetite particles on the thin carbon film on the TEM grid; (c) section analysis of the location shown in the micrograph—the cross-section line was horizontal and taken 150 nm from the bottom; (d) 3D image of the surface of the sample; (e) detailed 3D image of a location where no large particles were present. Scan size was (a) 2 or (b) 1 μm; the grayscale covers 50 nm.

HNO_3 and 1 mL of H_2O_2 in an ETHOS 900 microwave mineralizator (Millestone, Sydney, Australia). Deionized water was added to reach a total volume of 100 mL. The iron content was determined using a Spectroflame M120S apparatus (Spec-

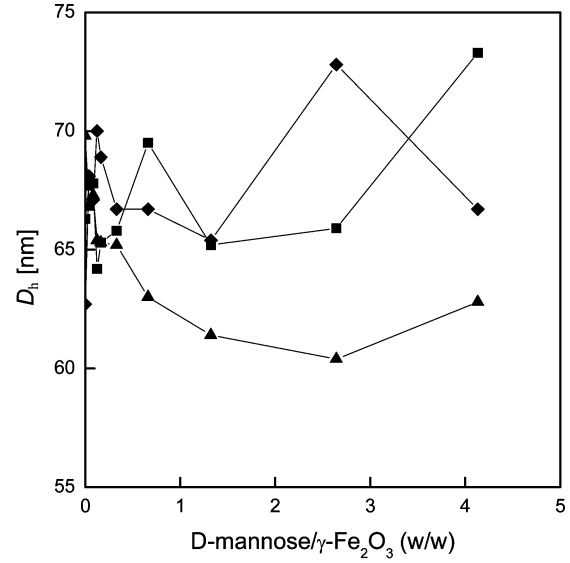

a

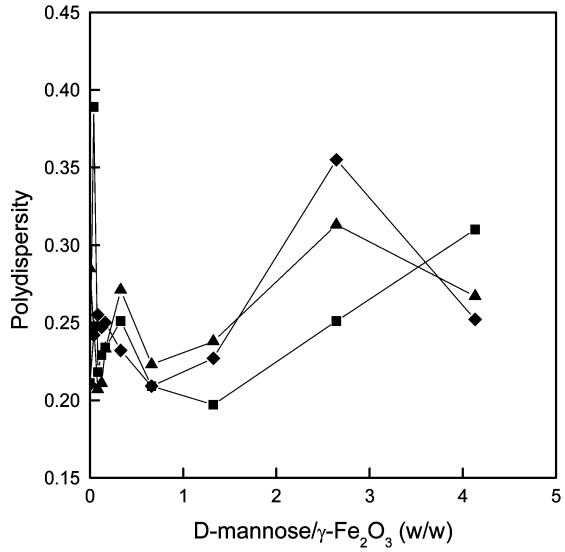

b

Figure 5. Dependence of (a) hydrodynamic particle diameter D_h and (b) polydispersity on the D-mannose/γ-Fe_2O_3 ratio, measured from dynamic light scattering experiments at three time points: day 1 (◆), 16 (■), and 51 (▲).

tro, Littleton, USA) calibrated with a standard Astasol solution (Analytika, Prague, Czech Republic). The measurements were repeated four times, and the average mean value was determined.

RESULTS AND DISCUSSION

Iron oxide colloids were prepared by two methods: (i) coprecipitation of Fe(II) and Fe(III) salts by ammonium in concentrated D-mannose solution (in situ coating) and (ii) precipitation followed by oxidation to maghemite (*21*) and slow addition of D-mannose solution (postsynthesis coating).

In Situ Precipitation of Iron Oxide in D-Mannose Solution. Magnetite was synthesized in a one-step process by alkaline coprecipitation of iron(II) and iron(III) precursors in an aqueous solution of D-mannose. This in situ coating, based on a modified Molday's procedure (*20*), is the easiest way to obtain surface-modified magnetic nanoparticles (run 1 in Table 1). The coating prevents particle aggregation. Elemental analysis of the resulting particles after washing revealed 58.9 wt % iron, 9.3 wt % carbon, and 2.6 wt % hydrogen, suggesting the conjugate contained about 30 wt % of D-mannose. D-Mannose is thought to be bound to the nanoparticles via a well-known coordination bond (chelate) formed between D-mannose and Fe(II) or Fe(III) on the surface of magnetite (*22*). The presence of magnetite

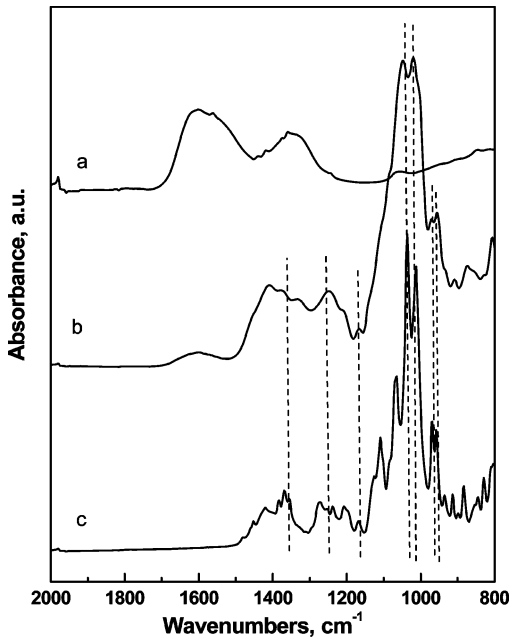

Figure 6. ATR FTIR spectra of magnetic particles before and after surface modification: spectrum of iron oxide (a) before modification and (b) after coating with D-mannose (run No. 4) and (c) spectrum of pure D-mannose.

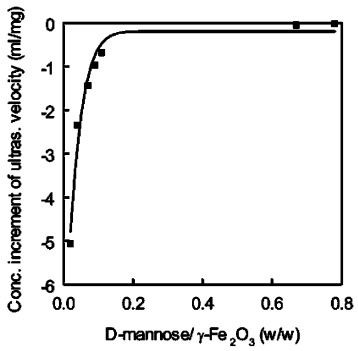

Figure 7. Dependence of the concentration increment of the ultrasonic velocity on the D-mannose/γ-Fe_2O_3 ratio.

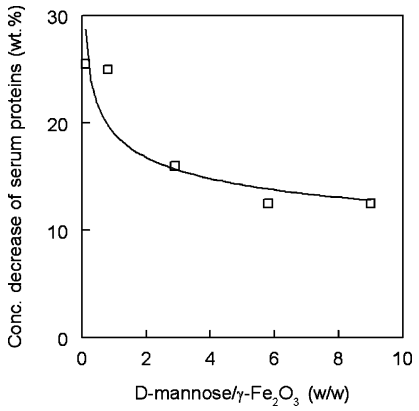

Figure 8. Effect of the D-mannose/iron oxide ratio on the decrease in serum protein concentration in culture medium, related to a standard (initial DMEM medium diluted with water 1/1 v/v), after protein sorption with D-mannose-modified iron oxide nanoparticles, as determined by UV spectrometry at 274 nm.

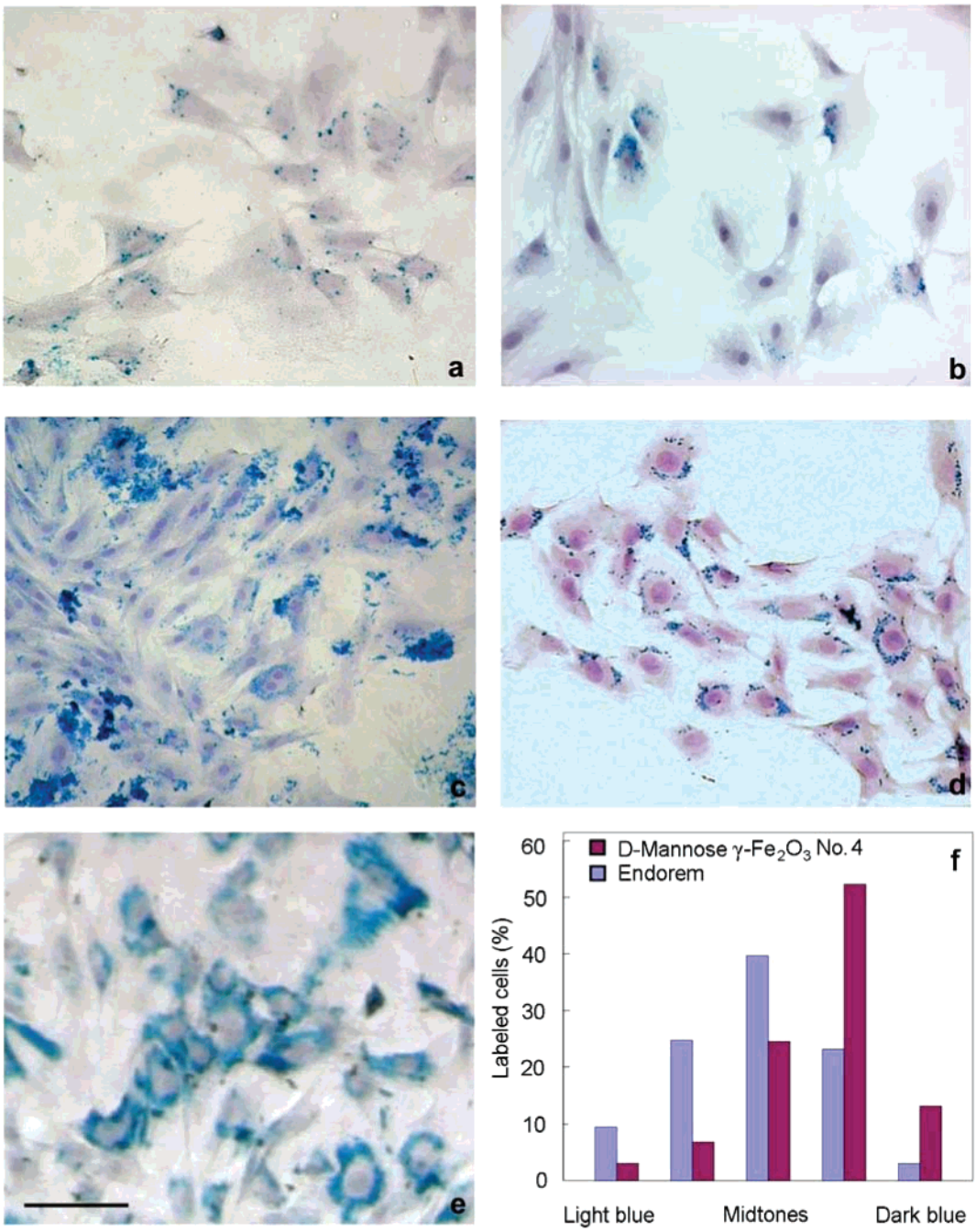

Figure 9. Microscopic observation of bone marrow stromal cells labeled with (a) Endorem (control experiment), (b) primary uncoated iron oxide nanoparticles No. 2, (c) undiluted (0.2 mg of iron oxide/mL) and (d) diluted (0.02 mg of iron oxide/mL) D-mannose-modified iron oxide nanoparticles No. 1, and (e) D-mannose-modified iron oxide nanoparticles No. 4. Scale bar: 50 μm. (f) Histograms showing the distribution of the intensity of Prussian blue staining in rMSCs labeled with Endorem or D-mannose-modified iron oxide nanoparticles No. 4.

spinel phase was confirmed by X-ray powder analysis (Figure 1). Due to the coating, only the most intense reflections (311 and 440) were observed. Significant broadening of the reflections indicates a very small particle size, in agreement with the TEM and AFM data.

Postsynthesis Iron Oxide Coating with D-Mannose. An iron oxide colloid was also obtained by a two-step procedure involving preparation of iron oxide cores in the first step (run 2 in Table 1) followed by addition of a stabilizer protecting them from aggregation and ensuring other necessary properties. Iron oxide cores were prepared by precipitation of iron salts, in particular $FeCl_2$ and $FeCl_3$, by increasing the pH followed by oxidation of the resulting magnetite with sodium hypochlorite. Oxidation resulted in maghemite (γ-Fe_2O_3), which is chemically stable and does not change its properties. This is in contrast to magnetite, which undergoes uncontrolled oxidation in the presence of oxygen. The conformation of the maghemite phase by Mössbauer spectroscopy and other magnetic properties were described in our previous report (*21*). D-Mannose was used as a stabilizer added to the primary iron oxide nanoparticles. The resulting particles were washed with water and freeze-dried to determine iron content and C and H content. Figure 2 summarizes the adsorption of D-mannose on the particles. At low D-mannose/γ-Fe_2O_3 ratios, the majority of D-mannose adsorbed to the particle surface; with increasing ratios, however, the efficiency of D-mannose adsorption initially decreased, then reached a plateau, and did not change further. It is interesting to note that after freeze drying, the product was rather voluminous without obvious agglomerates, indicating that D-mannose was attached to the iron oxide. Other supporting

evidence for such a claim is presented in the following sections; see the light scattering data, IR, and ultrasonic spectroscopy.

Nanoparticle Size Measurement by TEM, AFM, and DLS. The shapes and sizes of the magnetic nanoparticles obtained both in situ and by postsynthesis coating were observed using TEM. TEM images of the synthesized magnetic particles showed relatively high uniformity in terms of size and spherical shape. The presence of D-mannose during colloid preparation had a profound effect on the precipitation process. A TEM image of the iron oxide nanoparticles from run 1 (Figure 3a), precipitated in a concentrated D-mannose solution, shows their extremely fine size, ca. 2 nm (Table 1). This small size is due to the presence of D-mannose during precipitation, which interferes with the nucleation step of iron oxide formation, resulting in a smaller size compared with the postsynthesis method in which the coating is applied to the existing particles. The orientation of the magnetic particles is visible in Figure 3a. To confirm the TEM results, these particles were also studied by atomic force microscopy (AFM; Figure 4). A D-mannose layer containing iron oxide nanoparticles and many rounded, elevated structures (5−50 nm high) were noticeable in an AFM micrograph of magnetite particles spread across the carbon film on the TEM grid (Figure 4a). The surface structure is even more discernible at double magnification (Figure 4b), especially in the section analysis (Figure 4c). A plane lying 3.4−3.5 nm under the "surface" level can be distinguished in several places in Figure 4b. This plane is thought to be the surface of the carbon film, which is completely smooth as shown by AFM observation. The topography is illustrated in a 3D image of separated magnetite particles (Figure 4d) and in a detailed 3D image of a location where no large particles are present (Figure 4e). It can thus be concluded that the carbon film was covered with a 3.5-nm-thick layer of magnetite nanoparticles, which is in agreement with the TEM results. The layer contained rounded particle clusters 10−80 nm in size and many smaller particles (see the wrinkled surface in Figure 4e), which were otherwise not easily distinguishable. Some spots on the carbon film were not covered by the layer. Individual magnetite particles were not observed, indicating that all the iron oxide nanoparticles were stabilized with D-mannose. The iron oxide crystal growth was obviously retarded due to the unique structure of D-mannose present during precipitation. This is in contrast to the nanoparticles from run 3 (Table 1) obtained by postsynthesis coating of the primary bare colloid with D-mannose. TEM images of such particles (Figure 3c) showed no marked differences in either shape or size from uncoated iron oxide particles (2, Figure 3b). Their average diameter was 6−7 nm, and their polydispersity was PDI 1.3−1.5.

Iron oxide nanoparticle colloids obtained by postsynthesis coating were also investigated by dynamic light scattering measurements. The size calculated from DLS was ca. 10 times larger than that from TEM, mainly due to the effect of large particles on the hydrodynamic diameter. DLS provides the *z* average of the diameter, while TEM gives the number average. Figure 5 shows the dependence of hydrodynamic particle diameter and polydispersity on the D-mannose/γ-Fe_2O_3 ratio at three time points. D-Mannose-modified iron oxide particles were moderately larger than those that were uncoated due to the presence of a D-mannose hydrated shell. Moreover, Figure 5 documents the aging of the samples. Both the size and notably the polydispersity of uncoated iron oxide particles increased with storage time. This indicates aggregation of the particles without D-mannose protection. In contrast, the size and polydispersity of D-mannose-coated iron oxide nanoparticles did not dramatically change with time, implying that the particles do not aggregate (Figure 5). D-Mannose can thus be considered to be an effective stabilizer, preventing particle aggregation.

FTIR Spectra. The surface structure of the magnetic nanoparticles obtained by postsynthesis coating was analyzed by ATR FTIR spectroscopy. The infrared spectra of iron oxide before modification (run No. 2) and after coating with D-mannose (run 4) as well as the spectrum of pure D-mannose are shown in Figure 6a−c. Two broad bands of iron oxide dominate in the spectrum of the magnetic particles before modification (Figure 6a). The typical peaks of the C−H, C−O−H, and C−O−C vibrations of D-mannose (Figure 6c) are clearly distinguishable in the spectrum of the coated magnetic particles (Figure 6b). This indicates that the surface of the γ-Fe_2O_3 nanoparticles is covered with D-mannose (Figure 6). D-Mannose can be attached to iron oxide nanoparticles by the hydroxy group located on the C2 carbon in the axial position (*23*). This is a configuration specific to D-mannose, in contrast to, e.g., glucose and other common sugars that have this hydroxy group only in the equatorial position.

High-Resolution Ultrasonic Spectroscopy. Both uncoated and D-mannose-modified iron oxide nanoparticles were also characterized using high-resolution ultrasonic spectroscopy. Figure 7 shows the dependence of the concentration increment of the ultrasonic velocity on the amount of D-mannose added to the iron oxide. At low D-mannose/γ-Fe_2O_3 ratios, the ultrasonic velocity increased steeply with addition of D-mannose, which results from formation of a more ordered structure than in solution. After exceeding the critical D-mannose concentration, i.e., at a D-mannose/γ-Fe_2O_3 ratio > 0.065, the ultrasonic velocity almost did not change; that is, the excess D-mannose remained in solution. This indicates that until the critical D-mannose/γ-Fe_2O_3 ratio is reached, D-mannose molecules preferentially adsorb on the surface of iron oxide nanoparticles, forming a coat. Binding is obviously achieved via the D-mannose hydroxy group (*23*) at the carbon atom in position C2, possibly C3 and C4.

Protein Adsorption from Culture Medium. Adsorption of proteins from culture medium onto the iron oxide nanoparticles is an important tool for elucidating the transport of iron oxide in cells and also for nanoparticle coagulation. Iron oxide nanoparticles were thus mixed with serum-containing DMEM medium, the liquid separated by centrifugation, and the UV spectra of the supernatant recorded against a standard. The relative concentration decrease of serum proteins was correlated with the D-mannose/iron oxide ratio. Figure 8 indicates that even uncoated iron oxide nanoparticles adsorbed some serum proteins from the culture medium. With increasing D-mannose/iron oxide ratios used in the preparation of the nanoparticles, the amount of adsorbed serum proteins decreased. This is in agreement with published data on suppression of protein adsorption on saccharide-covered surfaces (*24*). The fact that D-mannose suppressed the nonspecific sorption of serum proteins on magnetic nanoparticles provides indirect evidence that the iron oxide particles were indeed coated with D-mannose. Moreover, it indicates that the cellular uptake mechanism of D-mannose-modified nanoparticles differs from that of PLL-modified ones (*25*).

Cell Labeling. Cell labeling with magnetic substances is an increasingly common method for in vivo cell monitoring and separation (*26*), as the labeled cells can be detected by magnetic resonance imaging. First, rat bone marrow stromal cells (rMSCs) labeled with either uncoated or surface-modified iron oxide nanoparticles were observed using an optical microscope. Cell labeling with Endorem served as a control (Figure 9a). Endorem has, however, a tendency to adhere to the surface of the cells, and it also sticks to the bottom of a vessel. Using the Prussian blue reaction, the cellular iron content was measured in rMSCs exposed to the nanoparticles.

Uncoated Iron Oxide. Uncoated iron oxide nanoparticles (No. 2) were used to label cells in order to elucidate the

importance of iron oxide modification/coating in subsequent experiments. Observation using an optical microscope with phase contrast revealed the iron oxide nanoparticles in rMSCs as dark dots. Cells in contact with the nanoparticles proliferated to some extent, and approximately 10% of the cells endocytosed the iron oxide (Figure 9b). Endocytosis might be explained by adsorption of proteins from the culture medium onto the iron oxide surface, subsequently inducing an undesirable partial coagulation of the particles. As the resulting coagulates were of a broad size distribution, only the smaller ones could penetrate the cells, whereas the larger ones were not internalized into the cells. In an attempt to increase the cell labeling, the iron oxide surface was modified with D-mannose.

D-Mannose-Modified Colloid. Modification of the colloid with D-mannose made the situation more complex, and differences were noted when the iron oxide was precipitated in a D-mannose solution compared to adding saccharide to the uncoated iron oxide nanoparticles. Cells in contact with D-mannose-modified nanoparticles No. 1 (prepared by precipitation in a concentrated D-mannose solution) proliferated well. If 10 μL of undiluted D-mannose-modified nanoparticles No. 1 was added to 1 mL of medium containing bone marrow stromal cells (to achieve a concentration of 0.2 mg of iron oxide/mL of medium), the nanoparticles were taken up by the cells (Figure 9c). A large percentage of cells was labeled (more than 80%; Table 1). However, some clumps of particles adhered to the surface of the cells and were difficult to wash out (Figure 9c). Thus, surface-bound iron oxide was indistinguishable from that internalized by the cells when observed by optical microscopy. The colloid was therefore diluted to concentrations of 0.1, 0.05, and 0.02 mg of iron oxide/mL of media. Improved results were already obtained at a concentration of 0.05 mg of iron oxide/mL, and at a concentration of 0.02 mg of iron oxide/mL, the cells were labeled with the nanoparticles without any iron oxide clusters adhering to the cell surface (Figure 9d); the percentage of labeled cells was still greater than 50% (Table 1). Compared with Endorem (0.11 mg of Fe_3O_4/mL), a lower concentration of D-mannose-modified iron oxide nanoparticles No. 1 was sufficient to label the cells. The very good ability of the cells to internalize the colloid can be explained by the extremely small size of the particles. Minimizing particle size was important for the ease of cellular internalization, but it reduced magnetic susceptibility at the same time. Moreover, colloid No. 1 was sensitive to aging; the particles coagulated within several days of storage. Modification by the postsynthesis coating of iron oxide nanoparticles with D-mannose was therefore developed. Table 1 summarizes the results of cell labeling experiments indicating that the degree of cell labeling depended on the D-mannose/γ-Fe_2O_3 ratio. The ratio 2.6/1 (colloid No. 4) can be considered as optimal, with ca. 80% of the cells being labeled. At a higher ratio (4.1/1; run 5) the particles adhered to the cell surface and the uptake of the nanoparticles did not significantly increase. This correlates with the results presented in Figure 2, which also documents that there is a limit to the ability of γ-Fe_2O_3 particles to adsorb D-mannose. Moreover, a high concentration of D-mannose results in an increased viscosity, promoting particle aggregation and adhesion to the cell surface. The mechanism responsible for the cellular internalization of ca. 10 nm nanoparticles is thought to be receptor-mediated endocytosis and/or diffusion through the cell membrane (*27*).

Image analysis tools were used to evaluate not only the percentage of labeled cells but also the intensity of Prussian blue staining. The resulting histograms (Figure 9f) show the distribution of the intensity of Prussian blue staining in rMSCs. In Endorem-labeled cells, the majority of cells (88%) were moderately stained, while in D-mannose-coated iron oxide No. 4 labeled cells, the staining intensity generally (90%) ranged from moderate to strong. These results confirm that the cells labeled with D-mannose-coated nanoparticles No. 4 contained a higher amount of iron per cell than did the cells with dextran-coated iron oxide.

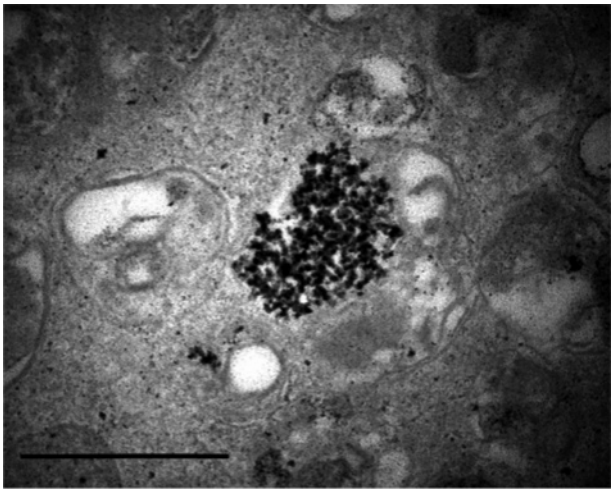

Figure 10. TEM micrograph of rMSCs labeled with D-mannose-modified iron oxide nanoparticles No. 4. Scale bar: 500 nm.

Table 2. r_1 and r_2 Relaxivities of D-mannose-coated Iron Oxide Nanoparticles No. 4 and Endorem and of rMSCs Labeled by These Contrast Agents

	phantoms containing a suspension of pure contrast agent (s^{-1}/mM Fe)		phantoms containing labeled cells (s^{-1}/million of cells/mL)	
	r_1	r_2	r_1	r_2
D-mannose-coated iron oxide nanoparticles	7.31 ± 0.11	140.4 ± 1.4	0.32 ± 0.04	12.1 ± 0.9
Endorem	19.8 ± 1.5	127 ± 9	0.18 ± 0.06	1.24 ± 0.15

Transmission Electron Microscopy of Labeled Cells. Light microscopy revealed that D-mannose-modified nanoparticles were distributed rather randomly in the cytoplasm. To further confirm that D-mannose-coated iron oxide nanoparticles were internalized by the cells rather than simply bound to the surface of the cells and visualize the location of the nanoparticles inside the cells after internalization, TEM images were taken. A TEM image (Figure 10) shows clusters of nanoparticles (No. 4) as black dots scattered in the cell cytoplasm. Cell membrane-bound nanoparticle clusters — as a result of endocytosis — were not detected. Since a highly D-mannose-specific and energy-independent transporter has been found on the surface of the majority of mammalian cells, D-mannose-coated nanoparticles are most likely transported into the cells via this mannose transporter.

MR Relaxometry. MR relaxometry enables quantification of relaxation times (and relaxivities), which are responsible for contrast enhancement in T_1- and T_2-weighted MR images. Table 2 compares the relaxivities of gelatin samples containing suspensions of two contrast agents, D-mannose-coated iron oxide nanoparticles No. 4 and commercially available Endorem, and the relaxivities of gelatin samples containing cells labeled by these contrast agents. A higher r_1 relaxivity was observed for Endorem and a higher r_2 relaxivity for D-mannose-coated iron oxide nanoparticles. Both r_1 and r_2 were higher in the case of D-mannose-coated iron oxide-labeled cells (in the case of r_2 almost 10-fold) than for Endorem-labeled cells. We hypothesize that the higher relaxivity of the D-mannose-coated iron oxide nanoparticles is responsible for not only such a huge increase in relaxivity but also the substantially higher internalization of D-mannose-coated iron oxide nanoparticles as the r_1 relaxivity

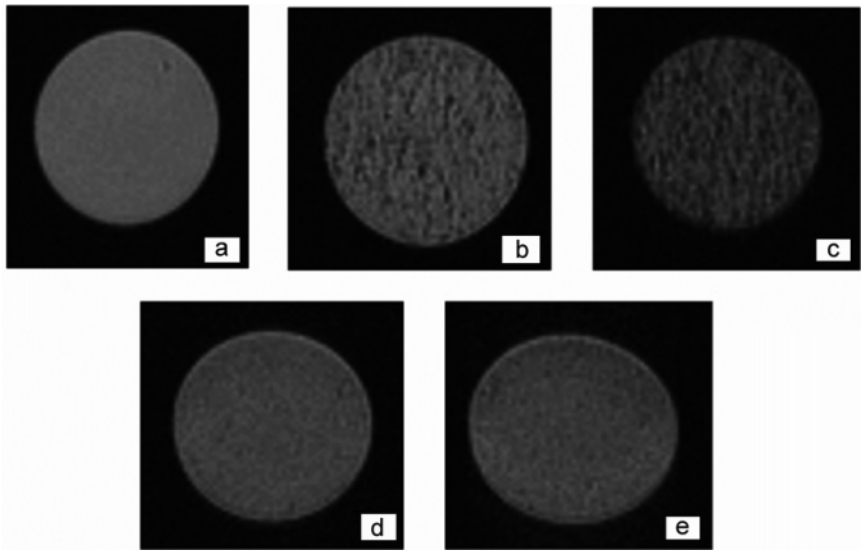

Figure 11. T_2-weighted MR images of gelatin phantoms containing (a) unlabeled cells, (b) 31 100 or (c) 62 200 cells labeled with D-mannose-coated iron oxide nanoparticles, and, for comparison, (d) 31 100 and (e) 62 200 cells labeled with Endorem.

of the D-mannose-coated iron oxide-labeled cells is also higher than the r_1 of Endorem-labeled cells, although D-mannose-coated iron oxide displayed a lower r_1 relaxivity than did Endorem. This hypothesis was confirmed by iron analysis of cell suspensions; the average amount of iron as determined by spectrophotometry after mineralization was 51.7 pg of iron per cell for D-mannose-coated iron oxide nanoparticles and 14.6 pg of iron per cell for Endorem-labeled cells.

These highly promising results were obtained with iron oxide nanoparticles coated by the postsynthesis method. Particles precipitated in situ in D-mannose solution did not display improved relaxivity, probably because they were too small, as reflected by the very low relaxivity of gelatin samples containing labeled cells: $r_2 = 0.114 \pm 0.006\ s^{-1}/10^6$ cells/mL. To mimic signal behavior in the tissue, in vitro imaging of labeled cells was performed. Phantoms with different numbers of rat MSCs labeled by Endorem or by D-mannose-coated iron oxide nanoparticles were prepared and suspended in gelatin. Unlabeled cells (Figure 11a) did not change the signal at all. Cells labeled with D-mannose-coated nanoparticles (Figure 11b,c) produced a visibly greater signal decrease than did Endorem-labeled cells (Figure 11d,e). These detectable changes in the MR signal correspond to 1.17 (Figure 11b,d) or 2.34 (Figure 11c,e) cells per image voxel, depending on the concentration of cells in the phantom. Since it was shown (*14*) that MSCs (300 000 cells in 5 μL) labeled with Endorem and implanted into the rat brain were clearly visible on T_2-weighted images, we believe that use of this novel cellular contrast agent would enable detection of very small numbers of labeled cells.

CONCLUSION

Iron oxide nanoparticles were produced by coprecipitation of Fe(II) and Fe(III) salts in an alkaline medium. The surface of the magnetic nanoparticles was modified by D-mannose, and the particles were characterized by several methods to confirm that D-mannose successfully coated the particles. The intracellular uptake of the D-mannose-coated nanoparticles by rMSCs was confirmed by both optical and transmission electron microscopy. Relaxometric measurements revealed that only postsynthesis-coated nanoparticles possessed very high r_2 relaxivity. D-Mannose-modified iron oxide nanoparticles are a promising tool for labeling living cells, particularly stem cells, for diagnostic and therapeutic applications in cell-based therapies due to their high relaxivities, which are responsible for contrast in MR imaging, and their easy internalization by cells. They can prove useful in human and veterinary medicine, biology, and microbiology for monitoring the fate of cells transplanted into a host organism, including their in vivo migration, localization, and differentiation, by means of noninvasive magnetic resonance.

ACKNOWLEDGMENT

The authors gratefully acknowledge support from the Grant Agency of the Czech Republic (grants 525/05/0311 and 309/06/1594), the Center for Cell Therapy and Tissue Repair (grant 1M0021620803), the Grant Agency of AS CR (grant KAN201110651), and the EC-FP6 project DiMI (LSHB-CT-2005-512146).

LITERATURE CITED

(1) Rosario, C. M., Yandava, B. D., Kosaras, B., Zurakowski, D., Sidman, R. L., and Snyder, E. Y. (1997) Differentiation of engrafted multipotent neural progenitors towards replacement of missing granule neurons in meander tail cerebellum may help determine the locus of mutant gene action. *Development 124*, 4213−24.

(2) Lu, D., Mahmood, A., Wang, L., Li, Y., Lu, M., and Chopp, M. (2001) Adult bone marrow stromal cells administered intravenously to rats after traumatic brain injury migrate into brain and improve neurological outcome. *NeuroReport 12*, 559−63.

(3) Nakano, K., Migita, M., Mochizuki, H., and Shimada, T. (2001) Differentiation of transplanted bone marrow cells in the adult mouse brain. *Transplantation 71*, 1735−40.

(4) Hawrylak, N., Ghosh, P., Broadus, J., Schlueter, C., Greenough, W. T., and Lauterbur, P. C. (1993) Nuclear magnetic resonance (NMR) imaging of iron oxide-labeled neural transplants. *Exp. Neurol. 121*, 81−92.

(5) Norman, A. B., Thomas, S. R., Pratt, R. G., Lu, S. Y., and Norgren, R. B. (1992) Magnetic resonance imaging of neural transplants in rat brain using a superparamagnetic contrast agent. *Brain Res. 594*, 279−83.

(6) Yeh, T., Zhang, W., Ildstad, S. T., and Ho, C. (1993) Intracellular labeling of T-cells with superparamagnetic contrast agents. *Magn. Reson. Med. 30*, 617−25.

(7) Yeh, T., Zhang, W., Ildstad, S. T., and Ho, C. (1995) In vivo dynamic MRI tracking of rat T-cells labeled with superparamagnetic iron-oxide particles. *Magn. Reson. Med. 33*, 200−208.

(8) Bulte, J. W., Brooks, R. A., Moskowitz, B. M., Bryant, L. H. J., and Frank, J. A. (1999) Relaxometry and magnetometry of the MR contrast agent MION-46L. *Magn. Reson. Med. 42*, 379−84.

(9) Shen, T., Weissleder, R., Papisov, M., Bogdanov, A. J., and Brady, T. J. (1993) Monocrystalline iron oxide nanocompounds (MION): physicochemical properties. *Magn. Reson. Med. 29*, 599−604.

(10) Bulte, J. W., Zhang, S. C., van Gelderen, P., Herynek, V., Jordan, E. K., Duncan, I. D., and Frank, J. A. (1999) Neurotransplantation of magnetically labeled oligodendrocyte progenitors: magnetic resonance tracking of cell migration and myelination. *Proc. Natl. Acad. Sci. U.S.A. 96*, 15256−61.

(11) Bulte, J. W., Douglas, T., Witwer, B., Zhang, S. C., Strable, E., Lewis, B. K., Zywicke, H., Miller, B., van Gelderen, P., Moskowitz, B. M., Duncan, I. D., and Frank, J. A. (2001) Magnetodendrimers allow endosomal magnetic labeling and in vivo tracking of stem cells. *Nat. Biotechnol. 19*, 1141−7.

(12) Modo, M., Cash, D., Mellodew, K., Williams, S. C. R., Fraser, S. E., Meade, T. J., Price, J., and Hodges, H. (2002) Tracking transplanted stem cell migration using bifunctional, contrast agent-enhanced, magnetic resonance imaging. *Neuroimage 17*, 803−811.

(13) Hoehn, M., Kustermann, E., Blunk, J., Wiedermann, D., Trapp, T., Wecker, S., Focking, M., Arnold, H., Hescheler, J., Fleischmann, B. K., Schwindt, W., and Buhrle, C. (2002) Monitoring of implanted stem cell migration in vivo: A highly resolved in vivo magnetic resonance imaging investigation of experimental stroke in rat. *Proc. Natl. Acad. Sci. U.S.A. 99*, 16267−72.

(14) Jendelová, P., Herynek, V., De Croos, J., Glogarová, K., Andersson, B., Hájek, M., and Syková, E. (2003) Imaging the fate of implanted bone marrow stromal cells labeled with superparamagnetic nanoparticles. *Magn. Reson. Med. 50*, 767−76.

(15) Jendelová, P., Herynek, V., Urdzikova, L., Glogarová, K., Kroupová, J., Bryja, V., Burian, M., Hájek, M., and Syková, E. (2004) MR tracking of transplanted bone marrow and embryonic stem cells labeled by iron oxide nanoparticles in rat brain and spinal cord. *J. Neurosci. Res. 76*, 232−43.

(16) Syková, E., Urdziková, L., Jendelová, P., Burian, M., Glogarová, K., and Hájek, M. (2005) Bone marrow cells - a tool for spinal cord injury repair. *Exp. Neurol. 193*, 261−2.

(17) Zhang, Y., and Zhang, J. (2005) Surface modification of monodisperse magnetite nanoparticle for improved intracellular uptake to breast cancer cells. *J. Colloid Interface Sci. 283*, 352−7.

(18) Zhang, J., Zhu, J., Bu, X., Cushion, M., Kinane, T. B., Avraham, H., and Koziel, H. (2005) Cdc42 and RhoB activation are required for mannose receptor-mediated phagocytosis by human alveolar macrophages. *Mol. Biol. Cell 16*, 824−34.

(19) Labský, J. (2003) Binding of D-mannose to poly(2-hydroxyethyl methacrylate) hydrogels by azo coupling. *Biomaterials 24*, 4031−6.

(20) Molday, R. S. (1984) Magnetic iron-dextran microspheres. U.S. Patent 4,452,773.

(21) Pollert, E., Knížek, K., Maryšsko, M., Závěta, K., Lančok, A., Boháček, J., Horák, D., and Babič, M. (2006) Magnetic poly(glycidyl methacrylate) microspheres containing maghemite prepared by emulsion polymerization. *J. Magn. Magn. Mater. 306*, 241−247.

(22) Geetha, K., Raghavan, M. S. S., Kulshreshtha, S. K., Sasikala, R., and Rao, C. P. (1995) Transition-metal saccharide chemistry-synthesis, spectroscopy, electrochemistry and magnetic-susceptibility studies of iron(III) complexes of monosaccharides and disaccharides. *Carbohydr. Res. 271*, 163−175.

(23) Koshikawa, M. K., and Hori, T. (2000) Adsorption selectivity of sugars toward hydrous zirconium(IV) and hydrous iron(III) oxide surfaces. *Phys. Chem. Chem. Phys. 2*, 1497−502.

(24) Zhu, J., and Marchard, R. E. (2006) Dendritic saccharide surfactant polymers as antifouling interface materials to reduce platelet adhesion. *Biomacromolecules 7*, 1036−41.

(25) Horák, D., Babič, M., Trchová, M., Jendelová, P., Glogarová, K., Lesný, P., Herynek, V., Hájek, M., and Syková, E. Poly(L-lysine)-modified iron oxide nanoparticles for stem cell labeling. *Bioconjugate Chem.*, in preparation.

(26) Olsvik, O., Popovic, T., Skjerve, E., Cudjoe, K. S., Hornes, E., Ugelstad, J., and Uhlen, M. (1994) Magnetic separation techniques in diagnostic microbiology. *Clin. Microbiol. Rev. 7*, 43−54.

(27) Dormer, K., Seeney, C., Lewelling, K., Lian, G., Gibson, D., and Johnson, M. (2005) Epithelial internalization of superparamagnetic nanoparticles and response to external magnetic field. *Biomaterials 24*, 2061−72.

BC060186C

Příloha č. 2

Poly(L-lysine)-Modified Iron Oxide Nanoparticles for Stem Cell Labeling

Michal Babič,[†,‡] Daniel Horák,[*,†,‡] Miroslava Trchová,[†] Pavla Jendelová,[‡,§] Kateřina Glogarová,[§] Petr Lesný,[‡,§] Vít Herynek,[‡,||] Milan Hájek,[‡,||] and Eva Syková[‡,§]

Institute of Macromolecular Chemistry, v. v. i., Academy of Sciences of the Czech Republic, Heyrovský Sq. 2, 162 06 Prague 6, Czech Republic, Center for Cell Therapy and Tissue Repair, Charles University, V Úvalu 84, 150 06 Prague 5, Czech Republic, Institute of Experimental Medicine, v. v. i., Academy of Sciences of the Czech Republic, Vídeňská 1083, 142 20 Prague 4, Czech Republic, and Institute of Clinical and Experimental Medicine, Vídeňská 1958/9, 140 21 Prague 4, Czech Republic. Received November 5, 2007; Revised Manuscript Received January 4, 2008

New surface-modified iron oxide nanoparticles were developed by precipitation of Fe(II) and Fe(III) salts with ammonium hydroxide and oxidation of the resulting magnetite with sodium hypochlorite, followed by the addition of poly(L-lysine) (PLL) solution. PLL of several molecular weights ranging from 146 (L-lysine) to 579 000 was tested as a coating to boost the intracellular uptake of the nanoparticles. The nanoparticles were characterized by TEM, dynamic light scattering, FTIR, and ultrasonic spectrometry. TEM revealed that the particles were ca. 6 nm in diameter, while FTIR showed that their surfaces were well-coated with PLL. The interaction of PLL-modified iron oxide nanoparticles with DMEM culture medium was verified by UV–vis spectroscopy. Rat bone marrow stromal cells (rMSCs) and human mesenchymal stem cells (hMSC) were labeled with PLL-modified iron oxide nanoparticles or with Endorem (control). Optical microscopy and TEM confirmed the presence of PLL-modified iron oxide nanoparticles inside the cells. Cellular uptake was very high (more than 92%) for PLL-modified nanoparticles that were coated with PLL (molecular weight 388 00) at a concentration of 0.02 mg PLL per milliliter of colloid. The cellular uptake of PLL-modified iron oxide was facilitated by its interaction with the negatively charged cell surface and subsequent endosomolytic uptake. The relaxivity of rMSCs labeled with PLL-modified iron oxide and the amount of iron in the cells were determined. PLL-modified iron oxide-labeled rMSCs were imaged *in vitro* and *in vivo* after intracerebral grafting into the contralateral hemisphere of the adult rat brain. The implanted cells were visible on magnetic resonance (MR) images as a hypointense area at the injection site and in the lesion. In comparison with Endorem, nanoparticles modified with PLL of an optimum molecular weight demonstrated a higher efficiency of intracellular uptake by MSC cells.

INTRODUCTION

Superparamagnetic iron oxide nanoparticles have been widely used for numerous *in vitro* and *in vivo* biomedical applications (*1*). Such applications exploit two major advantages of magnetic iron oxides: their low toxicity for humans (*2*) and their outstanding magnetic properties, which allow the targeting of drugs to a tumor area through external magnetic fields (*3*). Most *in vitro* applications have focused on immunoassays (*4, 5*), the detection and separation of cells, viruses (*6*), hormones (*7, 8*), oligonucleotides (*9*), DNA (*10*) and proteins (*11*). *In vivo* applications have concentrated on cell and tissue engineering, including cell tagging, tracking, and imaging (*12*) (magnetic resonance imaging, MRI); targeted drug delivery (*13, 14*); gene delivery systems and gene therapy (*15*); as well as targeted hyperthermia of cancers (*16*), tissue repair, and the detoxification of biological fluids (*17*). MRI makes use of the fact that magnetic nanoparticles generate a magnetic field and thus influence their immediate vicinity (*18*). In these applications, there is a growing need for the highly specific, efficient, and rapid internalization of nanoparticles into specific target cells, but this is severely limited by several factors (*19*): (i) nanoparticle aggregation (nanoparticles have a large surface/volume ratio and tend to agglomerate); (ii) the short half-life of the particles in blood circulation (when nanoparticles agglomerate, or adsorb plasma proteins, they are quickly eliminated from the bloodstream by macrophages of the mononuclear phagocyte system before they can reach the target cells); (iii) the low efficiency of the intracellular uptake of nanoparticles; and (iv) nonspecific targeting. Biocompatible polymers and targeting agents are therefore attached to the nanoparticle surface to prevent agglomeration, to make the nanoparticles more biocompatible, and to increase their nonspecific intracellular uptake (*20, 21*). All applications require that the nanoparticles have high magnetization values and a size smaller than 100 nm, with a narrow particle size distribution, so that the particles have uniform physical and chemical properties. Compared with paramagnetics, superparamagnetic iron oxide particles have higher molar relaxivities, and, when used as blood pool and tissue-specific agents, may offer advantages at low concentrations (*22*). The nature of the surface coating on the nanoparticles not only determines the overall size of the colloid, but also plays a significant role in the biokinetics and biodistribution of the nanoparticles in the body. Various biological molecules such as antibodies, proteins, targeting ligands, and so forth may also be bound to the nanoparticle surface to make the particles target-specific.

Since the introduction of particular contrast agents in MRI use in 1987, most superparamagnetic iron oxides (SPIO) and ultrasmall superparamegnetic iron oxides (USPIO) agents, taken up by macrophages, have been prepared using dextran or other types of polymer coatings to achieve good dispersion in water

* Corresponding author. Tel.: +420-296-809-260; Fax: +420-296-809-410; E-mail: horak@imc.cas.cz.

† Institute of Macromolecular Chemistry, v. v. i., Academy of Sciences of the Czech Republic.

‡ Center for Cell Therapy and Tissue Repair.

§ Institute of Experimental Medicine, v. v. i., Academy of Sciences of the Czech Republic.

|| Institute of Clinical and Experimental Medicine.

10.1021/bc700410z CCC: $40.75
Published on Web 02/21/2008

and selectivity (*23*). Dextran-coated nanoparticles, however, do not show sufficient cellular uptake to enable cell tracking, probably because of a relatively inefficient fluid-phase endocytosis pathway. Polymer coatings significantly increase the particle size, which may affect their penetration and metabolic clearance rate in the body. A few recent papers have reported the use of nonpolymer-coated superparamagnetic nanoparticle dispersions in MR imaging (*24*). They were prepared in the water phase and stabilized, e.g., by citrate (*25*) or tetramethylammonium hydroxide (*24*), providing some advantages over those that require additional polymer protection for stabilization. Nanoparticles without a polymer coating have a much smaller size for distinct biodistribution and metabolic clearance profile than conventional polymer-coated-particles. It is, however, not clear whether these particles can be taken up by cells.

Stem cells are the body's master cells and have a unique ability to renew and give rise to other specialized cell types for the development of a tissue (*26*). Cell transplantation is a powerful treatment method for many common diseases, including brain and spinal cord injury; however, current experiments with stem cells do not give information about the behavior of the transplanted cells in the host organism *in vivo*, especially about their migration and fate within the target structures and their potential neoplastic growth. The lack of these data represents a serious obstacle for the clinical use of cell therapy. Human medicine would benefit from the labeling of implanted stem cells and the use of noninvasive methods to image the labeled cells after implantation. Superparamagnetic particles coupled to the cells could target these cells to the desired site in the body.

The preparation of stable iron oxide colloids is not easy. The first paper of this series was focused on the labeling of stem cells with iron oxide nanoparticles coated with D-mannose (*27*). The objective of the present study was to investigate the use of poly(L-lysine) (PLL), which is commonly used to enhance cell adhesion to the surface of a culture dish in *in vitro* cell cultivation, as a prospective vehicle for iron oxide nanoparticle transport into cells. The endocytosis behavior of PLL-modified particles was determined using mesenchymal stem cells (MSCs) and compared with that of control and uncoated superparamagnetic iron oxide nanoparticles.

EXPERIMENTAL SECTION

Materials. $FeCl_2 \cdot 4H_2O$ and $FeCl_3 \cdot 6H_2O$ were purchased from Fluka (Buchs, Switzerland), sodium hypochlorite solution (NaOCl) from Bochemie (Bohumín, Czech Republic), and sodium citrate dihydrate from Lachema (Brno, Czech Republic). All other reagent-grade chemicals were purchased from Aldrich (Milwaukee, WI, USA) and used as received. L-Lysine (LL) and poly(L-lysine) (PLL) hydrobromide (M_w = 9200; 58 900; 93 800; 388 100; and 579 000) and gelatin were from Sigma (St. Louis, MO, USA) and the commercial contrast agent Endorem from Guerbet (Roissy, France). Ultrapure Q water ultrafiltered on a Milli-Q Gradient A10 system (Millipore, Molsheim, France) was used for the preparation of solutions.

Preparation of Uncoated Iron Oxide Nanoparticles and their Treatment with Poly(L-lysine) or L-Lysine. In a typical experiment, 12 mL of 0.2 M $FeCl_3$ aqueous solution was mixed with 12 mL of 0.5 M NH_4OH solution (less than an equimolar amount) under sonication (Sonicator W-385; Heat Systems-Ultrasonics, Inc., Farmingdale, NY, USA) at laboratory temperature for 2 min to form colloid $Fe(OH)_3$. Then, 6 mL of aqueous 0.2 M $FeCl_2$ was added under sonication and the mixture poured into 36 mL of 0.5 M NH_4OH aqueous solution. The resulting magnetite coagulate was left to grow for 15 min, the magnetically separated and repeatedly (7–10×) washed (peptized) with Q-water to remove all impurities (including NH_4Cl) remaining after the synthesis. Finally, 1.5 mL of 0.1 M sodium citrate was added under sonication, and the magnetite was oxidized by the slow addition of 1 mL of 5% sodium hypochlorite solution to the maghemite to enhance the redox stability. The above-described washing procedure was repeated to yield the primary colloid. 0.2 mL of aqueous L-lysine (LL) or poly(L-lysine) solution (concentration 1 mg/mL) was added dropwise with stirring to 10 mL of primary iron oxide colloid, diluted to a concentration of 2.2 mg iron oxide/mL. The obtained mixture was sonicated for 5 min and used in experiments.

Particle Characterization. The morphology of the colloids was observed by transmission electron microscopy (TEM) using a JEOL JEM 200 CX. Particle size distributions were obtained using Atlas image analysis software (Tescan, Brno, Czech Republic) (*27*). For the measurements, a drop of a dilute dispersion was spread on a carbon-coated copper grid, and the grid was air-dried at room temperature before viewing under the microscope. The particle size and distribution were determined by the measurement of at least 300 particles for each sample. Two types of mean particle size were calculated: the number-average particle size (D_n) and the weight-average particle size (D_w; $D_n = \Sigma D_i/N$ and $D_w = \Sigma D_i^4/\Sigma D_i^3$, where N is the number of particles). The particle size distribution was characterized by the polydispersity index (PDI = D_w/D_n). Moreover, the hydrodynamic diameter (*z*-average), polydispersity (from 0 - monodisperse particles - to 1 - polydisperse particles) from the cumulative analysis of time correlation functions, and the surface zeta potential were determined by dynamic light scattering (DLS) using an Autosizer Lo-C (Malvern Instruments Ltd., Malvern, Great Britain).

The PLL coating on the surface of the magnetic nanoparticles was examined using a Thermo Nicolet Nexus 870 FTIR spectrometer (Madison, WI, USA) in an H_2O-purged environment with DTGS (deuterated triglycine sulfate) detector. The Golden Gate single-reflection ATR system (Specac Ltd., Orpington, Great Britain) was used to measure the ATR spectra of powdered samples over a wavenumber range 400–4000 cm^{-1}. Typical parameters were as follows: 256 sample scans, resolution 4 cm^{-1}, Happ-Genzel apodization, KBr beamsplitter. The samples for measurement were prepared by freeze−drying purified PLL-coated nanoparticles (centrifuged four times at 14 000 rpm for 1 h).

Differences in ultrasonic velocity between the reference (water) and the iron oxide colloid were monitored under the slow addition of various amounts of PLL (M_w = 388 100) using an HR-US 102 ultrasonic spectrometer (Ultrasonic Scientific, Dublin, Ireland). In a typical experiment, 1 mL of iron oxide colloid (c = 18 mg/mL) was in the first cell and 1 mL of Q-water in the second cell as a reference. PLL solution (c = 1 mg/mL) was then simultaneously added in 10 μL aliquots to both cells with a Hamilton syringe.

In protein adsorption experiments, 1 mL of the colloid solution with a concentration of 22 mg of iron oxide/mL was mixed with 1 mL of DMEM/10% FBS (fetal bovine serum) on a Vortex-T Genie-2 for 1 h; subsequently, the liquid was separated from the solid by centrifugation (14 000 rpm) for 1 h and measured on a Perkin-Elmer Lambda 20 UV/vis spectrophotometer (Norwalk, CT, USA). An aqueous solution of DMEM/10% FBS (1/1 v/v) served as a standard.

To confirm that PLL was not released from PLL-coated iron oxide nanoparticles during contact with the culture medium, both uncoated (no. 1, Table 1) and PLL-coated iron oxides (no. 4; 22 mg of γ-Fe_2O_3/0.64 mL of water) were mixed with 1 mL of DMEM/10% FBS or 1 mL of 0.15 M NaCl solution for 1 h, and after magnetic separation the supernatant was hydrolyzed in 6 M HCl for 16 h at 115 °C. The concentration of L-lysine in the supernatant was determined by the standard FMOC/*N*-

Table 1. *In Vitro* Bone Marrow Stromal Cell (MSC) Labeling of Surface-Modified Iron Oxide Nanoparticles and Their Characteristics

		concentration					labeled cells[c] (%)	
no.	modification	modifier (mg/mL)	γ-Fe_2O_3 (mg/mL)	PLL/γ-Fe_2O_3 (w/w)	D_n[a] (nm)	PDI[b]	MSC (rat)	MSC (human)
1	none		2.2	0	6.05	1.46	27.9	
2	PLL[d]	0.005	2.2	0.002	6.2	1.32	48.6	
3	PLL[d]	0.01	2.2	0.005	6.2	1.37	65.5	
4	PLL[d]	0.02	2.2	0.009	5.5	1.30	92.2	87.5
Endorem	Dextran		11.2[e]		5.4	1.43	60.0	65.2

[a] D_n – number-average particle diameter determined from TEM. [b] PDI – polydispersity index (ratio of weight- to number-average particle diameter). [c] Average of 10 measurements. [d] M_w = 388 100. [e] mg of iron/mL.

(9-fluorenylmethoxycarbonyl)/ method and reverse-phase HPLC equipped with a Flouromonitor 4100 detector (both LDC Analytical, Riviera Beach, FL, USA) using Macherey-Nagel 125/4 Nucleosil 120-3 C-8 column (Düren, Germany).

Cell Cultures. The isolation of mesenchymal stem cells (MSC) was performed as previously described (*28*). To isolate rat bone marrow mesenchymal stem cells (rMSCs), the femurs of 4-week-old Wistar rats were dissected. The ends of the bones were cut, and the marrow extruded with 5 mL of DMEM with L-glutamine (PAA, Pasching, Austria), using a syringe. Marrow cells were cultivated in DMEM/10% FBS with 100 U/mL of penicillin and 100 U/mL of streptomycin. After 24 h, the nonadherent cells were removed by replacing the medium. The medium was changed every 2–3 days as the cells grew to confluence. The cells were lifted by incubation with 0.25 wt % trypsin.

Human mesenchymal stem cells (hMSC) were obtained from the bone marrows of healthy donors. Bone marrow aspirates were diluted with phosphate-buffered saline (PBS) and centrifuged through a density gradient (Ficoll-Paque Plus, GE Healthcare Life Sciences, Vienna, Austria) for 30 min at 1000 *g* (Hettich, Germany). Nucleated cells from the interface were cultivated in Alpha-Modified Eagle Medium (α-MEM, Gibco BRL, Paisley, Scotland) containing 10% FBS, 100 units/mL penicillin, and 0.1 mg/mL streptomycin. After 48 h, the nonadherent cells were removed by replacing the medium.

Transmission Electron Microscopy of Labeled Cells. For electron microscopic examination, rMSCs were fixed at 4 °C in 2.5% buffered glutaraldehyde for 1 h, then stained with 1% osmium tetroxide for 2 h. The cells were successfully dehydrated with increasing concentrations of ethanol, immersed in propylene oxide, and embedded in Epon 812 resin (Agar Scientific Ltd., Standsted, UK). The samples were cut into ultrathin sections (~60 nm), contrasted with 4% uranyl acetate and Reynold's lead citrate, and examined using a Philips Morgagni 268 electron microscope.

Quantitative Analysis of Labeled Cells. rMSCs were cultivated in duplicate on uncoated 6-well culture plates at a density 10^5 cells/mm^2. Endorem- or poly(L-lysine)-modified nanoparticles were added to the culture medium (10 μL/mL) for 72 h. The culture medium containing excess particles was removed, and the cell were washed with PBS (three times), fixed with 4% paraformaldehyde in 0.1 M PBS, and stained to produce Fe(III) ferrocyanide (Prussian Blue). Labeled and unlabeled cells were quantified using an inverted light microscope (Axiovert 200, Zeiss, Göttingen, Germany) by counting five random fields per well and three wells per run. The cells captured on each image were manually labeled as Prussian Blue positive or negative; the labeled cells were then counted and the staining intensity of the Prussian Blue positive cells was evaluated using the image analysis toolbox in *Matlab 6.1* (The MathWorks, Natick, MA, USA). The threshold was set in the image analysis toolbox for dark blue, and all cells above this threshold were considered intensely stained. Histograms of the intensity of the cytoplasmic staining were constructed.

Comparison of Relaxivity between rMSC Labeled with Endorem or PLL-Modified Iron Oxide. The following suspensions in 4% gelatin were prepared: pure contrast agent (Endorem or PLL-modified iron oxide no. 4), unlabeled rMSC (4000, 1200, and 200 cells per μL), and cells labeled with Endorem or with PLL-modified iron oxide (4000, 2000, 1600, 1200, 800, 400, or 200 cells per μL). MR relaxation times T_1 and T_2 were measured on an 0.5 T Bruker Minispec MQ20 relaxometer (Rheinstetten, Germany). The T_1 and T_2 values were converted to relaxivities r_1 and r_2; relaxation rates $R_1 = 1/T_1$ and $R_2 = 1/T_2$ were related to the actual concentrations of iron or to the cell concentration c: $r_1 = (R_1 - R_{1G})/c$ (l s^{-1} mmol^{-1}), $r_2 = (R_2 - R_{2G})/c$ (l s^{-1} mmol^{-1}), where R_{1G} and R_{2G} are the relaxation rates of pure 4% gelatin.

Iron Analysis. The amount of iron in the cells after mineralization was determined by spectrophotometry. Cell-containing samples were mineralized by the addition of 5 mL HNO_3 and 1 mL H_2O_2 in an ETHOS 900 microwave mineralizator (Millestone, Sydney, Australia). Deionized water was added to reach a total volume of 100 mL. The iron content was determined using Spectroflame M120S apparatus (Spectro, Littleton, MA, USA) calibrated with a standard Astasol solution (Analytika, Prague, Czech Republic). The measurements were repeated four times, and the mean value was determined.

Cell Grafting. Rats were anesthesized with isoflorane and mounted in a stereotactic frame. Using aseptic technique, a hole (1 mm) was drilled in the skull to expose the dura overlying the cortex. Poly(L-lysine)-modified iron oxide-labeled cells or Endorem-labeled cells (1000, 500, or 100 cells suspended in 2 μL of PBS) were slowly injected intracerebrally into the brain over a 10 min period. Unlabeled cells (10 000 in 5 μL of PBS) were injected as a control. The opening was closed by bone wax and the skin was sutured.

MR Imaging. MR images were obtained using a 4.7 T Bruker spectrometer equipped with a homemade surface coil. The rats were anesthesized by passive inhalation of 1.5–2% isoflorane in air. Breathing was monitored during the measurements. Sagittal, coronal, and transversal images were obtained by a fast gradient echo sequence for localizing the following T_2*-weighted axial and coronal images measured by a standard gradient echo sequence. Sequence parameters were as follows: repetition time T_R = 180 ms, echo time T_E = 12 ms, number of acquisitions AC = 48, matrix size 256 × 256, field of view FOV = 3.5 × 3.5 cm (axial images) or 3 × 6 cm (coronal images), slice thickness = 0.75 mm.

Phantoms containing labeled cells were measured by the same sequence with modified geometry parameters to obtain similar spatial resolution as in the *in vivo* measurements.

RESULTS AND DISCUSSION

Chemical Coprecipitation of Fe(II) and Fe(III) Salts and Postsynthesis Iron Oxide Coating with PLL. The key step in the formation of a stable magnetite/maghemite colloid consisted of the careful removal of all the impurities remaining after the synthesis of the magnetite and its oxidation. Purification

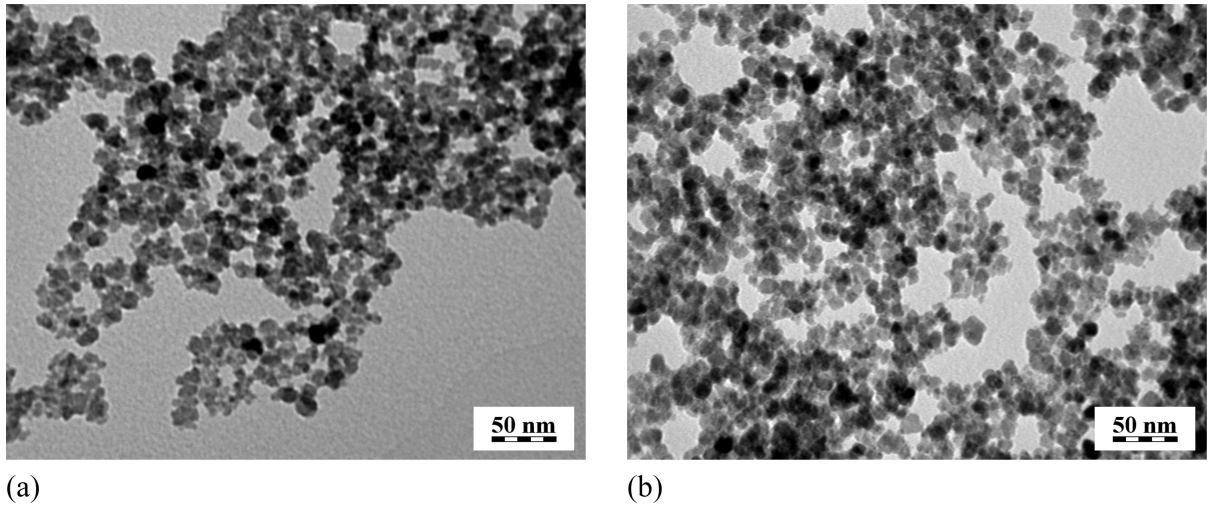

Figure 1. TEM micrographs of (a) uncoated iron oxide nanoparticles no. 1, and (b) PLL-modified iron oxide nanoparticles no. 4.

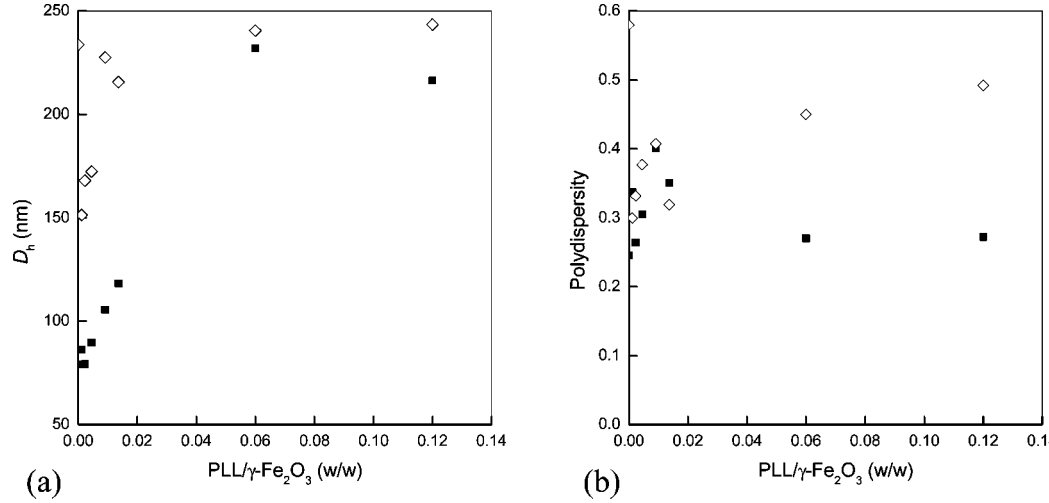

Figure 2. Dependence of (a) hydrodynamic particle diameter D_h and (b) polydispersity, measured by dynamic light scattering, on the PLL/γ-Fe_2O_3 ratio (□) 1 day and (◊) 152 days after synthesis.

was accomplished by magnetic separation in water. Washing with water peptized the particles. Colloidal stability was due to the charges of Fe(III) and citrate ions. Some characteristics of the prepared iron oxides are summarized in Table 1. TEM analysis indicates that dried, uncoated iron oxide particles showed a rather narrow size distribution (Figure 1a). The average size of uncoated nanoparticles no. 1 was about 6.5 nm (Table 1). The colloid showed high stability at neutral pH with no sedimentation observed even after 2 months. The stability is ascribed to the negative charges of the uncoated nanoparticles as documented by their low zeta potential (ca. −46 mV).

The surface modification of nanoparticles is a general strategy for enhancing the cells' permeability to nanoparticles. The transport of nanoparticles can be dramatically altered through the attachment of peptides (*29, 15*). It is expected that the nature of the attached poly(amino acid) strongly influences nanoparticle transport. In this report, the surface of the nanoparticles was modified by PLL (typically of M_w = 388 100) with the aim of promoting cellular uptake. Similarly as in a previous report (*27*), the postsynthesis coating of the primary iron oxide colloid with PLL changed neither the morphology nor the size of the iron oxide crystallites nos. 2–4 (Table 1, Figure 1b).

Figure 2a shows the dependence of the hydrodynamic particle diameter, measured by dynamic light scattering, on the PLL/iron oxide ratio for freshly prepared PLL-modified iron oxide nanoparticles (M_w of PLL = 388 100) and after 5 months of storage. It is normal that the hydrodynamic particle size is larger than the size obtained by TEM (*27*). The hydrodynamic size of freshly prepared particles appears to increase with the PLL/iron oxide ratio up to 0.06, probably due to a thickening of the shell. The hydrodynamic particle size is significantly larger after 5 months of storage, especially at lower PLL/iron oxide ratios,

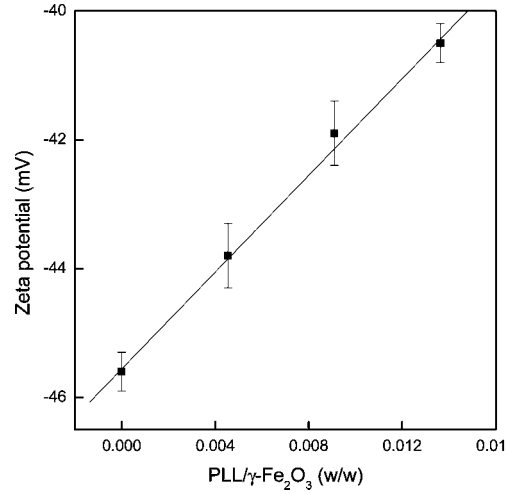

Figure 3. Dependence of zeta potential on the PLL/γ-Fe_2O_3 ratio.

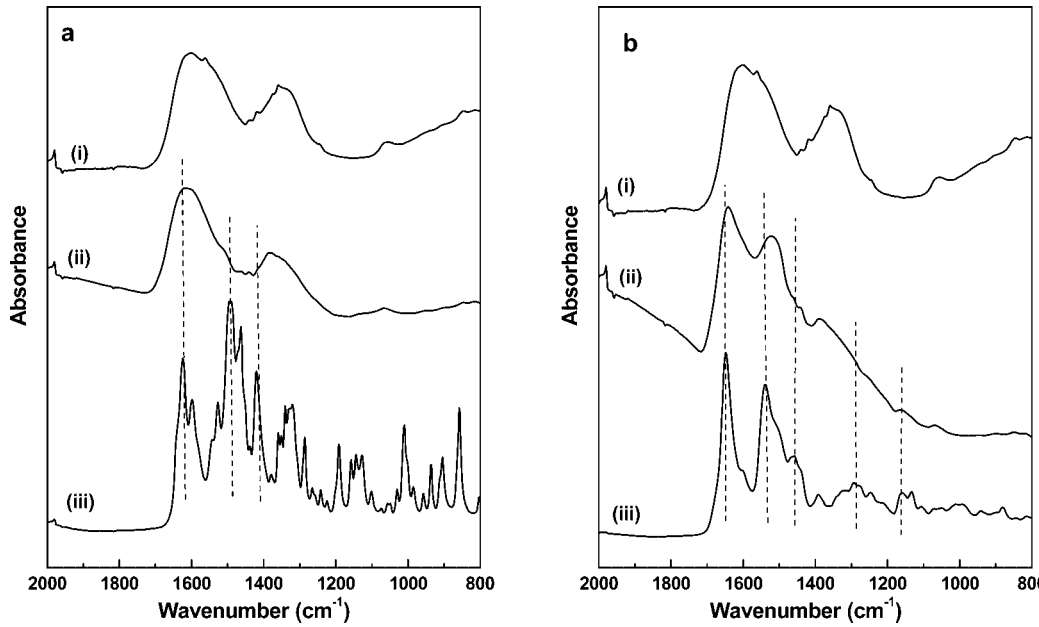

Figure 4. ATR FTIR spectra of magnetic γ-Fe_2O_3 particles before and after surface modification with (a) LL and (b) PLL; (i) iron oxide before modification, (ii) after coating, and (iii) spectrum of neat LL (a) and PLL (b).

Table 2. Concentration of L-Lysine in Hydrolyzed Supernatants after the Separation of Noncoated and PLL-Coated Iron Oxide Nanoparticles from the Medium[a]

sample	coating	medium	LL[b] (mg/mL)
1	PLL	NaCl	0.015
2		DMEM/FBS	0.419
3	PLL	DMEM/FBS	0.281
4[c]		DMEM/FBS	0.613

[a] 0.64 mL of colloid (34.7 mg γ-Fe_2O_3/ml). [b] L-Lysine after hydrolysis. [c] Control (no iron oxide particles in the medium).

because of particle aggregation. This can also be inferred from the analogous dependence of polydispersity (Figure 2b). A very high value of polydispersity was observed particularly in the absence of a PLL shell. Nevertheless, higher polydispersities were typical of all the particles after 5 months of storage (Figure 2b). Figure 3 documents an increase in zeta potential with increasing PLL/γ-Fe_2O_3 ratio, indicating that the negatively charged surface was compensated for by the positively charged PLL. This also shows that at the optimal ratio for cell labeling (0.009, see later) the zeta potential is still sufficiently low to repulse the nanoparticles.

FTIR Spectra. The structure of the surface and the efficiency of the coating of magnetic nanoparticles were analyzed by ATR FTIR spectroscopy. FTIR spectra of magnetic γ-Fe_2O_3 particles before and after surface modification with LL or PLL (M_w = 388 100) are shown in Figure 4. The spectra of pure LL and PLL are included for comparison. Two broad bands of iron oxide dominate the spectrum of the magnetic particles before modification. The spectrum of particles after modification with LL is very close to the spectrum of uncoated iron oxide (Figure 4a), confirming that LL did not coat the nanoparticles. As the molecules of LL have, at the same time, both acidic and basic character, their intermolecular interaction is stronger than the interaction with the particle surface. As a consequence, the particles are then poorly internalized by the cells (see later, Table 2).

The situation was different with PLL coating. The spectrum of particles after modification with PLL differs from the spectrum of uncoated iron oxide (Figure 4b). The main bands of PLL are clearly distinguishable in the spectrum of the modified particles. The Amide I band situated at 1648 cm^{-1} in the spectrum of pure PLL was only slightly shifted to higher wavenumbers by the coating (*30*). The Amide II band was shifted from 1539 cm^{-1} in the spectrum of pure PLL to 1502 cm^{-1} in the coating spectrum. We assume that the bands of $-CH_2-NH_3^+$ deformation and rocking vibrations influence the spectrum in this region. A broad, strong absorption above 1800 cm^{-1} (only the beginning is shown in Figure 4b) is observed in the spectrum, corresponding most probably to ionic interactions between PLL and the iron oxide particles. This strongly indicates that positive charges of the amine groups at the end of the PLL side chains interact with citrates complexed on the iron oxide surface as schematically illustrated in Figure 5. In contrast to the results observed with LL, the surface of γ-Fe_2O_3 nanoparticles was coated by PLL.

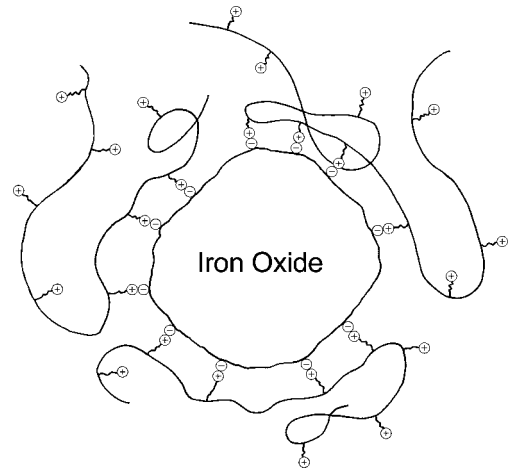

Figure 5. Schematic illustration of the interaction between PLL and a citrate-treated iron oxide nanoparticle.

High-Resolution Ultrasonic Spectroscopy. To investigate the process of PLL coating (M_w = 388 100) of the iron oxide nanoparticles in water, the colloid was monitored by high-resolution ultrasonic spectroscopy. The ultrasonic velocity increased with the addition of PLL. This is caused by an increase in the hydration layer of maghemite particles with hydrophilic PLL molecules, because water molecules are more organized in a hydration shell than in bulk (*31*). Figure 6 illustrates the

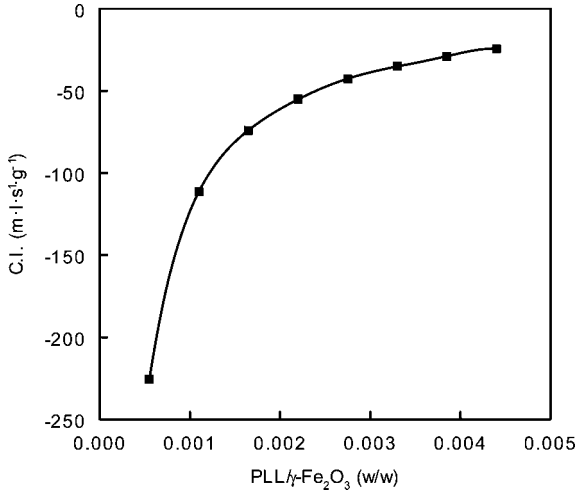

Figure 6. Dependence of the concentration increment of the ultrasonic velocity C.I. on PLL/γ-Fe_2O_3 ratio.

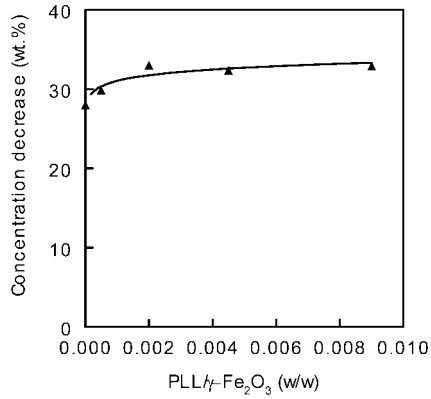

Figure 7. Effect of the PLL/iron oxide ratio on serum protein concentration in culture medium relative to a standard (DMEM/water 1/1 v/v) after adsorption by PLL-modified iron oxide nanoparticles (the concentration of serum proteins was determined by UV spectrometry at 274 nm).

concentration increment of the ultrasonic velocity depending on the amount of PLL added to the iron oxide. The largest increment in ultrasonic velocity was observed at PLL/γ-Fe_2O_3 ratios 0.0005–0.002 (w/w). The further addition of PLL solution did not significantly affect the hydration shell of the maghemite nanoparticles but resulted in a smaller increase in the increment. High-resolution ultrasonic spectroscopy thus provided another confirmation that PLL is indeed adsorbed on the particle surface. Binding is obviously achieved via the electrostatic attraction of opposite charges of PLL and iron oxide surface (Figure 5).

Protein Adsorption from Culture Medium. The adsorption of proteins from culture medium on iron oxide particles is important for elucidating both the transport of iron oxide into the cells and also nanoparticle coagulation. Iron oxide nanoparticles were mixed with serum-containing DMEM medium, the liquid was separated by centrifugation, and the UV spectra of the supernatant were measured against a standard. The relative decrease in the concentration of serum proteins was plotted against the PLL/iron oxide ratio. Figure 7 indicates that even uncoated iron oxide nanoparticles adsorbed some serum proteins from the culture medium. PLL (M_w = 388 100) modification of the iron oxide nanoparticles somewhat increased protein adsorption compared with uncoated iron oxide (Figure 7). The adsorption of serum proteins increased with increasing PLL concentration, reaching a plateau at a PLL/iron oxide ratio of 0.002. It is interesting to note that, while at higher PLL/iron oxide ratios protein adsorption did not increase, the percentage of labeled cells did (Table 1). It might be speculated that the entire PLL chain fully adheres onto the nanoparticle surface at PLL/iron oxide ratios 0.002 or less. The idea is also supported by the ultrasonic measurements. However, at higher ratios, all PLL chains remain attached to the iron oxide surface via their certain segments while their other parts move freely in the medium (Figure 5), facilitating cell labeling (see below). The free chain parts thus do not increase serum protein adsorption, but they can provide contact with the cell membrane.

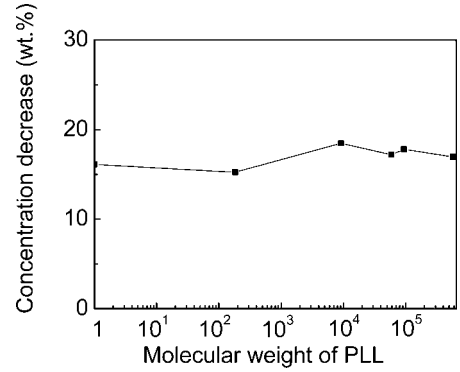

Figure 8. Effect of PLL molecular weight on serum protein concentration in culture medium relative to a standard (DMEM/water 1/1 v/v) after adsorption by PLL-modified iron oxide nanoparticles (the concentration of serum proteins was determined by UV spectrometry at 274 nm; PLL/iron oxide = 0.009 w/w—analogous to nanoparticles no. 4; Table 1).

To exclude the possibility that PLL dissociates from the iron oxide surface once mixed with serum, both uncoated (no. 1, Table 1) and PLL-coated nanoparticles (no. 4) were placed in DMEM/10% FBS medium or 0.15 M NaCl solution, magnetically separated, the supernatants hydrolyzed, and concentration of L-lysine was determined (Table 2). As expected, only traces of L-lysine were found in the supernatant from PLL-modified iron oxide during contact with the 0.15 M NaCl solution (sample 1, Table 2). This documents that PLL strongly associated with the iron oxide nanoparticles. The addition of uncoated iron oxide (sample 2) in DMEM/10% FBS induced a decrease in the amount of L-lysine in the hydrolyzed supernatant as compared with the control (sample 4), while the addition of PLL-coated iron oxide nanoparticles (sample 3) to DMEM/10% FBS led to a more pronounced decrease of L-lysine in the hydrolyzed supernatant. This is in accordance with our protein adsorption experiments (Figure 7). It should be noted that the total amount of L-lysine before hydrolysis and magnetic separation in sample 3 was higher than that in samples 2 and 4 (control), because in addition to serum L-lysine, it also contained L-lysine originating from the PLL coating. These experiments thus did not show the release of PLL from the PLL-coated iron oxide nanoparticles into the culture medium.

The effect of the molecular weight of PLL on the adsorption of FBS serum proteins from DMEM cultivation medium was also investigated by UV–vis spectrometry. The molecular weight of PLL did not significantly influence the adsorption of proteins from the DMEM medium on the surface of PLL-modified maghemite (Figure 8). It should be noted that this experiment was performed with another FBS charge than in the investigation of the effect of the PLL/iron oxide ratio on the concentration decrease in serum proteins, thus explaining the difference in the amount of adsorbed proteins (see Figures 7 and 8).

Cell Labeling. Cell labeling with Fe(III)/Fe(II)/paramagnetic substances is an increasingly common method for *in vivo* cell monitoring and separation (*32*), as the labeled cells can be detected by magnetic resonance imaging. The surface charac-

Table 3. Effect of PLL Molecular Weight on Percentage of rMSC Cells Labeled with PLL-Modified Iron Oxide Nanoparticles[a]

molecular weight	Endorem[b]	146	9200	58 900	93 800	388 100	579 000
percentage of labeled cells[c] (%)	58.6	80.6	87.6	84.7	90.4	92.2	90.5

[a] Concentration 2.2 mg of PLL-modified γ-Fe_2O_3/mL. [b] Control. [c] Average of 15 measurements.

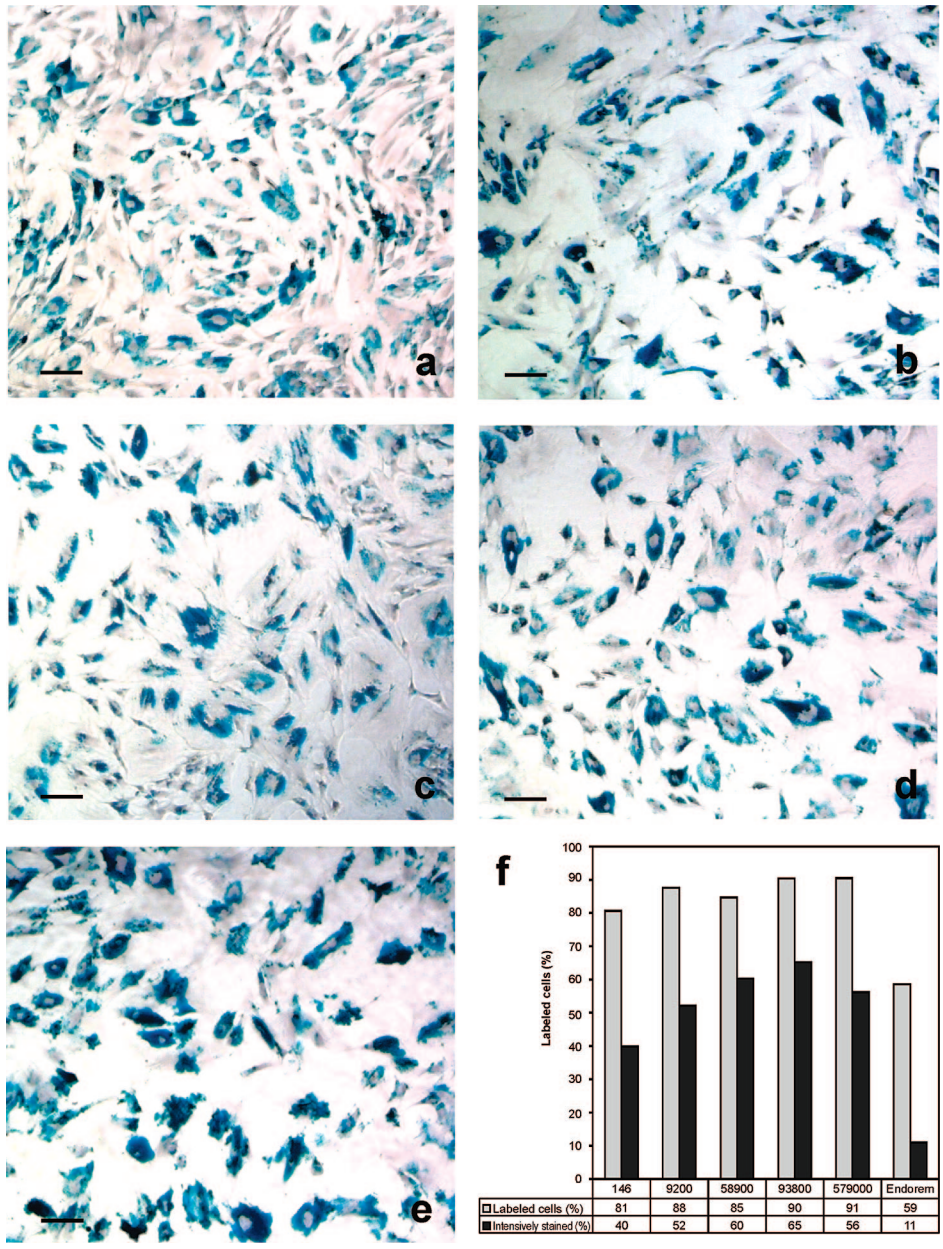

Figure 9. Microscopic observation of rMSCs labeled with PLL-modified iron oxide nanoparticles: effect of PLL molecular weight. M_w = (a) 146, (b) 9200, (c) 58 900, (d) 93 800, and (e) 579 000. Scale bar 50 μm. (f) Histograms of the percentage of the Prussian Blue stained PLL-coated iron oxide nanoparticle- and Endorem-labeled rMSC cells: effect of PLL molecular weight. Grey and black columns represent the percentage of labeled cells and strongly labeled cells, respectively, out of all the cells in the culture medium.

teristic of nanoparticles plays an important role in their internalization in cells. First, rMSCs labeled with either uncoated or surface-modified iron oxide nanoparticles were observed using an optical microscope. Cell labeling with Endorem served as a control. Endorem, however, shows a tendency to adhere on the surface of the cells, in addition to sticking to the bottom of the vessel. Using the Prussian Blue reaction, the cellular iron content was measured in MSCc exposed to the nanoparticles.

Primary Uncoated Iron Oxide. Primary uncoated iron oxide colloid no. 1 (Table 1) was tested for cell labeling to elucidate the importance of iron oxide modification/coating in subsequent experiments. Observation using an optical microscope with phase contrast revealed the iron oxide nanoparticles in rMSCs as dark dots. Cells in contact with the nanoparticles proliferated, and approximately one in every ten cells endocytosed the iron oxide. This might be explained by the formation of aggregates of sterically unstable particles due to the presence of electrolytes in the medium. As the resulting coagulates had a broad size distribution, only the small ones could penetrate into the cells, whereas the large ones were not internalized. In an attempt to increase cell labeling, the iron oxide surface was modified with PLL.

Poly(L-Lysine)-Modified Iron Oxide. PLL is a polycation due to the presence of NH_2 groups, widely used as a nonviral

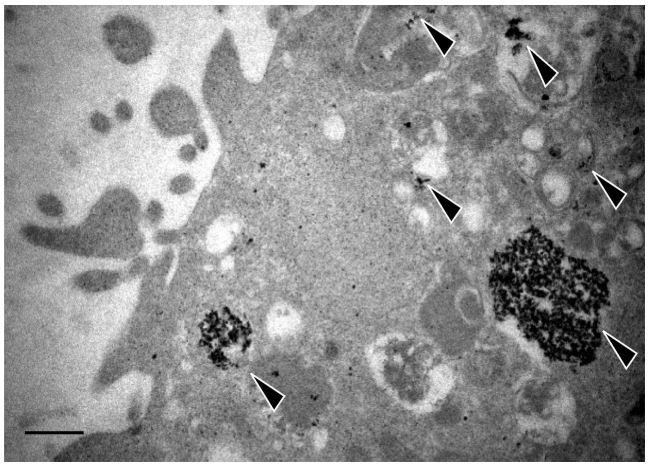

Figure 10. TEM micrographs of rMSC cells labeled with PLL-modified iron oxide nanoparticles (no. 3, Table 1). Scale bar 1 μm.

transfection agent for gene delivery and in DNA complexing thus promoting cell adhesion (*33*) through a positively charged interface clearly possessing an affinity for negatively charged cells. PLL is known to adsorb proteins not only from nutrient solutions, but also from cell membranes.

The results of both rat and human MSC cell labeling with PLL-modified maghemite nanoparticles (M_w of PLL = 388 100) are summarized in Table 1. It is clear that the degree of iron oxide internalization by the cells was PLL concentration-dependent. The higher the PLL concentration, the better the cell labeling (Table 1). The best result in terms of maximum cell labeling was achieved with 0.02 mg PLL per mL of colloid (Table 1, no. 4). The mechanism of PLL-mediated iron oxide uptake by the cells is assumed to be based on endocytosis and/or diffusion through the cell membranes (*34*). Cells took up much more PLL-modified nanoparticles than they did Endorem. Even a relatively low PLL concentration was sufficient for almost complete cell labeling. It can be thus assumed that increased endocytosis was induced by associates formed between PLL-coated nanoparticles and serum proteins. This is in accordance with both our protein adsorption experiments and also the L-lysine analysis of hydrolyzed supernatants (Table 2). The nanoparticles, however, aggregated at concentrations higher than 0.02 mg of PLL/mL. The results document a positive effect of PLL on intracellular nanoparticle uptake. This is in accordance with the published data on the cellular improved uptake of nanoparticles containing amino groups (*35*). Another approach to improve the uptake of nanoparticles into cells using PLL is based on combining a commercially available dextran-coated SPIO, such as Feridex (*36*) or Sinerem (*37*), and a commercially available transfection agent based on PLL (*38*). However, each combination of transfection agent and dextran-coated SPIO nanoparticles has to be carefully titrated and optimized for different cell cultures, since lower concentrations of transfection agent may result in insufficient cellular uptake, whereas higher concentrations may induce the precipitation of complexes or may be toxic for the cells (*39*). Also, magnetite cationic liposomes are known to promote the uptake of magnetic particles by target cells (*18*).

Table 4. Relaxivities r_1 and r_2 of Contrast Agent Suspensions and the Relaxation Rates of Suspensions of rMSCs Labeled with Contrast Agents

	relaxivities of phantoms containing suspension of pure contrast agent (s^{-1}/mmol Fe)		relaxation rates of phantoms containing labeled cells ($s^{-1}/10^6$ cells/mL)	
contrast agent	r_1	r_2	R_1	R_2
PLL-modified iron oxide no. 4	17.36	213	0.32	4.29
Endorem	19.65	126	0.18	1.24

Effect of PLL Molecular Weight. In the next series of experiments, L-lysine and PLL of several molecular weights, ranging up to 579 000, were chosen to test the cellular uptake of PLL-modified iron oxides (Table 3). Maghemite nanoparticles modified with L-lysine (M_w = 146) penetrated into the cells rather poorly, similarly to primary uncoated iron oxide particles, indicating again that LL did not coat the iron oxide (Figure 9). In contrast to LL-modified nanoparticles, the particles modified with PLL were internalized well by the cells. The efficiency of cell labeling increased with the molecular weight of PLL up to M_w = 388 100, which can be considered an optimum PLL molecular weight for γ-Fe_2O_3 nanoparticle modification. This is in accordance with earlier observations of inefficient mammalian cell labeling with low-molecular-weight PLL (*38*). On the other hand, particles coated with high-molecular-weight PLL (M_w = 579 000) showed lower cellular uptake (Table 2) and, moreover, adhered to the cell walls. This was indicated by the fact that the blue-stained areas were larger than the cells (Figure 9e). It is interesting to note that the efficiency of cell labeling with Endorem was higher in the experiments summarized in Table 1 than in those reported in Table 3, probably due to differences in the passage number of the cells used.

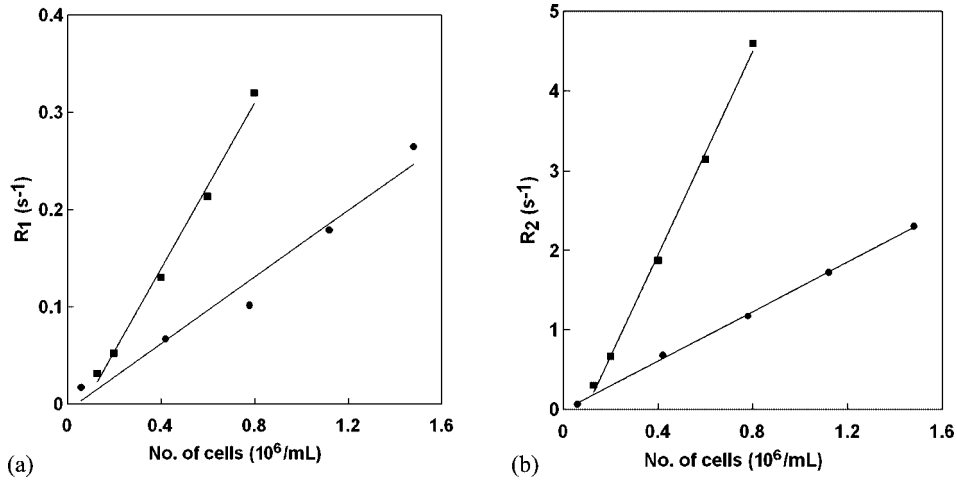

Figure 11. Proton relaxation rates (a) R_1 and (b) R_2 of rMSCs labeled with (•) Endorem and (■) PLL-modified iron oxide nanoparticles (no. 4, Table 1).

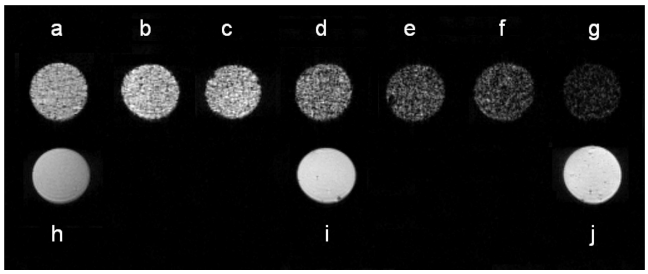

Figure 12. Gelatin phantoms containing (a) 200, (b) 400, (c) 800, (d) 1200, (e) 1600, (f) 2000, and (g) 4000 PLL-modified iron oxide (no. 4)-labeled cells per μL, and control samples with (h) 200, (i) 1200, and (j) 4000 unlabeled cells per μL.

Image analysis tools were used to evaluate not only the percentage of labeled cells, but also the intensity of Prussian Blue staining. The resulting histograms (Figure 9f) confirmed that the cells labeled with particles coated with higher-molecular-weight PLL (M_w > 58 900) were stained to a darker shade of blue, because they contained a greater amount of iron per cell than those labeled with particles coated with low-molecular-weight PLL. However, the intensity of Prussian Blue staining of particles modified with PLL of M_w = 579 000 was slightly decreased.

Transmission Electron Microscopy of Labeled Cells. To confirm the internalization of PLL-coated nanoparticles no. 3 by the cells rather than simply their bonding to the cell surface, and to visualize the location of the nanoparticles inside the cells after internalization, cells were examined by transmission electron microscopy (Figure 10). These observations revealed that the coated nanoparticles indeed crossed cell membranes and were internalized into the cells. They appeared as black dots evenly dispersed in the cell cytoplasm; cell membrane-bound nanoparticle clusters were not detected. The majority of the internalized PLL-coated nanoparticles were located in the lysosomes of the cells, which supports their intracellular trafficking. Nanoparticles are transported in endosomes and finally fused with lysosomes, a process during which the vesicle membranes disappear.

Comparison of Relaxivity between rMSC Labeled with Endorem and PLL-Modified Iron Oxide no. 4. MR relaxometry enables the quantification and proper comparison of relaxation times (and relaxivities), which are responsible for contrast enhancement in T_1-, T_2-, and T_2*-weighted MR images.

In Figure 11, the proton relaxation rates R_1 (a) and R_2 (b) of phantoms with labeled cells suspended in gelatin are plotted against the cell concentration. The relaxation rates of cells loaded with PLL-modified iron oxide nanoparticles were significantly higher than those of cells labeled with Endorem particles. Table 4 compares the relaxivities and relaxation rates of gelatin samples containing suspensions of the contrast agents or labeled cells relative to iron concentration or cell numbers, respectively. Relaxivity r_2 of PLL-modified iron oxide suspended in gelatin was 70% higher than that of Endorem. The difference between the relaxation rates of samples containing cells (related to the number of cells) labeled with PLL-modified nanoparticles and cells labeled with Endorem was much greater. This observation cannot be explained only by the higher relaxivity of the nanoparticles used; it is probably due to the better internalization of PLL-modified iron oxide nanoparticles in the cells. This hypothesis was confirmed by iron analysis of the cell suspensions, the average amounts of iron determined by spectrophotometry after mineralization were 41.5 pg of iron per cell for cells labeled with PLL-modified iron oxide no. 4 and 14.6 pg of iron per cell for Endorem-labeled cells.

***In Vitro* MR Imaging.** To check the sensitivity of the MRI technique and to mimic signal behavior in brain tissue, suspensions of unlabeled cells and cells labeled with PLL-modified iron oxide nanoparticles were imaged *in vitro*. Even the sample containing the lowest concentration (200 cells/μL which corresponds on average to 2 cells per image voxel) still provided visible contrast compared with a control phantom containing the same number of unlabeled cells (Figure 12). A similar set of experiments was performed in our previous work (*40*), in which MR images of gelatin phantoms showed a hypointense signal at the concentrations above 625 labeled cells per μL.

***In Vivo* MR Imaging.** Rats were examined 3 days after transplantation in an MR imager. Figure 13 shows that PLL-modified iron oxide (no. 4)-labeled cells were clearly discernible *in vivo*, even at low concentrations (1000 cells/2 μL). The iron oxide-labeled cell implants were visible as a hypointense area at the injection site. Cells labeled by PLL-modified iron oxide provide a better visible contrast than do Endorem-labeled cells. Labeling with PLL-modified iron oxide thus makes it possible to detect a lower number of cells in the tissue.

CONCLUSIONS

The preparation of new surface-modified iron oxide nanoparticles for stem labeling has been described and their

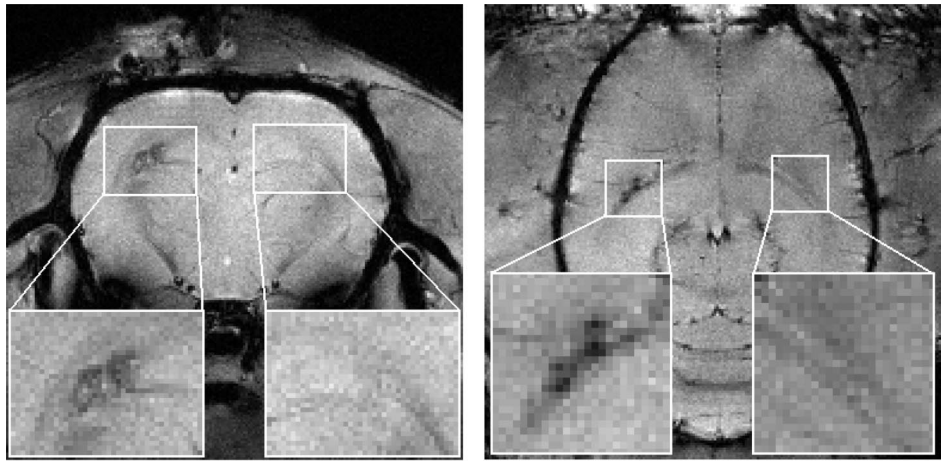

Figure 13. (a) Axial and (b) coronal MR images of a rat brain with 1000 cells labeled with PLL-modified iron oxide implanted into the left hemisphere and 1000 Endorem-labeled cells implanted into the right hemisphere. MR images were taken 3 days after implantation. Enlarged insets clearly show a hypointense signal in the left hemisphere; such a signal is not visible in the right one.

properties optimized. The structure of the polymer shell of the iron oxide core determined the efficacy of the nanoparticles' interaction with cells. A good colloidal stability has been obtained with poly(L-lysine) modifiers. Poly(L-lysine)-modified nanoparticles less than 10 nm in diameter were tested for cell labeling. PLL of high molecular weight ($M_w = 388\ 100$) proved to be the most effective surface-modifier for achieving the greatest internalization by rat bone marrow stromal cells. The accumulation of the magnetic particles in the cells was obviously facilitated by PLL-induced modification of the particles' surface charge. TEM examination of PLL-coated nanoparticles showed the successful internalization of the nanoparticles into lysosomes. Nanoparticles were found inside cells, mainly in endosomes. The cellular uptake of iron oxide nanoparticles was dependent on the concentration of PLL used in the iron oxide modification. At high concentrations, the nanoparticles started to aggregate in the culture medium. The cellular iron content was also dependent on the amount of added nanoparticles. Cell labeling with newly developed PLL-modified iron oxide was more efficient than that with a conventionally used agent (Endorem). Compared to Endorem, both the higher r_2 relaxivity of PLL-modified nanoparticles and their better internalization in the cells enabled easier MRI detection and tracking of cells in the tissue after transplantation. Moreover, the viability of PLL-coated iron oxide-labeled cells determined by a colorimetric essay was much higher than in cells labeled with Endorem (*41*). The newly developed PLL-modified iron oxide nanoparticles are expected to be nontoxic, similarly as analogous iron oxide−PLL complexes (*42*), the biodegradation of which and metabolic processes in cells have been reported earlier. The iron is introduced into the normal plasma iron pool and is then incorporated into the hemoglobin of red cells or metabolized (*43*). Compared with PLL modification of dextran-coated iron oxide nanoparticles (*44*), the advantage of our new procedure is that no dextran is necessary to produce the particles, thus simplifying their preparation. The developed nanoparticles are a promising tool for the noninvasive *in vivo* tracking of transplanted cells in the host organism and for monitoring the long-term effects of such transplantation.

ACKNOWLEDGMENT

The financial support of the Center for Cell Therapy and Tissue Repair (No. 1M0021620803), the Grant Agency of the Academy of Sciences of the Czech Republic (grant KAN200200651 and KAN201110651), and the Grant Agency of the Czech Republic (grant 203/05/2256 and 309/06/1594) is gratefully acknowledged.

LITERATURE CITED

(1) Pankhurst, Q. A., Connolly, J., Jones, S. K., and Dobson, J. (2003) Applications of magnetic nanoparticles in biomedicine. *J. Phys. D: Appl. Phys. 36*, R167–R181.

(2) Marchal, G., van Hecke, P., Demaerel, P., Decrop, E., Kennis, C., Baert, A. L., and van der Schueren, E. (1989) Detection of liver metastases with superparamagnetic iron oxide in 15 patients: Results of MR imaging at 1.5 T. *Am. J. Roentgenol. 152*, 771–775.

(3) Lubbe, A. S., Bergemann, C., Riess, H., Schriever, F., Reichardt, P., Possinger, K., Matthias, M., Dorken, B., Herrmann, F., Gurtler, R., Hohenberger, P., Haas, N., Sohr, R., Sander, B., Lemke, A. J., Ohlendorf, D., Huhnt, W., and Huhn, D. (1996) Clinical experiences with magnetic drag targeting: A phase I study with 4′-epidoxorubicin in 14 patients with advanced solid tumors. *Cancer Res. 56*, 4686–4693.

(4) Guesdon, J. L., Thiery, R., and Avrameas, S. (1978) Magnetic enzyme immunoassay for measuring human IgE. *J. Allergy Clin. Immunol. 6*, 23–27.

(5) Druet, E., Mahieu, P., Foidart, J. M., and Druet, P. (1982) Magnetic solid-phase enzyme immunoassay for the detection of anti-glomerular basement membrane antibodies. *J. Immunol. Methods 48*, 149–157.

(6) Gu, H., Ho, P. L., Tsang, K. W. T., Wang, L., and Xu, B. (2003) Using bifunctional magnetic nanoparticles to capture vancomycin-resistant Enterococci and other gram-positive bacteria at ultralow concentration. *J. Am. Chem. Soc. 125*, 15702–15703.

(7) Pazzagli, M., Kohen, F., Sufi, S., Masironi, B., and Cekan, S. Z. (1988) Immunometric assay for lutropin (hLH) based on the use of universal reagents for enzymatic labeling and magnetic separation and monitored by enhanced chemiluminescence. *J. Immunol. Methods 114*, 62–68.

(8) Vonk, G. P., and Schram, J. L. (1991) Dual-enzyme cascade-magnetic separation immunoassay for respiratory syncytial virus. *J. Immunol. Methods 137*, 133–139.

(9) Josephson, L., Perez, J. M., and Weissleder, R. (2001) Magnetic nanosensors for the detection of oligonucleotide sequences. *Angew. Chem., Int. Ed. 40*, 3204–3206.

(10) Patolsky, F., Weizmann, Y., Katz, E., and Willner, I. (2003) Magnetically amplified DNA assays (MADA): Sensing of viral DNA and single-base mismatches by using nucleic acid modified magnetic particles. *Angew. Chem., Int. Ed. 42*, 2372–2376.

(11) Nam, J. M., Thaxton, C. S., and Mirkin, C. A. (2003) Nanoparticle-based bio-bar codes for the ultrasensitive detection of proteins. *Science 301*, 1884–1886.

(12) Lewin, M., Carlesso, N., Tung, C. H., Tang, X. W., Cory, D., Scadden, D. T., and Weissleder, R. (2000) Tat peptide-derivatized magnetic nanoparticles allow in vivo tracking and recovery of progenitor cells. *Nat. Biotechnol. 18*, 410–414.

(13) Torchilin, V. P. (2000) Drug targeting. *Eur. J. Pharm. Sci. 11*, S81–S91.

(14) Häfeli, U. O. Magnetically modulated therapeutic systems. *Int. J. Pharm. 277*, 19–24.

(15) Xiang, J. J., Tang, J.-Q., Zhu, S.-G., Nie, X.-M., Lu, H.-B., Shen, S.-R., Li, X.-L., Tang, K., Zhou, M., and Li, G.-Y. (2003) IONP-PLL: A novel non-viral vector for efficient gene delivery. *J. Gene Med. 5*, 803–817.

(16) Jordan, A., Scholz, R., Maier-Hauff, K., Johannsen, M., Wust, P., Nadobny, J., Schirra, H., Schmidt, H., Deger, S., Loening, S., Lanksch, W., and Felix, R. (2001) Presentation of a new magnetic field therapy system for the treatment of human solid tumors with magnetic fluid hyperthermia. *J. Magn. Magn. Mater. 225*, 118–126.

(17) Gupta, A. K., and Gupta, M. (2005) Synthesis and surface engineering of iron oxide nanoparticles for biomedical applications. *Biomaterials 26*, 3995–4021.

(18) Shinkai, M. (2002) Functional magnetic particles for medical application. *J. Biosci. Bioeng. 94*, 606–613.

(19) Stella, B., Arpicco, S., Peracchia, M. T., Desmaele, D., Hoebeke, J., Renoir, M., D'Angelo, J., Cattel, L., and Couvreur, P. (2000) Design of folic acid-conjugated nanoparticles for drug targeting. *J. Pharm. Sci. 89*, 1452–1464.

(20) Zhang, Y., and Zhang, J. (2005) Surface modification of monodisperse magnetite nanoparticle for improved intracellular uptake to breast cancer cells. *J. Colloid Interface Sci. 283*, 352–357.

(21) Allen, M. J., MacRenaris, K. W., Venktasubramanian, P. N., and Meade, T. J. (2004) Cellular delivery of MRI contrast agents. *Chem. Biol. 11*, 301–307.

(22) Stark, D. D., Weissleder, R., Elizondo, G., Hahn, P. F., Saini, S., Todd, L. E., Wittenberg, J., and Ferrucci, J. T. (1988) Superparamagnetic iron oxide: Clinical application as a contrast agent for MR imaging of the liver. *Radiology 168*, 297–301.

(23) Molday, R. S., and MacKenzie, D. (1982) Immunospecific ferromagnetic iron-dextran reagents for the labeling and magnetic separation of cells. *J. Immunol. Methods 52*, 353–367.

(24) Cheng, F.-Y., Su, C.-H., Yang, Y.-S., Yeh, C.-S., Tsai, C.-Y., Wu, C.-L., Wu, M.-T., and Shieh, D.-B. (2005) Characterization of aqueous dispersions of Fe_3O_4 nanoparticles and their biomedical applications. *Biomaterials 26*, 729–738.

(25) Taupitz, M., Schnorr, J., Wagner, S. A., Abramjuk, C., Pilgrimm, H., Kivelitz, D., Schink, T., Hansel, J., Laub, G., Humogen, H., and Hamm, B. (2002) Coronary MR angiography: Experimental results with a monomer-stabilized blood pool contrast medium. *Radiology 222*, 120–126.

(26) Kiessling, A. A., Anderson, S. C. (2003) *Human embryonic stem cells, an introduction to the science and therapeutic potential*. Jones & Bartlett Publishers, USA.

(27) Horák, D., Babič, M., Jendelová, P., Herynek, V., Trchová, M., Pientka, Z., Pollert, E., Hájek, M., and Syková, E. (2007) D-mannose-modified iron oxide nanoparticles for stem cell labeling. *Bioconjugate Chem. 18*, 635–644.

(28) Azizi, S. A., Stokes, D., Augelli, B. J., DiGirolamo, C., and Prockop, D. J. (1998) Engraftment and migration of human bone marrow stromal cells implanted in the brains of albino rats–similarities to astrocyte grafts. *Proc. Natl. Acad. Sci. U.S.A. 95*, 3908–3913.

(29) Koch, A. M., Reynolds, F., Merkle, H. P., Weissleder, R., and Josephson, L. (2005) Transport of surface-modified nanoparticles through cell monolayers. *ChemBioChem 6*, 337–345.

(30) Socrates, G. (2001) In *Infrared and Raman Characteristic Group Frequencies*, pp 143–145, Wiley, New York.

(31) Van Durme, K., Delellio, L., Kudryashov, E., Buckin, V., and Van Mele, B. (2005) Exploration of high-resolution ultrasonic spectroscopy as an analytical tool to study demixing and remixing in poly(*N*-isopropyl acrylamide)/water solutions. *J. Polym. Sci., Part B: Polym. Phys. 43*, 1283–1295.

(32) Olsvik, O., Popovic, T., Skjerve, E., Cudjoe, K. S., Hornes, E., Ugelstad, J., and Uhlen, M. (1994) Magnetic separation techniques in diagnostic microbiology. *Clin. Microbiol. Rev. 7*, 43–54.

(33) Schatzlein, A. G. (2001) Non-viral vectors in cancer gene therapy: principles and progress. *Anticancer Drugs 12*, 275–304.

(34) Dormer, K., Seeney, C., Lewelling, K., Lian, G., Gibson, D., and Johnson, M. (2005) Epithelial internalization of superparamagnetic nanoparticles and response to external magnetic field. *Biomaterials 24*, 2061–2072.

(35) Petri-Fink, A., Chastellain, M., Juillerat-Jeanneret, L., Ferrari, A., and Hofmann, H. (2005) Development of functional superparamagnetic iron oxide nanoparticles for interaction with human cancer cells. *Biomaterials 26*, 2685–2694.

(36) Frank, J. A., Miller, B. R., Arbab, A. S., Zywicke, H. A., Jordan, E. K., Lewis, B. K., Bryant, L. H., and Bulte, J. W. M. (2003) Clinically applicable labeling of mammalian and stem cells by combining superparamagnetic iron oxides and transfection agents. *Radiology 228*, 480–487.

(37) Hoehn, M., Kustermann, E., Blunk, J., Wiedermann, D., Trapp, T., and Focking, M. (2002) Monitoring of implanted stem cell migration in vivo: A highly resolved in vivo magnetic resonance imaging investigation of experimantal stroke in rat. *Proc. Natl. Acad. Sci. U.S.A. 100*, 1073–1078.

(38) Arbab, A. S., Yocum, G. T., Wilson, L. B., Parwana, A., Jordan, E. K., Kalish, H., and Frank, J. A. (2004) Comparison of transfection agents in forming complexes with ferumoxides, cell labeling efficiency, and cellular viability. *Mol. Imaging 3*, 24–32.

(39) Kalish, H., Arbab, A. S., Miller, B. R., Lewis, B. K., Zywicke, H. A., Bulte, J. W., Bryant, L. H., and Frank, J. A. (2003) Combination of transfection agents and magnetic resonance contrast agents for cellular imaging: Relationship between relaxivities, electrostatic forces, and chemical composition. *Magn. Reson. Med. 50*, 275–282.

(40) Jendelová, P., Herynek, V., DeCroos, J., Glogarová, K., Andersson, B., Hájek, M., and Syková, E. (2003) Imaging the fate of implanted bone marrow stroma cells labeled with superparamagnetic nanoparticles. *Magn. Reson. Med. 50*, 767–776.

(41) Jendelová, P., Horák, D., Babič, M., Glogarová, K., Herynek, V., Hájek, M., and Syková, E. (2007) Modified iron oxide nanoparticles for *in vivo* cell imaging. *Regenerative Med. 2*, 635.

(42) Yocum, G. T., Wilson, L. B., Ashari, P., Jordan, E. K., Frank, J. A., and Arbab, A. S. (2005) Effect of human stem cells labeled with ferumoxides-poly-L-lysine on hematologic and biochemical measurements in rats. *Radiology 235*, 547–552.

(43) Weissleder, R., Stark, D. D., Engelstad, B. L., Bacon, B. R., Compton, C. C., White, D. L., Jacobs, P., and Lewis, J. (1989) Superparamagnetic iron oxide: Pharmacokinetics and toxicity. *Am. J. Roentgenol. 152*, 167–173.

(44) Arbab, A. S., Bashaw, L. A., Miller, B. R., Jordan, E. K., Lewis, B. K., Kalish, H., and Frank, J. A. (2003) Characterization of biophysical and metabolic properties of cells labeled with superparamagnetic iron oxide nanoparticles and transfection agent for cellular MR imaging. *Radiology 229*, 838–846.

BC700410Z

Příloha č. 3

Poly(*N*,*N*-dimethylacrylamide)-Coated Maghemite Nanoparticles for Stem Cell Labeling

Michal Babič,[†,‡] Daniel Horák,*[,†,‡] Pavla Jendelová,[‡,§] Kateřina Glogarová,[§] Vít Herynek,[‡,||] Miroslava Trchová,[†] Katarína Likavčanová,[§] Petr Lesný,[‡,§] Emil Pollert,[⊥] Milan Hájek,[‡,||] and Eva Syková[‡,§]

Institute of Macromolecular Chemistry, Academy of Sciences of the Czech Republic, Heyrovský Sq. 2, 162 06 Prague 6, Czech Republic, Center for Cell Therapy and Tissue Repair, Charles University, V Úvalu 84, 150 06 Prague 5, Czech Republic, Institute of Experimental Medicine, Academy of Sciences of the Czech Republic, Vídeňská 1083, 142 20 Prague 4, Czech Republic, Institute for Clinical and Experimental Medicine, Vídeňská 1958/9, 140 21 Prague 4, Czech Republic, and Institute of Physics, Academy of Sciences of the Czech Republic, Cukrovarnická 10, 162 53 Prague 6, Czech Republic. Received September 3, 2008; Revised Manuscript Received November 13, 2008

Maghemite (γ-Fe_2O_3) nanoparticles were obtained by the coprecipitation of Fe(II) and Fe (III) salts with ammonium hydroxide followed by oxidation with sodium hypochlorite. Solution radical polymerization of *N,N*-dimethylacrylamide (DMAAm) in the presence of maghemite nanoparticles yielded poly(*N,N*-dimethylacrylamide) (PDMAAm)-coated maghemite nanoparticles. The presence of PDMAAm on the maghemite particle surface was confirmed by elemental analysis and ATR FTIR spectroscopy. Other methods of nanoparticle characterization involved scanning and transmission electron microscopy, atomic adsorption spectroscopy (AAS), and dynamic light scattering (DLS). The conversion of DMAAm during polymerization and the molecular weight of PDMAAm bound to maghemite were determined by using gas and size-exclusion chromatography, respectively. The effect of ionic 4,4′-azobis(4-cyanovaleric acid) (ACVA) initiator on nanoparticle morphology was elucidated. The nanoparticles exhibited long-term colloidal stability in water or physiological buffer. Rat and human bone marrow mesenchymal stem cells (MSCs) were labeled with uncoated and PDMAAm-coated maghemite nanoparticles and with Endorem as a control. Uptake of the nanoparticles was evaluated by Prussian Blue staining, transmission electron microscopy, T_2-MR relaxometry, and iron content analysis. Significant differences in labeling efficiency were found for human and rat cells. PDMAAm-modified nanoparticles demonstrated a higher efficiency of intracellular uptake into human cells in comparison with that of dextran-modified (Endorem) and unmodified nanoparticles. In gelatin, even a small number of labeled cells changed the contrast in MR images. PDMAAm-coated nanoparticles provided the highest T_2 relaxivity of all the investigated particles. In vivo MR imaging of PDMAAm-modified iron oxide-labeled rMSCs implanted in a rat brain confirmed their better resolution compared with Endorem-labeled cells.

INTRODUCTION

Recently, superparamagnetic iron oxide nanoparticles have found widespread application in medicine, in particular as contrast agents in magnetic resonance imaging (MRI) (*1*). Contrast agents in MRI improve the detection and characterization of lesions by changing the signal intensity of target tissues when compared with the surrounding tissue (*2*). Understanding the interactions between the nanoparticles and cells is crucial for improving their behavior in vivo and in vitro. The direct use of nanoparticles as in vivo MRI contrast agents results in their biofouling in the blood plasma and the formation of aggregates that are quickly sequestered by cells of the reticular endothelial system (RES) such as macrophages. Both small particle size and surface chemical structures are key parameters determining the blood half-life in the circulation, opsonization, biokinetics, and the biodistribution of magnetic nanoparticles (*3–5*). It is therefore essential to engineer the surface of the iron oxide to minimize biofouling and the aggregation of the particles under physicochemical conditions (i.e., high salt and protein concentrations) for long periods. Surface modifications of magnetic iron oxide nanoparticles with biocompatible polymers are potentially beneficial for preparing MR contrast agents for in vivo applications. Such particles can circulate in the plasma for long periods by escaping uptake by the RES. Iron oxide nanoparticles coated with dextran and its derivates, such as Feridex (Endorem) and Resovist, are commercially available. Iron oxide nanoparticles also show potential for in vitro cell labeling followed by in vivo MRI tracking, an approach that is being investigated for stem cell therapy (*6, 7*). Dextran-coated agents are, however, insufficiently taken up by the cells during cultivation; consequently, modifications of the iron oxide surface are attempted in order to increase the internalization of the nanoparticles. One promising approach toward increasing the local concentration of the nanoparticles in cells is to conjugate them with targeting molecules that have a high affinity for tumor cells (*8–10*). Target-specific molecules, including monoclonal antibodies (*11*), proteins (*12*), peptides, and folic acid (*10*), have been investigated to increase the site-specific accumulation of MR contrast agents in tumor cells. Several transfection agents have been suggested to facilitate the effective magnetic labeling of cells by endocytosis into endosomes (*13*). These are mostly cationic, positively charged compounds (*14*). Superparamagnetic

* To whom correspondence should be addressed. E-mail: horak@imc.cas.cz.

† Institute of Macromolecular Chemistry, Academy of Sciences of the Czech Republic.

‡ Charles University.

§ Institute of Experimental Medicine, Academy of Sciences of the Czech Republic.

|| Institute for Clinical and Experimental Medicine.

⊥ Institute of Physics, Academy of Sciences of the Czech Republic.

10.1021/bc800373x CCC: $40.75
Published on Web 01/14/2009

iron oxide nanoparticles have thus been incorporated into hemoglobin within red cells, short human immunodeficiency virus-transactivator transcription (TAT) proteins (*15*), polyamines (polycationic poly(L-lysine) (PLL) (*16*)), magnetodendrimers (*17*), and antigen-specific internalizing monoclonal antibodies (*18*). The complexing of PLL with iron oxide occurs through electrostatic interactions of the negatively charged iron oxide nanoparticles with the polycation, allowing for the efficient incorporation of iron oxide nanoparticles into endosomes for magnetic cell labeling. A disadvantage of PLL-modified iron oxides is, however, that they aggregate in the presence of some electrolytes.

In our previous reports, the efficiency of cellular uptake was investigated following D-mannose and PLL modification of the iron oxide surface (*19, 20*). These systems were relatively stable in cell culture media; however, their further modification with antibodies, enzymes, or proteins, was difficult. In an attempt to design a novel coating of iron oxide nanoparticles that would not only ensure their very good colloidal stability but also enable the subsequent covalent attachment of highly specific biomolecules (antibodies, enzymes, peptides, etc.), PDMAAm was selected. Its advantage consists in the easy formation of homogeneous networks and copolymers with various functional monomers (*21*). Our preliminary biological experiments confirmed not only the nontoxicity of the PDMAAm coating but also its ability to enhance cellular uptake. In this study, PDMAAm coating of iron oxide particles was investigated in more detail utilizing in vitro cell labeling followed by MR cell tracking. As a model, rat and human mesenchymal stem cells (rMSCs and hMSCs) were labeled with PDMAAm-coated nanoparticles, and nanoparticle internalization into cells was visualized with light and TEM microscopy. In addition, the effect of PDMAAm-coated iron oxide nanoparticles on cell viability and labeling efficiency was quantified. Moreover, MR relaxometry of labeled cells was used to measure relaxation times, which are responsible for contrast enhancement in MR images.

EXPERIMENTAL SECTION

Materials. *N*,*N*-Dimethylacrylamide (DMAAm; Aldrich, Milwaukee, USA) was distilled (56 °C/266 Pa). 4,4′-Azobis(4-cyanovaleric acid) (ACVA), $FeCl_2 \cdot 4H_2O$, and $FeCl_3 \cdot 6H_2O$ were purchased from Fluka (Buchs, Switzerland) and used without further purification. All other chemicals were supplied by Aldrich and used as received. Endorem, a MRI contrast agent based on superparamagnetic dextran-coated iron oxide nanoparticles, was obtained from Guerbet (Roissy, France). Ultrapure Q water ultrafiltered on a Milli-Q Gradient A10 system (Millipore, Molsheim, France) was used for preparation of the solutions.

Preparation of Ferrofluid. Two procedures are generally used for the preparation of iron oxide nanoparticles: an in situ and a stepwise method. In this report, a two-step procedure was used. Colloidal $Fe(OH)_3$ was first precipitated from $FeCl_3 \cdot 6H_2O$ added to less than an equimolar amount of ammonia, followed by the addition of $FeCl_2 \cdot 4H_2O$ (molar ratio Fe(III)/Fe(II) = 2). Mixing was simply achieved by rapid sonication. The mixture was then poured into an excess of ammonia, and a magnetite (Fe_3O_4) coagulate was formed. The key step in the formation of a stable magnetite colloid after the synthesis consists in its careful purification from all impurities by washing and magnetic separation in water, a process called peptization. Briefly, 12 mL 0.2 M $FeCl_3 \cdot 6H_2O$ aqueous solution was mixed with 12 mL 0.5 M NH_4OH solution under sonication (Sonicator W-385; Heat Systems-Ultrasonics, Inc., Farmingdale, USA) for 2 min at laboratory temperature to form the $Fe(OH)_3$ colloid. Then, 6 mL of 0.2 M $FeCl_2 \cdot 4H_2O$ aqueous solution was added under sonication and the mixture poured into 36 mL of 0.5 M NH_4OH aqueous solution. The resulting magnetite coagulate was left to grow for 15 min, magnetically separated, and repeatedly (7−10×) washed with Q-water to remove all impurities (including NH_4Cl) remaining after the synthesis. The above-formed pure magnetite was sonicated for 3 min with 2 mL of 0.1 M sodium citrate solution and oxidized at room temperature with 1.5 mL of 5 wt % sodium hypochlorite to maghemite. The precipitate was again repeatedly (7×) washed with Q-water using magnetic separation/decantation to obtain a stable colloid.

Coating by Solution Radical Polymerization of DMAAm in the Presence of Maghemite Nanoparticles. In a typical experiment, 1 g of DMAAm and 0.01 g of ACVA initiator were dissolved in 30 mL of aqueous colloid containing 0.5 g of γ-Fe_2O_3, and the mixture was purged with nitrogen to remove oxygen for 10 min. PDMAAm was synthesized under stirring (400 rpm) at 70 °C for 8 h. The resulting colloid was washed 8 times with water by centrifugation/redispersion to remove excessive polymer, unreacted monomer, and initiator, and redispersed.

For comparison, iron oxide nanoparticles were also encapsulated in neat PDMAAm added to the particles, followed by a thorough purification by repetitive centrifugation/redispersion in water.

Characterization of the Particles. The particles were observed in a scanning electron microscope (SEM, JEOL JSM 6400). A drop of particle dispersion was smeared between glasses for microscopy to obtain a thin layer, dried, and surface-coated with a 4-nm platinum layer using a SCD 050 sputtering device (BalTech, Lichtenstein). Transmission electron microscopy (TEM) was performed on a JEOL JEM 200 CX to determine the particle size of the iron oxides. The average diameter and particle size distribution PDI (weight-number-average particle diameter ratio D_w/D_n) were obtained by statistical analysis of at least 500 particles using the Atlas program (Tescan Brno, Czech Republic). The X-ray diffraction measurement was carried out with a Bruker D8 diffractometer using Cu Kα radiation and a Sol-X energy dispersive detector. The amount of iron in the coated nanoparticles was found by AAS (Perkin-Elmer 3110) of an extract of the sample obtained with dilute HCl (1:1) at 80 °C for 1 h. The amount of PDMAAm bound to the particles after polymerization was determined after their lyophilization by elemental analysis (Perkin-Elmer 2400 Series II CHNS/O Analyzer, Shelton, CT, USA).

The coating of PDMAAm on the surface of magnetic nanoparticles was investigated using a Thermo Nicolet NEXUS 870 FTIR Spectrometer (Madison, WI, USA) in a water-purged environment with a DTGS detector in the wavenumber range from 400 to 4000 cm^{-1}. A Golden Gate Heated Diamond ATR Top-Plate (MKII Golden Gate single reflection ATR system) (Specac Ltd., Orpington, Great Britain) was used for measuring the spectra of powdered samples by ATR spectroscopy. Typical parameters used were 256 sample scans, 4 cm^{-1} resolution, Happ-Genzel apodization, and KBr beamsplitter.

The hydrodynamic diameter D_h and the zeta-potential of both the unwashed colloid (0.2 mL of original colloid diluted to 2 mL) and the colloid repeatedly (8×) washed with water through ultracentrifugation/redispersion were determined by dynamic light scattering (DLS) with an Autosizer Lo-C (Malvern Instruments Ltd., Malvern, UK). Colloidal stability was evaluated visually according to the presence of sediment on the bottom of the vial.

To determine the molecular weight (M_w) of PDMAAm bound to maghemite, maghemite was first dissolved in concentrated HCl. The resulting dark yellow solution was diluted with water and PDMAAm separated on a PD 10 desalting column (Amersham Biosciences, Buckinghamshire, UK). Finally, PD-

MAAm was lyophilized and dissolved in acetate buffer ($c \sim 3$ mg/mL). The M_w was determined by size-exclusion chromatography in an aqueous methanol solution on a Shimadzu HPLC system equipped with RI, UV, and multiangle light scattering DAWN EOS (Wyatt Co., USA) detectors using a mobile phase consisting of 20% 0.3 M acetate buffer (pH 6.5; 0.5 g/L NaN_3) and 80% methanol (flow rate 0.5 mL/min) with a GPC column TSKgel G6000PW (300 × 7.8 mm; 15 μm; Tosoh Bioscience, Japan).

The conversion versus DMAAm polymerization time was calculated from the concentration of monomers during polymerization monitored after the addition of hydrochinone (50 mg/mL) by a GC Perkin-Elmer (Norwalk, CT, USA) with FID detector using 30 m length, 0.32 mm inner diameter Rtx-624 column with 1.8 μm thick film (Restek, Bellefonte, PA, USA). Calibration was performed using an external standard.

Cell Cultures and Cell Labeling. In vitro cellular uptake experiments were performed using rat and human bone marrow mesenchymal stem cells. Rat bone marrow mesenchymal stem cells (rMSCs) were obtained from the tibia and femur of 4-week-old Wistar rats. The ends of the bones were cut, and the marrow was extruded with Dulbecco's modified Eagle's medium (DMEM, PAA Laboratories, Linz, Austria) by using a needle and a syringe (*22*). Marrow cells were plated in a 75-cm^2 tissue culture flask (TPP, Trasadingen, Switzerland) in DMEM medium containing 10% fetal bovine serum (FBS, PAA Laboratories, Linz, Austria), 100 units/mL penicillin (Gibco BRL, Paisley, Scotland), and 0.1 mg/mL streptomycin (Gibco BRL). After 24 h, the nonadherent cells were removed by replacing the medium.

Human bone marrow mesenchymal stem cells (hMSCs) were obtained from the bone marrow of healthy donors after obtaining informed consent. Bone marrow aspirates were diluted in phosphate-buffered saline (PBS) and centrifuged through a density gradient (Ficoll-Paque Plus, GE Healthcare Life Sciences, Vienna, Austria) for 30 min at 1000 *g* (*22, 23*). Nucleated cells from the interface were plated in a 75-cm^2 tissue culture flask in α-modified Eagle's medium (α-MEM, Gibco BRL) containing 10% FBS, 100 units/mL penicillin, and 0.1 mg/mL streptomycin. After 48 h, the nonadherent cells were removed by replacing the medium.

Both types of cells were cultured in a humidified 5% CO_2 incubator. The medium was replaced every 3 days as the cells grew to confluence. The cells were labeled with iron oxide nanoparticles. For cell labeling, either uncoated γ-Fe_2O_3 nanoparticles, the contrast agent Endorem, or PDMAAm-coated γ-Fe_2O_3 nanoparticles were used at the same concentration −15 μg Fe_2O_3/mL of media. After 72 h, the contrast agent was washed out by replacing the culture medium.

Transmission Electron Microscopy (TEM). Nanoparticle localization inside the cells was observed by transmission electron microscopy. MSCs were incubated with the nanoparticles for 72 h, transferred onto polylysine-coated coverslips, fixed in 2.5% glutaraldehyde in 0.1 M Sörensen buffer for 48 h at 4 °C, and stained by 1% osmium tetraoxide in 0.1 M Sörensen buffer for 2 h. Cells were then dehydrated in ethanol, immersed in propylene oxide, and flat embedded in Epon 812 using gelatin capsules. After polymerization for 72 h at 60 °C, coverslips were removed by liquid nitrogen. Ultrathin sections of 60 nm were examined with a Philips Morgagni 268D transmission electron microscope (FEI Inc., Hillsboro, OR, USA).

Cell Viability. The viability of cells was analyzed using a colorimetric assay based on the cleavage of the tetrazolium salt WST-1 (4-[3-(4-iodophenyl)-2-(4-nitrophenyl)-2*H*-5-tetrazolio]-1,3-benzene disulfonate) (Roche Diagnostics, Mannheim, Germany) to a highly water-soluble formazan dye by mitochondrial dehydrogenases in viable cells (*24*). rMSCs or hMSCs (2nd and 5th passages) were plated on 96-well plates (TPP, Trasadingen, Switzerland) at a density of 5×10^3 cells/well. The cells were cultured and labeled with iron oxide nanoparticles as described above. Twelve wells of each cell type were labeled with Endorem and 12 wells with PDMAAm-coated maghemite nanoparticles, and 12 wells were not labeled and served as control samples. On the day that nanoparticles were withdrawn (day 3), 10 μL of the WST-1 solution was added to 100 μL of culture medium per well, and the cells were kept in the incubator (37 °C) for an additional 2 h. The absorbance was measured using an ELISA plate reader (Tecan Spectra, Tecan Trading, Switzerland) at a wavelength of 450 nm.

Labeling Efficiency and Staining Intensity. Labeling efficiency was determined by manually counting the number of Prussian Blue-stained and unstained cells in 96-well plates and measuring the staining intensity of Prussian Blue-stained cells colorimetrically. Twelve optical fields from each plate were scanned using an Axioplan Imaging II microscope at 100× magnification using a 10×/0.75 objective lens, an AxioCam digital camera, and AxioVision 4 software (microscope setup from Zeiss, Oberkochen, Germany). All of the cells in the scanned images were manually labeled as Prussian Blue-stained or unstained using Jasc Paint Shop Pro 8 (Corel Corporation, Ottawa, Canada). The scanned images with manually labeled cells were processed by the Image analysis toolbox of MATLAB software (The MathWorks, Inc., MA, USA). Before the analysis, we validated the colorimetric scale from the image colors corresponding to the increasing intensities of the Prussian Blue staining of the cells. Then we processed each Prussian Blue-stained cell in the image and determined the intensity of the cytoplasmic staining as the intensity of the color of the cytoplasm on the scale. As a result, two parameters were obtained: (i) the presence or absence of a label inside the cells expressed as the percentage of labeled cells and (ii) the amount of label inside the cells, which correlates with the intensity of the staining.

In Vitro MR Relaxometry and MR Imaging of Labeled Cells Suspended in Gelatin. MR relaxometry of the particles was performed using a Bruker MiniSpec 0.5 T relaxometer and a Bruker BioSpec 4.7 T imager (both Etlingen, Germany). The latter apparatus was also used for MR imaging. Two types of labeled cells, rat and human MSCs, were dispersed in gelatin in the following concentrations: 50, 100, 200, 400, and 800 cells/μL. Control samples containing suspensions of unlabeled cells and Endorem-labeled cells were measured at the same concentrations. For T_1 relaxometry, the standard saturation recovery sequence was used; T_2 relaxometry was performed with a CPMG multispin−echo sequence. Measured relaxation times were converted to relaxation rates and related to cell concentrations. MR imaging was performed with T_2-weighted turbo-spin echo (effective echo time TE = 35 ms, repetition time TR = 3 s) and T_2*-weighted gradient echo (TE = 5 ms, TR = 100 ms) sequences that are commonly used in in vivo measurements.

Iron Analysis. The amount of iron in the cells after mineralization was determined by spectrophotometry. Cell-containing samples were mineralized by the addition of 5 mL of HNO_3 and 1 mL of H_2O_2 in an ETHOS 900 microwave mineralizator (Millestone, Sydney, Australia). Deionized water was added to reach a total volume of 100 mL. The iron content was determined using a Spectroflame M120S apparatus (Spectro, Littleton, MA, USA) calibrated with a standard Astasol solution (Analytika, Prague, Czech Republic). The measurements were repeated four times, and the average mean value was determined.

Cell Grafting. The rats ($n = 5$) were anesthetized with isoflorane and mounted in a stereotactic frame. Using an aseptic technique, a burr hole (1 mm) was made in the skull to expose the dura overlying the cortex. PDMAAm-modified iron oxide-

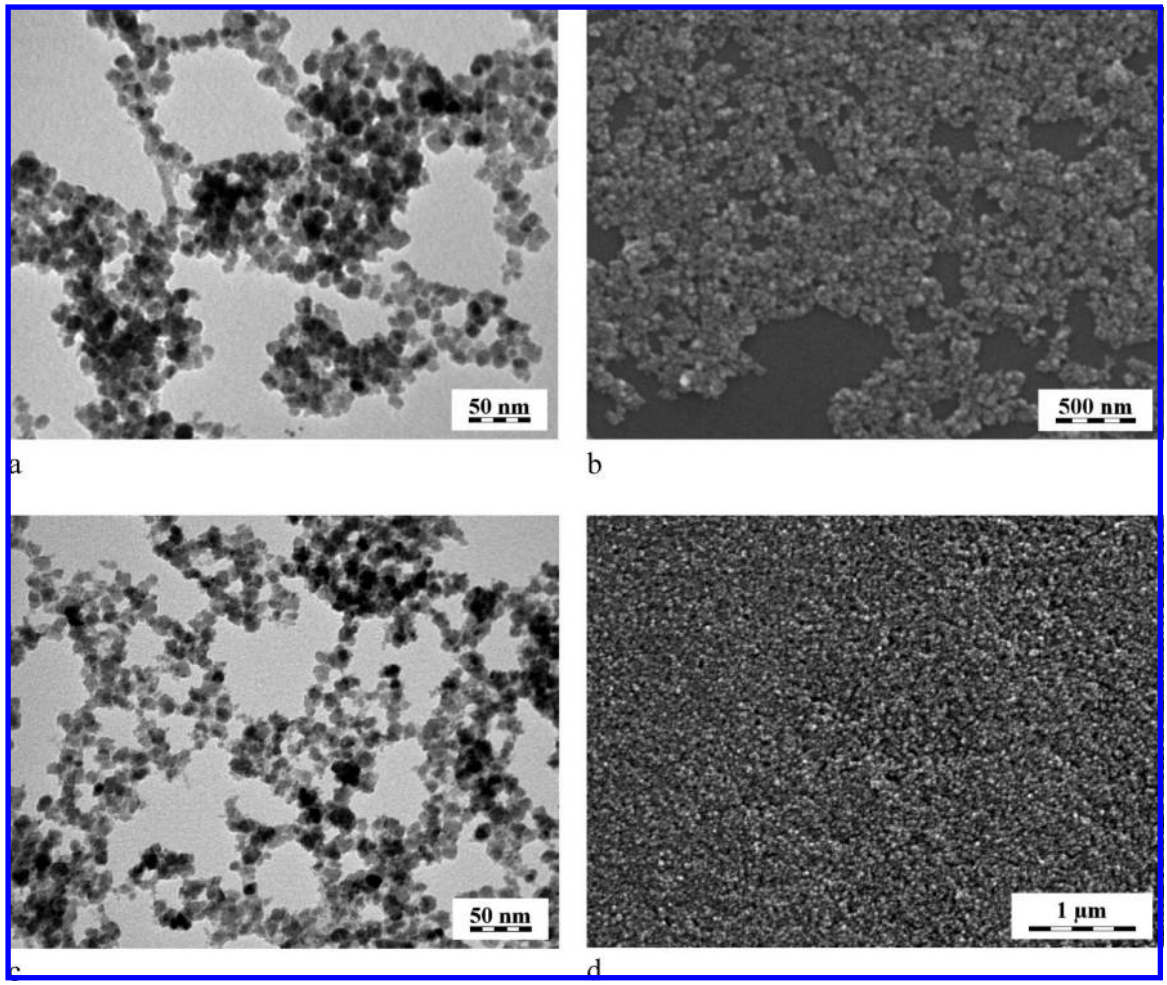

Figure 1. (a,c) TEM and (b,d) SEM micrographs of (a,b) primary uncoated γ-Fe_2O_3 particles No. 1 and (c,d) particles coated with PDMAAm by solution polymerization No. 5.

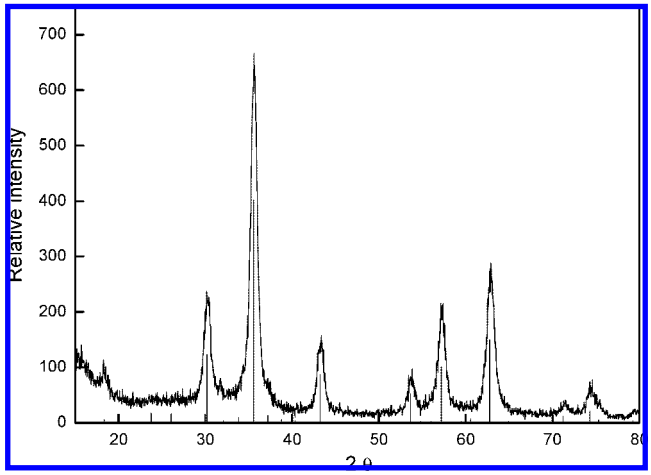

Figure 2. X-ray diagram of synthesized γ-Fe_2O_3 nanoparticles. Vertical bars, γ-Fe_2O_3 standard.

labeled cells or Endorem-labeled cells (5,000 cells suspended in 5 μL of PBS) were slowly injected intracerebrally into the brain over a 10-min period using a Hamilton syringe. Unlabeled cells were injected as a control. The opening was closed by bone wax, and the skin was sutured.

MR Imaging. The in vivo MR images were obtained on a 4.7 T Bruker imager equipped with a homemade surface coil. The rat was anesthetized by passive inhalation of 1.5−2% isoflorane in air. Breathing was monitored during the measurements. Single sagittal, coronal, and transversal images were obtained by a fast gradient echo sequence for localizing, then both T_2-weighted (turbospin echo sequence, TE = 35 ms, TR = 3 s, number of acquisitions AC = 8, matrix size 256 × 256, field of view FOV = 3.5 × 3.5 cm, slice thickness 0.75 mm) and T_2*-weighted (gradient echo sequence, TE = 12 ms, TR = 180 ms, number of acquisitions AC = 48, same geometry) axial images were acquired.

RESULTS AND DISCUSSION

Preparation of Maghemite. Maghemite (γ-Fe_2O_3) nanoparticles are one of the most commonly used ferric oxide particles because of their simple synthesis and chemical stability. Their advantage is that iron participates in human metabolism and is thus well tolerated by the living organism. First, magnetite was precipitated; its colloidal stability was achieved by charges induced by Fe^{3+} ions. However, because the above colloid is chemically unstable, undergoing uncontrolled oxidation upon contact with air, it was controllably chemically oxidized to maghemite, which shows long-term stability in either alkaline or acidic media. The ultimate advantage of the above procedure consists in the simplicity of purification by magnetic separation/decantation, which is much more convenient than the commonly used but more elaborate and time-consuming method of ultracentrifugation.

TEM and SEM images (Figure 1a,b) show agglomerated maghemite particles in a dry state. The agglomerates consist of primary particles with an average size D_n = 6.3 nm and a polydispersity index PDI = 1.33. X-ray diffraction measure-

Table 1. Modification of Maghemite Nanoparticles by the Solution Polymerization of DMAAm

sample	polymerization feed			colloidal stability[e]	D_h[c] (nm)	bound PDMAAm[d] (wt %)
	γ-Fe_2O_3 (g)	DMAAm (g)	ACVA (mg)			
1[a]	0.5	0	0	−	127 ± 3	0
2[b]	0.5	0.5	0	−	161 ± 3	0.21
3	0.5	0.375	3.8	aggr.	n.a.	
4	0.5	0.5	5	++	81.4 ± 0.6	0.7
5	0.5	1	10	++	56.9 ± 0.3	1.2
6	0.5	1.5	15	+	171 ± 5	1.95
7	0.5	1	5	++	77.8 ± 0.3	1.52
8	0.5	1	15	+	172 ± 22	1.7
9	0.5	1	20	aggr.	n.a.	2.74
10	0.5	1	30	aggr.	n.a.	4.95
11	0.5	0.375	10	++	55 ± 5	1.03
12	0.5	0.5	10	++	67 ± 3	1.1
13	0.5	1.5	10	aggr.	328 ± 4	1.06
14	0.5	2	10	aggr.	614 ± 12	1.6
15	1	1	10	++	76.6 ± 0.5	2.1
16	1.5	1	10	++	83.5 ± 0.2	0.88
17	2	1	10	++	75.1 ± 0.1	0.96
18	2.5	1	10	++	76 ± 0.5	0.74

[a] Primary uncoated γ-Fe_2O_3 (control). [b] PDMAAm solution was added to neat γ-Fe_2O_3 particles. [c] D_h, hydrodynamic diameter determined by dynamic light scattering. [d] From elemental analysis. [e] −, poor stability (aggregation within a week); +, high stability (no sediment after 3 months of storage); ++, very high stability (no sediment after 6 months of storage).

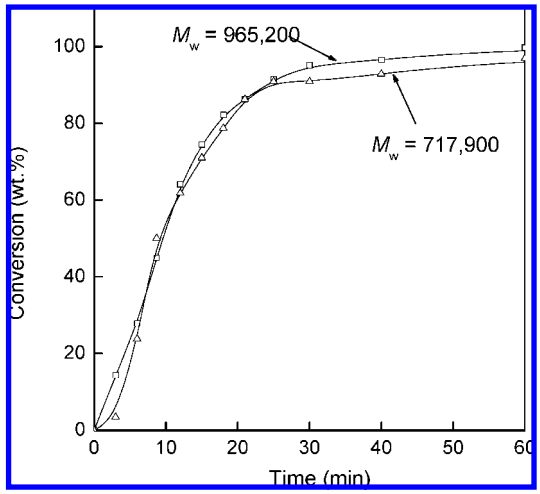

Figure 3. Conversion curves of DMAAm in solution polymerization in (Δ) the presence and (□) absence of γ-Fe_2O_3.

ments of the synthesized particles evidenced the typical spinel structure of γ-Fe_2O_3 (Figure 2). With respect to a small size of the crystallites, weak superstructural patterns indicated for the standard material were not detectable. Detailed Mössbauer spectra were published elsewhere (*25*).

Solution Radical Polymerization of DMAAm in the Presence of Maghemite Nanoparticles. The surface modification of nanoparticles is a general strategy for enhancing the permeability of nanoparticle-based therapeutics. To modify the iron oxide surface, the solution radical polymerization of DMAAm in aqueous ferrofluid was investigated. This could produce a dispersion of maghemite nanoparticles stable in a medium suitable for subsequent polymerization of DMAAm, thus facilitating their subsequent incorporation in the polymer microspheres. At the same time, it provides a model for investigating the effect of iron oxide nanoparticles on the polymerization process. In the system, ACVA was preferred over 2,2′-azobisisobutyronitrile (AIBN) as an initiator because its solubility in an aqueous monomer solution is much higher than that of AIBN. An additional advantage of ACVA consists in its carboxyl group's ability to interact with iron oxide. The polymerization conditions are summarized in Table 1. The effect of several polymerization parameters, such as the concentrations

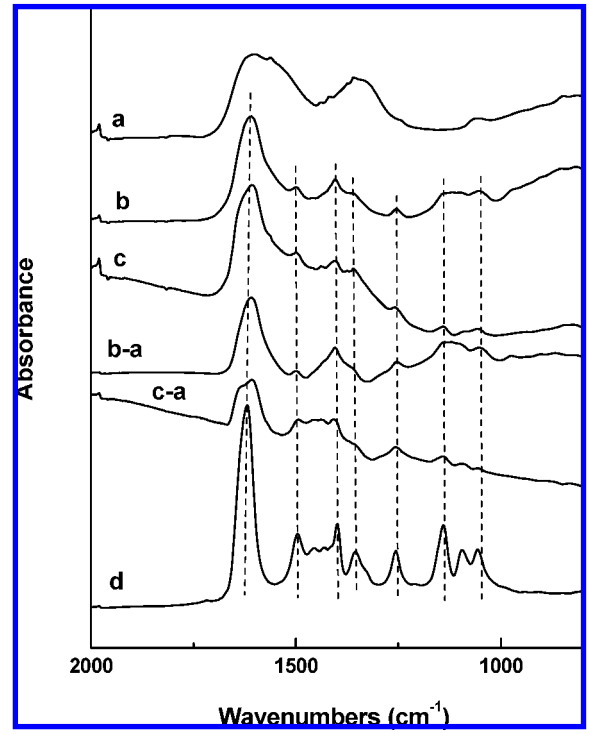

Figure 4. ATR FTIR spectra of γ-Fe_2O_3 nanoparticles before and after surface modification with PDMAAm. (a) Before modification, (b) coating by solution polymerization in the presence of γ-Fe_2O_3 nanoparticles No. 3, (c) coating by encapsulation of γ-Fe_2O_3 nanoparticles in the polymer No. 2, (b-a) and (c-a) the corresponding differential spectra of coated and uncoated γ-Fe_2O_3, and (d) pure PDMAAm.

of the monomer, the initiator, and the iron oxide in the feed, on particle size and the amount of PDMAAm bound to the particles was investigated. For the sake of comparison, the characteristics of neat (uncoated) maghemite nanoparticles and of nanoparticles coated with a solution of preprepared PDMAAm are also shown in Table 1.

Conversion Curves. Conversion curves were determined in order to estimate the effect of maghemite on the polymerization process. The presence of maghemite colloid in the feed affected the molecular weight of the resulting PDMAAm compared to solution radical polymerization without maghemite. The mo-

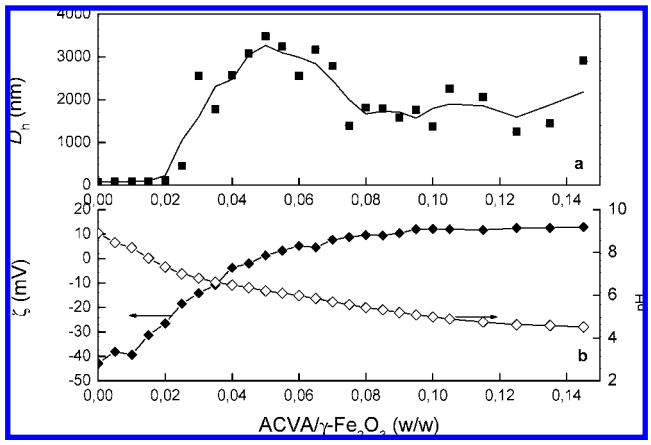

Figure 5. Dependence of the (■) hydrodynamic diameter D_h (a), (◆) ζ-potential, and (◇) pH (b) on the ACVA/γ-Fe_2O_3 ratio.

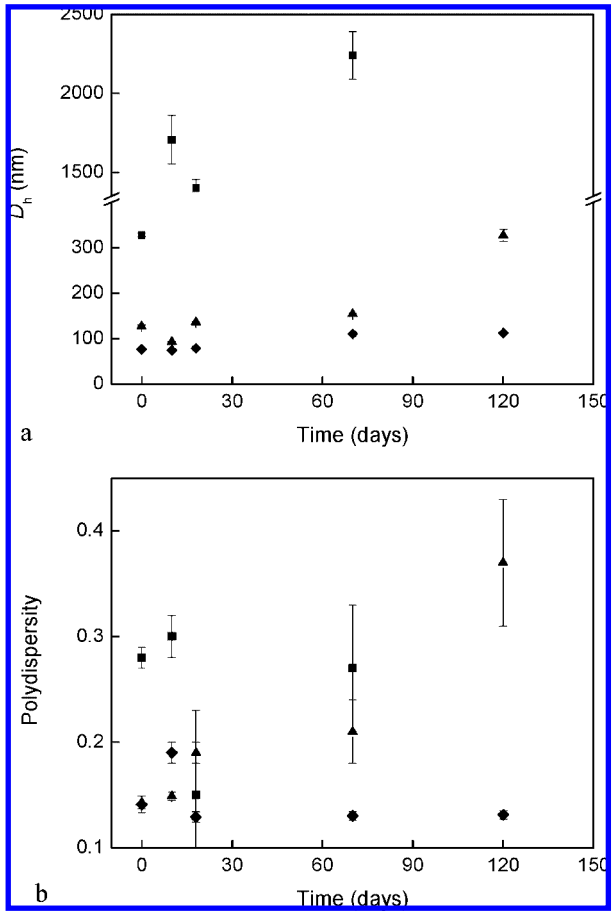

Figure 6. Dependence of the (a) hydrodynamic particle diameter D_h and (b) polydispersity, measured by dynamic light scattering, on storage time; (▲) uncoated γ-Fe_2O_3 No. 1, PDMAAm-coated γ-Fe_2O_3 (◆) No. 18, and (■) No. 13.

lecular weight of PDMAAm prepared in the presence of maghemite was 717,900, i.e., lower than that prepared in its absence (965,200). This can be attributed to the growing polymer chains probably terminating on the nanoparticle surface as documented by the slower consumption of monomers in the initial and final stages of the polymerization (Figure 3). Because of the termination, PDMAAm can be attached to the maghemite surface. The possible complexation of the ACVA initiator with maghemite Fe atoms can contribute to additional DMAAm initiation. At γ-Fe_2O_3/DMAAm ratios of 0.5/0.375 (w/w) and lower, free PDMAAm was present in the mixture after polymerization. The colloidal stability then decreased with an increasing γ-Fe_2O_3/DMAAm ratio.

FTIR Spectra. The structure of the surface and the efficiency of the coating of magnetic nanoparticles were analyzed by surface-sensitive ATR FTIR spectroscopy. FTIR spectra of iron oxide before modification, after coating by solution radical polymerization in the presence of γ-Fe_2O_3 nanoparticles, after coating by encapsulation of maghemite nanoparticles in the polymer, the corresponding differential spectra of coated and uncoated surfaces, and the spectrum of pure PDMAAm are shown in Figure 4. The spectrum of coating by encapsulation of maghemite γ-Fe_2O_3 nanoparticles (see corresponding differential spectrum) is relatively weak and is very close to the spectrum of pure PDMAAm. This signifies that some amount of polymer adheres to the surface of the nanoparticles. The spectrum of coating by solution radical polymerization in the presence of maghemite nanoparticles (see corresponding differential spectrum) is stronger and differs from the spectrum of pure PDMAAm in some aspects. The band of Amide I (*26*) observed at 1618 cm^{-1} is shifted to 1608 cm^{-1}, and the intensity of the band of Amide II observed at 1404 cm^{-1} increased after polymerization. The peaks of CH_3 deformation vibration at about 1495 and 1354 cm^{-1} decreased in their relative intensity. We hypothesize that these changes correspond to the interaction of the protonated NH^+ groups of PDMAAm with citrates complexed on the iron oxide surface. Citrate is adsorbed on the ferric oxide surface via one or two carboxylate moieties, allowing the use of one of the ungrafted carboxylic acid groups to bind a polycation. This confirms that the PDMAAm shell has effectively formed at the surface of the iron oxide particles.

DLS, TEM, and Elemental Analysis. Particle size and its distribution have a strong effect on the physical and biochemical properties of colloidal dispersions. Many methods have been described for the measurement of average particle size, such as electron microscopy, dynamic light scattering, and chromatographic methods; the former two techniques were used in this study.

ACVA-initiated solution polymerization of DMAAm in the presence of maghemite nanoparticles produced a very stable colloid, with the particles typically in the hydrodynamic size (D_h) range of 50−170 nm. Because DLS provides information on the hydrodynamic particle size of whole particle clusters, including polymer coating layers and the magnetic core, the size of the iron oxide core alone was examined by TEM. Figure 1c,d shows TEM and SEM images of the obtained DMAAm-coated nanoparticles with an average size $D_n = 7.5$ nm and a polydispersity index PDI = 1.20. A comparison of Figure 1a,b and Figure 1c,d reveals that both the shape and the size of the particles after the coating process effectively did not change from those of the uncoated particles. It is worth pointing out that the particle size determined by TEM was smaller compared with the particles size of the same latex obtained from DLS measurements (Table 1). These results confirm the presence of a hydrophilic polymer hairy layer on the particle surface, which increases the value of the average hydrodynamic diameter during the DLS measurements and which is collapsed onto the particle surface during the drying of the TEM sample. It should also be remembered that while TEM provides the number-average particle size, DLS gives the z-average, which is sensitive to large-size particles.

Effect of the Reaction Parameters. The effect of the amount of the monomer in the polymerization feed on colloidal stability, hydrodynamic particle size, and the percentage of PDMAAm bound to the particles (determined from elemental analysis) at a constant initiator concentration (1 wt % in the monomers) is documented in Table 1 for experiments Nos. 3−6. Particles aggregated at low amounts of bound PDMAAm. The percentage

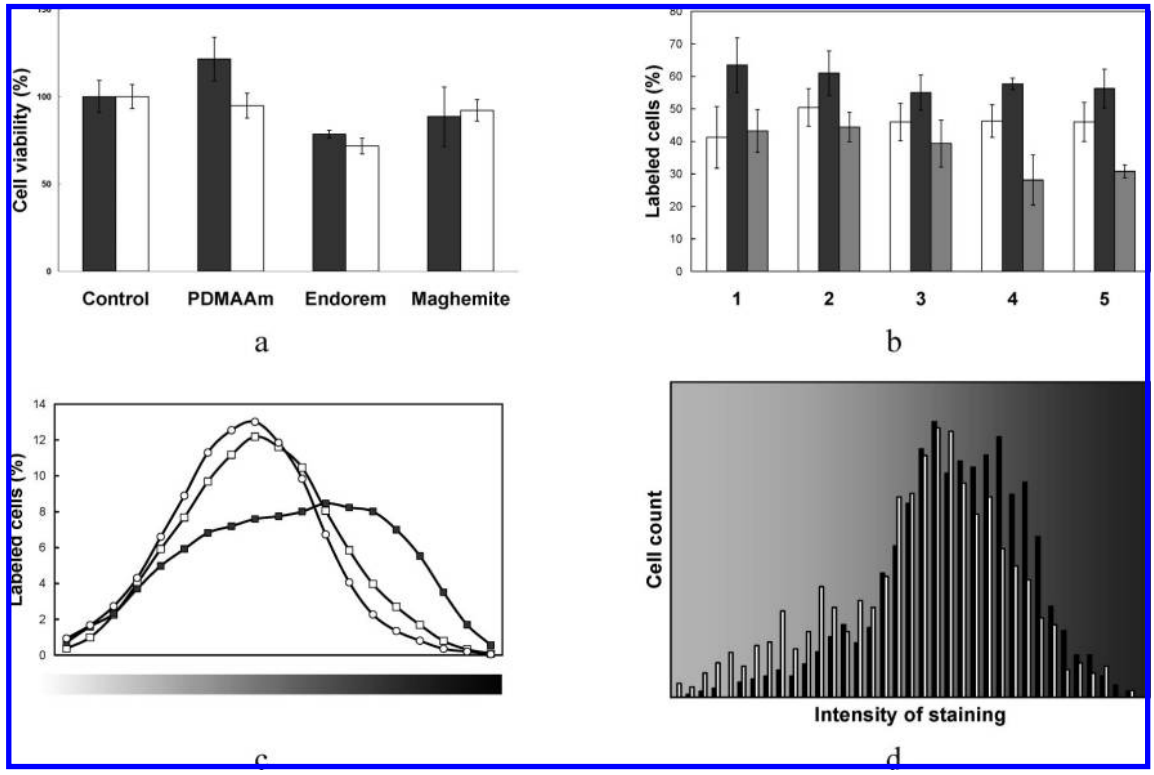

Figure 7. (a) Viability of rat (■) and human MSCs (□) labeled with several types of iron oxide nanoparticles. PDMAAm-coated nanoparticles No. 7 were used. (b) Labeling efficiency (expressed as the percentage of labeled cells) of rat MSCs from the 1st−5th passage (columns 1−5) labeled with uncoated γ-Fe_2O_3 (□), PDMAAm-coated γ-Fe_2O_3 No. 7 nanoparticles (■), and Endorem (gray square). (c) Distribution of the intensity of Prussian Blue staining (*x*-axis) of rMSCs labeled with uncoated γ-Fe_2O_3 (□), PDMAAm-coated γ-Fe_2O_3 nanoparticles (■), and Endorem (○). (d) Histograms of the intensity of staining of rat and human MSCs; note that hMSCs (■) are more intensively labeled than rMSCs (□).

Table 2. Cell Labeling Efficiency with Surface-Modified and Unmodified Iron Oxide Nanoparticles

	percentage of labeled cells	
	rMSC	hMSC
Endorem	39 ± 6	68 ± 5
uncoated γ-Fe_2O_3	46 ± 5	70 ± 5
PDMAAm-coated γ-Fe_2O_3	59 ± 5	82 ± 5

of bound PDMAAm generally reached up to ca. 2 wt %, while free PDMAAm was removed during washing. The more DMAAm in the polymerization feed, the more PDMAAm was bound to the particles.

The effect of the amount of initiator in the feed on colloidal stability, hydrodynamic particle diameter, and the percentage of bound PDMAAm is documented in Table 1 for experiments Nos. 5 and 7−10. At <10 mg of ACVA in the polymerization feed, the D_h of the resulting particles was smaller than that of the primary maghemite particles (Table 1). This can be explained by the steric repulsion of PDMAAm chains on their surface, which decreases the number of particle associates measured by DLS. At higher ACVA amounts, the stability of the colloidal system was lost, and the particles aggregated. Both the hydrodynamic particle size D_h and the percentage of bound PDMAAm determined from elemental analysis increased with increasing amounts of the initiator in the feed up to 15 mg of ACVA (Nos. 5, 7, and 8 in Table 1). The increasing percentage of bound PDMAAm at higher initiator concentrations can be ascribed to a larger number of carboxyl groups available to anchor more PDMAAm chains on the maghemite particle and/or a greater tendency toward particle aggregation. To explain why steric stabilization occurred only at concentrations lower than 15 mg of ACVA in the feed, ACVA was added to the maghemite colloid, and hydrodynamic diameter D_h, ζ-potential, and pH were monitored depending on the ACVA/γ-Fe_2O_3 ratio. With the ACVA/γ-Fe_2O_3 ratio increasing from ∼0.02 (w/w), hydrodynamic diameter sharply increased (Figure 5a). This can be explained by the increase of ζ-potential from ca. −43 mV, reaching a critical value at −30 mV and accompanied by a steep decrease of pH till the ACVA/γ-Fe_2O_3 ratio reached 0.02 (Figure 5b). It should be noted that ± 30 mV is the limiting value for effective electrostatic stabilization. Further ACVA addition thus increased ζ-potential up to 13 mV, which was inadequate to stabilize the particles; consequently, they aggregated. The coating efficiency of PDMAAm was further deduced from a comparison of maghemite modified by solution radical polymerization of DMAAm with a sample obtained by the addition of separately prepared PDMAAm to the maghemite colloid. The data shown in Table 1 (Nos. 2 and 4) argue in favor of solution polymerization.

The effect of the amount of the monomer in the polymerization feed at constant amounts of initiator and maghemite is shown in Table 1 for experiments No. 5 and 11−14. Particle aggregation occurred with amounts of 1.5 g or more DMAAm in the feed, probably because of the undesirable physical cross-linking of PDMAAm chains and the increased viscosity of the reaction mixture. At a constant amount of initiator in the feed, the percentage of PDMAAm bound to the particles did not change with increasing amounts of DMAAm (with the exception of No. 14 in Table 1 because of the high viscosity of the mixture), thus documenting the key role of the amount of initiator on encapsulation efficiency.

The effect of the amount of γ-Fe_2O_3 added in the feed under otherwise identical conditions is documented by experiments No. 5 and 15−18 in Table 1. While the particle diameter was almost constant (within the experimental error), the amount of bound PDMAAm decreased with increasing amounts of γ-Fe_2O_3 in the feed, as expected.

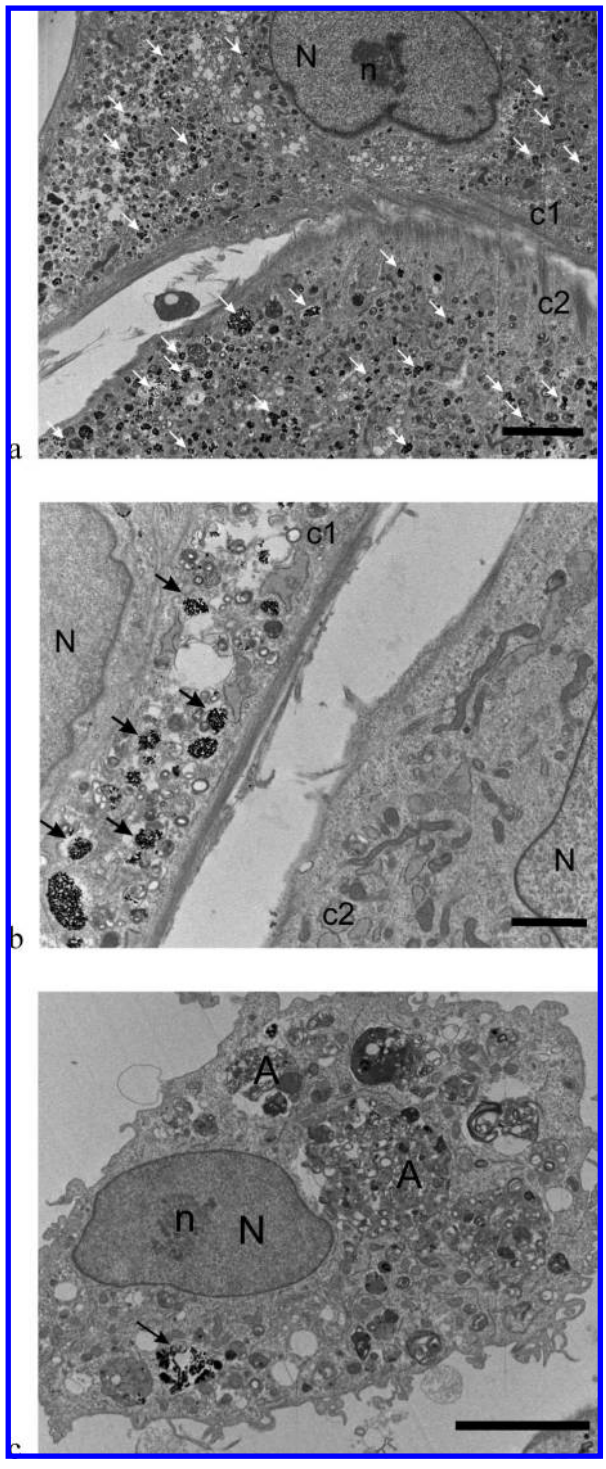

Figure 8. TEM micrographs of rMSCs labeled with (a) PDMAAm-coated γ-Fe_2O_3 nanoparticles, (b) Endorem, and (c) uncoated γ-Fe_2O_3. Arrows indicate nanoparticles inside the endosomes. A, autophagosome; N, nucleus; n, nucleolus; c1 and c2, cell 1 and cell 2, respectively. Scale bar: a,c, 500 nm; b, 200 nm.

Colloidal Stability. The long-term colloidal stability of PDMAAm-coated maghemite nanoparticles is of utmost importance for prospective biological applications. The stability of some dispersions over time was determined by DLS (Figure 6). Almost no increase in the hydrodynamic size and consistently low polydispersity over several months were observed in colloid No. 18, thus documenting its perfect stability in water due to the presence of the PDMAAm coating. The colloidal stability of such samples is denoted as very high in Table 1. The good colloidal stability suggests that the stabilization of the maghemite nanoparticles was primarily dependent on the steric repulsion of the attached hydrophilic PDMAAm chains. In comparison, uncoated nanoparticles No. 1 were unstable. Both the hydrodynamic diameter and polydispersity of these particles increased with time because of aggregation. Similarly, the stability of nanoparticles No. 13, prepared in the presence of large amounts of monomer, was poor. This can be explained by the high viscosity of the polymerization mixture, as a consequence of which the PDMAAm chains could entangle, resulting in particle aggregation. This is documented by the extremely large size and polydispersity determined by DLS in Figure 6a,b.

Viability of Cells. In order to examine the acute toxicity of PDMAAm-coated maghemite nanoparticles, both rMSCs and hMSCs were incubated for 72 h with sample No. 7, uncoated nanoparticles No. 1, and Endorem (control) at concentrations of 15 μg γ-Fe_2O_3/mL, and cell viability was assessed using the WST-1 assay. The viability of both rat and human MSCs labeled with PDMA nanoparticles did not markedly decrease compared to that of unlabeled MSCs (control). When mesenchymal stem cells were labeled with Endorem, their viability decreased by 32%, and uncoated nanoparticles decreased the viability by 15% (Figure 7a). However, the TEM images showed that the cells labeled with uncoated nanoparticles were undergoing programmed cell death (see below); therefore, in long-term follow up the viability would be affected.

Cell Labeling Efficiency. To investigate the role of the PDMAAm coating and its effect on the internalization of the maghemite nanoparticles by target cells, both hMSCs and rMSCs were incubated with PDMAAm-coated nanoparticles No. 7 or Endorem; uncoated maghemite nanoparticles served as controls. The uptake of nanoparticles into the cells (expressed as the percentage of labeled cells) was investigated using Prussian Blue staining. The cellular uptake of particles generally depends on the cell type and the particle size and surface properties, including surface charge and surface hydrophilicity (*27, 28*). It also depends on the number of passages of the cells, which is a characteristic physiological cell property. The lower the passage, the more efficient the cell labeling. The most intensive staining of any iron oxide nanoparticles was thus observed for cells from the first and second passages, while the intensity of the blue staining decreased in the fifth passage (only 30% of cells were labeled with Endorem). rMSCs cultured with PDMAAm-coated maghemite nanoparticles showed considerably higher nanoparticle uptake (59%) than those cultured with Endorem (39%; Table 2). This means that the number of rMSCs labeled by PDMAAm-coated γ-Fe_2O_3 was more than 50% higher than the number labeled by Endorem. Moreover, the labeling efficiency (percentage of labeled cells) was stable and was not dependent on the number of passages (Figure 7b). Even higher PDMAAm-nanoparticle uptake was observed in hMSCs (82%; Table 2), whereas Endorem uptake was 68%. The number of hMSCs labeled by PDMAAm-coated γ-Fe_2O_3 was thus more than 20% greater than the number labeled by Endorem. Histograms showing the intensity of Prussian Blue staining, which corresponds to the amount of label inside the cell, revealed that more cells were intensely stained with PDMAAm-coated nanoparticles than with Endorem or maghemite (Figure 7c). These results were even more apparent or amplified in hMSCs (Figure 7d). Although a relatively large number of cells were labeled with uncoated maghemite nanoparticles, the advantage of the PDMAAm coating consists in the possibility of its modification, thus introducing desired functional groups. An additional substantial advantage of PDMAAm-coated γ-Fe_2O_3 exists in the stability of the formed colloid, in contrast to uncoated γ-Fe_2O_3 nanoparticles that coagulate after the addition of the culture media. Coagulation of uncoated maghemite nanoparticles also leads to the attachment of the nanoparticles

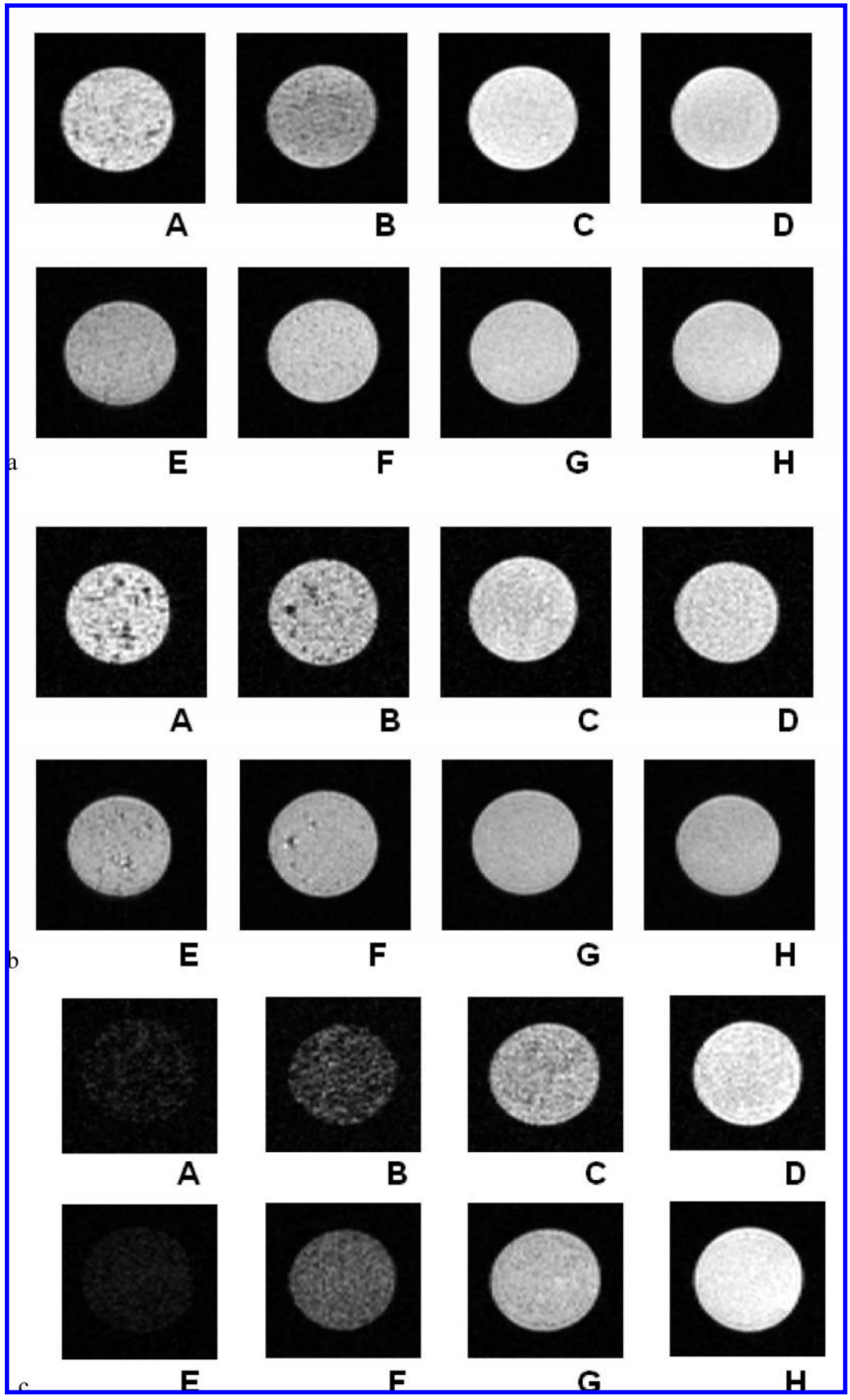

Figure 9. MRI of phantoms containing labeled (a) human and (b) rat mesenchymal stem cells suspended in gelatin measured by a T_2*-weighted gradient echo sequence (A−D) and by a T_2-weighted turbo-spin echo sequence (E−H). A,E, cells labeled by PDMAA-coated maghemite nanoparticles No. 7; B,F, cells labeled by uncoated maghemite nanoparticles No. 1; C,G, cells labeled by Endorem; D,H, unlabeled cells. Each sample (0.5 mL) contained 25,000 cells, yielding on average 1 cell per image voxel. For comparison, an MRI of phantoms containing a high number (400,000) of labeled human cells is shown in c; the phantoms are in the same order as in a.

Table 3. Relaxation Rates r_1 and r_2 (Related to Cell Concentration) of hMSCs and rMSCs Labeled with Endorem (Control), Uncoated (Control) No. 1, and PDMAAm-Coated Maghemite Nanoparticles No. 7, and the Amount of Iron Internalized Inside the Cells[a]

	hMSCs ($s^{-1}/10^6$) cells/mL)				rMSC ($s^{-1}/10^6$ cells/mL)			
	r_1 (0.5 T)	r_2 (0.5 T)	r_2 (4.7 T)	Fe (pg/cell)	r_1 (0.5 T)	r_2 (0.5 T)	r_2 (4.7 T)	Fe (pg/cell)
Endorem	undetectable	0.88 ± 0.34	1.7 ± 0.5	3.2 ± 0.5	0.21 ± 0.19	0.13 ± 0.14	0.72 ± 0.09	undetectable
uncoated γ-Fe_2O_3	0.52 ± 0.09	7.13 ± 0.77	9.8 ± 3.3	17.1 ± 0.3	0.55 ± 0.20	3.67 ± 0.62	4.95 ± 0.17	29.3 ± 4.9
PDMAAm-coated γ-Fe_2O_3	1.19 ± 0.04	27.26 ± 0.24	40.8 ± 1.6	36.9 ± 0.5	0.41 ± 0.13	2.91 ± 0.50	4.18 ± 0.40	23.2 ± 2.9

[a] Measured at 0.5 and 4.7 T.

Figure 10. T_2-weighed MR image of a rat brain with 5,000 rMSCs labeled with PDMAAm-coated nanoparticles No. 7 or Endorem, implanted in the left or right hemisphere, respectively. White and black arrows indicate the injection sites in the head and the nanoparticles in the brain, respectively.

to the cell surface. This effect is also responsible for the high labeling efficiency of uncoated maghemite nanoparticles. It was difficult to distinguish using light microscopy whether the nanoparticles were inside the cells or just attached to the cell surface. Cells with iron oxides attached to the surface are better targets for macrophages after transplantation, and iron oxides incorporated into macrophages can also give a false positive signal on MRI.

TEM Images. Intracellular uptake was also visualized with TEM as it provides higher resolution than does light microscopy. While these methods cannot provide a quantitative measurement of cellular uptake, they demonstrate the importance of visualization to determine the distribution of particles on a cellular and subcellular level. PDMAAm chains are thought to form a complex with surface charges on the cell surface or else have an affinity with the cell membrane that facilitates endocytosis. A TEM image (Figure 8) shows that the cells internalized the PDMAAm-coated maghemite nanoparticles in large numbers and accumulated them in endosomes. Organelles and cell structures were not affected by the presence of coated nanoparticles inside the cells. However, the majority of cells labeled with uncoated maghemite were undergoing programmed cell death, probably by autophagia. The cells contained large autophagosomes, recognized in micrographs as membrane bound organelles with other organelles clearly contained within them, together with uncoated nanoparticles (Figure 8b). MSCs stained with Endorem showed a heterogeneous distribution of the nanoparticles. Some of the cells contained numerous endosomes filled with nanoparticles, others only a few or none (Figure 8c). The results obtained from TEM images are in agreement with those of our colorimetric analysis of the intensity of Prussian Blue staining (Figure 7c) as well as with those obtained from MR relaxometry (see text below and Table 3).

NMR Relaxometry. The iron oxide concentration of labeled rat and human cells was assessed using MR relaxometry. Relaxation rates measured at 0.5 and 4.7 T are listed in Table 3. Relaxation rates r_1 and r_2 are related to the number of cells per mL after subtracting the contribution of unlabeled cells. At a higher field strength (4.7 T), the contribution of all the particles to total r_1 was negligible; the values are therefore not provided. PDMAAm-coated iron oxide-labeled human cells provided significantly higher r_1 and r_2 at both 0.5 and 4.7 T fields than Endorem- and uncoated-iron-oxide-labeled cells. Large differences were obtained in the relaxation rates of PDMAAm-labeled human and rat cells, with r_2 several times higher for human cells. PDMAAm-coated iron oxide-labeled rat cells provided higher relaxation rates than Endorem-labeled ones; however, they were quite comparable to data obtained from uncoated-iron-oxide-labeled cells. Iron analysis proved that the higher relaxation rates of PDMAAm-coated or uncoated iron-oxide-labeled cells compared with Endorem-labeled ones are caused mainly by higher iron internalization (Table 3). It is interesting to note that human cells prefer PDMAAm-coated nanoparticles to both Endorem and uncoated ones, whereas in the case of rat cells, uncoated iron particles are internalized slightly better than PDMAAm-coated ones (both nanoparticles are internalized at a markedly higher rate than Endorem). These results are in good agreement with the relaxometry results.

MR Imaging of Cells after Nanoparticle Internalization in Gelatin. Gelatin samples with suspended cells labeled by PDMAAm-coated iron oxide nanoparticles, Endorem, and bare particles were examined by MRI to evaluate the potential of PDMAAm-coated iron oxide nanoparticles as a targeted MR contrast agent. Figure 9 compares MR images of cell phantoms. The T_2-and T_2*-weighted MR images of phantoms containing cells incubated with PDMAAm-coated and uncoated iron oxide nanoparticles show a significant negative contrast enhancement (signal darkening) over those containing cells labeled with Endorem and unlabeled cells (Figure 9a,b). As the MR images are normalized during processing, it is not possible to decide (based on observation with the naked eye) which of the two types of nanoparticles provides better contrast. However, the MR image of phantoms containing a high number of cells (Figure 9c) unambiguously proves that cells labeled by PDMAAm-coated iron oxide nanoparticles show significantly higher negative contrast enhancement. The results thus confirm that there is a preferential uptake of PDMAAm-coated iron oxide nanoparicles, i.e., the amount of internalized iron is markedly higher (see also Table 3), especially in human cells.

In Vivo MR Imaging. Magnetic labeling and MRI were used to noninvasively monitor cells injected into rats. PDMAAm-coated iron-oxide- and Endorem-labeled rMSCs (5,000 cells in 5 μL of PBS) were injected into the left and right rat hemispheres, respectively. Only cells labeled with PDMAAm-coated iron-oxide nanoparicles (left hemisphere) were detected (Figure 10).

CONCLUSIONS

In this article, PDMAAm-coated γ-Fe_2O_3 nanoparticles were obtained by the solution radical polymerization of DMAAm in the presence of maghemite nanoparticles obtained by the

chemical coprecipitation of Fe(II) and Fe (III) salts with ammonium hydroxide and subsequent oxidation with sodium hypochlorite. The presence of the PDMAAm coating on the maghemite surface was confirmed by both elemental analysis and ATR FTIR spectroscopy. PDMAAm coating provided good dispersibility of the magnetic nanoparticles in an aqueous medium and substantially improved iron oxide colloidal stability in the culture medium compared with uncoated maghemite, which immediately precipitated or aggregated within 1 h. A key parameter determining the amount of PDMAAm bound on maghemite nanoparticles is the amount of initiator in the polymerization feed. The amount of the initiator also influences the stability of the colloid. A narrow range of reaction conditions (5−15 mg of ACVA in the feed) was found under which particle aggregation was avoided, and at the same time, PDMAAm coating of the particles was high. DLS data revealed that the particle sizes were not altered even after several months of incubation in water. The surface of the particles is the determining factor for the efficiency of cellular uptake. Magnetic cellular labeling was evaluated by Prussian Blue staining for iron content, T_2 relaxometry, and MR imaging of labeled cell suspensions. PDMAAm coating did not adversely affect the penetration of the iron oxide nanoparticles into cells. After 72 h of culture in media containing 15 μg of iron oxide per 1 mL, the morphology and viability of both rMSCs as well as hMSCs were close to those of unlabeled cells, suggesting the biocompatibility of the nanoparticles. PDMAAm-coated maghemite nanoparticles turned out to be particularly suitable for labeling rat and human MSCs for in vivo MR cell tracking. The PDMAAm-coated maghemite nanoparticles were shown to be taken up by the target cells at significantly higher levels than were Endorem nanoparticles coated with dextran, thus allowing a minimum amount of imaging agent to be used. In addition, the labeling was not dependent on cell passage number, which can be particularly useful for cell expansion. Significant contrast enhancement was demonstrated by cells labeled with PDMAAm-coated maghemite nanoparticles and implanted in a rat brain over cells labeled with Endorem.

The fact that PDMAAm coating of iron oxide nanoparticles improves cellular uptake is, to the best of our knowledge, a new observation yet to be published. In subsequent research, PDMAAm-coated maghemite nanoparticles can be further modified by covalent attachment of highly specific biomolecules (antibodies, peptides, etc.) to make labeling more specific. In potential applications, cells can be labeled in vitro with the nanoparticles prior to transplantation. After transplantation of the labeled cells, in vivo imaging monitors cell migration throughout the body. The ability to track the extent of migration following direct implantation or systemic injection in vivo using noninvasive MR imaging techniques is the greatest advantage of the described procedure. Cellular monitoring is particularly important for evaluating cell-based therapies.

ACKNOWLEDGMENT

The financial support of the Center for Cell Therapy and Tissue Repair No. 1M0538, the Grant Agency of AS CR (grants KAN201110651 and KAN200200651), the Grant Agency of the Czech Republic (203/09/1242) and the EC-FP6 project DiMI (LSHB-CT-2005-512146) is gratefully acknowledged.

LITERATURE CITED

(1) Lewin, M., Carlesso, N., Tung, C. H., Tang, X. W., Cory, D., Scadden, D. T., and Weissleder, R. (2000) Tat peptide-derivatized magnetic nanoparticles allow in vivo tracking and recovery of progenitor cells. *Nat. Biotechnol. 18*, 410–414.

(2) Modo, M., Hoehn, M., and Bulte, J. W. (2005) Cellular MR imaging. *Mol. Imaging 4*, 143–64.

(3) Wilhelm, C., Billotey, C., Roger, J., Pons, J. N., Bacri, J. C., and Gazeau, F. (2003) Intracellular uptake of anionic superparamagnetic nanoparticles as a function of their surface coating. *Biomaterials 24*, 1001–1011.

(4) Metz, S., Bonaterra, G., Rudelius, M., Settles, M., Rummeny, E. J., and Daldrup-Link, H. E. (2004) Capacity of human monocytes to phagocytose approved iron oxide MR contrast agents in vivo. *Eur. Radiol. 14*, 1851–1858.

(5) Muller, K., Skepper, J. N., Posfai, M., Trivedi, R., Horwath, S., Corot, C., Lancelot, E., Thompson, P. W., Brown, A. P., and Gillard, J. H. (2007) Effect of ultrasmall superparamagnetic iron oxide nanoparticles (Ferumoxtran-10) on human monocyte-macrophages in vitro. *Biomaterials 28*, 1629–1642.

(6) Hinds, K. A., Hill, J. M., Shapiro, E. M., Laukkanen, M. O., Silva, A. C., Combs, C. A., Varney, T. R., Balaban, R. S., Koretsky, A. P., and Dunbar, C. E. (2003) Highly efficient endosomal labeling of progenitor and stem cells with large magnetic particles allows magnetic resonance imaging of single cells. *Blood 102*, 867–872.

(7) Syková, E., and Jendelová, P. (2007) Migration, fate and in vivo imaging of adult stem cells in the CNS. *Cell Death Differ. 14*, 1336–1342.

(8) Veiseh, O., Sun, C., Gunn, J., Kohler, N., Gabikian, P., Lee, D., Bhattarai, N., Ellenbogen, R., Sze, R., Hallahan, A., Olson, J., and Zhang, M. (2005) Optical and MRI multifunctional nanoprobe for targeting glicomas. *Nano Lett. 5*, 1003–1008.

(9) Huh, Y. M., Jun, Y. W., Song, H. T., Kim, S., Choi, J. S., Lee, J. H., Yoon, S., Kim, K. S., Shin, J. S., Suh, J. S., and Cheon, J. (2005) In vivo magnetic resonance detection of cancer by using multifunctional magnetic nanocrystals. *J. Am. Chem. Soc. 127*, 12387–12391.

(10) Sun, C., Sze, R., and Zhang, M. (2006) Folic acid-PEG conjugated superparamagnetic nanoparticles for targeted cellular uptake and detection by MRI. *J. Biomed. Mater. Res. 78A*, 550–557.

(11) Tiefenauer, L. X., Kuhne, G., and Andres, R. Y. (1993) Antibody-magnetite nanoparticles: in vitro characterization of a potential tumor-specific contrast agent for magnetic resonance imaging. *Bioconjugate Chem. 4*, 347–352.

(12) Kresse, M., Wagner, S., Pfefferer, D., Lawaczek, R., Elste, V., and Semmler, W. (1998) Targeting of ultrasmall superparamagnetic iron oxide (USPIO) particles to tumor cells in vivo by using transferring receptor pathways. *Magn. Reson. Med. 40*, 236–242.

(13) Arbab, A. S., Bashaw, L. A., Miller, R. B., Jordan, E. K., Lewis, B. K., Kalish, H., and Frank, J. A. (2003) Characterization of biophysical and metabolic properties of cells labeled with superparamagnetic iron oxide nanoparticles and transfection agent for cellular MR imaging. *Radiology 229*, 838–846.

(14) Gershon, H., Ghirlando, R., Guttman, S. B., and Minsky, A. (1993) Mode of formation and structural features of DNA-cationic liposome complexes used for transfection. *Biochemistry 32*, 7143–7151.

(15) Jesephson, L., Tung, C. H., Moore, A., and Weissleder, R. (1999) Highly-efficient intracellular magnetic labeling with novel superparamagnetic-tat peptide conjugates. *Bioconjugate Chem. 10*, 186–171.

(16) Kostura, L., Kraitchman, D. L., Mackay, A. M., Pittenger, M. F., and Bulte, J. W. M. (2004) Feridex labeling of mesenchymal stem cells inhibits chondrogenesis but not adipogenesis or osteogenesis. *NMR Biomed. 17*, 513–517.

(17) Strable, E., Bulte, J. W. M., Moskowitz, B., Vivekanandan, K., and Douglas, T. (2001) Synthesis and characterization of soluble iron oxide-dendrimer composites. *Chem. Mater. 13*, 2201–2209.

(18) Bulte, J. W., Zhang, S., van Gelderen, P., Herynek, V., Jordan, E. K., Duncan, I. D., and Frank, J. A. (1999) Neurotransplantation of magnetically labeled oligodendrocyte progenitors: Magnetic resonance tracking of cell migration and myelination. *Proc. Natl. Acad. Sci. U.S.A. 96*, 15256–15261.

(19) Horák, D., Babič, M., Jendelová, P., Herynek, V., Trchová, M., Pientka, Z., Pollert, E., Hájek, M., and Syková, E. (2007) D-mannose-modified iron oxide nanoparticles for stem cell labeling. *Bioconjugate Chem. 18*, 635–644.

(20) Babič, M., Horák, D., Trchová, M., Jendelová, P., Glogarová, K., Lesný, P., Herynek, V., Hájek, M., and Syková, E. (2008) Poly(L-lysine)-modified iron oxide nanoparticles for stem cell labeling. *Bioconjugate Chem. 19*, 740–750.

(21) Orakdogen, N., and Okay, O. (2006) Reentrant conformation transition in poly(*N,N*-dimethylacrylamide) hydrogels in water-organic solvent mixtures. *Polymer 47*, 561–568.

(22) Azizi, S. A., Stokes, D., Augelli, B. J., DiGirolamo, C., and Prockop, D. J. (1998) Engraftment and migration of human bone marrow stromal cells implanted in the brains of albino rats: Similarities to astrocyte grafts. *Proc. Natl. Acad. Sci. U.S.A. 95*, 3908–3913.

(23) Pittenger, M. F., Mackay, A. M., Beck, S. C., Jaiswal, R. K., Douglas, R., Mosca, J. D., Moorman, M. A., Simonetti, D. W., Craig, S., and Marshak, D. R. (1999) Multilineage potential of adult human mesenchymal stem cells. *Science 284*, 143–147.

(24) Ishiyama, M., Shiga, M., Sasamoto, K., Mizoguchi, M., and He, P. (1993) A new sulfonated tetrazolium salt that produces a highly water-soluble formazan dye. *Chem. Pharm. Bull. 41*, 1118–1122.

(25) Závěta, K., Kančík, A., Maryško, M., Pollert, E., and Horák, D. (2006) Superparamagnetic properties of γ-Fe_2O_3 particles: Mössbauer spectroscopy and d.c. magnetic measurements. *Czech. J. Phys. 56* (Suppl. E), 83–91.

(26) Socrates, G. (2001) In *Infrared and Raman Characteristic Group Frequencies*, pp 143−145, Wiley, New York.

(27) Sun, R., Dittrich, J., Le-Huu, M., Mueller, M. M., Bedke, J., Kartenbeck, J., Lehman, J. K., Krueger, R., Bock, M., Huss, R., Seliger, C., Grone, H. J., Misselwitz, B., Semmler, W., and Kiessling, F. (2005) Physical and biological characterization of superparamagnetic iron oxide- and ultrasmall superparamagnetic iron oxide-labeled cells: A comparison. *Invest. Radiol. 40*, 504–513.

(28) Bentzen, E. L., Tomlinson, I. D., Mason, J., Gresch, P., Warnement, M. R., Wright, D., Sanders-Bush, E., Blakely, R., and Rosenthal, S. (2005) Surface modification to reduce non-specific binding of quantum dots in live cell assays. *Bioconjugate Chem. 16*, 1488–1494.

BC800373X

Příloha č. 4

Journal of Magnetism and Magnetic Materials 321 (2009) 1539–1547

Contents lists available at ScienceDirect

Journal of Magnetism and Magnetic Materials

journal homepage: www.elsevier.com/locate/jmmm

Effect of different magnetic nanoparticle coatings on the efficiency of stem cell labeling

Daniel Horák [a,b,*], Michal Babič [a,b], Pavla Jendelová [c,b], Vít Herynek [d], Miroslava Trchová [a], Katarina Likavčanová [c], Miroslava Kapcalová [c], Milan Hájek [b,d], Eva Syková [c,b]

[a] Institute of Macromolecular Chemistry, AS CR, Heyrovský Sq. 2, 162 06 Prague 6, Czech Republic
[b] Center for Cell Therapy and Tissue Repair, Charles University, V Úvalu 84, 150 06 Prague 5, Czech Republic
[c] Institute of Experimental Medicine, AS CR, Vídeňská 1083, 142 20 Prague 4, Czech Republic
[d] Institute of Clinical and Experimental Medicine, Vídeňská 1958/9, 140 21 Prague 4, Czech Republic

ARTICLE INFO

Available online 21 February 2009

Keywords:
Magnetic nanoparticles
Maghemite
MRI
Stem cells
Biocompatibility
Contrast agent

ABSTRACT

Maghemite nanoparticles with various coatings were prepared by the coprecipitation method and characterized by transmission electron microscopy, dynamic light scattering and IR in terms of morphology, size, polydispersity and surface coating. The labeling efficiency and the viability of both rat and human mesenchymal stem cells labeled with Endorem®, poly(L-lysine) (PLL)-modified Endorem®, uncoated γ-Fe_2O_3, D-mannose-, PLL- or poly(*N*,*N*-dimethylacrylamide) (PDMAAm)-coated γ-Fe_2O_3 nanoparticles were compared. Coated γ-Fe_2O_3 nanoparticles labeled cells better than did Endorem®. High relaxation rates and *in vitro* magnetic resonance imaging of cells labeled with coated nanoparticles showed clearly visible contrast compared with unlabeled cells or cells labeled with Endorem®.

1. Introduction

A distinctive feature of superparamagnetic nanoparticles is that they are attracted by a magnet, but they are not retained upon removal of the applied external magnetic field. Superparamagnetic iron oxide nanoparticles used in cell labeling and tracking [1,2], cell sorting [3,4] and as magnetic resonance contrast agents are very important in the emerging fields of nanomedicine [5] and nanoscience [6]. They improve contrast to increase the sensitivity needed for early detection of even the smallest tumors by magnetic resonance imaging. Non-invasive imaging of cell migration and, specifically, of genetically engineered stem and progenitor cells has long been sought [7]. The fabrication of iron oxide nanoparticles is usually based on the precipitation of iron salts with bases [8,9] or the thermal decomposition of organometallic precursors [10]. One of the difficulties in synthesizing uniformly sized iron oxides is the intrinsic agglomeration of magnetic nanoparticles; the formed aggregates are then quickly sequestered by cells of the reticular endothelial system. To avoid macrophage recognition, particles are surface-protected by a layer of hydrophilic groups [11]. Various organic coatings have been used to optimize the delivery of magnetic nanoparticles to or into cells: antibodies, targeting ligands to cell receptors [12], amphiphilic coatings such as poly(ethylene glycol) [13], dendrimers [14], transfection agents such as HIV-derived TAT protein [15], protamine sulphate, and poly(L-lysine) (PLL) on dextran-coated iron oxides [16]. The most common labeling approach is based on combining a commercially available contrast agents based on dextran-coated nanoparticles, such as Feridex® or Sinerem®, and a commercially available transfection agent, for example Superfect™, poly(L-lysine) (PLL), Lipofectamin, or Fugene™ [17]. However, each combination of transfection agent and nanoparticle has to be carefully titrated and optimized for different cell cultures, since lower concentrations of the transfection agent may result in insufficient cellular uptake, whereas higher concentrations may induce the precipitation of complexes or may be toxic to the cells [18]. Therefore, we prepared different types of nanoparticles that combined high labeling efficiency with low iron concentrations, thus resulting in high cell viability.

In the current study, iron oxide cores were prepared by the well-known precipitation of iron salts, in particular $FeCl_2$ and $FeCl_3$, by increasing the pH with ammonium hydroxide, followed by the oxidation of the resulting magnetite with sodium hypochlorite [19]. Oxidation resulted in maghemite (γ-Fe_2O_3), which is chemically stable and does not change its properties. This is in contrast to magnetite, which undergoes uncontrolled oxidation in the presence of oxygen. Confirmation of the maghemite phase by Mössbauer spectroscopy and its other magnetic properties were described in our previous report [20]. The primary uncoated maghemite nanoparticles, which are highly

* Corresponding author at: Institute of Macromolecular Chemistry AS CR, Heyrovský Sq. 2, 162 06 Prague 6, Czech Republic. Tel.: +420 296809260; fax: +420 296809410.
E-mail address: horak@imc.cas.cz (D. Horák).

0304-8853/$ - see front matter © 2009 Elsevier B.V. All rights reserved.
doi:10.1016/j.jmmm.2009.02.082

unstable in saline solutions, were used in cell experiments as a control or served as cores for subsequent coating to prevent particle aggregation during long-term utilization.

The coating of iron oxide colloidal nanoparticles was achieved by three methods. The first method involved a one-step synthesis of D-mannose-coated nanoparticles by the *in situ* alkaline coprecipitation of iron precursors in an aqueous solution of D-mannose, alternatively the coating was done post-synthesis [19]. In the second, a two-step post-synthesis procedure, PLL stabilizer protecting the nanoparticles from aggregation was added to the primary uncoated maghemite cores obtained by the above precipitation in the first step [21]. While D-mannose-coated nanoparticles were prepared at D-mannose/γ-Fe_2O_3 ratios on the order of units, the PLL/iron oxide ratio was lower by an order of magnitude in the synthesis of PLL-coated nanoparticles [19,21]. Finally, the post-synthesis coating of maghemite was achieved by the solution radical polymerization of *N,N*-dimethylacrylamide (DMAAm) in the presence of γ-Fe_2O_3 nanoparticles [22]. The nanoparticles were compared with commercially available dextran-coated iron oxide nanoparticles (Endorem®, Guerbet, Roissy, France) and poly(L-lysine) ($M_w = 93{,}800$) coated Endorem®. All the nanoparticles were analyzed by transmission electron microscopy (TEM) and dynamic light scattering (DLS) to obtain information on their size, shape, and distribution; FTIR spectra were recorded to confirm the coating [19,21,22].

2. DLS and TEM

Fig. 1 shows TEM images of all four types of the nanoparticles. Similarly as in previous reports [19,21,22], the post-synthesis coating of the primary iron oxide colloid with either PLL or poly(*N,N*-dimethylacrylamide) (PDMAAm) changed neither the morphology or the size of the iron oxide crystallites, which was about 10 nm (Fig. 1c and d) and did not differ from that of uncoated maghemite (Fig. 1a). A noticeable difference was, however, found for *in situ* coating with D-mannose. These nanoparticles were much smaller with a typical diameter of about 2 nm (Fig. 1b).

Iron oxide nanoparticle colloids obtained by post-synthesis coating were also investigated by dynamic light scattering. The hydrodynamic diameter of the nanoparticles calculated from DLS was about 10 times larger than that from TEM (Table 1), which is quite normal [19]. This is due to the fact that the hydrodynamic nanoparticle diameter is measured in their dispersion state in water, in contrast with TEM which analyzes the particle core. Moreover, DLS provides the *z*-average of the diameter, which is strongly affected by the presence of large particles, while TEM gives the number average. Moreover, the formation of iron oxide aggregates in water cannot be ruled out. Table 1 shows the dependence of the hydrodynamic particle diameter, measured by dynamic light scattering of uncoated, D-mannose-, PLL- and PDMAAm-coated γ-Fe_2O_3, on time ranging from 1 to 150 days after synthesis. Coated iron oxide particles were moderately larger than those uncoated due to the presence of a thick hydrated coating shell. The increased hydrodynamic particle size of PLL-coated maghemite nanoparticles 150 days after synthesis can be attributed to particle aggregation. This can also be inferred from the higher polydispersity of such samples. On the other hand PDMAAm-coated γ-Fe_2O_3 were colloidally stable in aqueous solutions as well as in cell culture medium for at least 6 months.

Table 1
Hydrodynamic diameters D_h (nm) of differently coated γ-Fe_2O_3 nanoparticles over time.

Nanoparticles	1st day	30th day	90th day	150th day
Uncoated γ-Fe_2O_3	63	66	70	512
D-mannose-coated γ-Fe_2O_3	73	66	61	83
PLL-coated γ-Fe_2O_3	90	128	145	166
PDMAAm-coated γ-Fe_2O_3	78	80	85	110

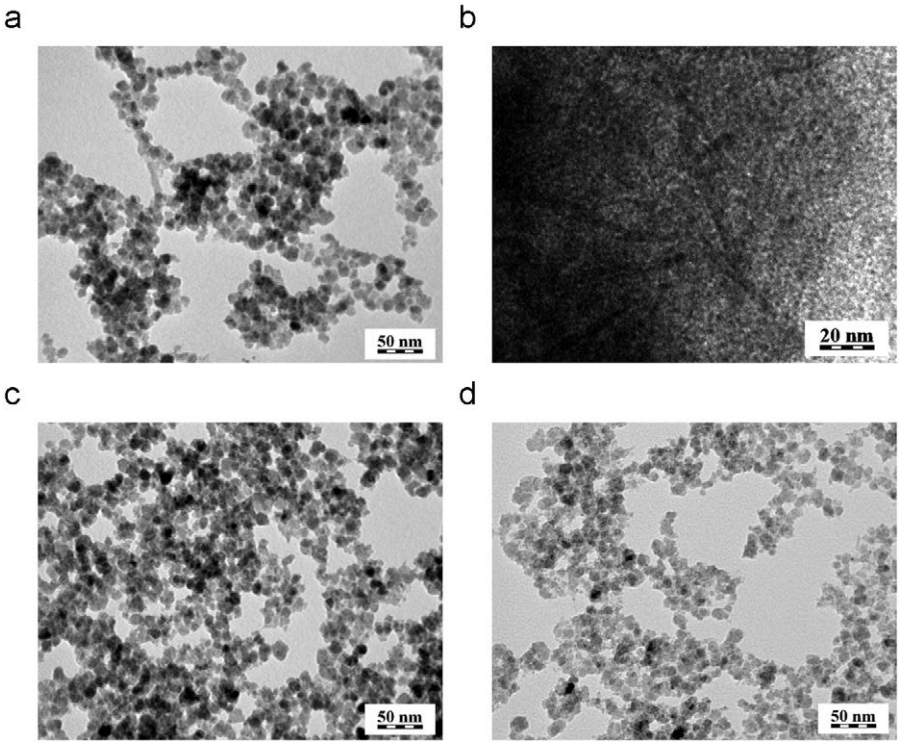

Fig. 1. TEM images of (a) uncoated, (b) D-mannose-, (c) PLL- and (d) PDMAAm-coated γ-Fe_2O_3 nanoparticles.

3. FTIR spectra

The structure of the surface and the efficiency of the coating of magnetic nanoparticles were analyzed by surface sensitive ATR FTIR spectroscopy. FTIR spectra of magnetic γ-Fe_2O_3 particles before and after coating with D-mannose, PLL, and by radical polymerization of DMAAm in the presence of γ-Fe_2O_3 nanoparticles are shown in Fig. 2. Two broad bands of iron oxide dominate in the spectrum of the magnetic particles before modification (Fig. 2a). The typical peaks of the C–H, C–OH, and C–O–C vibrations present in the spectrum (Fig. 2b) indicate that the surface of the γ-Fe_2O_3 nanoparticles was covered with D-mannose [19]. D-mannose can be attached to iron oxide nanoparticles by the hydroxy group located on the C2 carbon in the axial position [23]. This is a configuration specific to D-mannose, in contrast to, e.g., glucose and other common sugars that have this hydroxy group only in the equatorial position.

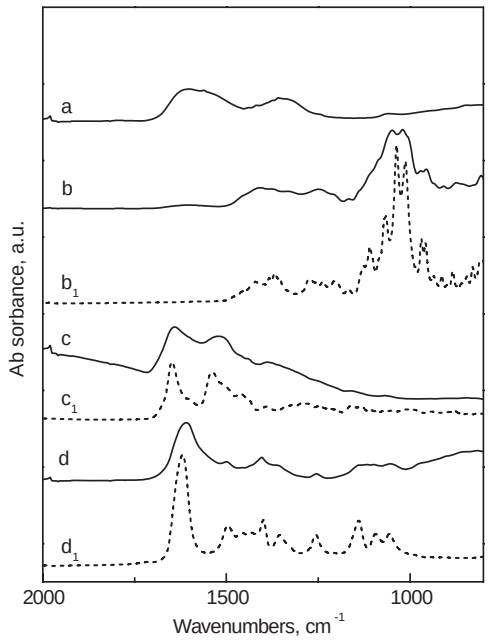

Fig. 2. ATR FTIR spectra of maghemite nanoparticles before (a) and after surface modification with (b) D-mannose, (c) PLL and (d) PDMAAm. Spectra of corresponding pure (b_1) D-mannose, (c_1) PLL and (d_1) PDMAAm are shown for comparison (dash).

The spectrum of particles after modification with PLL (Fig. 2c) differed from the spectrum of uncoated iron oxide (Fig. 2a). The band of Amide I situated at 1648 cm^{-1} in the spectrum of pure PLL was only slightly shifted to higher wavelengths by the coating [21]. The Amide II band was shifted from 1539 cm^{-1} in the spectrum of pure PLL to 1502 cm^{-1} in the spectrum of coated nanoparticles. We assume that the bands of $-CH_2-NH_3^+$ deformation and rocking vibrations influence the spectrum in this region. A broad, strong absorption above 1800 cm^{-1} (only the beginning is shown in Fig. 2c) was observed in the spectrum, corresponding most probably to ionic interactions between PLL and the iron oxide particles. This strongly indicates that positive charges of the amine groups terminating the PLL side chains interact with citrates complexed on the iron oxide surface.

The spectrum of the coating formed by the solution radical polymerization of DMAAm in the presence of maghemite nanoparticles (Fig. 2d) also differed from the spectrum of uncoated particles. The band of Amide I observed at 1618 cm^{-1} in the spectrum of pure PLL was shifted to 1608 cm^{-1} and the intensity of the band of Amide II observed at 1404 cm^{-1} increased after the polymerization. The peaks of CH_3 deformation vibration at about 1495 and 1354 cm^{-1} decreased in their relative intensity [22]. We hypothesize that these changes correspond to the interaction of the protonated NH^+ groups of PDMAAm with citrates complexed on the iron oxide surface. Citrate is adsorbed on the ferric oxide surface via one or two carboxylate moieties, allowing the use of one of the ungrafted carboxylic acid groups to bind a polycation. This confirms that a PDMAAm shell has been effectively formed at the surface of the iron oxide particles.

4. Cell labeling

As a model for cell labeling, mesenchymal stem cells (MSCs) were investigated, since they are already used in human clinical studies for the treatment of heart ischemic diseases [24,25], ischemic limbs [26,27] and spinal cord injury [28,29]. The cells were labeled with D-mannose-, PLL-, PDMAAm-, and dextran-coated iron oxide nanoparticles (Endorem®), PLL-coated Endorem® and uncoated γ-Fe_2O_3 nanoparticles. A nanoparticle suspension (1.54 μg of iron per 1 mL for all types of nanoparticles) was added to the cell culture. After 72 h, the nanoparticles were washed out by replacing the culture medium. The viability of rat

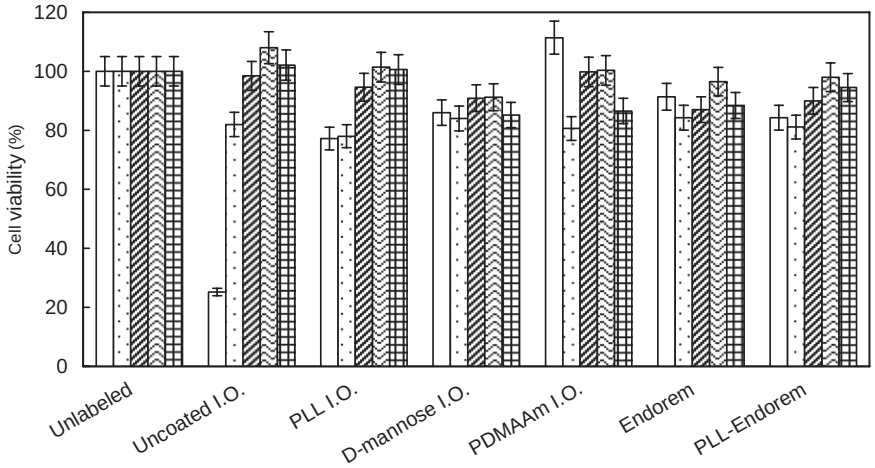

Fig. 3. Viability of unlabeled rat MSCs from the 1st to 5th passages (left to right columns, respectively), labeled with uncoated iron oxide, PLL-, D-mannose-, and PDMAAm-coated iron oxide nanoparticles, Endorem® and PLL-modified Endorem®.

(r) MSCs (1st to 5th passage) or human (h) MSCs (2nd to 4th passage) labeled with different superparamagnetic maghemite nanoparticles was determined using a WST-1 colorimetric assay based on the cleavage of the tetrazolium salt (4-[3-(4-iodophenyl)-2-(4-nitrophenyl)-2H-5-tetrazolio]-1,3-benzene disulfonate) to a highly water-soluble formazan dye by mitochondrial dehydrogenases in viable cells [30]. The viability of MSCs, irrespective of the number of passages (length of cultivation), labeled with D-mannose-, PLL-, PDMAAm-coated iron oxide nanoparticles, PLL-coated Endorem® or Endorem® did not decrease under 75% compared to unlabeled MSCs (Fig. 3). The only marked drop in viability was observed in the cells of the 1st passage labeled with uncoated maghemite nanoparticles due to many cells undergoing apoptosis. Some decrease in viability under 80% was detected in the 1st and 2nd passages of cells labeled with PLL-coated iron oxide nanoparticles: however, the decrease was not significant and

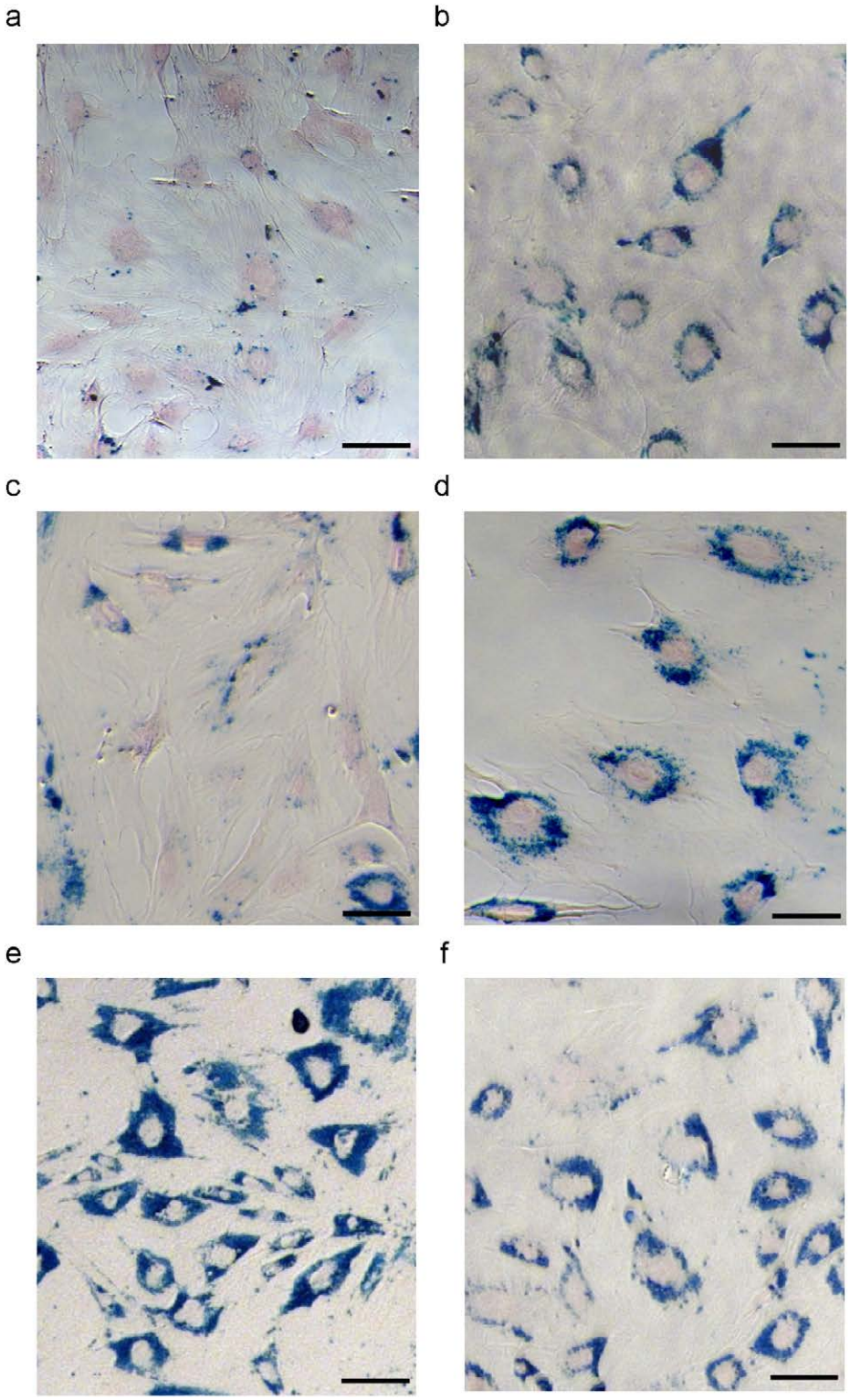

Fig. 4. Photomicrographs of Prussian Blue stained rMSCs labeled with (a) Endorem®, (b) PLL-modified Endorem®, (c) uncoated γ-Fe_2O_3, (d) D-mannose-coated γ-Fe_2O_3, (e) PLL-coated γ-Fe_2O_3 and (f) PDMAAm-coated γ-Fe_2O_3 nanoparticles. Counterstained with nuclear fast red, scale bar 100 μm.

can be explained by the heterogeneity of the cell populations in the culture. These results are in agreement with earlier published findings [19,21], where similar viabilities were detected in human and rat MSCs. In previous experiments, the cell viability dropped to as low as 50% if the concentration of Endorem® was higher than 0.11 μg of Fe_3O_4/mL [31].

Labeling efficiency was determined by relaxometry, spectrophotometrical iron content analysis and by manual evaluation of Prussian Blue stained nanoparticle-labeled MSCs (Fig. 4). The cells took up smaller amounts of Endorem® and uncoated maghemite nanoparticles (less intensive staining for iron) than of D-mannose-, PLL-, PDMAAm-coated nanoparticles or PLL-coated Endorem® (Fig. 4). The percentage of labeled hMSCs and rMSCs is summarized in Table 2. Comparing hMSCs and rMSCs, the trends in labeling were the same: however, a higher percentage of labeled hMSCs was found. This can be partly explained by using cells from the 2nd to 4th passages, which represent the best time for labeling (see below). The best results for hMSC labeling were obtained with PLL-coated γ-Fe_2O_3 nanoparticles, followed by D-mannose-coated ones, PDMAAm-coated ones, PLL-coated Endorem®, uncoated γ-Fe_2O_3 nanoparticles and Endorem®. The distribution of the intensity of Prussian Blue staining is shown in Fig. 5. The percentage of intensely stained rMSCs was highest in cells labeled with PLL-coated γ-Fe_2O_3 nanoparticles, followed by PDMAAm-coated ones, D-mannose-coated ones, PLL-coated Endorem®, uncoated γ-Fe_2O_3 nanoparticles and Endorem®.

Table 2
Percentage of human and rat MSCs labeled with differently coated γ-Fe_2O_3 nanoparticles.

Nanoparticles	Labeled cells (%)	
	hMSCs	rMSCs
Uncoated γ-Fe_2O_3	74±6	44±5
Mannose-coated γ-Fe_2O_3	84±5	57±6
PLL-coated γ-Fe_2O_3	84±4	72±5
PDMAAm-coated γ-Fe_2O_3	77±6	59±6
Endorem®	62±5	37±6
PLL-coated Endorem®	77±5	49±9

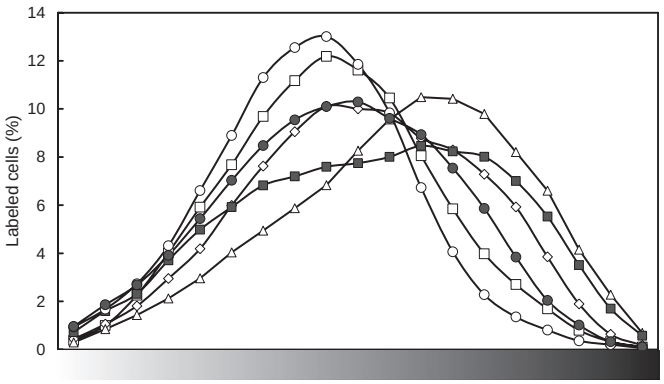

Fig. 5. Distribution of the intensity of Prussian Blue staining (*x*-axis) in rMSCs labeled with (□) uncoated, (◇) D-mannose-coated, (△) PLL-coated, (■) PDMAAm-coated iron oxide nanoparticles, (*o*) Endorem® and (●) PLL-coated Endorem®.

The efficiency of labeling with different nanoparticles was dependent on the number of cell passages (Fig. 6), with lower passages being labeled more efficiently than higher ones. The most pronounced effect of cultivation time was observed in Endorem®- and PLL-coated Endorem®-labeled cells. Endorem® was also the least efficient labeling agent of all the tested nanoparticles. This can be explained by the low concentration of iron, which did not affect cell viability, but did affect labeling efficiency. The best efficiency of labeling, up to 70–80%, was achieved with PLL-coated γ-Fe_2O_3 nanoparticles. The PLL coating of Endorem® increased the labeling efficiency of Endorem®; however, it did not reach the level of PLL-coated γ-Fe_2O_3 nanoparticles. This might be due to the larger size of the nanoparticles, since Endorem® itself has a diameter of about 130 nm and the PLL coating increased the size to 145–260 nm. D-mannose- and PDMAAm-coated γ-Fe_2O_3 nanoparticles achieved labeling efficiencies of around 60% (Fig. 6) that were less dependent on time in culture/number of passages than in the case of PLL-coated γ-Fe_2O_3 nanoparticles or PLL-coated Endorem®. In general, nanoparticle uptake seems to be related to cell expansion and proliferation. The first passage contains the most heterogeneous population; therefore, the nanoparticle uptake varies depending not only on the type of coating, but also on the cell types present in the culture. The highest labeling efficiency was obtained during the 2nd–4th passages when the cells are growing and expanding rapidly. The 2nd–3rd passages are mostly used in cell therapy experiments. At the 5th passage, cell growth and expansion are not so robust nor is the nanoparticle uptake.

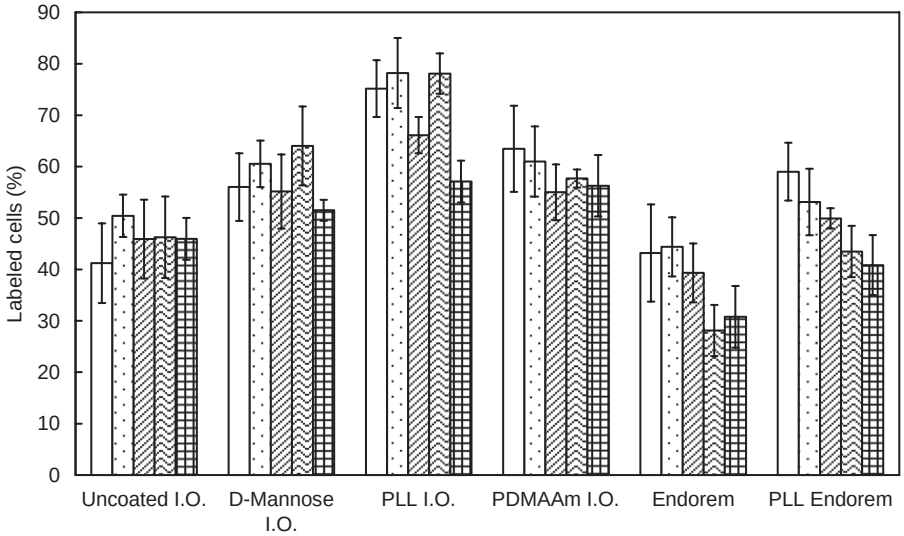

Fig. 6. Labeling efficiency of rat MSCs from the 1st to 5th passages (left to right columns, respectively) with uncoated iron oxide, D-mannose-, PLL- and PDMAAm-coated iron oxide nanoparticles, Endorem® and PLL-modified Endorem®.

The internalization of coated γ-Fe_2O_3 nanoparticles by rat and human MSCs was verified on 65-nm-ultrathin sections of cells embedded in epoxy resin using TEM. Large numbers of free magnetic nanoparticles were mostly seen inside numerous vacuoles (Fig. 7). A small number of nanoparticles were dispersed within the cytoplasm (Fig. 7f), but the cells, organelles and cell structures were not affected by the presence of coated nanoparticles inside the cells. However, the majority of cells labeled with uncoated maghemite were undergoing programmed cell death, probably by autophagia. The cells contained large autophagosomes, recognized in micrographs as membrane-bound organelles with other organelles clearly contained within them, together with uncoated nanoparticles (Fig. 7b). MSCs stained with Endorem® showed a heterogeneous distribution of the nanoparticles. Some of the cells contained numerous endosomes filled with nanoparticles, others only a few or none (Fig. 7a). In the cells labeled with PLL-coated γ-Fe_2O_3 nanoparticles, nanoparticle clusters were seen in higher numbers in all cells (Fig. 7c and d) than in Endorem®-labeled cells. This finding is in agreement with the results obtained from Prussian Blue staining. D-mannose-coated nanoparticles were present in large numbers in all of the cells (Fig. 7e). Nanoparticles were seen dispersed also in the cytoplasma not only in membrane-bound vacuoles (Fig. 7f). PLL-coated γ-Fe_2O_3 nanoparticles appeared as large numbers of clusters inside the vacuoles in the cells (Fig. 7g and h). Likewise, PDMAAm-coated γ-Fe_2O_3 nanoparticles were also seen in large numbers in the cells (Fig. 7i and j) and were not harmful to either the nucleus or other organelles. The mechanism of nanoparticle uptake into the cells is presumably different depending on the type of the coating. While D-mannose-coated iron oxide nanoparticles are taken up by the mannose transport that is present in the majority of mammalian cells, PLL serves as a transfection agent and PLL-coated nanoparticles are therefore entering the cell via the different charges of PLL and the cell surface. This can be confirmed by our findings that the PLL-coated nanoparticle clusters are mainly found close to the cell surface. PDMAAm-coated γ-Fe_2O_3 nanoparticles and Endorem® are taken up by endocytosis, which can be facilitated in the case of PDMAAm-coated nanoparticles by their positive surface charge interacting with the negatively charged cell membrane and their smaller diameter compared to that of Endorem®.

5. MR relaxometry

Suspensions of contrast agents at different concentrations were prepared together with suspensions of rat and human MSCs labeled with Endorem®, PLL-coated Endorem®, uncoated γ-Fe_2O_3 nanoparticles and D-mannose-, PLL- and PDMAAm-coated γ-Fe_2O_3 nanoparticles in 4% gelatin and examined by MR relaxometry. T_2 relaxation times were measured at different field strengths of 0.5, 3 and 4.7 T, converted to relaxivities r_2 and, after deducting the contribution of pure gelatin, related to actual iron concentration c, i.e., $r_2 = (1/T_2 - 1/T_{2gel})/c$. In the samples containing labeled cells, the relaxation rate R_2 was related after deducting the contribution of unlabeled cells to 10^6 cells in 1 mL.

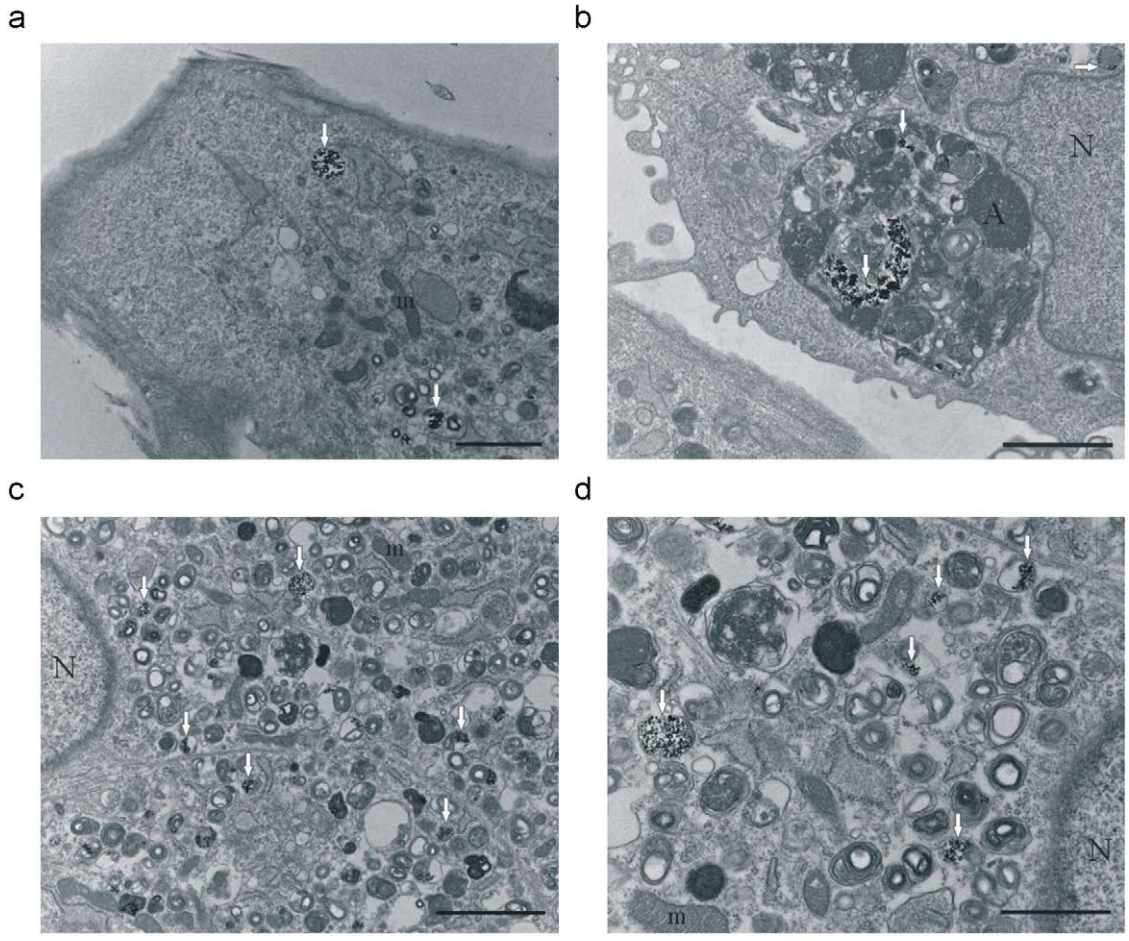

Fig. 7. TEM micrographs of rMSCs labeled with (a) Endorem®, (b) uncoated γ-Fe_2O_3, (c, d) PLL-coated Endorem®, (e, f) D-mannose-, (g, h) PLL- and (i, j) PDMAAm-coated γ-Fe_2O_3 nanoparticles (arrows). Arrows and arrow head indicate nanoparticles inside the endosome/autophagosome and in the cytoplasma, respectively. A-autophagosome, m-mitochondrion, N-nucleus, n-nucleolus. Scale bar (d, f, j) 1 μm, (a, b, c) 2 μm, (g, h, i) 5 μm, (e) 10 μm.

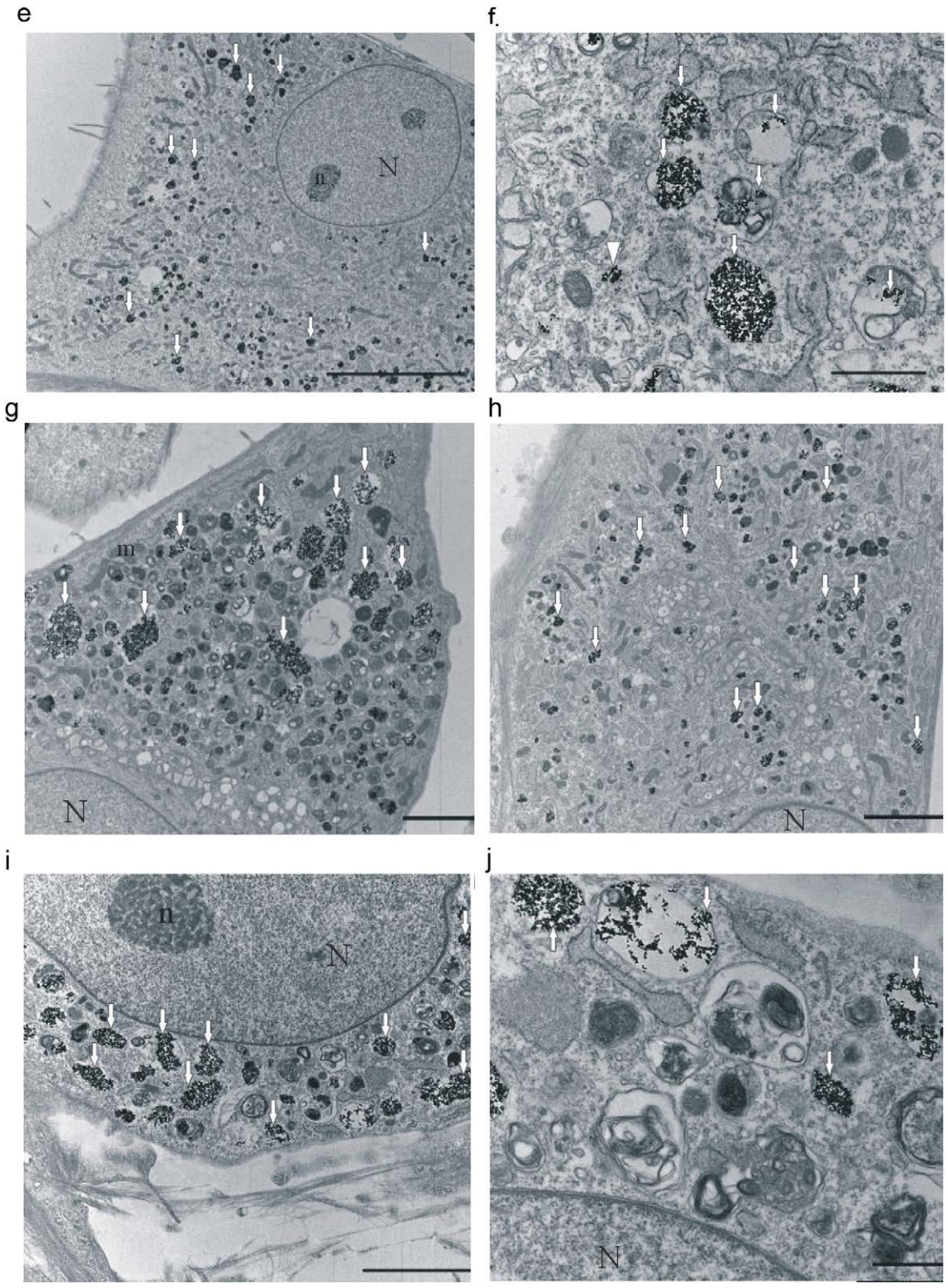

Fig. 7. (*Continued*)

Surface modification strongly affected the relaxivity properties of the γ-Fe_2O_3 nanoparticles (Table 3). As expected, uncoated γ-Fe_2O_3 nanoparticles achieved the highest r_2 relaxivity, where the distance between the water molecules and the particles was smallest. PLL- and D-mannose-coated nanoparticles also reached higher r_2 relaxivities than did the commercial contrast agents including Endorem®. On the other hand, PDMAAm-coated particles had a lower relaxivity than the commercially available contrast agent.

As the nanoparticles are intended for T_2 contrast enhancement only, r_1 relaxivities are not important for their characterization and thus they were not considered.

However, for cell detection not only is the relaxivity of the cellular contrast agent important, but also the absolute amount of

the contrast agent inside the cells. Therefore, a crucial role is played by the uptake of the nanoparticles into the cells, which in turn is strongly affected by the surface modification of the particles [32,33]. Compared with the conventionally used contrast agent Endorem®, the newly coated γ-Fe_2O_3 nanoparticles entered the cells more easily and significantly higher amounts of iron were detected inside the cells by spectrophotometry after mineralization (Table 4). Improved cellular uptake significantly contributes to the higher R_2 relaxation rate of cells labeled by modified iron oxide nanoparticles. Both higher relaxivity and greater uptake improved the relaxation rate R_2 per 10^6 cells labeled with uncoated iron oxide, D-mannose- or PLL-coated nanoparticles. Higher cellular uptake also significantly increased the R_2 relaxation rate of cells labeled by PDMAAm-coated nanoparticles, although the relaxivity of pure PDMAAm-coated nanoparticles was much lower than that of Endorem®. The amount of iron inside the cells in the case of labeling with modified iron oxide nanoparticles was up to ten times higher than in the case of cells labeled with Endorem® (Table 4).

The relaxivity r_2 of iron oxide crystals strongly depended on the field strength [34]. Relaxivity field dependence was observed in suspensions of pure contrast agents (Table 3). The behavior of cell suspensions differs, probably due to the clustering of iron oxide nanoparticles inside the cells. This clustering probably differs among different cell types and might be affected by the internal cellular environment (Table 4).

Table 3
Relaxivities r_2 (s^{-1}/mM) of rMSCs labeled with D-mannose-, PLL-, PDMAAm-coated γ-Fe_2O_3 nanoparticles and commercial contrast agents.

Field strength (T)	0.5	3	4.7
Uncoated γ-Fe_2O_3	383±87	429±13	549±22
D-mannose-coated γ-Fe_2O_3	409±14	434±19	509±16
PLL-coated γ-Fe_2O_3	413±23	432±26	492±30
PDMAAm-coated γ-Fe_2O_3	46±18	83±46	89±22
PLL-Endorem®	87±16	246±11	290±1
Endorem®	156±4	174±6	235±7
Sinerem®	129±4	114±6	177±5
Resovist®	217±4	207±24	265±7

6. *In vitro* MR imaging of cell suspensions

To check the sensitivity of the magnetic resonance imaging (MRI) using a 4.7 T Bruker spectrometer and to compare different types of γ-Fe_2O_3 nanoparticles to commercially available Endorem®, rMSCs were labeled with nanoparticles and suspended in gelatin. The concentration of cells was 50,000 cells/mL, which represents 2 cells per image voxel on average. Even this low number of cells labeled by PLL-coated Endorem® (Fig. 8c), PLL-coated iron oxide nanoparticles (Fig. 8d), D-mannose-coated iron oxide (Fig. 8e) or PDMAAm-coated iron oxide (Fig. 8f), or uncoated iron oxide nanoparticles (Fig. 8g) provided visible contrast on MR images compared to samples containing unlabeled cells (Fig. 8a) or cells labeled by Endorem® without any transfection agent (Fig. 8b), which did not provide any contrast. As Endorem®-labeled cells can be detected at numbers of 70 or more [35], the newly synthesized particles represent a significant improvement in cell detection using MRI.

Surface modification of iron oxide nanoparticles with D-mannose, PLL or PDMAAm also had a strong impact on cell viability. The mechanism of nanoparticle internalization into the cells differed depending on the type of coating. Iron oxide nanoparticles are believed to be biodegradable with the iron being used/recycled by cells through normal biochemical pathways for iron metabolism [36]. Non-invasive MR imaging of D-mannose-, PLL- and PDMAAm-coated iron oxide nanoparticle-labeled cells has been demonstrated, opening up possibilities for tracking grafted cells as well as monitoring their migration, proliferation and differentiation in a host organism.

Acknowledgements

The financial support of the Center for Cell Therapy and Tissue Repair No. 1M0021620803, the Grant Agency of AS CR (Grants KAN201110651 and KAN200200651), the Grant Agency of the Czech Republic (Grants 203/09/1242 and 309/08H/079) and the EC-FP6 project DiMI (LSHB-CT-2005-512146) is gratefully acknowledged.

Table 4
Relaxation rates R_2 ($s^{-1}/10^6$ cells/mL) of rMSCs and hMSCs labeled with several types of iron oxide nanoparticles and the amount of iron internalized inside the cells.

Field strength (T)	0.5		4.7		Fe content (pg/cells)	
	rMSC	hMSC	rMSC	hMSC	rMSC	hMSC
Uncoated γ-Fe_2O_3	3.67±0.62	7.13±0.77	4.95±0.17	4.88±1.65	29.3±4.9	17.1±0.3
Mannose-coated γ-Fe_2O_3	4.12±0.13	46.63±0.79	4.92±0.58	32.07±1.10	21.1±3.5	34.6±0.5
PLL-coated γ-Fe_2O_3	4.27±0.08	10.77±0.62	5.98±0.82	8.90±0.39	24.5±4.1	27.1±0.4
PDMAAm-coated γ-Fe_2O_3	2.91±0.50	27.26±0.24	4.18±0.40	20.42±0.78	23.2±2.9	36.9±0.5
Endorem®	0.13±0.14	0.88±0.33	0.72±0.09	0.83±0.27	–[a]	3.2±0.5
PLL-coated Endorem®	2.23±0.08	4.44±0.12	3.95±0.62	4.02±0.27	16.3±4.1	12.1±0.5

[a] Undetectable.

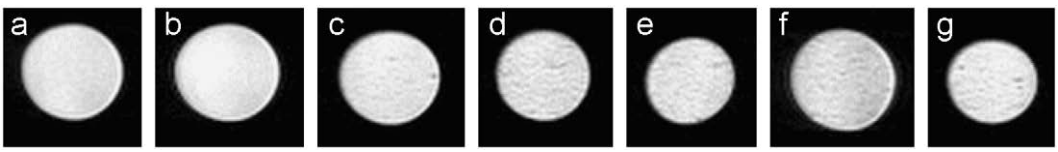

Fig. 8. MRI images of gelatin phantoms containing (a) unlabeled or (b–g) labeled rat mesenchymal stem cells measured by a T_2-weighted turbo-spin echo sequence. Test tubes contained 25,000 cells in 0.5 mL. Cells were labeled with (b) Endorem®, (c) PLL-coated Endorem®, (d) PLL-coated iron oxide, (e) D-mannose-coated iron oxide, (f) PDMAAm-coated iron oxide and (g) uncoated iron oxide nanoparticles.

References

[1] A.S. Arbab, G.T. Yocum, H. Kalish, et al., Blood 104 (2004) 1217.
[2] J.W. Bulte, Methods Mol. Med. 124 (2006) 419.
[3] E.A. Schellenberger, D. Sosnovik, et al., Bioconj. Chem. 15 (2004) 1062.
[4] M. Shinkai, A. Ito, et al., J. Biosci. Bioeng. 100 (2005) 1.
[5] E.V. Groman, J.C. Bouchard, et al., Bioconj. Chem. 18 (2007) 1763.
[6] S.H. Sun, H. Zeng, D.B. Robinson, J. Am. Chem. Soc. 126 (2004) 273.
[7] M. Lewin, N. Carlesso, C.-H. Tung, et al., Nat. Biotechnol. 18 (2000) 410.
[8] R. Massart, IEEE Trans. Magn. 17 (1981) 1247.
[9] S.A. Morisson, C.L. Cahill, et al., J. Nanosci. Nanotechnol. 5 (2005) 1323.
[10] D. Horák, M. Babič, et al., J. Sep. Sci. 30 (2007) 1751.
[11] Q.-L. Fan, K.G. Neoh, E.-T. Kang, et al., Biomaterials 28 (2007) 5426.
[12] F. Sonvico, S. Mornet, S. Vasseur, et al., Bioconj. Chem. 16 (2005) 1181.
[13] A.K. Gupta, A.S. Curtis, J. Mater. Sci. Mater. Med. 15 (2004) 493.
[14] J.W. Bulte, T. Douglas, B. Witwer, et al., Nat. Biotechnol. 19 (2001) 1141.
[15] P. Kircher, J.R. Allport, M. Zhao, et al., Radiology 225 (2002) 453.
[16] A. Omidkhoda, H. Mozdarani, et al., Toxicol. in Vitro 21 (2007) 1191.
[17] J.A. Frank, B.R. Miller, et al., Radiology 228 (2003) 480.
[18] H. Kalish, A.S. Arbab, et al., Magn. Reson. Med. 50 (2003) 275.
[19] D. Horák, M. Babič, P. Jendelová, et al., Bioconj. Chem. 18 (2007) 635.
[20] E. Pollert, K. Knížek, M. Maryško, et al., J. Magn. Magn. Mater. 306 (2006) 241.
[21] M. Babič, D. Horák, M. Trchová, et al., Bioconj. Chem. 19 (2008) 740.
[22] M. Babič, D. Horák, P. Jendelová, et al., Bioconj. Chem. 20 (2009) 283.
[23] M.K. Koshikawa, T. Hori, Phys. Chem. Chem. Phys. 2 (2000) 1497.
[24] V. Schachinger, S. Erbs, A. Elsasser, et al., Eur. Heart J. 27 (2006) 2775.
[25] M. Hendrikx, K. Hensen, C. Clijsters, et al., Circulation 114 (2006) I101.
[26] T. Bartsch, M. Brehm, et al., J. Cardiovasc. Nurs. 21 (2006) 430.
[27] K. Esato, K. Hamano, T.S. Li, et al., Cell Transplant 11 (2002) 747.
[28] G.A. Moviglia, R. Fernandez Vina, J.A. Brizuela, et al., Cytotherapy 8 (2006) 202.
[29] E. Syková, A. Homola, R. Mazanec, et al., Cell Transplant 15 (2006) 675.
[30] M. Ishiyama, M. Shiga, K. Sasamoto, et al., Chem. Pharm. Bull. 41 (1993) 1118.
[31] P. Jendelová, D. Horák, M. Babič, et al., Regenerative Med. 2 (2007) 635.
[32] A.K. Gupta, M. Gupta, Biomaterials 26 (2005) 1565.
[33] A.K. Gupta, A.S. Curtis, Biomaterials 25 (2004) 3029.
[34] J. Vymazal, R.A. Brooks, et al., Magn. Reson. Med. 27 (1992) 368.
[35] P. Jendelová, V. Herynek, J. DeCroos, et al., Magn. Reson. Med. 50 (2003) 767.
[36] J.W.M. Bulte, D.L. Kraitchman, NMR Biomed. 17 (2004) 484.

Příloha č. 5

Daniel Horák
Michal Babič
Hana Macková
Milan J. Beneš

Institute of Macromolecular Chemistry, Academy of Sciences of the Czech Republic, Prague, Czech Republic

Review

Preparation and properties of magnetic nano- and microsized particles for biological and environmental separations

The paper presents a critical overview on magnetic nanoparticles and microspheres used as separation media in different fields of chemistry, biochemistry, biology, and environment protection. The preparation of most widely used magnetic iron oxides in appropriate form, their coating or encapsulation in polymer microspheres, and functionalization is discussed in the first part. In the second part, new developments in the main application areas of magnetic composite particles for separation and catalytical purposes are briefly described. They cover separations and isolations of toxic inorganic and organic ions, proteins, and other biopolymers, cells, and microorganisms. Only selected number of relevant papers could be included due to the restricted extent of the review.

Keywords: Cells / Enzymes / Functionalization / Heterogeneous polymerization / Iron oxide

Received: March 1, 2007; revised: April 5, 2007; accepted: April 5, 2007

DOI 10.1002/jssc.200700088

1 Introduction

Magnetic field-based separations using magnetic nano- and microparticles have received considerable attention in recent two decades. They opened widespread opportunities for application in chemistry, biochemistry, biology, and medicine [1, 2]. Above all, they enable rapid and easy removal of functionalized magnetic particle-bound compounds and organisms from complex heterogeneous reaction mixtures both on micro- and pilot plant scale. In addition to easy manipulation, possible automation, and miniaturization, no dilution of the sample or loss of the carrier occur during washing. Fast and cost-effective separation of magnetic carriers from the reaction mixture without filtration or centrifugation makes the magnetic materials useful not only in daily laboratory work, but also in production practice. Similar to chromatographic separations, analogous interactions are realized on magnetic particles starting from general nonspecific (ionic, hydrophobic, hydrogen bond), through group-specific (dye ligand, immobilized metal affinity chromatography (IMAC), chelating), up to specific affinity interactions (antigen – antibody, avidin – biotin, enzyme – inhibitor, *etc.*). Such systems offer sophisticated analysis, separation, and purification of compounds starting from inorganic ions, biopolymers (enzymes, antibodies, nucleic acids, and other proteins), to cell populations. For these applications, magnetic particles of suitable size (nano-, micro-) and with modified surface are required carrying functional ionic groups (strongly or weakly basic, or acid), selected dye ligands (*e.g.*, Cibachrom Blue F3GA) or chelates of transition metals, and, finally, a bound component of affinity pair. Typically, the magnetic particles are of the "core-shell" type. Magnetic core is preferably coated with inert low- or high-molecular-weight compound preventing at the same time undesirable nonspecific interactions and ensuring stabilization. A number of procedures are available to obtain such particles: (i) preparation of parent particles of the required size and magnetic properties, (ii) coating of their surface with low- or high-molecular-weight compound or their encapsulation in polymers and inorganic materials, (iii) functionalization to introduce required groups for the intended application.

Control of particles by a magnetic field can be advantageously applied also in the opposite direction, not for

Correspondence: Dr. Daniel Horák, Institute of Macromolecular Chemistry, Academy of Sciences of the Czech Republic, Heyrovsky Sq. 2, 162 06 Prague 6, Czech Republic
E-mail: horak@imc.cas.cz
Fax: +420-296-809410

Abbreviations: **ATRP,** atom transfer radical polymerization; **GMA,** glycidyl methacrylate; **HEMA,** 2-hydroxyethyl methacrylate; **IMAC,** immobilized metal affinity chromatography; **IDA,** iminodiacetic acid; **IMS,** immunomagnetic separation; **KPS,** potassium persulfate; **MRI,** magnetic resonance imaging; **NMP,** nitroxide-mediated polymerization; **NOM,** natural organic materials; **PHEMA,** poly(2-hydroxyethyl methacrylate); **PS,** polystyrene; **PVA,** poly(vinyl alcohol); reversible addition fragmentation chain transfer; **SPION,** superparamagnetic iron oxide nanoparticles

separation, but for the localization of functionalized magnetic particles at the required site in the organism, *e.g.*, in *in vivo* targeting chemotherapeutic drug delivery systems and in hyperthermia (controlled heating of magnetic particles by alternating electric field for triggering and necrotization of solid tumors). Superparamagnetic nanoparticles are traced in aqueous environment in magnetic resonance imaging (MRI) for the visualization of tissues and monitoring labeled cells in tissue repair, *etc.* [3]. Other biomedical applications include magnetofection. Also for these applications, the particles must have combined properties of high magnetic saturation, biocompatibility, and interactive functions at the surface.

Diagnostic (immunoassays) and therapeutic applications of magnetic particles were recently reviewed [3 – 7] and therefore will not be covered in this review. Preparation and application of magnetic particles in various fields was also described in numerous monographs [2, 8 – 20] and review articles [3, 5, 6, 21 – 52]. Magnetic particles are also the subject of a plethora of patent literature and many companies market various magnetic carriers and instruments for their separation, manipulation, and monitoring (Table 1). To complete the picture, it is also necessary to mention the use of magnetic particles in electrotechnique and as magnetically controllable sealants [12]. These are not covered in this article, although they found widespread applications. It is the aim of this paper to review methods of magnetic particle preparation, and to describe their properties as well as applications of these systems in the separation of biologically active species. The survey is by no means complete. It only demonstrates the wealth of the work done in the field and many directions pursued up to the end of 2006.

1.1 Ideal *versus* real magnetic support

The use of magnetic materials in practice depends on their properties, including magnetization, morphology, shape, size, polydispersity, to name just the most important. Out of many conceivable shapes (rod, wire, tube, membrane, slab, irregular, *etc.*), the bead form is essential for practical applications if the best possible hydrodynamic (flow) properties are required. It offers important practical advantages of easy handling both in batch and continuous separation processes. Irregularly shaped particles are much more susceptible to mechanical attrition and breakdown to "fines" than spherical ones. In contrast to conventional particles with a broad particle size distribution, monodisperse microspheres (or at least with a narrow size distribution) provide a great advantage, because they possess uniform physical and chemical properties and do not aggregate in liquids so easily as polydisperse particles do. Large particles have the disadvantage of a small specific surface area available for the attachment of functional groups or immobilization of biomolecules (including enzymes). This is the reason why microspheres (micrometer-size and smaller) are required, because they ensure a sufficiently high specific surface area available for the immobilization of reactive groups, enzymes, and other biologically active compounds and boost the catalytic activity in phase transfer reactions. However, too small a particle may cease to be magnetically responsive. The magnetic susceptibility of magnetic microspheres needs to be as high as possible. In practice, a compromise between active surface and sufficient magnetic properties must be, therefore, found.

Particles for magnetic separations available in the market are coated or encapsulated with synthetic or natural polymers, or also inorganic materials. Polystyrene (PS) or poly(methyl methacrylate) (PMMA) are historically most frequently used matrices for magnetic microparticles. Despite their widespread use, they show some drawbacks in connection with their hydrophobicity. PS exhibits residual nonspecific protein adsorption which produces an undesirable background signaling, *e.g.*, in immunoassays. PS is not easy to chemically modify to introduce specific ligands or recognition groups. Moreover, the hydrophobic nature of PS hinders swelling in polar solvents like water and alcohol. This led to the idea to investigate magnetic poly(2-hydroxyethyl methacrylate) (PHEMA)-based microspheres. PHEMA was selected as a hydrophilic support (hydrogel) since it offers the advantage of biocompatibility and low nonspecific adsorption which are so important in the biomedical field. PHEMA has a long history of application as a biocompatible, nontoxic, mechanically stable material with decreased nonspecific protein adsorption (compared with hydrophobic matrixes) [53]. The reactivity of the hydroxy group, however, is low and it is therefore necessary to introduce functional groups on the matrix (amino, poly(ethylenimine), tosyl group) to enable binding or immobilization of various ligands. Other polymers leading to magnetic microparticles with functional groups include polysaccharides, dextran, albumin, cellulose, poly(lactic acid), *etc.*

2 Preparation of magnetic microspheres

Magnetic microspheres consist mostly of superparamagnetic cores embedded in a polymer shell protecting the analyte from a direct contact with the metal (mostly iron) oxide. The advantage of polymer shell surrounding the magnetic core consists in the possibility of surface functionalization and subsequent immobilization of a target biomolecule. The magnetic colloid (ferrofluid) is an important starting component in the preparation of magnetic polymer nano- and microspheres. Various methods and materials were used for their synthesis. The

factors, such as the carrier type (chemical composition, particle size, porosity, hydrophilic or hydrophobic character, magnetic properties, and minimal nonspecific sorption of analytes) and immobilization procedure can be broadly varied. Magnetic properties of the microspheres are mostly determined by the selection of magnetic material, its weight concentration, and distribution inside the polymer particles.

2.1 Magnetic cores

2.1.1 Magnetic characteristics

To describe magnetic properties of the material, a relationship between magnetization M (magnetic polarization) and magnetic field H inside substances has to be determined. According to the behavior of the material in magnetic field, substances (except supraconductors) can be divided into two groups. First group involves materials with weak magnetic behavior. Their magnetization reaches only small values. On the other hand, substances belonging to the second group with strong magnetic behavior reach high values of magnetization. Substances with weak magnetic behavior are classified into paramagnetic and diamagnetic ones. They show a linear dependence on field intensity and magnetization (Fig. 1a) described as

$$M(r) = \chi_m H(r) \quad (1)$$

where χ_m is magnetic susceptibility. It has small negative values for diamagnets (typically (10^{-6}) and small positive values for paramagnets (typically 0 – 0.01), the temperature dependence of which is described by Curie law

$$\chi_m = C/T \quad (2)$$

where T is absolute temperature (in °K) and C is the Curie constant characteristic of each substance. Both groups of the materials are not suitable to design media for separation and transport. Substances with strong magnetic behavior caused by spontaneous ordering of uncompensated magnetic moments of atoms into magnetic domains are classified as ferromagnets, ferrimagnets, antiferromagnets, and others. They differ from para/diamagnets not only by higher magnetization and susceptibility ($0.01 - 10^6$), but also by a complex dependence of magnetization on the field intensity, the so-called hysteresis loop (Fig. 1b).

Magnetic ordering always exists below a certain critical temperature, called the Curie temperature T_C for ferromagnets and Neel temperature T_N for ferrimagnets and antiferromagnets. Below the critical temperature, an increasing field applied to ferromagnetic substance increases magnetization to saturation magnetization M_S

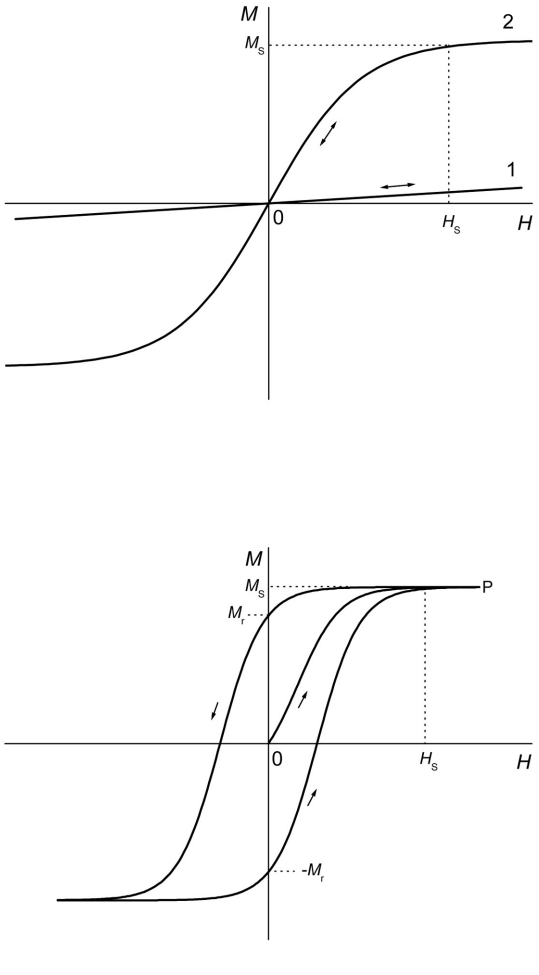

Figure 1. (a) Magnetization curve of a paramagnetic (1) and a superparamagnetic (2) material possessing zero remanence. The superparamagnetic material (2) reaches much higher values of both magnetization M and saturated magnetization M_S. (b) Magnetic hysteresis loop of a ferromagnet. Magnetization M of a sample, which was not magnetized in the initial state, increases with increase in field intensity H primarily according to the 0 – P curve. The curve slope corresponds to the definition of susceptibility (see Section 2.1.1.1). The magnetization decreases with a consequent decrease in the field intensity – see the arrow. Repeated cyclic changes of the field intensity cause cyclic changes of the magnetization as the arrows show. The magnetization curve is similar if the sample does not reach the saturation magnetization M_S.

(Fig. 1b). The M_S value is a very important characteristic of any magnetic material and is dependent on temperature. Below T_C (T_N), the M_S value decreases with an increase in temperature. Another important characteristic is the value of magnetization corresponding to the zero applied field, called remanent magnetization (M_r) (Fig. 1b). The zero M_r value can be achieved either by applying magnetic field with opposite orientation (coercive field H_C), or by a temperature increase above T_C (T_N).

Materials lose their magnetic properties and become paramagnetic above the T_C or T_N. It can be said that the material has lost its magnetic history, which also affects the general magnetic behavior. T_C (T_N) temperature is therefore a very important characteristic.

Superparamagnetic behavior can be described as a combination of paramagnetic and ferromagnetic behavior. Superparamagnetic materials show mostly a linear dependence of magnetization on the field intensity below T_C (T_N) temperature, as paramagnets do, but the magnetization is almost constant after reaching the M_S value (Fig. 1a). In comparison with ferromagnets, superparamagnetic substances do not exhibit any hysteresis and have zero remanence (Fig. 1a). Their magnetic susceptibility is between that of ferromagnetic and paramagnetic materials. Superparamagnetism is exhibited by very small (1 – 30 nm) crystallites of the material, which is ferro/ferrimagnetic in the bulk state. This was observed for different materials, such as iron oxides, ferrites, alloys (Fe-C, Fe-Co), *etc*. Complex superparamagnetic behavior depends not only on material composition, crystallite size, and temperature, but is also influenced by the adjacent particles and the character of their surface. Due to the nanometric particle size, each particle affects the magnetic behavior of adjacent particles by its generated magnetic field [54, 55]. The character and composition of the surface plays a crucial role in the behavior of the particle material in contrast to volume (bulk) properties. Surface-bound surfactants and residual compounds from the particle preparation thus have a considerable impact on the magnetic properties [55 – 57].

2.1.2 Requirements of inorganic nanoparticles as cores of polymer microspheres

Several essential features are expected from inorganic magnetic core materials: (i) good response to the applied external magnetic field – the better the response, the lower the necessary intensity of the applied field and the better the process dynamics, (ii) very low remanence – the lower the remanence, the better the particle dispersibility after switching off the external magnetic field. Zero remanence causes no magnetic interactions between the particles (aggregation) after the removal of external field, (iii) small size (diameter); most of the separation/transport processes are heterogeneous, *i.e.*, the smaller the particles the higher the surface available for potential interactions, (iv) good chemical stability at different pH and redox conditions, (v) reasonable price, and (vi) easy production.

Superparamagnetic or paramagnetic particles with low Curie temperature (up to *ca*. 100°C) fulfill the requirements. Low Curie temperature (temperature of transition from the ordered ferri-/ferromagnetic to paramagnetic state) is a prerequisite for controlling magnetism. The diameter of superparamagnetic particles is in the nanometer range. Superparamagnetic particles also give a sufficient response to the applied magnetic field and have almost zero remanence. Colloid dispersions of magnetic nanoparticles (typically magnetite or maghemite) in water or nonpolar solvents called magnetic fluids or ferrofluids were recently reviewed in several papers [51, 58] and monographs [10, 13].

2.1.3 Iron oxides/ferrites

Term "iron oxides" covers numerous families of substances generally described by the formula $Fe_xO_yH_z$ (in most of the cases, $z = 0$). Chemical formula of ferrites is generally expressed as $MO \cdot Fe_2O_3$. Transition metals like Mn, Co, Zn, Cu, and Ni are typical M atoms in the ferrite structure. The material (with M = Fe) called magnetite belongs to the ferrite family as well. Out of the materials, magnetite and maghemite have an exceptional importance. They have the highest saturation magnetization (80 – 100 $A \cdot m^2kg^{-1}$), which is two orders of magnitude higher than in other iron oxides [59]. The superparamagnetic behavior was observed for their crystallites with a diameter below 30 nm. Such crystallites are commonly named superparamagnetic iron oxide nanoparticles (SPION). The saturation magnetization of SPION is usually 20 – 50% lower than in the bulk state. Biocompatibility of SPIONs was recently reviewed [6]. Both superparamagnetic substances are easy to prepare at a reasonable price. Iron oxide-based ferrofluids often contain a mixture of maghemite and magnetite.

Magnetite, Fe_3O_4 ($FeO \cdot Fe_2O_3$) is a black, ferrimagnetic oxide with an inverse spinel structure containing both Fe(II) and Fe(III) ions [59]. It is often used as a precursor of maghemite. Its micrometer-size crystallites (Fig. 2a and b) have been widely used for the production of magnetic tapes and in other industrial applications due to their high M_S. It should be, however, noted that micrometer-sized magnetite has a nonzero remanence. SPION particles therefore prevail as core materials for separation/transport processes.

Also maghemite, γ-Fe_2O_3, is a reddish brown black ferrimagnetic material, isostructural with magnetite, but with cation deficient site. It is an important magnetic pigment with properties similar to Fe_3O_4 [59]. Due to its similarity with magnetite it is commonly classified as ferrite, although it does not have a proper composition. It is usually prepared from magnetite by oxidation. As an oxidizing agent, hydrogen peroxide [60], ferric nitrate [61], and air [62] can be employed. Maghemite is more suitable for biological applications due to its higher stability.

2.1.4 Preparation of superparamagnetic iron oxide and ferrite nanoparticles

Many methods are available for tailoring size, distribution, and magnetic properties of the nanoparticles by controlling reaction and process parameters. Unfortu-

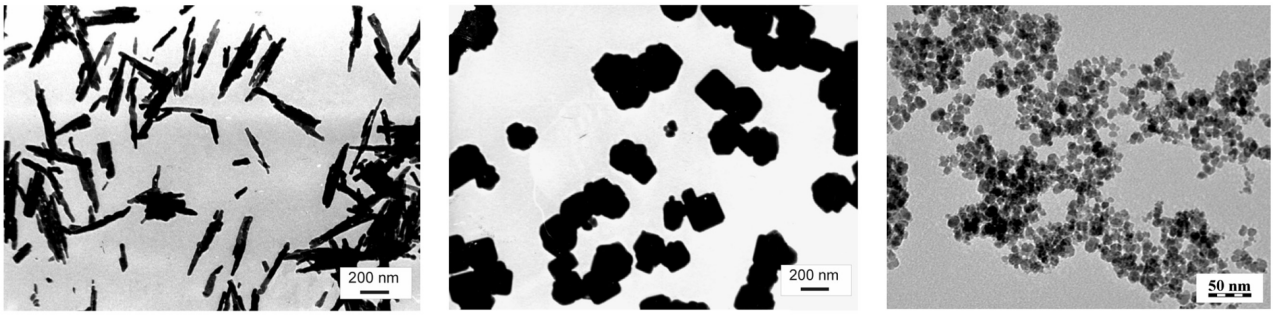

Figure 2. Scanning electron micrograph of (a) needle-like and (b) cubic magnetite, (c) transmission electron micrograph of citric acid-stabilized maghemite obtained by coprecipitation.

nately, methods yielding monodisperse nanoparticles with excellent magnetic properties often make impossible the chemical modification (functionalization) of the material surface. Thus a compromise has to be carefully found depending on the prospective application. Among a plethora of techniques developed for the preparation of magnetic materials, only those suitable for separation media are discussed further.

2.1.4.1 Mechanical procedures

Historically, superparamagnetic magnetite was prepared by wet grinding of bulk magnetite in organic solvents in the presence of large amounts of oleic acid as the surfactant. The surfactant facilitated grinding and also inhibited the particle agglomeration. The process was performed in a ball mill and the typical charge was 4 vol.% magnetite, 10 – 20 vol.% surfactant, and the rest was a solvent [63]. Because the procedure was costly and time consuming and the particles had a broad size distribution, it was replaced by chemical and thermal methods.

2.1.4.2 Chemical procedures

2.1.4.2.1 Coprecipitation with bases

It is the most widespread method of SPION preparation performed in water, resulting in a rather narrow particle size distribution compared with the wet grinding process. The process provides magnetite particles up to 10 nm in diameter (Fig. 2c). In general, the synthesis can be expressed by the following equation:

$$2\,Fe^{3+} + Fe^{2+} + 8\,OH^- \rightarrow Fe_3O_4 + 4\,H_2O \qquad (3)$$

Typically, ammonia solution is added under stirring to a water solution of trivalent and divalent iron salts at a molar ratio of Fe(III)/Fe(II) near 2, or *vice versa* [64]. The procedure depends on the type and concentrations of salts (chlorides being predominant) and base, addition of chelating agents, temperature, rate of addition, and aging. The precipitate is left to grow and then repeatedly washed with distilled water by magnetic separation until the colloid is formed by the process called peptization.

Formation of the product and particle morphology is affected by different parameters of the coprecipitation process. A rapid pH increase in the range of 8.5 – 10 is essential [65]. Slow addition of a base may lead to the formation of a brown nonmagnetic precipitate, probably hydroxides. Rapid introduction of alkali into the solution under intensive agitation permits simultaneous precipitation of both Fe(II) and Fe(III) hydroxides resulting in a black magnetite precipitate. Also, iron salt solution can be slowly added to the base. If strong bases such as NaOH, KOH, and LiOH are used, nonmagnetic products may be obtained. Ammonium hydroxide is therefore preferred, where such an effect was not observed. Precipitation and aging of the precipitate also depend on temperature, the appropriate one being typically 25 – 80°C to obtain particles smaller than 10 nm [65]. The dependence of particle growth on the aging process was described.

Water-based colloidal oxides are mostly prepared in the absence of surfactants [66, 67]. Stabilization is then achieved by electric charges on the particles, *e.g.*, from perchlorate, citrate, nitrate or tetramethylammonium ions, providing alkaline or acidic ferrofluid [67, 68]. The dispersion is then stable due to electrostatic repulsion of the particles carrying the same charge. Its stability, however, is very sensitive to electrolytes present in the medium and is limited only to extremely high or low pH and low ionic strength. Colloid particles form aggregates of 5 – 100 magnetite nanoparticles depending on the surface charge. Precipitated nanoparticles can be stabilized (peptized) in water or nonpolar liquids by the addition of a surfactant with a proper hydrophilic/hydrophobic balance. As surfactants, various low-molecular-weight compounds, such as higher fatty acids [69] and saccharides were reported [70, 71]. The effect of different surfactants on size and magnetic properties of maghemite nanoparticles was already reported [72]. Ferrofluids can be stabilized also by the addition of various polymers, such as

polysaccharides [73], typically dextran [74 – 77], poly(vinyl alcohol) (PVA) [78 – 84], poly(ethylene glycol) (PEG) [85], poly(oxyethylene-*co*-propene) bisphosphonates [86], poly(methacrylic acid), polyacrylamide, *etc.* The well-known dextran-stabilized magnetite available under the trade names Feridex I.V.® (http://www.advancedmagnetics.com/doc/prod/feridex. htm), Combidex® (http://www.advancedmagnetics.com/doc/prod/combidex.htm), Endorem®, and Resovist® found applications as a contrast agent in MRI of liver, spleen, and bone marrow, or for tumor or cell hyperthermia [87 – 90]. PEG coating became popular due to its very good biocompatibility. To improve the adsorption of PEG on the particles during coprecipitation, chemical bonding by silanization of magnetite with (trimethoxysilyl)PEG was proposed [91]. Stabilization is generally achieved either by coprecipitation of ferrous/ferric salts in a polymer solution (*in situ* synthesis), or a polymer solution is added after the precipitation (postsynthesis modification). The presence of a dissolved polymer during the formation of magnetic particles influences the precipitation, nucleation, and stability of resulting colloid particles. Polymer stabilizers improve not only the stability of the colloid, but also boost surface properties of the particles and contribute to their biocompatibility.

In addition to magnetite, particles of other ferrites are prepared by the coprecipitation of corresponding divalent metals salts, such as Co(II), Cu(II), Ni(II), Mn(II), and Fe(III) with an alkali [92 – 97]. Unlike magnetite, Co and Ni ferrites are formed at higher temperatures (80 – 100°C) [98]. Both, the duration of aging and the pH of the medium, affect the diameter of the resulting particles after precipitation [92]. Other parameters influencing the coprecipitation of Co(II) and Fe(III) salts include temperature and nature of precipitant [99]. Strong alkali hydroxides (LiOH, KOH, NaOH) are preferred to NH_4OH in the preparation of ferrites. Co, Mn, and Ni ferrites have generally slightly higher magnetic susceptibility and saturation magnetization than magnetite. Their application in biology and medicine, however, is limited due to the toxicity of their divalent metals.

2.1.4.2.2 Thermolysis of organometallic precursors

A two-step thermal decomposition of iron pentacarbonyl in the presence of a stabilizing polymer provides 10 – 20 nm (alternatively up to 25 nm) monodisperse magnetite nanoparticles [100]. The process is based on the formation of primary Fe nanoparticles in a nonpolar liquid followed by their subsequent oxidation to magnetite particles. The decomposition temperature plays the crucial role in the determination of the particle size and polydispersity [101]. Surfactant (*e.g.*, oleic acid) has to be used; it can, however, hinder subsequent surface modification. Decomposition of iron pentacarbonyl was also used for the preparation of maghemite [102]. Alternatively, spherical maghemite nanoparticles are formed by the rapid injection of iron cupferon complex in trioctylamine at 300°C [103].

2.1.4.2.3 Hydrothermal procedure

Generally, hydrothermal processes are reactions of mixed oxides or hydroxides of iron and other selected metals carried out in water under supercritical conditions, *i.e.*, at temperatures above 200°C and under a pressure higher than 14 MPa. Water plays the role of a hydrolytic reactant. Size and morphology of the product are controlled by reaction time and temperature. Purity of the forming solid phase depends on pH. Two main chemical processes lead to the formation of ferrites under hydrothermal conditions: (i) neutralization (or hydrolysis) and oxidation of Fe(II) and divalent metal ions [104] and (ii) neutralization of mixed metal hydroxides [105]. Alternative modifications include the use of mixed metal oxides [106] or ethylene glycol under supercritical conditions [107]. Hydrothermal procedures are experimentally demanding and the resulting properties, such as magnetic behavior, particle size, size distribution, do not offset the technical complications.

2.1.5 Metals, alloys, and other compounds

Magnetic fluids based on various amorphous metal nanoparticles, such as Co, Fe, FeCo, and FePt are obtained by metal carbonyl decomposition [108 – 111]. Due to the above mentioned toxicity of Co, only iron and iron alloys can be considered for bioapplications. A great advantage of iron magnetic fluids consists in their saturation magnetization higher than that of the conventional SPION ferrofluids. Well-dispersed iron particles were prepared by the thermal decomposition of iron pentacarbonyl in organic liquid media of different polarities [112]. Polymer stabilizers influenced the decomposition of iron pentacarbonyl and undesirable oxidation of iron nanoparticles [113]. Magnetite, maghemite, and akaganeite (β-FeOOH) were formed in the air at various humidities. The uncontrolled oxidation was accompanied by the deterioration of magnetic properties, which limits applications of iron nanoparticles. Also ultrafine amorphous Fe-C nanoparticles were obtained by the decomposition of iron pentacarbonyl [114]. Alternatively, iron nitride magnetic fluid was synthesized from the gas reaction of iron carbonyl and ammonia [115]. The fluid had a high M_S and was expected to be more stable against oxidation than pure iron. However, this was not confirmed [116].

2.1.6 Surface modification of magnetic nanoparticles

Surface modification of magnetic nanoparticles is necessary for three reasons: (i) it stabilizes colloid dispersion, (ii) ensures biocompatibility and prevents undesirable

interactions with components of the medium (nonspecific interactions with proteins, phosphates, *etc.*), and (iii) facilitates attachment of functional groups necessary for interaction-based applications (ionic, chelating, biospecific separation, targeting, *etc.*).

Colloids modified with various low-molecular-weight chelating agents possess substantially higher stability than those stabilized conventionally. The agents are linked to surface Fe(III) and Fe(II) ions (or other M(II) metal ions in ferrites) possessing unsaturated valences in the crystal lattice *via* a coordination bond. The first large group contains agents possessing one or more carboxyl groups, possibly in combination with OH, NH_2, or SH groups. It includes highly chelating ethylenediaminetetraacetic acid (EDTA) [117], tartaric, citric, and (disulfanyl)succinic acids (DMSA), which substantially broaden the scope of applicable pH [118]. Simple amino acids provide weaker bonds. The second group includes agents carrying phosphorous ligands, such as phosphoric acid and one or more of its derivatives, *e.g.*, phosphates, di- and polyphosphates, phosphonates and diphosphonates, monoesters of acid [119 – 121]. They are often combined with COOH, NH_2, OH, SH groups. Some strongly chelating agents (diphosphonates, EDTA) partly dissolve the oxides or change their structure.

Polyfunctional low-molecular-weight chelating agents containing reactive groups besides moieties binding the iron oxide are suitable for a more sophisticated functionalization. DMSA-modified maghemite contains free sulfanyl groups suitable for various reactions including immobilization *via* disulfidic bonds [122]. Other modifications take advantage of primary amino groups introduced by the reaction of maghemite with [(2-aminoethyl)hydroxymethylen]bisphosphonic or [(5-aminopentyl)hydroxymethylen]bisphosphonic acid [121]. To prepare magnetic nanoparticles carrying amino groups, silanization with (3-aminopropyl)trialkoxysilanes is common [123 – 126]. PEGylated maghemite was obtained by three-step functionalization starting from silanization with (3-aminopropyl)trimethoxysilane, followed by Schiff base formation with oxidized dextran and amino-PEG [127].

Polymers with groups interacting with surface ions of magnetic oxides are useful also for the modification. Stability of the coating depends on the type of the interaction. While one carboxyl group of a low-molecular-weight compound ensures a weak bond, attachment to more carboxyl groups of the polymer is more stable, even in the absence of convenient mutual 1,2 or 1,3 arrangement. Poly(acrylic acid) [128 – 131], carboxymethylated polysaccharides [132 – 135], and other natural polymers containing carboxyl groups (hyaluronic, alginic, pectic acid, heparin [136]) were thus used to coat magnetic oxides. Alginic acid carrying chelating OH and carboxyl groups provided even stronger bonds. Aldehyde groups were introduced into dextran-coated iron oxide nanoparticles to immobilize and detect DNA [137]. Strong binding of PVA was achieved by crosslinking PVA with glutaraldehyde [82] or by coating iron oxide nanoparticles with PVA functionalized with carboxyl, thiol [138], or phosphate groups [139]. Poly(2-methoxyethyl methacrylate) shell rendered magnetite nanoparticles thermoresponsive [140]. Magnetite nanoparticles coated with cationic polyethylenimine simplified the purification of plasmid DNA from bacterial cells [141].

2.1.6.1 Magnetic particles by grafting

Several "living" radical polymerization techniques, such as nitroxide-mediated polymerization (NMP), atom transfer radical polymerization (ATRP), and reversible addition fragmentation chain transfer (RAFT) have been developed in recent years and also employed for grafting polymers on magnetic nanoparticles, yielding magnetic core-polymer shell particles stable in liquids. They show characteristics of "living" systems, *e.g.*, predefined molecular weight, narrow molecular weight distribution, and active polymer end groups. A major difference between conventional and controlled radical polymerization is the lifetime of the propagating radical during reaction. While in conventional radical polymerization the radicals generated by the decomposition of the initiator undergo propagation and terminate within seconds, the lifetime of the living radical can be extended up to several hours.

2.1.6.1.1 NMP

NMP often employs 2,2,6,6-tetramethylpiperidinyl-1-oxyl (TEMPO) to reversibly deactivate/trap growing polymer radicals making them dormant. This reduces the probability of bimolecular termination. Because monomer can only add to the growing polymer radical between its activation and deactivation reactions, the rate of polymerization is slower than in conventional free radical polymerization. By initiating polymer radicals at nearly the same instant, polymers with narrow molecular weight distribution are synthesized by NMP. Being a free radical process, NMP is relatively insensitive to impurities. It can be performed without the need to purify solvents or reagents, unlike conventional living polymerization processes (*e.g.*, ionic and group transfer polymerization). Additionally, NMP can be performed in commonly used heterogeneous systems, such as suspension and emulsion. The system uses various alkoxyamines to polymerize vinyl monomers yielding polymers of moderately low polydispersities and relatively low molecular weights. PS and poly(3-vinylpyridine) were thus directly attached on 10 nm magnetite nanoparticles by the method of "grafting from" the surface (Fig. 3). 4-Hydroxy-1-[(2′-hydroxy-1-phenylethyl)oxy]-2,2,6,6-tetramethylpiperidine (TEMPO-based alkoxyamine) initiator with a phosphoric acid

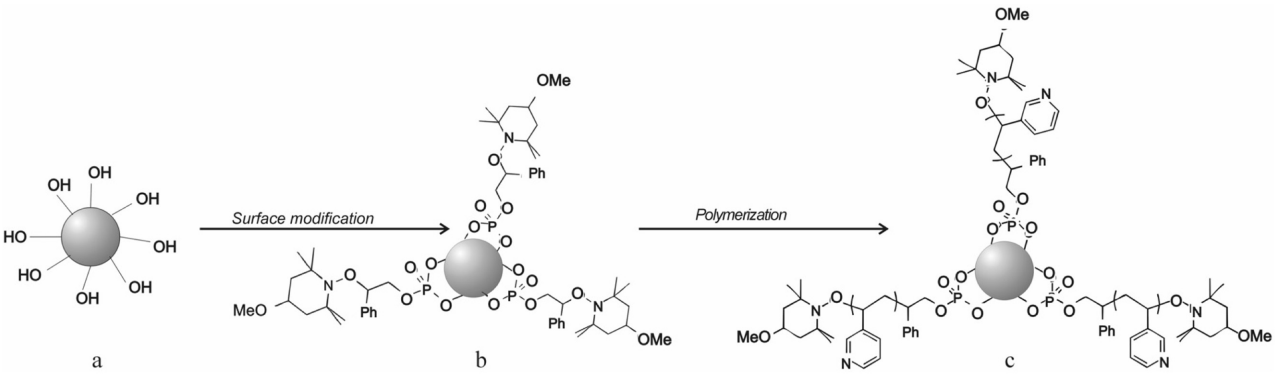

Figure 3. Surface-initiated NMP of 3-vinylpyridine on magnetite nanoparticles. (a) Starting, (b) initiator-modified, and (c) resulting poly(3-vinylpyridine) brush/magnetite core nanoparticles.

group was chemisorbed on the surface of magnetite initiating NMP of styrene and 3-vinylpyridine. With this method, it was possible to control the length of polymers grafted on the nanoparticles. PSt- and poly(3-vinylpyridine)-modified magnetite particles were *ca.* 50 nm in diameter and formed fine and stable dispersions in appropriate solvents [142].

2.1.6.1.2 ATRP

ATRP is an efficient route for synthesizing polymers with well-controlled molecular weight, low polydispersity, and novel architectures. The advantage of ATRP over the traditional living processes is its great tolerance to protonic reagents. The fast and reversible equilibrium between growing radicals and dormant species results in a low and constant concentration of growing radicals, which, along with the fast initiation and negligible irreversible termination, makes the polymerization proceed in a living manner. ATRP has succeeded in the polymerization of methacrylates, acrylates, styrene, and functional monomers, such as 2-hydroxyethyl methacrylate (HEMA) and 2-(dimethylamino)ethyl methacrylate, or in grafting PEG monomethacrylate onto magnetic nanoparticle surface to produce "brush" morphology. The surface of magnetic nanoparticles is first modified with a suitable initiator, *e.g.*, 2-bromo-2-methylpropanoic acid [140], trichloro[4-(chloromethyl)phenyl]silane [143], 3-chloropropanoic acid [144], 12-(2-bromopropanoyloxy)-dodecanoic acid [145], trichloro{2-[4-(chlorosulfonyl)phenyl]ethyl}silane [146]. One end group of the initiator is chemically attached to iron oxide core (*via* COOH or OH) and the other end has a functional group (*e.g.*, $-CH_2(C_6H_5)CHBr$, $-OCOCHBrCH_3$, $-OCOC(CH_3)_2Br$) facilitating polymerization of the respective monomer in a suitable solvent under the catalysis of, *e.g.*, CuBr, CuCl, and amine (*N,N,N′,N″,N‴*-pentamethyldiethylenetriamine). The advantage of the method consists in the formation of uniform chains on the surface of iron oxide, whereas the disadvantage is a rather low conversion (10 – 15 wt.%) and difficult practicability in water.

2.1.6.1.3 RAFT

RAFT has recently emerged as a promising controlled radical polymerization technique due to its versatility and simplicity. Its main advantage consists in that the polymer is free from the contamination with metal catalyst. The RAFT technique is compatible with almost all of the conventional monomers for radical polymerization. The polymerization conditions are similar to the conventional radical polymerization, but with the addition of selected thiocarbonylthio chain transfer agents, such as trithiocarbonates, (dibenzyl trithiocarbonate), dithioesters (phenylethyl dithiobenzoate), dithiocarbamates, xanthates, *etc.* The requirements for an effective RAFT agent are that both rates of addition and fragmentation must be fast relative to the rate of propagation and the expelled radical must be capable of reinitiating polymerization. The first requirement is ensured by the rapid consumption of the initial RAFT agent and fast equilibration of the dormant and active species, while the second requirement ensures the continuity of the chain process. The conception was applied onto the preparation of 5 nm magnetic PS and poly(acrylic acid) particles. Peroxidic or hydroperoxidic groups were introduced on the surface of magnetite by an O_2/O_3 treatment thermally initiating RAFT polymerization of styrene and acrylic acid in the presence of a chain transfer agent [147].

2.2 Preparation of magnetic polymer microspheres

Magnetic polymer microspheres are composites of an inorganic and organic material. A variety of methodologies were used for their preparation. Every method, however, has its limitations in terms of the amount of magnetic material encapsulated in the particles, their size,

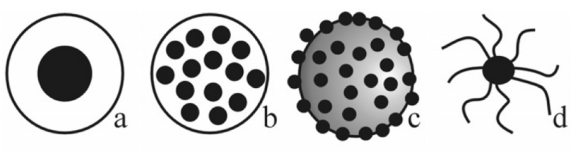

Figure 4. Different morphologies of composite magnetic polymer microspheres. (a) Single-core, (b) multicore, (c) strawberry and (d) brush (hair) morphology.

and polydispersity. No method can fulfil all the requirements expected from the use of microspheres, *e.g.*, to produce functionalized monodisperse spherical particles completely encapsulating magnetic cores, control the size, and with a biocompatible surface. The desirable affinity of a polymer, or a monomer to a magnetic filler is often ensured by functional groups (OH, COOH, $PO(OH)_2$, NH_2), suitably selected environment, or electrostatic interactions. Various preparation methods provide magnetic polymer microspheres differing in morphology (Fig. 4a – d), including magnetic core – polymer shell (Fig. 4a), magnetic multicores homogeneously dispersed within the polymer matrix (Fig. 4b), magnetic nanoparticles located on the surface of a polymer core ("strawberry" morphology, Fig. 4c), "brush" (hair) morphology (polymer chains attached to the magnetic core, Fig. 4d).

Nanocomposite microspheres can be prepared from separately obtained polymers and magnetic cores (phase-separation, solvent evaporation, layer-by-layer process). Alternatively, they are *in situ* precipitated in/on polymer microspheres, *e.g.*, by chemical metal oxide deposition. Out of the methods, heterogeneous polymerizations in the presence of magnetic nanoparticles are by far most frequently used. They involve polymerization in a continuous (often aqueous) phase in the presence of inorganic particles by suspension, dispersion, emulsion, miniemulsion, and microemulsion polymerization methods.

2.2.1 Composite microspheres obtained from separately prepared magnetic cores and polymers

2.2.1.1 Phase separation method

Phase separation involves the formation of water-in-oil or oil-in-water emulsion. The polymer is precipitated from the continuous phase onto the magnetic particle by a change of pH, temperature, ionic strength, or by the addition of precipitants. Magnetic HSA microspheres, 0.8 – 1 μm in diameter, were prepared by dispersing sufficient amounts of magnetically responsive material (γ-Fe_2O_3, 26 nm in size) with albumin in cottonseed oil containing sorbitan sesquioleat [148]. The system was subjected to chemical (glutaraldehyde) or thermal (130°C) crosslinking. In thermal crosslinking, intramolecular disulfide bridges between free SH groups on adjacent protein albumin chains were formed. Heat-stabilized magnetic albumin microspheres were more stable than chemically crosslinked ones. In another example, Fe_3O_4 and poly(D,L-lactide-*co*-ethylene glycol) were dispersed in acetone by sonication and the dispersion was dropped into water. After the polymer was precipitated and solvent evaporated, the magnetic spherical particles were obtained with the size range of 100 – 200 nm and Fe content from 0.5 to 5.2 wt.%. Properties of magnetic particles were controlled by changing the molecular weight and ratio of the lactide and ethylene glycol blocks [149].

2.2.1.2 Solvent evaporation method

Solvent evaporation is the easiest way to encapsulate magnetic particles in a polymer. The resulting microparticles, however, are polydisperse and usually rather large. The magnetic material is dispersed in a polymer solution (typically dichloromethane) and then emulsified with a surfactant until the solvent evaporates. Magnetic spherical particles (125 – 250 μm) were prepared from a chloroform solution of poly(vinyl butyral) containing magnetite, which was stirred in water with PVA, sodium dodecyl sulfate (SDS) and Pluronic F6800 (ethylene oxide/propylene oxide block copolymer) emulsifiers until chloroform was evaporated [150].

2.2.1.3 Layer-by-layer process

The layer-by-layer method is based on the electrostatic attraction between the oppositely charged particles. It produces coated colloids of different shapes, sizes, uniform layers of diverse compositions and controllable thickness [151]. As an example, monosized magnetic latex particles were prepared by a two-step procedure using anionic iron oxide (5 – 10 nm) and cationic polymer latexes. Core-shell particles (470 – 150 nm) based on poly(styrene-*co*-2-aminoethyl methacrylate) and poly(styrene-*co*-*N*-isopropylacrylamide) functionalized with 2-aminoethyl methacrylate or poly(*N*-isopropylacrylamide-*co*-*N*,*N*′-methylenebisacrylamide-*co*-2-aminoethyl methacrylate) were prepared by precipitation polymerization. Iron oxide nanoparticles were then adsorbed on the latexes *via* electrostatic interaction depending on the concentration and type of nanoparticles. The highest adsorption was achieved with pure cationic poly(*N*-isopropylacrylamide) latexes [152, 153].

2.2.1.4 Sol – gel transition

The sol – gel process involves the transition of a system from a liquid ("sol") into a solid ("gel") phase. In a typical sol – gel process, the precursor is subjected to a series of hydrolysis and polymerization reactions to form a colloidal suspension, the particles then aggregate in a new phase, the gel. Magnetic bead cellulose, 100 μm – 1.1 mm in size, was obtained by thermal sol – gel transition (90°C) of viscose in the presence of a ferrite powder

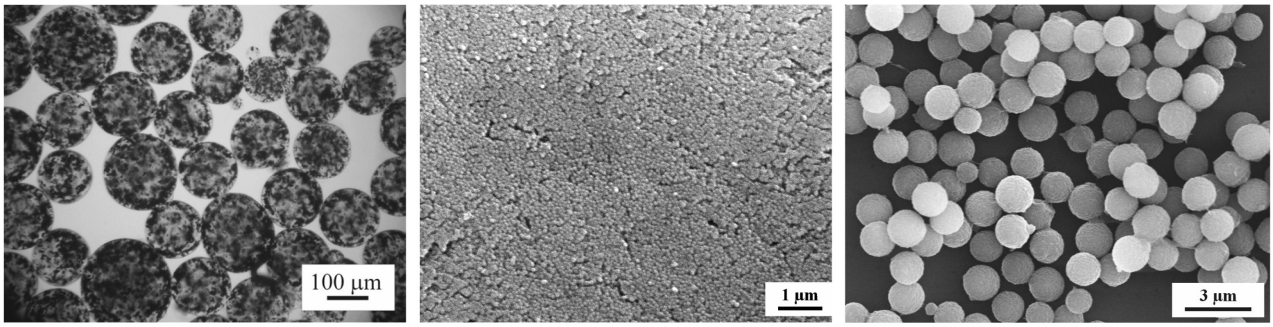

Figure 5. (a) Optical micrograph of 125 – 250 μm magnetic bead cellulose. (b) Scanning electron micrograph of 77 nm magnetic PGMA microspheres obtained by emulsion polymerization. (c) 1.5 μm magnetic poly(2-hydroxyethyl methacrylate-*co*-ethylene dimethacrylate) microspheres obtained by dispersion polymerization.

(< 10 μm) suspended in chlorobezene using oleic acid as a stabilizer (Fig. 5a) [154]. Silica-coated magnetite was obtained by the sol – gel transition of tetraethyl orthosilicate in propan-2-ol by the addition of aqueous ammonia at room temperature. The surface of the particles was modified with [3-(glycidyloxy)propyl]trimethoxysilane and iminodiacetic acid (IDA) [155]. Magnetic calcium alginate particles with bis(2,4,4-trimethylpentyl) phosphinic acid as an extractant of metal ions were prepared by dropping maghemite dispersion in sodium alginate and extractant into a $CaCl_2$ bath [156].

2.2.2 Preparation of magnetic nanoparticles in porous microspheres

Magnetic compounds can be obtained *in situ* inside the polymer matrix by the same techniques as used in the preparation of magnetic colloids, *e.g.*, by coprecipitation, decomposition of metal carbonyls, or reduction of metal salts [157]. The key to success is to use such a medium, in which the prospective magnetic compound does not coagulate, which penetrates the microspheres, either into the pores or swells the particles. Alternatively, conventional supports (seed particles) were "postmagnetized" by the treatment (impregnation) with magnetic ferrofluid, or by chemical metal deposition [158]. Probably the best known magnetic monodisperse polymer microspheres were developed by Ugelstad in a multistep procedure [159], which are commercially available from Dynal. Iron oxides formed *in situ* by the precipitation of Fe(II) and Fe(III) salts with a base (NH_4OH or NaOH) inside the preformed porous monodisperse polymer microspheres produced by the staged templated suspension polymerization (method of activated swelling) followed by coating [160]. However, the multistep process is tedious requiring the preparation of monosized seed particles, usually by emulsion polymerization, in the very beginning.

Impregnation of 0.2 – 0.4 mm hypercrosslinked poly(styrene-*co*-divinylbenzene) microspheres having high specific surface area and 2 – 3 nm pore diameter with $Co_2(CO)_8$ in propan-2-ol, evaporation of the solvent, and following thermolysis resulted in discrete 2 nm Co nanoparticles. An increase in the Co content was accompanied by an increase in the mean microsphere diameter due to an increase in the population of large Co nanoparticles (up to 15 nm). The controlled nanoparticle growth over a wide range of Co concentrations was attributed to nanoscale hypercrosslinked PS cavities, which physically restricted the size of growing Co nanoparticles [161].

2.2.3 Preparation of magnetic microspheres by heterogeneous polymerization techniques in the presence of magnetic nanoparticles

Various monomers are polymerized in the presence of magnetic dispersions to yield magnetic microspheres. In these systems, the type and size of magnetic nanoparticles, their polydispersity and good dispersibility, or stability in an appropriate medium are important. Although polymerization techniques are traditionally classified into suspension, emulsion, miniemulsion, microemulsion or dispersion methods, it is not always possible to place a given system in a particular category. In the same manner, the presence of the polymer during the precipitation affects the quality and stability of the forming magnetic colloid, and magnetic nanoparticles present in the polymerization also influence reaction kinetics and precipitation and stability of the system. According to the recent information, magnetic material should possess higher affinity to monomers forming polymer chains and, at the same time, have minimal interaction with all other components of the system. This does not depend much on the phase, in which the magnetic material is dispersed, but rather on the kind of stabilizer of the nanoparticles and on whether they thermodynamically prefer (especially in the interaction with

common emulsifiers and stabilizers) to stay at the interphase boundary, where they act as a colloidal stabilizer.

2.2.3.1 Suspension polymerization

Suspension polymerization is the oldest of all heterogeneous polymerization techniques. It provides microspheres of broad size distribution with diameters ranging from micrometers to millimeters. The suspension procedure is an effective platform for the encapsulation of not only magnetic colloids, but also drugs. Monomer, magnetic filler, and initiator make a separate phase in the form of droplets dispersed in the continuous phase (typically aqueous). The droplets are stabilized either by inorganic colloidal stabilizers, or by polymer surfactants to prevent aggregation. Polymerization proceeds in droplets, which transform into microspheres.

Preparation of hydrophobic polymer microspheres is most illustrative. Here, the dispersed phase typically consists of a styrene and divinylbenzene monomer mixture, and porogen agents (*e.g.*, toluene/heptane mixture), initiator (2,2′-azobisisobutyronitrile, AIBN). It also contains 3 – 4 μm iron particles. The dispersed phase is stirred in the continuous aqueous phase (typically at 400 rpm). Depending on the reaction conditions, resulting microspheres are often 65 – 300 μm in size and contain 2 – 7 wt.% Fe [162]. Magnetic poly(styrene-*co*-divinylbenzene-*co*-glycidyl methacrylate) microspheres were prepared by modified suspension polymerization and the microspheres were reacted with ethylenediamine and Cibachrom Blue F3GA as a dye ligand for affinity protein adsorption [163].

Since hydrophilic polymers mostly cannot be prepared in an aqueous phase, inverse suspension polymerization was developed. As an example, magnetic, molecularly imprinted poly(4-vinylpyridine-*co*-ethylene dimethacrylate) particles were prepared by inverse suspension polymerization in the presence of 2,4-dichlorophenoxyacetic acid and [3-(methacryloxy)propyl]trimethoxysilane-modified magnetic nanoparticles in silicone oil. A highly viscous dispersion phase avoided coalescence of the dispersed droplets. Other reasons why silicone oil was suitable as a continuous phase were its nonpolarity, immiscibility with the monomer mixture, and low cost. The redox initiator dibenzoyl peroxide/dimethylaniline initiated the polymerization at 10°C. The diameter of the resulting magnetic microspheres was 20 μm and the Fe_3O_4 content amounted to 1.1 wt.% [164]. Another example of magnetic hydrophilic polymer microspheres prepared by the water-in-oil inverse suspension polymerization is spherical thermosensitive poly(*N*-isopropylacrylamide) microspheres. Ferrofluid and ammonium persulfate (APS) solution were added to *N*-isopropylacrylamide and *N,N*(-methylenebisacrylamide monomer phase containing Igepal CO-520 (poly(oxyethylene)nonylphenyl ether) under sonication. The potential of this technology for a new contactless controllable drug releasing system was exemplarily demonstrated using Rhodamine B and Methylene Blue as drug-analogous substances. Depending on the stirring speed (800 – 2000 rpm) and surfactant, microspheres with a size of 10 – 200 μm were obtained [165]. The presence of the magnetic colloids allowed an inductive heating of the particles using an alternating magnetic field above the polymer volume phase transition temperature (~35°C). This resulted in a pronounced microsphere deswelling accompanied with a release of the encapsulated substances.

2.2.3.2 Emulsion polymerization

It is a process in which a monomer is emulsified in aqueous continuous phase and transformed into latex by polymerization. The size of resulting nano- and micospheres ranges from tens of nanometers to one micrometer. Microspheres are stabilized with emulsifiers or protective colloids adsorbed on surface. Several emulsion polymerization mechanisms were proposed, the most recognized being micellar and homogeneous nucleation. In seeded emulsion polymerization, the concentration of the emulsifier has to be lower than its critical micellar concentration in order to avoid the formation of new micelles free of any magnetic material. The least possible solubility of the monomer in the continuous phase is required. Nonionic initiators are often used to avoid chain growth in the continuous phase [166].

In principle, two concepts exist for the preparation of magnetic microspheres by emulsion polymerization. In the first one, magnetic nanoparticles are dispersed in the monomer phase, possibly also with an organic solvent. The latter one consists of dispersing magnetic nanoparticles in the continuous, typically aqueous phase stabilized preferably by a hydrophilic compound. While the first concept is applicable to polymerizations of hydrophobic monomers, the other one is suitable for hydrophilic monomers. The initiator is always dissolved in the continuous phase. A typical example of polymerization of a hydrophobic monomer is AIBN- or potassium persulfate (KPS)-initiated seeded emulsion copolymerization of styrene and divinylbenzene. Oleic acid-stabilized magnetic nanoparticles in octane (γ-Fe_2O_3, diameter 7 nm) were emulsified in water containing nonionogenic Triton X-405 surfactant [poly(oxyethylene) isooctylphenyl ether]. The dispersion was added to a styrene and divinylbenzene mixture, AIBN was admixed, and the mixture stirred at laboratory temperature to enable monomer droplets with the initiator to adsorb onto the ferrofluid drops. Polymerization was started by heating the reaction mixture. If the polymerization was initiated with KPS, aqueous solution of the initiator was added until the emulsion of maghemite was swollen with the monomer. While the oil-soluble AIBN initiator produced hemisphere-type latex particles, much more homogeneous

microspheres were produced with KPS. The microspheres had an extremely low sedimentation rate [167]. An example of the inverse emulsion polymerization is the copolymerization of acrylamide with *N,N′*-methylenebisacrylamide in dodecane. Sodium citrate-stabilized maghemite was added to aqueous solution of the monomers, the dispersed phase was stabilized with Span 80 and the polymerization initiated with 2,2′-azobis(2-isobutyramidine). Size of the resulting microspheres was surprisingly large, 10 – 60 μm [168]. Another example is copolymerization of HEMA and methacrylic acid. The magnetic material stabilized with poly(oxyethylene-*block*-methacrylic acid) was mixed with monomers and then added to a mixture of decane and poly(ethene-*co*-butene)-*block*-poly(ethylene oxide), and finally the initiator 2,2′-azobis(2-methylbutanonitrile) was added. The microspheres formed by the polymerization were 50 – 250 nm in diameter [169].

A less common procedure involves dispersing magnetic nanoparticles in an aqueous continuous phase assuming the homogeneous nucleation mechanism, which is based on a limited solubility of the monomer in the continuous phase. The initiation then starts in the continuous phase, followed by the growth of oligomer chains, their precipitation when reaching the critical chain length, and finally nuclei and particle formation. The dispersed phase consisted of glycidyl methacrylate (GMA); aqueous ferrofluid was stabilized with dextran, (carboxymethyl)dextran or [2-(diethylamino)ethyl]dextran or D-mannose [170]. Disponil AES 60 (sodium poly(oxyethylene) alkylaryl ether sulfate) served as an emulsifier and 4,4′-azobis(4-cyanopentanoic acid) or APS as an initiator. Depending on the reaction conditions, microspheres were obtained in the size range of 70 – 400 nm (Fig. 5b).

The emulsifier-free emulsion polymerization, which is a special type of the emulsion polymerization, provided magnetic poly(styrene-*co*-butyl acrylate-*co*-methacrylic acid) microspheres [171]. Ferrofluid (Fe_3O_4) stabilized with dodecyl sulfate, KPS, and a mixture of a polar solvent (methanol, ethanol, or acetone) and water constituted the continuous phase; monomers formed the dispersed phase. The aqueous phase was homogenized at room temperature, and then the dispersed phase was added for 5 min. Depending on the polymerization conditions, monodisperse 100 – 400 nm microspheres were prepared. The magnetite nanoparticles (~10 wt.%) were localized at the surfaces of the microspheres.

2.2.3.3 Microemulsion polymerization

Microemulsion is defined as a stable isotropic and optically transparent dispersion of two immiscible liquids prepared in the presence of a stabilizing system, which can be a surfactant, a mixture of surfactants, or a mixture of a surfactant and a cosurfactant [172]. To prepare a thermodynamically stable microemulsion (a large amount of the surfactant (*ca.* 10 – 15 wt.%) is required), the weight fraction of the dispersed liquid at the same time does not exceed 10 – 15 wt.%. Microemulsion polymerization produces very small particles, typically 12 – 30 nm in size; as a result, their specific surface area is very large (~450 m^2/g). Surprisingly large (1 – 5 μm) homogeneous polymer-coated magnetite-containing microparticles were obtained by dispersing 10 nm oleic acid-stabilized magnetite nanoparticles in styrene, divinylbenzene, methacrylic acid, and acrylamide microemulsion polymerized in a continuous phase containing emulsifier (SDS), coemulsifier (cetyl alcohol), and KPS [173]. Submicrometer-sized magnetic hydrophilic polymer particles were prepared by 2,2′-azobisisobutyronitrile-initiated inverse microemulsion polymerization of acrylamide and *N,N′*-methylenebisacrylamide added to a suspension of trisodium citrate-stabilized iron oxide nanoparticles. Aqueous phase was dispersed in Aerosol OT (sodium bis(2-ethylhexyl) sulfosuccinate) surfactant in toluene solution to form a water/oil microemulsion. The particle size ranging from 80 to 180 nm was controlled by the concentration of the water-soluble crosslinker and the surfactant/water ratio. The magnetite content in polymer particles was 5 – 23 wt.%, which is in agreement with its concentration in the initial recipe thus confirming the total incorporation of iron oxide nanoparticles [174].

2.2.3.4 Miniemulsion polymerization

Miniemulsions are prepared under high mechanical shear (sonication, homogenizers) and are distinguished by high stability. They consist of mostly homogeneous monodisperse droplets in the range of 30 – 500 nm obtained using a low-molecular-weight costabilizer, which is soluble in the dispersed, but insoluble in the continuous (water) phase. A typical costabilizer is hexadecane, which reduces the diffusion of monomers from smaller to larger monomer droplets (Ostwald ripening) resulting in a relatively long stability of the miniemulsion system. An anionic, cationic, or nonionic surfactant present in the continuous phase prevents coalescence during particle collision. In the second step, the droplets (sometimes called nanoreactors) are polymerized without changing their identity, in contrast to microemulsions, where the droplets do not retain their identity [175].

A styrene miniemulsion was prepared using the following recipe. Styrene and the hydrophobic agent (costabilizer) hexadecane were added to SDS (surfactant) solution in water and the miniemulsion was obtained by sonication. For the encapsulation, styrene miniemulsion and water-based SDS-stabilized magnetite dispersion (~10 nm) were mixed and cosonified. To start the polymerization, KPS was added and the temperature increased. After completion of the polymerization, the

latex particles had a size of about 60 nm and the content of magnetite was 20 – 35 wt.% [176].

Polyacrylamide particles (60 – 160 nm) containing nanosized magnetic iron oxide were prepared by AIBN-initiated inverse miniemulsion polymerization. First, acrylamide, *N*,*N*′-methylenebisacrylamide, and methacrylic acid-stabilized magnetic fluid were homogenously mixed in a dilute aqueous ammonium and the dispersion was then added to a Span 80 (sorbitol monooleate) solution in cyclohexane under stirring. Miniemulsion was obtained by sonication. The size of superparamagnetic polymer particles was about 100 nm. The magnetite content in the particles was 13 wt.%, which was in agreement with the magnetite concentration in the feed [177]. Similarly, thermosensitive magnetic poly(*N*-isopropylacrylamide-*co*-methacrylic acid) particles were obtained in cyclohexane with the Span 80 emulsifier [178].

Finally, an emulsifier-free miniemulsion polymerization employing 10 nm oleic acid-stabilized magnetite (Fe_3O_4) nanoparticles for the encapsulation in PS microspheres used 2,2′-azobis(2-isobutyramidine) dihydrochloride as a cationic water-soluble initiator and hexadecane as a hydrophobic agent (costabilizer) [179]. The resulting 100 – 300 nm microspheres were monodisperse.

2.2.3.5 Dispersion polymerization

The original investigations of the dispersion polymerization, which is a kind of the precipitation polymerization, can be traced to ICI industrial research aimed at developing nonaqueous dispersion coating technology [180]. The dispersion polymerization is advantageous because micrometer-size polymer microspheres of a narrow size distribution can be obtained in a single step, *i.e.*, the process is simple and without tedious operations. The technique may be a useful alternative to the complicated Ugelstad method. Of utmost importance for the technique is the appropriate selection of the reaction medium, in which the monomer(s) is (are) soluble, but not the polymer and magnetic material. By heating the polymerization mixture, the initiator is decomposed and oligomer radicals are formed. The oligomeric chains do not remain dissolved in the medium, but precipitate when reaching the critical chain length. The chains associate forming nuclei, which aggregate and at the same time adsorb the stabilizer forming primary mature particles containing magnetic cores. Under the condition that no new nuclei are formed, the primary particles grow and reach the same (uniform) size. Two mechanisms of particle growth then follow. The first consists in the polymerization inside the particles, which are swollen with the monomer and oligomer chains. The second involves the particles growing by accumulation on the surface of polymers formed by solution polymerization [181, 182].

As an example, acetate butyrate cellulose-stabilized and dibenzoyl peroxide-initiated dispersion polymerization of HEMA in toluene/2-methylpropan-1-ol mixture in the presence of iron oxide needles (*ca.* 100×500 nm) or cubes produced 1 – 2 μm magnetic microspheres [183]. To obtain crosslinked microspheres, ethylene dimethacrylate (EDMA) was added 2 h after the start of the polymerization (Fig. 5c). Similar microspheres were prepared by the dispersion polymerization of GMA using AIBN as an initiator and poly(vinyl pyrrolidone) (PVP) stabilizer in an alcohol/water medium in the presence of iron oxide needles [184]. The amount of iron found in the microspheres was typically 12 – 15 wt.%.

3 Applications of magnetic particles in separations

Magnetic particles permit manipulation and *in vitro* separation of selected target species in the presence of other suspended solids. The isolated or purified species include simple inorganic compounds and biomolecules, such as antibodies, peptides, nucleic acids, enzymes, and even cells, bacteria, and viruses. It is thus possible to separate them directly from process liquors or complex biological mixtures, like fermentation broth, cell disruptates, blood or plasma, tissues, foodstuffs, whey, soil, or from water of different sources. Magnetic separations eliminate pretreatment, such as centrifugation, or filtration. The separations are fast, gentle, and scalable, easily automated and can be used in situations, in which other techniques are impossible or impractical to perform. With the exception of wastewater treatment, they are, however, employed mostly only on laboratory scale.

3.1 Ion exchange separations

Ion exchange-based separations on a magnetic support were already developed years ago, tested on pilot-plant scale and finally used successfully on production scale. Microparticles with weakly acidic (COOH), weakly (NH_2) and strongly basic groups ($N^+(CH_3)_3$) found applications in water treatment providing drinking water supplies from low quality resources, sewage treatment, and purification of industrial wastewaters [185 – 188]. Magnetic supports carrying carboxylic groups were obtained by Ce(IV)-initiated grafting of acrylic acid to magnetite coated with crosslinked PVA [189, 190]. Both batch and continuous procedures were developed for desalting brackish water, or the treatment of industrial and household wastewater. The magnetic support with carboxylate groups in Na form found applications in removal of nickel from electroplating rinse water. A weakly basic

magnetic exchanger was able to decolorize the pulp mill eluent [191]. The magnetic ion exchanger with quaternary ammonium groups removed particulates as well as dissolved compounds from water [192]. A strongly basic magnetic ion exchanger effectively removed negatively charged colloid turbidity and dyes in one-step coagulation process [192]. A cost-effective process was developed for a continuous removal of dissolved organic compounds from natural organic materials (NOM) [193]. In 1995, MIEX® magnetic ion exchangers were introduced for the removal of NOM from ambient raw water (http://www.environmental-expert.com/technology/orica/ScaleupAUSAWAFC97.pdf), which was superior to the standard coagulation process [194 – 197]. NOM are undesirable in water resources because they react with chlorine and other organochlorine compounds forming trihalomethanes which are harmful to health and deteriorate the taste of water. Pretreatment of water with MIEX ozonization and disinfection resin significantly reduced the content of the dissolved organic compound and bromide ions [198]. MIEX can remove a majority of hydrophilic and significant amounts of hydrophobic compounds from the biologically treated wastewater before using the membrane system [199]. Magnetic ion exchangers also found applications in the isolation of enzymes and other proteins. By combining the cation and anion exchange, bovine whey proteins were fractionated and purified [200, 201]. Basic proteins adsorbed first on a cation exchanger (quantitatively lactoferin and lactoperoxidase, and some immunoglobulins). Then, they were partly separated by desorption with increase in the concentration of NaCl in elution buffer. The anion exchanger bound serum albumin and selectively β-lactoglobulin. Lysozyme was also adsorbed on a cation exchanger [201]. Magnetic (diethylaminoethyl)agarose (DEAE-Magarose®) effectively bound DNA from crude cell lysates [1, 202].

Magnetic chelating ion exchangers, such as a methacrylate-based sorbent with immobilized ethylenediamine, effectively adsorbed toxic cations in the order, Cu(II) > Pb(II) > Cd(II) > Hg(II), under competition [203]. Sorption of Pb(II) was investigated on hexamethylenediamine analog [204]. Magnetic chelating resins found broad applications in IMAC. If they contained chelates of transition metal ions such as Ni(II), Co(II), Zn(II), Ni(II), Fe(III), they bound proteins possessing affinity to metal ions *via* the ligand. IMAC provided a mild and rapid prepurification step in HPLC [205]. A new adsorptive capture technique, termed "high gradient magnetic fishing" (HGMF), was developed for the isolation of hexahistidine-tagged L1 coat protein of human papillomavirus type 16 on two types of silanized metal chelator particles derivatized with IDA [206]. The particles were micrometer sized, superparamagnetic, and nonporous. Protein isolation from extracts of *E. coli* lysate was demonstrated on the magnetic agarose adsorbent with bound iminodiacetic groups in the Cu(II) or Zn(II) form [207]. A methacrylate sorbent with IDA ligand and chelated Ni(II) or Fe(III) specifically bound human immunoglobulins, porcin pepsin and other phosphoproteins. Magnetite nanoparticles coated with silica with IDA groups in the Zn(II) form separated bovine hemoglobin and BSA [208]. A porous methacrylate sorbent with cysteine groupings in the Fe(III) form specifically bound ferritin [209] and catalase [210]. Analogous adsorbents with bound histidin in the Fe(III) form or glutamic acid in the Cu(II) form adsorbed catalase [211] or cytochrome C [212], respectively. Cytochrome C adsorbed also on a magnetic methacrylate support with polyethylenimine in the Cu(II) form [213]. Magnetic alginate support with immobilized Cu(II) had specificity for bovine hemoglobin [214].

3.2 Separations based on affinity interactions

Affinity chromatography is a method of choice for the separation of biochemical mixtures, based on biological interactions of two complementary components, differing in types of specificity, such as between antibody and antigen/virus/cell, lectin and polysaccharide/glycoprotein/cell surface receptor/cell, nucleic acid and complementary base sequence/histone/nucleic acid polymerase, biotin and avidin/streptavidin, *etc*. Out of the plethora of applications described for column affinity chromatography, the most important interactions were realized also on magnetic supports.

3.2.1 Isolation of enzymes and other proteins

Affinity separations and purifications of proteins and peptides on magnetic particles were recently reviewed [215 – 217]. Briefly, they include magnetic dye-ligand chromatography, magnetic supports with chelates of transition metals and affinity ligands for the isolation of complementary substances. Magnetic supports with reactive dyes, *e.g.*, Cibachrom Blue F3GA, or Procion Red 120, were used as group-selective ligands for the isolation and purification of lysozyme [218], albumin, alcohol dehydrogenase [218], and lactate dehydrogenase [219]. Magnetic supports with chelates of transition metals (IMAC – see Section 3.1) found widespread applications in the purification of cytochrome C, uricase, hemoglobin, *etc.* Magnetic alginate microparticles (crosslinked with Ca(II)) were used for specific purification of amylases [220]. Finally, typical affinity ligands for the isolation of complementary substances include bound protein A or G for the separation of immunoglobulins [221], and bound streptavidin for the isolation of biotinylated proteins. Other examples are monoclonal antibodies (mAb) for interferon [222], or soybean trypsin inhibitor and benzamidine for the separation of trypsin [223]. Affinity interactions can be used also for the detoxifica-

tion of biological fluids [224, 225]. Tumor necrosis factor α and interleukin were thus adsorbed on the magnetic support with the corresponding monoclonal or polyclonal antibody [226, 227].

3.2.2 Separations of nucleic acids

Selective separation of DNA and RNA is an important tool in clinical diagnostics of microorganisms and viruses, genomic profiling, gene manipulation, *etc.* The separation is commonly performed using functionalized magnetic supports [228], many of which are commercially available. The separation of a nucleic acid is always an integral part of a multistep identification procedure. It often precedes or follows PCR which is known as a specific and sensitive method for the direct identification of microorganisms. Two basic principles are used for the separation of target nucleic acid from a mixture. The magnetic support is functionalized with streptavidin, or with a short oligonucleotide [229 – 231]. While in the first method the target nucleic acid or oligonucleotide is modified with biotin, in the other one the target complementary nucleic acid or oligonucleotide is bound by hybridization. The target nucleic acid can be separated either by capturing on the solid phase (sequence or hybridization capture) or by retaining the background on the solid phase (substractive hybridization) [232]. Originally, both approaches were multistep ones. Selective capture, however, was also attempted in a single hybridization step directly on the solid phase. The application of nested primers reduced the occurrence of false results caused by the presence of extracellular inhibitors in the samples. Such a combination of PCR and immunomagnetic separation (IMS) reduced the identification time of diagnostically important genes for a target organism and increased both the specificity and sensitivity of the method. The magnetic capture hybridization PCR (MCH-PCR) took advantage of the capture probe to separate DNA template for the detection of pathogens, such as *Escherichia coli*, *Bacillus cereus* and *B. thuringiensis*, *Mycobacterium paratuberculosis*, or *Staphylococcus* from food and other sources by DNA hybridization and biotin – streptavidin-based magnetic separation. The effect of inhibitors present in the samples on PCR amplification was thus eliminated [233, 234]. Similarly, false negative results could be avoided by the isolation of lactic acid bacteria DNA in the presence of PEG and sodium chloride on magnetic poly(HEMA-*co*-GMA) (P(HEMA-*co*-GMA)) microspheres containing carboxyl groups [235]. Microbial DNA was isolated from different probiotic dairy products, such as cheese, yoghurt, and fermented milk products, or from *Trichophyton* fungi [236] and Baikal sediments [237]; finally, it was checked by PCR. The PCR amplicons were used also as templates in the robot-assisted DNA sequencing. The biotin-labeled amplicons from the target genes were bound to streptavidin-modified magnetic support and then made single-stranded by denaturing with NaOH or heat. The support-bound and free dissolved strands were magnetically separated and recovered for sequencing [238].

3.2.3 Cell separation and detection

A variety of magnetic cell separation methods have been described for the isolation of cells already in the 1990′ [44, 46, 239, 240]. The magnetic cell separation is beneficial in terms of the direct isolation of target cells from crude biological samples, such as blood, bone marrow, stool, food, water, soil, *etc.* The sheer forces associated with the separation are minimal compared with centrifugation or filtration, the isolated cells are pure, viable and unaltered, and automation is possible. It is easy to separate magnetic cells, such as erythrocytes and magnetotactic bacteria. Nonmagnetic cells have to be magnetically labeled with magnetic particles *via* affinity ligands, typically antibodies against specific cell surface epitopes. Magnetic labels do not need to be detached from target microbial cells since the attachment to immunomagnetic beads has no effect on their growth and cells continue to multiply. Magnetically labeled cells can be directly used for cultivation or the cells can be disrupted and analyzed. Magnetic separation of the cells is performed in two modes, either direct or indirect. In the direct method, an affinity ligand-coupled magnetic particle binds the cells forming a stable magnetic conjugate. In the indirect method, the cells sensitized with a primary affinity ligand are first incubated with a primary antibody against the target structure and the formed conjugate is then captured by an appropriate affinity magnetic support with an immobilized secondary antibody. The support can be functionalized with protein A or protein G which bind the antibody of the conjugate. If the antibody in the first step is biotinylated, the magnetic support contains bound streptavidin (or avidin). The indirect technique is the method of choice if a cocktail of mAb is used. Alternatively, the target cells are isolated by the depletion of the unwanted cells, the advantage of which is that the target cells remain unlabeled in the separation process [239]. Another classification of magnetic cell separation includes negative or positive selection. While in the former case, all unwanted cell types are removed from the sample, in the latter the target cells are isolated from the cell suspension. The immunomagnetic cell separation is mostly based on the antigen – antibody interaction, where an antibody is coupled to the magnetic microparticles usually by a covalent bond or adsorption *via* amino, carboxyl, hydroxy, tosyl, hydrazide groups of the carrier, possibly with streptavidin and protein A or G. IMSs found applications especially in food, clinical, veterinary, and environmental microbiology for the detection of pathogenic microorganisms. Examples include numerous separations and

Table 1. Examples of some commercial magnetic particles

Product	Company	Note
Adembeads	Ademtech, Pessac, France http://www.ademtech.com	200, 300, 500 nm; amine, carboxylic acid, streptavidin, protein A and G, histidine, antibodies
Combidex, Feridex	Advanced Magnetics, Cambridge, USA http://www.advancedmagnetics.com	>8 – 10 nm
AGOWA® mag Particles	Agowa, Berlin, Germany http://www.agowa.de	>53 μm
BioMag®	Bangs Laboratories, Fishers, USA, http://www.bangslabs.com	Monodisperse 3 – 12 μm PS particles; amine, carboxylic acid, biotin, proteins A and G, streptavidin, antibodies
BcMag®	Bioclone, San Diego, USA http://www.bioclon.com	1 or 5 μm silica particles; amine, carboxylic acid, aldehyde, epoxy, hydrazide, IDA
M-PVA Magnetic Beads	Chemagen Biopolymer Technology, Baesweiler, Germany http://www.chemagen.de	2 μm PVA particles; amine, carboxylic acid, aldehyde, epoxy, streptravidin
fluidMAG	Chemicell, Berlin, Germany http://www.chemicell.com	0.5 – 1 μm silica particles; amine, carboxylic acid, cyanuric, OH, hydrazide, carbodiimides, protein A, G
MagaPhase®	Cortex Biochem, San Leandro, USA www.cortex-biochem.com	Cellulose, acrolein, polyacrylamide; amine, carboxylic acid, OH, aldehyde
Dynabeads®	Invitrogen, Carlsbad, USA http://www.invitrogen.com	Amine, carboxylic acid, epoxy, tosyl, streptavidin, protein A and G, antibodies
MagSi	MagnaMedics, Aachen, Germany http://www.magnamedics.com	Monodisperse 150 nm – 20 μm silica, gelatin; amine, carboxylic acid, C18, sulfo, aldehyde, thiol, streptavidin, protein A, G, fluorescent
MagSense	MagSense Life Sciences, West Lafayette, USA http://www.magsenselifesci.com	1 μm carboxylic acid
Estapor®	Merck, Fontenay, France http://www.estapor.com	Monodisperse 700 nm – 2 μm PS particles; amine, carboxylic acid, OH
Nanomag, Micromer®	Micromod Partikeltechnologie, Rostock, Germany http://www.micromod.de	Monodisperse 250 nm – 12 μm silica particles; amine, carboxylic acid, thiol, epoxy, avidin, biotin, albumin, streptavidin, protein A, antibodies
MicroBeads®	Miltenyi Biotec, Bergisch Gladbach, Germany http://www.miltenyibiotec.com	50 nm antibodies
SupraMag®	PolyMicrospheres, Indianapolis, USA http://www.polymicrospheres.com	Monodisperse 0.2 – 500 μm PS particles; amine, thiol, chloromethyl, OH
Sera-Mag®	Seradyn, Indianapolis, USA http://www.seradyn.com	1 μm PS particles; amine, carboxylic acid, thiol, epoxy, biotin, albumin, streptavidin
SPHERO®	Spherotech, Lake Forest, USA http://www.spherotech.com	Monodisperse 1 – 20 μm PS particles; amine, carboxylic acid, epoxy, biotin, avidin, protein G, antibodies

For details, see http://www.magneticmicrosphere.com/suppliers/magnetic_microspheres.php and the manufacturers' web sites.

subsequent determinations of microbial pathogens, such as *E. coli*, *Salmonella enteritidis*, *Staphylococcus aureus*, and *Listeria monocytogenes* in foodstuffs [241 – 243]. Commercial magnetic particles are available for the detection of most important microbial pathogens (see Table 1; *e.g.*, anti-*Salmonella* magnetic particles, (http://www.invitro-

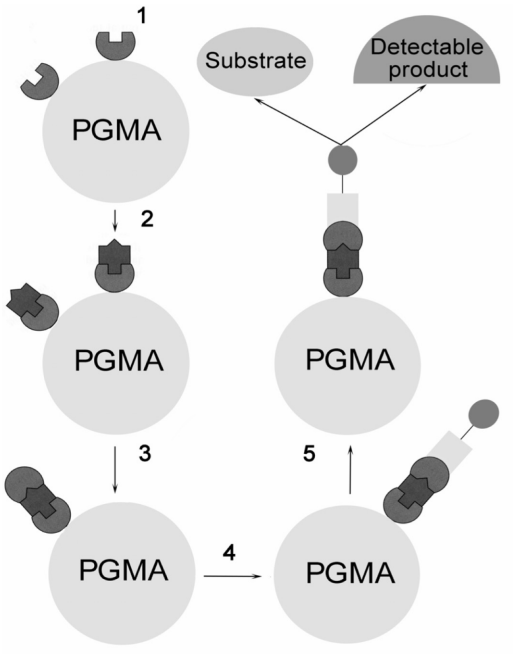

Figure 6. Sandwich enzyme immunoassay. First step: covalent attachment of antibody (IgG) to the magnetic PGMA microspheres, saturation of the solid phase surface with BSA; second step: incubation with the sample; third step: addition of the second antibody (IgY); fourth step: addition of the anti-IgY antibody–enzyme complex; fifth step: addition of enzyme substrate, removal of microspheres and absorbance measurement.

gen.com/content.cfm?pageid=11049). The IMS is often associated with the PCR (IMS-PCR) to identify target cells in processed foods, where extracellular inhibitors are present. The method successfully and quickly identifies nontypical *Salmonella* strains isolated from the human stool and rabbit meat [244]. Magnetic hydrophilic microspheres, based, *e.g.*, on P(HEMA-*co*-EDMA) functionalized with polyclonal *Salmonella* antibodies [245] are preferred for IMS of *Salmonella* cells to hydrophobic ones. IMS of cells thus solved problems associated with false negative PCR results caused by PCR inhibitors present in processed food products, *e.g.*, milk powder and dried eggs. IMS cannot, however, eliminate intracellular PCR inhibitors in *Salmonella* cells isolated from field samples. Magnetically captured cells can also be detected by ELISA. As an example, sandwich ELISA for the detection of *Campylobacter jejuni* in food or clinical and environmental samples using magnetic poly(GMA) (PGMA) microspheres with an immobilized antibody is shown in Fig. 6 [246]. Compared with conventional microbiological separation methods, which take approximately 5 days and are laborious and time consuming, both the number of washing steps and overall time for the *Campylobacter* detection are substantially reduced. Magnetic particles are used also for the isolation and detection of parasites, *e.g.*, *Cryptosporidium* in water. In biomedicine, removal of cancer cells from the bone marrow is probably the most important application of the IMS. Together with the isolation of a plethora of other human cell subsets from the blood, this is, however, beyond the scope of this review.

3.3 Other separations

Iron oxides and ferrites interact with many compounds including proteins, higher carboxylic acids, chelating agents, *etc.*, which seriously impedes the majority of their biological applications. Iron oxide particles have to be therefore properly coated or embedded in polymer microspheres. The adsorption ability of magnetic oxides, however, can be utilized not only for coating, but also for the convenient removal of strongly interacting compounds from water media. Magnetic hydrated iron oxide embedded in a macroporous ion exchanger is thus effective in the removal of As(III) and As(V) traces [247] or heavy metal ions, like Zn(II) and Cu(II) from water [248]. The azo dye Acid Red B was effectively removed by adsorption on Cu or Mn ferrite ($CuFe_2O_4$ or $MnFe_2O_4$) [249, 250]. Also catalytic properties are closely related to the sorption ability of magnetite, maghemite, and Cu, Mn, Co ferrites. They catalyze the decomposition of hydrogen peroxide providing highly reactive hydroxyl radicals which can be utilized for the decolorization of wastewaters containing synthetic dyes or polycyclic aromatic hydrocarbons [251].

3.4 Immobilized enzymes and nucleic acids

Immobilization of enzymes on magnetic nanoparticles imparts them potentially unique properties. In contrast to micrometer-sized particles, a highly specific surface area of the nanoparticles facilitates the immobilization of a larger amount of enzyme, which is accompanied by an increased specific enzyme activity. The easy dispersibility of the nanoparticles also enables smooth contact with the substrate alleviating mass-transfer limitations. This lowers the detection limit and speeds up the analysis time [252]. Like in conventional polymer supports, various enzymes were immobilized *via* chemical bonds on coated or embedded magnetic nanoparticles. The enzymes include glucoamylase [253], cytochrome c oxidase [254], β-lactamase [255], chymotrypsin [256–258], alcohol dehydrogenase [259, 260], glucose oxidase, galactose oxidase, urease [261], neuramidinase [262, 263], papain [264], DNase [265], RNase [266], *etc.* Enzymes immobilized on magnetic supports generally have higher thermal and storage stability facilitating repeated applications, but lower activity than free enzymes in solution. Trypsin-immobilized magnetic polymer particles smaller than 1 μm can digest proteins in microchip (μ-chip) protease microreactor. This helps to elucidate pri-

mary structure of the proteins and their post-translation modification. A unique fingerprint for each protein called a "peptide map" can thus be obtained. Digestion in μ-chip immobilized magnetic enzyme reactor (IMER) using magnetic nano- and microparticles is a preferable alternative to the conventional batch mode for numerous large globular and highly glycosylated proteins [267]. On-line connection with mass spectrometer opens the route to automated, high-throughput proteomic devices, which significantly simplifies proteomic analysis protocols without compromising the quality and specificity of analysis.

4 Conclusions

Functionalized magnetic nano- and microparticles have evolved into a powerful instrument for separation, diagnostics, catalytic, and many other systems employed, *e.g.*, in chemistry, biochemistry, biology, environment protection, *etc*. In the first part of this review, various procedures for preparation, characterization, coating, or embedding of magnetic materials, including their functionalization, have been summarized. The materials differ both in the type and the size. The applications of the particles are presented in the second part of the review. They are limited only to the applications assisted with separations/isolations and catalytic effects of both the unmodified and modified magnetic particles. Other important applications, such as MRI, drug targeting, hyperthermia, diagnostic, *etc*., could not be described. Some directions discussed in the review are already established and belong to a standard laboratory practice, other new analytical procedures and IMSs are permanently appearing especially on the laboratory scale. Together with improvements in the design of new sophisticated methods for magnetic particle preparation and characterization, quite new separation strategies can be foreseen. Besides the amenability of magnetic separations to automation and miniaturization, the isolations on large industrial scale will undoubtedly continue to grow in the near future as well. Magnetic isolations can be targeted to high value-added compounds present in low concentrations in various raw materials. The limiting factors are the cost of magnetic separation media and availability of effective magnetic separators.

Financial support of the Ministry of Education, Youth and Sports of the Czech Republic (grant 2B06053), Academy of Sciences of the Czech Republic (grant KAN200200651) and Grant Agency of the Czech Republic (grant 525/05/0311) is gratefully acknowledged.

5 References

[1] Levison, P. R., Badger, S. E., Dennis, J., Hathi, P., *et al.*, *J. Chromatogr. A* 1998, *816*, 107 – 111.
[2] Hafeli, U., Schutt, W., Teller, J., Zborowski, M. (Eds.), *Scientific and Clinical Applications of Magnetic Carriers*, Kluwer Academic Publishers, New York 1997.
[3] Taupitz, M., Schmitz, S., Hamm, B., *Rofo-Fortschr. Rontg.* 2003, *175*, 752 – 765.
[4] Gupta, A. K., Gupta, M., *Biomaterials* 2005, *26*, 3995 – 4021.
[5] Hafeli, U. O., *Int. J. Pharm.* 2004, *277*, 19 – 24.
[6] Mornet, S., Vasseur, S., Grasset, F., Duguet, E., *J. Mater. Chem.* 2004, *14*, 2161 – 2175.
[7] Schillinger, U., Brill, T., Rudolph, C., Huth, S., *et al.*, *J. Magn. Magn. Mater.* 2005, *293*, 501 – 508.
[8] Craik, D. J., *Magnetic Oxides*, John Wiley&Sons, London 1975.
[9] Pelizzetti, E. (Ed.), *Fine Particles Science and Technology: From Micro to Nanoparticles*, Springer, London 1996.
[10] Berkovsky, B. M., (Ed.), *Magnetic Fluids and Applications Handbook*, Begell House Publishers, New York 1996.
[11] Arshady, R., *Radiolabeled and Magnetic Particulates in Medicine & Biology*, Citus Books, London 2001.
[12] Berkovsky, B. M., Krakov, M. S., Medvedev, V. F., *Magnetic Fluids: Engineering Applications*, Oxford University Press, New York 1993.
[13] Blums, E. S., Cebers, A. O., Maiorov, M. M., *Magnetic Fluids*, Walter de Gruyter, Berlin 1997.
[14] Halbreich, A., Roger, J., Pons, J. N., Da Silva, M. F., *et al.*, in: Arshady, R. (Ed.), *Radiolabeled and Magnetic Particulates in Medicine & Biology*, Citus Books, London 2001, pp. 459 – 493.
[15] Liberti, P. A., Charappa, J. N., Hovsepian, A. C., Rao, C. G., Pelizzetti, E., in: Pelizzetti, E. (Ed.), *Fine Particle Science and Technology: From Micro to Nanoparticles*, Kluwer Academic Publishers, Dordrecht 1996, pp. 777 – 790.
[16] Morales, M. P., Ocana, M., Gonzales-Carreno, T., Serna, C. J., Pelizzetti, E., in: Pelizzetti, E. (Ed.), *Fine Particle Science and Technology: From Micro to Nanoparticles* Kluwer Academic Publishers, Dordrecht 1996, pp. 197 – 208.
[17] Pouliquen, D., Arshady, R., in: Arshady, R. (Ed.), *Radiolabeled and Magnetic Particulates in Medicine & Biology*, Citus Books, London 2001, pp. 430 – 457.
[18] Pouliquen, D., Arshady, R., in: Arshady, R. (Ed.), *Radiolabeled and Magnetic Particulates in Medicine & Biology*, Citus Books, London 2001, pp. 495 – 523.
[19] Šafařík, I., Šafaříková, M., in: Wilson, I. D., Adlard, T. R., Poole, C. F., Cool, M. (Eds.), *Encyclopedia of Separation Science*, Academic Press, London 2000, pp. 2163 – 2170.
[20] Šafařík, I., Šafaříková, M., in: Wilson, I. D., Adlard, T. R., Poole, C. F., Cool, M. (Eds.), *Encyclopedia of Separation Science*, Academic Press, London 2000, pp. 2260 – 2267.
[21] Allen, M. J., Meade, T. J., *Met. Ions Biol. Syst.* 2004, *42*, 1 – 38.
[22] Anzai, Y., Prince, M. R., *J. Magn. Reson. Imaging* 1997, *7*, 75 – 81.
[23] Bahadur, D., Giri, J., *Sadhana-Acad. Proc. Eng. Sci.* 2003, *28*, 639 – 656.
[24] Berry, C. C., Curtis, A. S. G., *J. Phys. D Appl. Phys.* 2003, *36*, R198 – R206.
[25] Blankenberg, F. G., *J. Cell. Biochem.* 2003, *90*, 443 – 453.
[26] Brasch, R. C., *Radiology* 1992, *183*, 1 – 11.
[27] Brigger, I., Dubernet, C., Couvreur, P., *Adv. Drug Deliv. Rev.* 2002, *54*, 631 – 651.
[28] Bulte, J. W. M., Kraitchman, D. L., *NMR Biomed.* 2004, *17*, 484 – 499.
[29] Frank, J. A., Anderson, S. A., Kalsih, H., Jordan, E. K., *et al.*, *Cytotherapy* 2004, *6*, 621 – 625.
[30] Gabrielsen, O. S., Huet, J., *Methods Enzymol.* 1993, *218*, 508 – 525.
[31] Haukanes, B. I., Kvam, C., *Biotechnology* 1993, *11*, 60 – 63.
[32] Huke, B., Lucke, M., *Rep. Prog. Phys.* 2004, *67*, 1731 – 1768.
[33] Hyeon, T., *Chem. Commun.* 2003, 927 – 934.
[34] Jolivet, J. P., Tronc, E., Chaneac, C., *C. R. Chim.* 2002, *5*, 659 – 664.
[35] Kemshead, J. T., Ugelstad, J., *Mol. Cell. Biochem.* 1985, *67*, 11 – 18.

[36] Kemshead, J. T., Gibson, F., *Pharm. Int.* 1985, *6*, 153 – 157.
[37] Mainardes, R. M., Silva, L. P., *Curr. Drug Targets* 2004, *5*, 449 – 455.
[38] Meade, T. J., Taylor, A. K., Bull, S. R., *Curr. Opin. Neurobiol.* 2003, *13*, 597 – 602.
[39] Moroz, P., Jones, S. K., Gray, B. N., *Int. J. Hyperthermia* 2002, *18*, 267 – 284.
[40] Muller-Schulte, D., *Magn. Electr. Sep.* 2000, *10*, 141 – 159.
[41] Neuberger, T., Schopf, B., Hofmann, H., Hofmann, M., von Rechenberg, B., *J. Magn. Magn. Mater.* 2005, *293*, 483 – 496.
[42] Pankhurst, Q. A., Connolly, J., Jones, S. K., Dobson, J., *J. Phys. D Appl. Phys.* 2003, *36*, R167 – R181.
[43] Parker, D. L., Tsuruda, J. S., Goodrich, K. C., Alexander, A. L., Buswell, H. R., *Invest. Radiol.* 1998, *33*, 560 – 572.
[44] Šafařík, I., Šafaříková, M., *J. Chromatogr. B* 1999, *722*, 33 – 53.
[45] Šafařík, I., Šafaříková, M., *Monatsh. Chem.* 2002, *133*, 737 – 759.
[46] Šafařík, I., Šafaříková, M., Forsythe, S. J., *J. Appl. Bacteriol.* 1995, *78*, 575 – 585.
[47] Šafaříková, M., Šafařík, I., *Magn. Electr. Sep.* 2001, *10*, 223 – 252.
[48] Setchell, C. H., *J. Chem. Technol. Biotechnol. B* 1985, *35*, 175 – 182.
[49] Shinkai, M., *J. Biosci. Bioeng.* 2002, *94*, 606 – 613.
[50] Tanimoto, A., in: Arshady, R. (Ed.), *Radiolabeled and Magnetic Particulates in Medicine & Biology, MML Series Vol. 3*, Citus Books, London 2001, pp. 525 – 558.
[51] Willard, M. A., Kurihara, L. K., Carpenter, E. E., Calvin, S., Harris, V. G., *Int. Mater. Rev.* 2004, *49*, 125 – 170.
[52] Vatta, L. L., Sanderson, R. D., Koch, K. R., *Pure Appl. Chem.* 2006, *78*, 1793 – 1801.
[53] Wichterle, O., Lim, D., *Nature* 1960, *185*, 117 – 118.
[54] Zeng, H., Zheng, M., Skomski, R., Sellmyer, D. J., *et al.*, *J. Appl. Phys.* 2000, *87*, 4718 – 4720.
[55] Burke, N. A. D., Stover, H. D. H., Dawson, F. P., *Chem. Mater.* 2002, *14*, 4752 – 4761.
[56] Moumen, N., Lisiecki, I., Pileni, M. P., Briois, V., *Supramol. Sci.* 1995, *2*, 161 – 168.
[57] Bui, Q. T., Pankhurst, Q. A., Zulqarnain, K., *IEEE Trans. Magn.* 1998, *34*, 2117 – 2119.
[58] Jeong, U., Teng, X., Wang, Y., Yang, H., Y., X., *Adv. Mater.* 2007, *19*, 33 – 60.
[59] Cornell, R. M., Schwertmann, U., *The Iron Oxides: Structure, Properties, Reactions, Occurence and Uses*, VCH Publishers, Weinheim 1997.
[60] US Patent 5,928,958, 1999.
[61] Bee, A., Massart, R., Neveu, S., *J. Magn. Magn. Mater.* 1995, *149*, 6 – 9.
[62] Carpenter, E. E., Long, J. W., Rolison, D. R., Logan, M. S., *et al.*, *J. Appl. Phys.* 2006, *99*, 3.
[63] US Patent 3,215,572, 1965.
[64] Massart, R., *C. R. Hebd. Seances. Acad. Sci., Paris C* 1980, *291*, 1 – 3.
[65] Zaitsev, V. M., Shliomis, M. I., *Dokl. Akad. Nauk SSSR* 1969, *188*, 1261.
[66] Jolivet, J. P., Massart, R., Fruchart, J. M., *Nouv. J. Chim.* 1983, *7*, 325 – 331.
[67] Massart, R., *IEEE Trans. Magn.* 1981, *17*, 1247 – 1248.
[68] Bacri, J. C., Perzynski, R., Salin, D., Cabuil, V., Massart, R., *J. Magn. Magn. Mater.* 1986, *62*, 36 – 46.
[69] Rocchiccioli-Deltcheff, C., Franck, R., Cabuil, V., Massart, R., *J. Chem. Res. Synop.* 1987, 126 – 129.
[70] WO Patent 9,505,669A1, 1995.
[71] US Patent 5,248,492, 1993.
[72] Shafi, K. V. P. M., Ulman, A., Yan, X. Z., Yang, N. L., *et al.*, *Langmuir* 2001, *17*, 5093 – 5097.
[73] DE Patent 19,624,426 A1, 1988.
[74] Jiang, W. Q., Yang, H. C., Yang, S. Y., Horng, H. E., *et al.*, *J. Magn. Magn. Mater.* 2004, *283*, 210 – 214.
[75] US Patent 5,698,271, 1997.
[76] US Patent 4,452,773, 1984.
[77] Kawaguchi, T., Hasegawa, M., *J. Mater. Sci. Mater. Med.* 2000, *11*, 31 – 35.
[78] Pardoe, H., Chua-Anusorn, W., St. Pierre, T. G., Dobson, J., *J. Magn. Magn. Mater.* 2001, *225*, 41 – 46.
[79] Chastellain, A., Petri, A., Hofmann, H., *J. Colloid Interface Sci.* 2004, *278*, 353 – 360.
[80] Qiu, X., Winnik, F., *Chin. J. Polym. Sci.* 2000, *18*, 535 – 539.
[81] Lin, H., Watanabe, Y., Kimura, M., Hanabusa, K., Shirai, H., *J. Appl. Polym. Sci.* 2003, *87*, 1239 – 1247.
[82] Xue, B., Tong, X. D., Sun, Y., *Sep. Sci. Technol.* 2001, *36*, 2449 – 2461.
[83] Hofmann, H., Petri-Fink, A., Steitz, B., von Rechenberg, B. *et al.*, in: Laudon, M., Romanowicz, B. (Eds.), *NSTI Nanotech*, Cambridge 2005.
[84] Kumar, R. V., Koltypin, Y., Cohen, Y. S., Cohen, Y., *et al.*, *J. Mater. Chem.* 2000, *10*, 1125 – 1129.
[85] Zhang, Y., Kohler, N., Zhang, M. Q., *Biomaterials* 2002, *23*, 1553 – 1561.
[86] Dumazet-Bonnamour, I., Le Perchec, P., *Colloids Surf. A* 2000, *173*, 61 – 71.
[87] Jordan, A., Scholz, R., Wust, P., Schirra, H., *et al.*, *J. Magn. Magn. Mater.* 1999, *194*, 185 – 196.
[88] Brusentsov, N. A., Nikitin, L. V., Brusentsova, T. N., Kuznetsov, A. A. *et al.*, *J. Magn. Magn. Mater.* 2002, *252*, 378 – 380.
[89] Kuznetsov, V. D., Brusentsova, T. N., Brusentsov, N. A., Nikiforov, V. N., Danilkin, M. I., *Russ. Phys. J.* 2005, *48*, 156 – 162.
[90] Jordan, A., Scholz, R., Maier-Hauff, K., van Landeghem, F. K. H., *et al.*, *J. Neurooncol.* 2006, *78*, 7 – 14.
[91] Butterworth, M. D., Illum, L., Davis, S. S., *Colloids Surf. A* 2001, *179*, 93 – 102.
[92] Tamura, H., Matijevic, E., *J. Colloid Interface Sci.* 1982, *90*, 100 – 109.
[93] Regazzoni, A. E., Matijevic, E., *Colloids Surf.* 1983, *6*, 189 – 201.
[94] Sato, T., Iijima, T., Seki, M., Inagaki, N., *J. Magn. Magn. Mater.* 1987, *65*, 252 – 256.
[95] Schuele, W. J., Deetscreek, V. D., *J. Appl. Phys.* 1962, *33*, 1136 – 1140.
[96] Tirado, J. L., Thomas, J. M., Jefferson, D. A., Millward, G. R., Charles, S. W., *J. Chem. Soc. Chem. Commun.* 1987, 365 – 368.
[97] Vandenberghe, R. E., Vanleerberghe, R., Degrave, E., Robbrecht, G., *J. Magn. Magn. Mater.* 1980, *15*, 1117 – 1118.
[98] Tanaka, T., Tamagawa, N., *Jpn. J. Appl. Phys.* 1967, *6*, 1096 – 1100.
[99] Wolfe, R., North, J. C., *Appl. Phys. Lett.* 1974, *25*, 122 – 124.
[100] Gonzales, M., Krishnan, K. M., *J. Magn. Magn. Mater.* 2005, *293*, 265 – 270.
[101] Pei, W., Kumada, H., Natusme, T., Saito, H., Ishio, S., *J. Magn. Magn. Mater.* 2007, *310*, 2375 – 2377.
[102] Hyeon, T., Lee, S. S., Park, J., Chung, Y., Bin Na, H., *J. Am. Chem. Soc.* 2001, *123*, 12798 – 12801.
[103] Rockenberger, J., Scher, E. C., Alivisatos, A. P., *J. Am. Chem. Soc.* 1999, *121*, 11595 – 11596.
[104] Matijevic, E., in: Hench, L. L., Ulrich, D. R. (Eds.), *Science of Ceramic Chemical Processing*, Wiley, New York 1986, p. 463.
[105] Rozman, M., Drofenik, M., *J. Am. Ceram. Soc.* 1995, *78*, 2449 – 2455.
[106] Makovec, D., Drofenik, M., Znidarsic, A., *J. Am. Ceram. Soc.* 1999, *82*, 1113 – 1120.
[107] Inoue, M., Nishikawa, T., Inui, T., *J. Mater. Res.* 1998, *13*, 856 – 860.
[108] Wagener, M., Gunther, B., Blums, E., *J. Magn. Magn. Mater.* 1999, *201*, 18 – 22.

[109] Hyeon, T., Park, J., Joo, J., Kim, S. W., *Abstr. Pap. Am. Chem. Soc.* 2003, *225*, U437 – U437.

[110] Behrens, S., Bonnemann, H., Matoussevitch, N., Gorschinski, A., *et al.*, *J. Phys. Condens. Matter* 2006, *18*, S2543 – S2561.

[111] Sato, T., *IEEE Trans. Magn.* 1970, *6*, 795 – 799.

[112] Scholten, P. C., *IEEE Trans. Magn.* 1980, *16*, 221 – 225.

[113] Griffiths, C. H., Ohoro, M. P., Smith, T. W., *J. Appl. Phys.* 1979, *50*, 7108 – 7115.

[114] Linderoth, S., Balcells, L., Labarta, A., Tejada, J., *et al.*, *J. Magn. Magn. Mater.* 1993, *124*, 269 – 276.

[115] Nakatani, I., Hijikata, M., Ozawa, K., *J. Magn. Magn. Mater.* 1993, *122*, 10 – 14.

[116] Lee, H. S., Nakatani, I., *J. Magn. Magn. Mater.* 1999, *201*, 23 – 26.

[117] Blesa, M. A., Borghi, E. B., Maroto, A. J. G., Regazzoni, A. E., *J. Colloid Interface Sci.* 1984, *98*, 295 – 305.

[118] Fauconnier, N., Bee, A., Roger, J., Pons, J. N., *J. Mol. Liq.* 1999, *83*, 233 – 242.

[119] Portet, D., Denizot, B., Rump, E., Lejeune, J. J., Jallet, P., *J. Colloid Interface Sci.* 2001, *238*, 37 – 42.

[120] WO Patent 9,603,653A1, 1996.

[121] Beneš, M., Hrubý, M., Rittich, B., Španová, A., Czech Patent Appl. PV 2004-392.

[122] Fauconnier, N., Pons, J. N., Roger, J., Bee, A., *J. Colloid Interface Sci.* 1997, *194*, 427 – 433.

[123] Bruce, I. J., Sen, T., *Langmuir* 2005, *21*, 7029 – 7035.

[124] del Campo, A., Sen, T., Lellouche, J. P., Bruce, I. J., *J. Magn. Magn. Mater.* 2005, *293*, 33 – 40.

[125] Sen, T., van de Waterbeemd, M., Bruce, I. J., *6th International Conference on Scientific and Clinical Applications of Magnetic Carriers*, Krems, Austria 2006.

[126] Yamaura, M., Camilo, R. L., Sampaio, L. C., Macedo, M. A. *et al.*, *J. Magn. Magn. Mater.* 2004, *279*, 210 – 217.

[127] Mornet, S., Portier, J., Duguet, E., *J. Magn. Magn. Mater.* 2005, *293*, 127 – 134.

[128] US Patent 5,160,725, 1992.

[129] MataZamora, M. E., Arriola, H., Nava, N., Saniger, J. M., *J. Magn. Magn. Mater.* 1996, *161*, L6 – L10.

[130] Nesterova, M. V., Walton, S. A., Webb, J., *J. Inorg. Biochem.* 2000, *79*, 109 – 118.

[131] Huang, S. H., Liao, M. H., Chen, D. H., *Sep. Purif. Technol.* 2006, *51*, 113 – 117.

[132] Hasegawa, M., Hanaichi, T., Shoji, H., Kawaguchi, T., Maruno, S., *Jpn. J. Appl. Phys.* 1998, *37*, 1029 – 1032.

[133] Gansau, C., Buske, N., Gross, C., Weitschies, W., *Eur. Cell. Mater.* 2002, *20*, 158 – 159.

[134] US Patent 6,599,498, 2003.

[135] Schwalbe, M., Buske, N., Vetterlein, M., Hoffken, K., *et al.*, *Z. Phys. Chem.* 2006, *220*, 125 – 131.

[136] Beneš, M., Lenfeld, J., Španová, A., Rittich, B., Bílková, Z., Czech Patent Appl. PV 2004 – 391.

[137] Fuentes, M., Mateo, C., Rodriguez, A., Casqueiro, M., *et al.*, *Biosens. Bioelectron.* 2006, *21*, 1574 – 1580.

[138] Petri-Fink, A., Chastellain, M., Juillerat-Jeanneret, L., Ferrari, A., Hofmann, H., *Biomaterials* 2005, *26*, 2685 – 2694.

[139] Mohapatra, S., Pramanik, N., Ghosh, S. K., Pramanik, P., *J. Nanosci. Nanotechnol.* 2006, *6*, 823 – 829.

[140] Gelbrich, T., Feyen, M., Schmidt, A. M., *Macromolecules* 2006, *39*, 3469 – 3472.

[141] Chiang, C. L., Sung, C. S., *J. Magn. Magn. Mater.* 2006, *302*, 7 – 13.

[142] Matsuno, R., Yamamoto, K., Otsuka, H., Takahara, A., *Macromolecules* 2004, *37*, 2203 – 2209.

[143] Hu, F. X., Neoh, K. G., Cen, L., Kang, E. T., *Biomacromolecules* 2006, *7*, 809 – 816.

[144] Vestal, C. R., Zhang, Z. J., *J. Am. Chem. Soc.* 2002, *124*, 14312 – 14313.

[145] Gravano, S. M., Dumas, R., Liu, K., Patten, T. E., *J. Polym. Sci., Polym. Chem. Ed.* 2005, *43*, 3675 – 3688.

[146] Marutani, E., Yamamoto, S., Ninjbadgar, T., Tsujii, Y., *et al.*, *Polymer* 2004, *45*, 2231 – 2235.

[147] Wang, W. C., Neoh, K. G., Kang, E. T., *Macromol. Rapid Commun.* 2006, *27*, 1665 – 1669.

[148] Chatterje, J., Haik, Y., Chen, C. J., *Colloid Polym. Sci.* 2001, *279*, 1073 – 1081.

[149] Ren, J., Hong, H. Y., Ren, T. B., Teng, X. R., *React. Funct. Polym.* 2006, *66*, 944 – 951.

[150] Tanyolac, D., Ozdural, A. R., *React. Funct. Polym.* 2000, *43*, 279 – 286.

[151] Yang, H., Jiang, W., Lu, Y., *Mater. Lett.* 2007, *61*, 2789 – 2793.

[152] Sauzedde, F., Elaissari, A., Pichot, C., *Colloid Polym. Sci.* 1999, *277*, 1041 – 1050.

[153] Sauzedde, F., Elaissari, A., Pichot, C., *Colloid Polym. Sci.* 1999, *277*, 846 – 855.

[154] Lenfeld, J., *Angew. Makromol. Chem.* 1993, *212*, 147 – 155.

[155] Ma, Z. Y., Guan, Y. P., Liu, H. Z., *J. Magn. Magn. Mater.* 2006, *301*, 469 – 477.

[156] Ngomsik, A. F., Bee, A., Siaugue, J. M., Cabuil, V., Cote, G., *Water Res.* 2006, *40*, 1848 – 1856.

[157] Sahiner, N., *Colloid Polym. Sci.* 2006, *285*, 283 – 292.

[158] Furusawa, K., Nagashima, K., Anzai, C., *Colloid Polym. Sci.* 1994, *9*, 1104 – 1110.

[159] US Patent 4,774,265, 1988.

[160] Ugelstad, J., Berge, A., Ellingsen, T., Schmid, R., *et al.*, *Prog. Polym. Sci.* 1992, *17*, 87 – 161.

[161] Sidorov, S. N., Bronstein, L. M., Davankov, V. A., Tsyurupa, M. P. *et al.*, *Chem. Mater.* 1999, *11*, 3210 – 3215.

[162] Maria, L. C. D., Leite, M. C. A. M., Costa, M. A. S., Ribeiro, J. M. S. *et al.*, *Eur. Polym. J.* 2003, *39*, 843 – 846.

[163] Ma, Z. Y., Guan, Y. P., Liu, H. Z., *React. Funct. Polym.* 2006, *66*, 618 – 624.

[164] Wang, X. B., Ding, X. B., Zheng, Z. H., Hu, X. H., *et al.*, *Macromol. Rapid Commun.* 2006, *27*, 1180 – 1184.

[165] Muller-Schulte, D., Schmitz-Rode, T., *J. Magn. Magn. Mater.* 2006, *302*, 267 – 271.

[166] Elaissari, A., Sauzedde, F., Montagne, F., Pichot, C., in: Elaissari, A. (Ed.), *Colloidal Polymers: Synthesis and Characterization*, Marcel Dekker, New York 2003, pp. 285 – 317.

[167] Montagne, F., Mondain-Monval, O., Pichot, C., Elaissari, A., *J. Polym. Sci. A, Polym. Chem. Ed.* 2006, *44*, 2642 – 2656.

[168] Menager, C., Sandre, O., Mangili, J., Cabuil, V., *Polymer* 2004, *45*, 2475 – 2481.

[169] Wormuth, K., *J. Colloid Interface Sci.* 2001, *241*, 366 – 377.

[170] Horák, D., Chekina, N., *J. Appl. Polym. Sci.* 2006, *102*, 4348 – 4357.

[171] Xie, G., Zhang, Q. Y., Luo, Z. P., Wu, M., Li, T. H., *J. Appl. Polym. Sci.* 2003, *87*, 1733 – 1738.

[172] Larpent, C., in: Elaissari, A. (Ed.), *Colloidal Polymers: Synthesis and Characterization*, Marcel Dekker, New York 2003, pp. 145 – 187.

[173] Liu, Z. L., Yang, X. B., Yao, K. L., Du, G. H., Liu, Z. S., *J. Magn. Magn. Mater.* 2006, *302*, 529 – 535.

[174] Deng, Y., Wang, L., Yang, W., Fu, S., Elaissari, A., *J. Magn. Magn. Mater.* 2003, *257*, 69 – 78.

[175] Landfester, K., in: Elaissari, A. (Ed.), *Colloidal Polymers: Synthesis and Characterization*, Marcel Dekker, New York 2003, pp. 225 – 243.

[176] Ramirez, L. P., Landfester, K., *Macromol. Chem. Phys.* 2003, *204*, 22 – 31.

[177] Xu, Z. Z., Wang, C. C., Yang, W. L., Deng, Y. H., Fu, S. K., *J. Magn. Magn. Mater.* 2004, *277*, 136 – 143.

[178] Lin, C. L., Chiu, W. Y., Don, T. M., *J. Appl. Polym. Sci.* 2006, *100*, 3987 – 3996.

[179] Faridi-Majidi, R., Sharifi-Sanjani, N., Agend, F., *Thin Solid Films* 2006, *515*, 368 – 374.

[180] Barrett, K. E., *Dispersion Polymerization in Organic Media*, Wiley, Chichester 1975.

[181] US Patent 5,976,426, 1999.

[182] Li, X., Sun, Z., *J. Appl. Polym. Sci.* 1995, *58*, 1991 – 1997.

[183] Horák, D., Boháček, J., Šubrt, M., *J. Polym. Sci. A, Polym. Chem. Ed.* 2000, *38*, 1161 – 1171.

[184] Horák, D., *J. Polym. Sci. A, Polym. Chem. Ed.* 2001, *39*, 3707 – 3715.

[185] Bolto, B. A., Eldridge, R. J., Kotowski, M., Pawlowski, L., *et al.*, *React. Polym.* 1984, *2*, 223 – 231.

[186] Bolto, B. A., *Desalination* 1996, *106*, 137 – 143.

[187] Bolto, B. A., *Waste Manage* 1990, *10*, 11 – 21.

[188] Bolto, B. A., Swinton, E. A., Nadebaum, P. R., Murtagh, R. W., *Water Sci. Technol.* 1982, *14*, 523 – 534.

[189] Bolto, B. A., Dixon, D. R., Eldridge, R. J., *J. Appl. Polym. Sci.* 1978, *22*, 1977 – 1982.

[190] Clemence, L. J., Eldridge, R. J., Lydiate, J., *React. Polym.* 1984, *2*, 197 – 207.

[191] Bolto, B. A., Dixon, D. R., Swinton, E. A., Weiss, D. E., *J. Chem. Technol. Biotechnol.* 1979, *29*, 325 – 331.

[192] Anderson, N. J., Bolto, B. A., Eldridge, R. J., Kolarik, L. O., Swinton, E. A., *Water Res.* 1980, *14*, 967 – 973.

[193] Eldridge, R. J., *Rev. Chem. Eng.* 1995, *11*, 185 – 228.

[194] Singer, P. C., Bilyk, K., *Water Res.* 2002, *36*, 4009 – 4022.

[195] Boyer, T. H., Singer, P. C., *Water Res.* 2005, *39*, 1265 – 1276.

[196] Boyer, T. H., Singer, P. C., *Water Res.* 2006, *40*, 2865 – 2876.

[197] Shorrock, K., Drage, B., *Water Environ. J.* 2006, *20*, 65 – 70.

[198] Wert, E. C., Edwards-Brandt, J. C., Singer, P. C., Budd, G. C., *Ozone Sci. Eng.* 2005, *27*, 371 – 379.

[199] Zhang, R., Vigneswaran, S., Ngo, H. H., Nguyen, H., *Desalination* 2006, *192*, 296 – 302.

[200] Heeboll-Nielsen, A., Justesen, S. F. L., Thomas, O. R. T., *J. Biotechnol.* 2004, *113*, 247 – 262.

[201] Heeboll-Nielsen, A., Justesen, S. F. L., Hobley, T. J., Thomas, O. R. T., *Sep. Sci. Technol.* 2004, *39*, 2891 – 2914.

[202] Levison, P. R., Badger, S. E., Hathi, P., Davies, M. J., *et al.*, *J. Chromatogr. A* 1998, *827*, 337 – 344.

[203] Denizli, A., Ozkan, G., Arica, M. Y., *J. Appl. Polym. Sci.* 2000, *78*, 81 – 89.

[204] Denizli, A., Satiroglu, N., Patir, S., Bektas, S., Genc, O., *J. Macromol. Sci., Pure Appl. Chem.* 2000, *37*, 1647 – 1662.

[205] O'Brien, S. M., Thomas, O. R. T., Dunnill, P., *J. Biotechnol.* 1996, *50*, 13 – 25.

[206] Heeboll-Nielsen, A., Choe, W. S., Middelberg, A. P. J., Thomas, O. R. T., *Biotechnol. Prog.* 2003, *19*, 887 – 898.

[207] Abudiab, T., Beitle, R. R., *J. Chromatogr. A* 1998, *795*, 211 – 217.

[208] Ma, Z.-Y., Liu, X.-Q., Guan, Y.-P., Liu, H.-Z., *Colloids Surf. A* 2006, *275*, 87 – 91.

[209] Yavuz, H., Odabasi, M., Akgol, S., Denizli, A., *J. Biomater. Sci., Polym. Ed.* 2005, *16*, 673 – 684.

[210] Sari, M., Akgol, S., Karatas, M., Denizli, A., *Ind. Eng. Chem. Res.* 2006, *45*, 3036 – 3043.

[211] Akgol, S., Denizli, A., *J. Mol. Catal. B.* 2004, *28*, 7 – 14.

[212] Altintas, E. B., Yavuz, H., Say, R., Denizli, A., *J. Biomater. Sci., Polym. Ed.* 2006, *17*, 213 – 226.

[213] Turkmen, D., Yavuz, H., Denizli, A., *Int. J. Biol. Macromol.* 2006, *38*, 126 – 133.

[214] Šafařík, I., Šabatková, Z., Šafaříková, M., *6th International Conference on Scientific and Clinical Applications of Magnetic Carriers*, Krems, Austria 2006.

[215] Franzreb, M., Siemann-Herzberg, M., Hobley, T. J., Thomas, O. R., *Appl. Microbiol. Biotechnol.* 2006, *70*, 505 – 516.

[216] Šafařík, I., Šafaříková, M., *Biomagn. Res. Technol.* 2004, *2*, 1 – 17.

[217] Gu, H. W., Xu, K. M., Xu, C. J., Xu, B., *Chem. Commun.* 2006, 941 – 949.

[218] Tong, X. D., Xue, B., Sun, Y., *Biotechnol. Prog.* 2001, *17*, 134 – 139.

[219] Ennis, M. P., Wisdom, G. B., *Appl. Biochem. Biotechnol.* 1991, *30*, 155 – 164.

[220] Šafaříková, M., Roy, I., Gupta, M. N., Šafařík, I., *J. Biotechnol.* 2003, *105*, 255 – 260.

[221] Liu, X. Q., Guan, Y. P., Yang, Y., Ma, Z. Y., *et al.*, *J. Appl. Polym. Sci.* 2004, *94*, 2205 – 2211.

[222] Cao, Y., Bai, G., Chen, J. Q., Tian, W. *et al.*, *J. Chromatogr. B* 2006, *833*, 236 – 244.

[223] Hubbuch, J. J., Thomas, O. R. T., *Biotechnol. Bioeng.* 2002, *79*, 301 – 313.

[224] Falkenhagen, D., Brandl, M., Hartmann, J., Kellner, K. H. *et al.*, *Ther. Apher. Dial.* 2006, *10*, 154 – 159.

[225] Chen, H., Kaminski, M. D., Liu, X., Mertz, C. J. *et al.*, *Med. Hypotheses* 2007, *68*, 1071 – 1079.

[226] Schwanzer-Pfeiffer, D., Mitteregger, R., Rossmanith, E., Falkenhagen, D., *Int. J. Artif. Organs* 2006, *29*, 1140 – 1147.

[227] Weber, C., Falkenhagen, D., in: Hafeli, U., Schüt, W., Teller, J., Zborovski, M. (Eds.), *Scientific and Clinical Applications of Magnetic Carriers*, Plenum Press, New York 1997, pp. 371 – 379.

[228] Akutsu, J., Tojo, Y., Segawa, O., Obata, K. *et al.*, *Biotechnol. Bioeng.* 2004, *86*, 667 – 671.

[229] Albretsen, C., Kalland, K. H., Haukanes, B. I., Havarstein, L. S., Kleppe, K., *Anal. Biochem.* 1990, *189*, 40 – 50.

[230] Georgieva, J., Milling, A., Orfanos, C. E., Geilen, C. C., *Melanoma Res.* 2002, *12*, 309 – 317.

[231] Hornes, E., Korsnes, L., *Genet. Anal. Tech. Appl.* 1990, *7*, 145 – 150.

[232] Archer, M. J., Lin, B. C., Wang, Z., Stenger, D. A., *Anal. Biochem.* 2006, *355*, 285 – 297.

[233] Chen, J. R., Johnson, R., Griffiths, M., *Appl. Environ. Microbiol.* 1998, *64*, 147 – 152.

[234] Chen, J., Griffiths, M. W., *Methods Biotechnol.* 2001, *14*, 107 – 110.

[235] Křížová, J., Španová, A., Rittich, B., Horák, D., *J. Chromatogr. A* 2005, *1064*, 247 – 253.

[236] Rittich, B., Španová, A., Horák, D., Beneš, M. J., *et al.*, *Colloids Surf. B* 2006, *52*, 143 – 148.

[237] Španová, A., Rittich, B., Styriak, I., Styriakova, I., Horák, D., *J. Chromatogr. A* 2006, *1130*, 115 – 121.

[238] Olsvik, O., Popovic, T., Skjerve, E., Cudjoe, K. S., *et al.*, *Clin. Microbiol. Rev.* 1994, *7*, 43 – 54.

[239] Miltenyi, S., in: Morstyn, G., Sheridan, W. (Eds.), *Cell Therapy: Stem Cell Transplantation, Gene Therapy, and Cellular Immunotherapy*, Cambridge University Press, Cambridge 1996, pp. 213 – 220.

[240] Radbruch, A., Mechtold, B., Thiel, A., Miltenyi, S., Pfluger, E., *Methods in Cell Biology*, Academic Press, San Diego 1994, *Vol. 42*, pp. 387 – 403.

[241] Parmar, N., Easter, M. C., Forsythe, S. J., *Lett. Appl. Microbiol.* 1992, *15*, 175 – 178.

[242] Skjerve, E., Rorvik, L. M., Olsvik, O., *Appl. Environ. Microbiol.* 1990, *56*, 3478 – 3481.

[243] Payne, M. J., Campbell, S., Kroll, R. G., *Food Microbiol.* 1993, *10*, 75 – 83.

[244] Španová, A., Rittich, B., Karpíšková, R., Čechová, L., Škapová, D., *Bioseparation* 2000, *9*, 379 – 384.

[245] Špánová, A., Rittich, B., Horák, D., Lenfeld, J., *et al.*, *J. Chromatogr. A* 2003, *1009*, 215 – 221.

[246] Horák, D., Hochel, I., *e-Polymers* 2005, http://www.e-polymers.org/061 (2005) .

[247] DeMarco, M. J., SenGupta, A. K., Greenleaf, J. E., *Water Res.* 2003, *37*, 164 – 176.

[248] Cumbal, L., Greenleaf, J., Leun, D., SenGupta, A. K., *React. Funct. Polym.* 2003, *54*, 167 – 180.

[249] Wu, R. C., Qu, H. H., He, H., Yu, Y. B., *Appl. Catal. B, Environ.* 2004, *48*, 49 – 56.

[250] Wu, R., Qu, J., *J. Chem. Technol. Biotechnol.* 2005, *80*, 20 – 27.

[251] Baldrian, P., Merhautova, V., Gabriel, J., Nerud, F., *et al.*, *Appl. Catal. B, Environ.* 2006, *66*, 258 – 264.

[252] Rossi, L. M., Quach, A. D., Rosenzweig, Z., *Anal. Bioanal. Chem.* 2004, *380*, 606 – 613.

[253] Bahar, T., Celebi, S. S., *J. Appl. Polym. Sci.* 1999, *72*, 69 – 73.

[254] de Cuyper, M., Joniau, M., *Biotechnol. Appl. Biochem.* 1992, *16*, 201 – 210.

[255] Gao, X., Yu, K. M. K., Tam, K. Y., Tsang, S. C., *Chem. Commun.* 2003, 2998 – 2999.

[256] Izmailov, A. F., Kiselev, M. V., Vakurov, A. V., Gladilin, A. K., Levashov, A. V., *Prikl. Biokhim. Mikrobiol.* 2000, *36*, 68 – 73.

[257] Koneracká, M., Kopčanský, P., Timko, M., Ramchand, C. N. *et al.*, *J. Mol. Catal. B, Enzym.* 2002, *18*, 13 – 18.

[258] Shimomura, M., Ohta, M., Sugiyama, N., Oshima, K., *et al.*, *Polym. J.* 1999, *31*, 274 – 278.

[259] Chen, D. H., Liao, M. H., *J. Mol. Catal. B, Enzym.* 2002, *16*, 283 – 291.

[260] Liao, M. H., Chen, D. H., *J. Mol. Catal. B, Enzym.* 2002, *18*, 81 – 87.

[261] Varlan, A. R., Sansen, W., Van Loey, A., Hendrickx, M., *Biosens. Bioelectron.* 1996, *11*, 443 – 448.

[262] Bílková, Z., Slováková, M., Horák, D., Lenfeld, J., Churácek, J., *J. Chromatogr. B* 2002, *770*, 177 – 181.

[263] Bílková, Z., Slováková, M., Lyčka, A., Horák, D., *et al.*, *J. Chromatogr. B* 2002, *770*, 25 – 34.

[264] Korecká, L., Ježová, J., Bílková, Z., Beneš, M., *et al.*, *J. Magn. Magn. Mater.* 2005, *293*, 349 – 357.

[265] Rittich, B., Španová, A., Ohlashennyy, Y., Lenfeld, J., *et al.*, *J. Chromatogr. B* 2002, *774*, 25 – 31.

[266] Horák, D., Rittich, B., Šafář, J., Španová, A., *et al.*, *Biotechnol. Prog.* 2001, *17*, 447 – 452.

[267] Bílková, Z., Slováková, M., Minc, N., Futterer, C., *et al.*, *Electrophoresis* 2006, *27*, 1811 – 1824.

Příloha č. 6

Poly(*N*,*N*-dimethylacrylamide)-Based Microspheres Prepared by Heterogeneous Polymerizations

Michal Babič, Daniel Horák*

PDMAAm microspheres have been obtained by inverse suspension, inverse emulsion, and dispersion polymerization. Conventional inverse suspension polymerization in toluene/trichloroethene is modified by the use of ultrasound. The resulting hydrogel microspheres are examined by dynamic light scattering and scanning electron microscopy to afford the morphology, dispersity, and size of the microspheres. Inverse suspension polymerization yields 100-μm particles, while those obtained by inverse emulsion polymerization are 0.13–1 μm in diameter. While the inverse techniques produce particles of broad size distribution, monodisperse microspheres are obtained by the Kraton G 1650-stabilized dispersion polymerization of DMAAm in a toluene/heptane medium. The particle size and polydispersity could be controlled by the addition of water into the dispersed phase, and by varying the cellulose acetate butyrate or Kraton G 1650 concentration and the toluene/trichloroethene or toluene/heptane ratio.

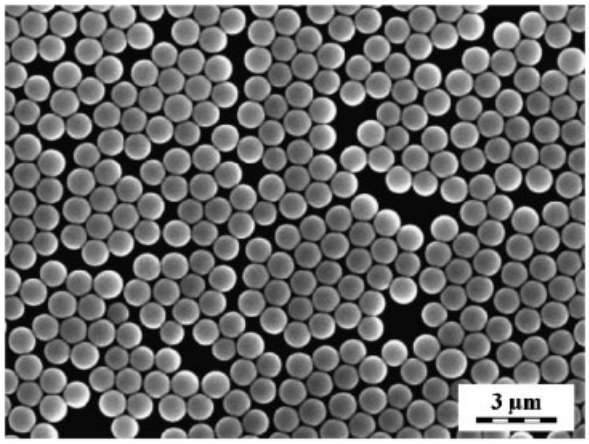

Introduction

The scientific and practical interest in poly(*N*,*N*-dimethylacrylamide) (PDMAAm) is increasing because of its high hydrophilicity and thermal responsivity.[1,2] PDMAAm copolymers are known to produce smart polymers that are used in oil recovery[3] and in slow-release medical materials.[4] Solid-phase-supported PDMAAm has also been used as a solvent-free system in organic reactions[5] and metal catalysis,[6] and is promising in the separation of nucleic acid (DNA) in microfluid systems. Unlike acrylamide (AAm), *N*,*N*-dimethylacrylamide (DMAAm) does not show strong hydrogen bond interactions. Poly(*N*-substituted methacrylamide)s are inert, non-toxic, and biocompatible,[7,8] which makes them suitable for substitution of AAm.

Copolymerization of DMAAm enables tailoring of the hydrophilic/hydrophobic character of the resulting products. DMAAm has been employed to adjust the lower critical solution temperature (LCST) of poly[(*N*-isopropylacrylamide)-*co*-DMAAm] in water to approx. 37 °C because both of the monomers exhibited similar reactivity.[9] An

M. Babič, D. Horák
Institute of Macromolecular Chemistry, Academy of Sciences of the Czech Republic, Heyrovský Sq. 2, 162 06 Prague 6, Czech Republic
E-mail: horak@imc.cas.cz

Macromol. React. Eng. **2007**, *1*, 86–94

DOI: 10.1002/mren.200600008

increase in the length of the hydrophilic DMAAm segments of the copolymer increased the LCST.[10] DMAAm copolymers with hydrophobic comonomers such as allyl methacrylate undergo thermal phase separation.[11] Moreover, copolymerization makes possible the incorporation of small amounts of a monomer that contains a reactive chemical function with the potential for polymer modification, which is attractive for the immobilization of biological molecules.

PDMAAm-based microspheres have been rarely described in the literature. In order to utilize the particles in applications, precise control of their properties is important. Their size, size uniformity, functionality, morphology, and the degree of crosslinking are main concerns in controlling their properties. The present report is devoted to the synthesis of crosslinked and uncrosslinked PDMAAm microspheres by inverse suspension, inverse emulsion, and dispersion polymerization. Attention is paid to the effect of numerous parameters, such as the crosslinker content, initiator, stabilizer, and monomer concentrations, and composition of the solvent system on the morphology, size, and polydispersity of PDMAAm hydrogel particles.

Experimental Part

Materials

DMAAm (Aldrich, Milwaukee, USA) was distilled (56 °C at 267 Pa), *N*,*N*′-methylenebisacrylamide (MBAAm, Aldrich), and cellulose acetate butyrate (CAB 381-20, Eastman Chemical Company, Kingsport, USA) were used as received. Kraton G 1650 (Shell, Houston, USA) is polystyrene-*block*-(hydrogenated polybutadiene)-*block*-polystyrene with $\overline{M}_w = 74\ 000$, $\overline{M}_n = 70\ 000$, and a polystyrene/hydrogenated polybutadiene ratio of 29/71 w/w. Medical grade petroleum ether was from Kulich, Hradec Králové, Czech Republic. Ammonium persulfate (APS) was from Lachema, Brno, Czech Republic, 2,2′-azoisobutyronitrile (AIBN) was obtained from Fluka, Buchs, Switzerland and recrystallized from ethanol. All other solvents and chemicals were from Aldrich and used as received.

Preparation of Poly(DMAAm-*co*-MBAAm) Particles

Inverse Suspension Polymerization

In a typical experiment, a mixture of 8.55 g of DMAAm, 0.45 g of MBAAm, 3 g of water, and 0.09 g of APS as the polymerization initiator was dispersed in a continuous phase that contained a solution of 1.36 g of CAB suspension stabilizer in 43 g of toluene (Tol) and 25 g of trichloroethene (TCE) in a glass 100 mL reactor equipped with a mechanical anchor stirrer. The reactor was purged with nitrogen for 10 min, the stirring speed was adjusted to 400 rpm, and the mixture was polymerized at 70 °C for 8 h. The resulting beads were washed by repeated decantations with Tol (6×) to remove excessive CAB, 1/1 Tol/ethyl acetate mixture (5×), ethyl acetate (5×), 1/1 ethyl acetate/acetone mixture (5×), acetone (5×), and finally with water. The particles thus obtained were then freeze-dried.

Inverse Emulsion Polymerization

The above-described reactor was used. Briefly, water (2 g) was dispersed under 5 min of sonication (Ultrasonic Homogenizer 4710 Series, Cole-Palmer Instruments, USA, 30% power) in the continuous phase (solution of 3 g of CAB in a Tol/TCE mixture 10/58 $g \cdot g^{-1}$), the mixture was ice-cooled and a solution of 0.02 g of AIBN initiator in 1.9 g of DMAAm and 0.1 g of MBAAm was added, and again sonicated (30% power, 1 min) under cooling. After purging the mixture with nitrogen for 10 min, polymerization proceeded with stirring (400 rpm) at 70 °C for 8 h. The resulting particles were washed with Tol (5×) and ethyl acetate before transferring them into diethyl ether. Finally the particles were dried.

Dispersion Polymerization

Dispersion polymerization was conducted in a glass 30 mL reaction vessel equipped with an anchor stirrer (400 rpm). In a typical procedure, 27 g of a mixture of 17.5 g of heptane and 9.5 g of Tol with 0.27 g of dissolved Kraton G 1650 stabilizer, 1 g of DMAAm, and 0.01 g of AIBN was charged in the reactor and the system was purged with nitrogen for 10 min. The reactor was then heated at 70 °C with stirring for 8 h. At the end of the reaction, the polymer was removed and washed with petroleum ether (30 mL, six times each) and finally dried. If the colloid did not sediment, the sample was centrifuged at 14 000 rpm before washing.

Characterization

Particle size was determined at 25 °C by dynamic light scattering (DLS) with an AutoSizer Lo-C (Malvern, UK). The measured diameter is the *z*-average diameter (D_z). The average particle sizes (weight-average (D_w) and number-average (D_n)) and the polydispersity index ($PDI = D_w/D_n$) were obtained from optical (Meopta Přerov, Czech Republic, digital camera Minolta Dimage A1) or scanning electron microscopy (SEM, JEOL JSM 6400) photographs using Atlas software (Tescan Digital Microscopy Imaging, Brno, Czech Republic) by counting some 500 microspheres. The water regain of the microspheres was measured in fritted glass columns at room temperature.[12]

Results and Discussion

Inverse Suspension Polymerization of DMAAm

Suspension polymerization is a process in which monomers are dispersed as liquid droplets in a continuous phase by stirring and then polymerized essentially by the

bulk polymerization mechanism. The advantage of suspension polymerization is that it is suitable for the preparation of porous particles in contrast to emulsion and dispersion polymerizations. Suspension polymerization of a water-soluble monomer, such as DMAAm, is always much more challenging than that of water-insoluble compounds. In order to prepare PDMAAm microspheres, crosslinking is needed as it prevents polymer dissolution in water. In this study, DMAAm is copolymerized with MBAAm crosslinker. However, it should be noted that the maximum degree of crosslinking is limited to 20 wt.-% of MBAAm in the monomer phase, because MBAAm is not soluble at higher concentrations. DMAAm is suspension-polymerized in an inverse mode in a Tol/TCE mixture; the polymerization is stabilized with CAB and initiated with APS. A Tol/TCE mixture has been selected as a medium that dissolves the suspension stabilizer and prevents the droplets from sedimentation (which occurs in neat Tol). Because DMAAm dissolves in the Tol/TCE mixture, water, which is insoluble in this medium, has been added to act as an extraction agent for the monomer. In the absence of water, the polymerization does not produce any particles, only a microgel. As DMAAm is more soluble in water than in Tol/TCE, its solubility in the continuous phase is thus restricted and the monomer droplets are formed. The obtained P(DMAAm-*co*-MBAAm) particles are of spherical shape, mostly approx. 60 μm in diameter irrespective of the content of the MBAAm crosslinker. At the same time, the particle size distribution is broad, which is typical of any suspension polymerization (Figure 1a,b). Swelling in water (characterized by water regain) is the most important single property of any hydrogel particle. As follows from Figure 1 and Table 1, low-crosslinked P(DMAAm-*co*-MBAAm) beads possess a substantial swelling ability in water (approx. 1.6 mL of water per g of dry polymer particles). As expected, increasing the content of MBAAm leads to a decrease in swelling.

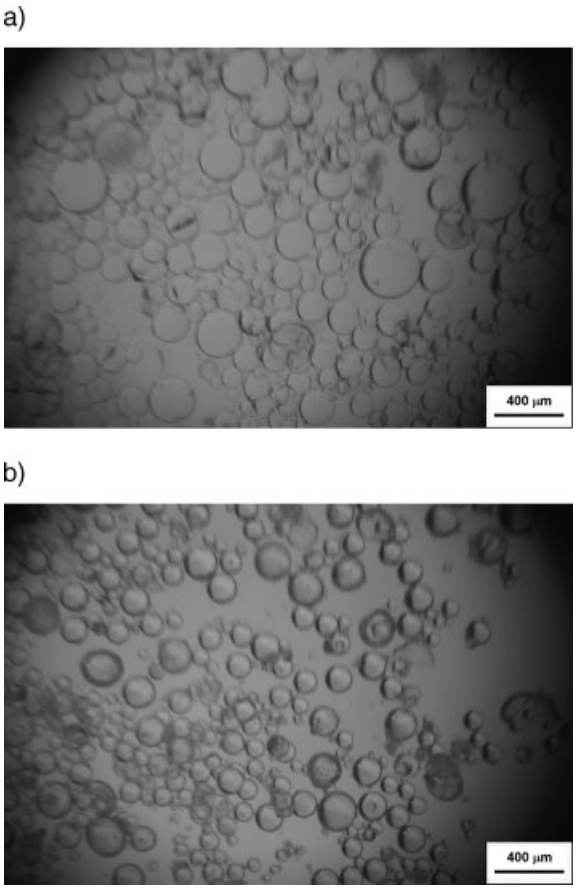

Figure 1. Optical microscopy of a) water-swollen and b) dry P(DMAAm-*co*-5%MBAAm) microspheres obtained by inverse suspension polymerization in Tol/TCE.

Table 1. Effect of MBAAm crosslinker on swelling of PDMAAm particles prepared by inverse suspension polymerization in water.

Sample[a)]	MBAAm content	$D_{n,\ wet}$	$D_{n,\ dry}$	Water regain
	wt.-%	μm	μm	$mL \cdot g^{-1}$
1	2.5	74	63	1.56
2	5	120	50	1.66
3	10	65	61	0.90
4	20	66	59	0.72

[a)]Polymerization conditions (weight ratios): dispersed/continuous phase 12/80, water/monomers 3/9, APS 1% (relative to monomers), Tol/TCE 43/25, CAB 2% in the continuous phase; 70 °C for 8 h.

Inverse Emulsion Polymerization of DMAAm

Inverse emulsion polymerization of DMAAm is similar to the inverse suspension polymerization, with the exception of the intensive monomeric phase homogenization under high-shear mixing (sonication) into a continuous medium formed by the CAB solution in Tol/TCE. CAB is an effective polymeric emulsifier and dispersed monomer minidroplets are formed in the medium. Another substantial difference from the suspension polymerization consists in the selection of an initiator: oil-soluble AIBN has been used instead of water-soluble APS. These changes evidently cause particle nucleation and the subsequent propagation reaction to occur primarily in the small-sized polymerization loci, which introduces segregation effects.[13] However, the effect of homogenization conditions on the particle size distribution and the prediction of poly-

Macromol. React. Eng. **2007**, *1*, 86–94

Macromolecular Journals

DOI: 10.1002/mren.200600008

Table 2. Effect of MBAAm crosslinker concentration, water content, AIBN initiator concentration in the monomers, CAB stabilizer concentration in the polymerization feed, and Tol/TCE ratio on the D_n and PDI of P(DMAAm-*co*-MBAAm) microspheres prepared by inverse emulsion polymerization.

Sample[a)]	MBAAm[c)]	Water	CAB[d)]	AIBN[e)]	Tol/TCE	D_n	PDI
	wt.-%	g	wt.-%	wt.-%	$g \cdot g^{-1}$	μm	
5	5	2	4	1	10/58	0.87	1.18
6	5	3	4	1	10/58	0.95	1.28
7	5	4	4	1	10/58	1.35	1.13
8[b)]	5	4	3.7	1	10/58	0.28	1.71
9[b)]	10	4	3.7	1	10/58	0.13	2.80
10[b)]	5	4	4.9	1	10/58	0.25	3.86
11[b)]	5	4	6.2	1	10/58	0.29	3.19
12	5	2	4	0.5	10/58	0.54	1.51
13	5	2	4	1.5	10/58	0.99	1.37
14	5	2	4	2	10/58	0.93	1.17
15	5	2	4	2.5	10/58	0.74	1.36
17	5	2	4	1	20/48	0.69	1.16
18	5	2	4	1	34/34	0.31	2.46
19	5	2	4	1	48/20	0.27	2.54

[a)]Polymerization conditions: 2.8 wt.-% of monomers in the feed, 70 °C for 8 h; [b)]11 wt.-% of monomers in the feed; [c)]Relative to monomers; [d)]Relative to feed; [e)]Relative to monomers.

merization mechanisms are far from being established. A given polymerization system cannot always be easily classified, if at all, as one of the 'classical' polymerization mechanisms (dispersion, emulsion, and suspension polymerization).[14]

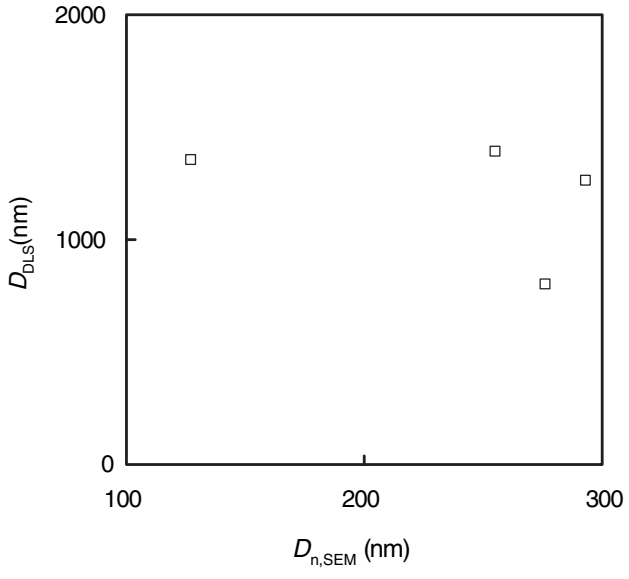

Figure 2. Correlation of P(DMAAm-*co*-5%MBAAm) microsphere size by DLS (D_{DLS}) and SEM ($D_{n,SEM}$).

The recipes for inverse emulsion polymerization of DMAAm and some characteristics of the products are shown in Table 2. The resulting PDMAAm microspheres have been measured by two independent methods: DLS and SEM. DLS measurement in water is feasible because the microspheres are crosslinked. This is in contrast to the particles obtained by the dispersion polymerization, which are uncrosslinked and, therefore, water soluble. Figure 2 compares the microsphere diameter determined by both of these methods. The diameters found by DLS are substantially larger than those determined by SEM, because the former technique measures the diameter of water-swollen particles, whereas the latter determines the unswollen size of the particles in the dry state. Moreover, while the SEM shows number-average diameters, scattering techniques measure *z*-average diameters, which are sensitive to large particles, while the number-average diameter is strongly influenced by the presence of small ones. According to SEM, the size of the P(DMAAm-*co*-MBAAm) microspheres prepared by inverse emulsion polymerization is substantially smaller (typically in the submicrometer range, Figure 3) than those obtained by inverse suspension polymerization.

To better control the size and polydispersity of the microspheres, the effect of the main experimental parameters (water/monomer and Tol/TCE ratio, crosslinking degree, and concentration of initiator and stabilizer) on the

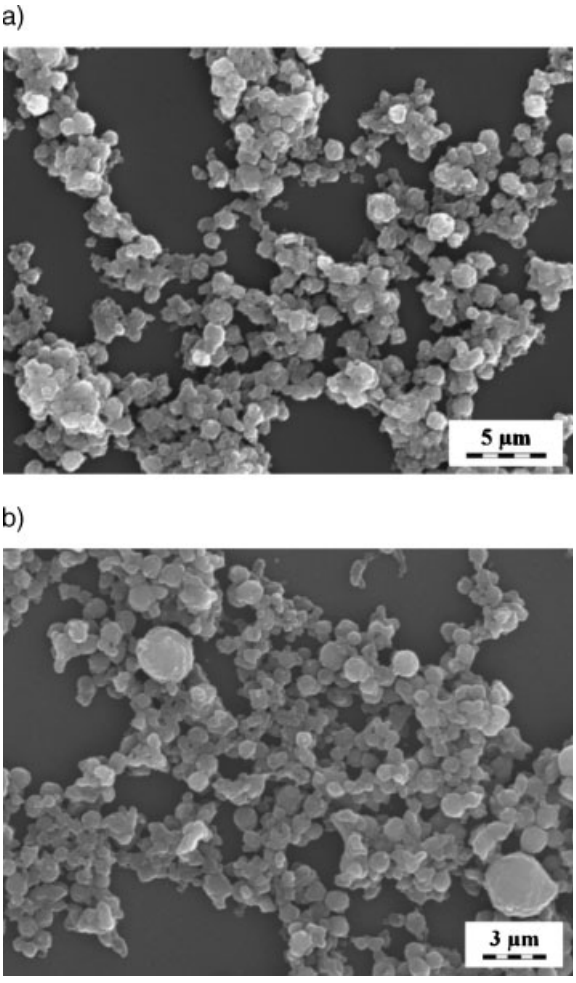

Figure 3. SEM of P(DMAAm-*co*-5%MBAAm) microspheres obtained by inverse emulsion polymerization in Tol/TCE. a) Run 5 and b) run 18 in Table 2.

morphology of the emulsion particles have been investigated.

Effect of Water Addition

In analogy to the suspension polymerization, addition of water to the system is of primary importance to keep the monomer in the dispersed phase and not allow its transfer into the continuous phase. In the absence of water or with addition of 1 g of water to the feed, only a microgel is formed. Microspheres result from the mixtures containing 2–4 g of water, and a macrogel is formed with five and more grams of water in the feed because of the disruption of the micelles. The effect of the amount of water added to the feed is listed in Table 2, samples 5–7. The microsphere size increases with increasing water content in the range of 2–4 g probably because their solubility is improved. This is in agreement with a general observation that a change in the system that tends to enhance the solubility of the polymer initially formed causes an increase in the particle size.[15] The microspheres, however, are not monodisperse.

Effect of Crosslinking

As follows from Table 2 (samples 8 and 9), the P(DMAAm-*co*-MBAAm) microsphere size decreases with increasing MBAAm crosslinker content. A similar effect has been observed in other systems, where the microspheres are formed from monomer minidroplets, and it has been explained by two factors.[16] One factor is the hardness of the primary microspheres with a high degree of crosslinking, which prevents particle growth. The second factor may be the larger size of MBAAm with two double bonds compared with DMAAm, which lowers the solubility and favors the formation of smaller minidroplets. Attempts to crosslink DMAAm with ethylene dimethacrylate (EDMA) by inverse emulsion polymerization do not produce the desired microspheres. At relatively low EDMA concentrations (up to 4 wt.-%), a microgel is formed. A block polymer is then formed at and above 6 wt.-% of EDMA.

Effect of CAB Concentration

CAB has been used as a polymeric emulsifier. In contrast to the inverse suspension polymerization, the inverse emulsion polymerization requires rather a high CAB concentration, which is accompanied by an enhanced viscosity of the continuous phase. As a result, the particle size distribution is broad (Table 2, samples 9–11) because relatively large particles are formed because of incomplete mixing at high CAB concentrations in the polymerization mixture (4.9 and 6.2 wt.-%). There are also other possible factors that lead to broad particle size distributions at higher contents of the emulsifier in the feed:[17] 1) its higher concentration is favorable to the formation of more particle nuclei, and 2) the higher contents lead to changes in the polarity and solvency of the media, thus increasing the possibility of secondary nucleation during the polymerization. Generally, the higher the emulsifier concentration, the greater the chance of secondary nucleation. An optimal emulsifier concentration is thus needed to prepare more uniform polymer particles.

Effect of Initiator Concentration

In contrast to the suspension polymerization, the initiator is soluble in the continuous medium but not in the monomer in the emulsion polymerization. Accordingly, emulsion polymerization of DMAAm in the Tol/TCE medium is initiated with AIBN and not with APS initiator, as the former is soluble in the organic (continuous) and not in the aqueous (dispersed) phase. A pronounced dependence of the microsphere size on the AIBN concentration is not observed (Table 2, samples 5 and 12–15): the particle size distribution remains broad. The probable reason is that the generation rate of the oligomers is much faster

Macromol. React. Eng. **2007**, *1*, 86–94

Macromolecular Journals

DOI: 10.1002/mren.200600008

than the absorption of the CAB because of the fast decomposition rate of the AIBN initiator at higher temperatures.

Effect of Tol/TCE Ratio

This effect has been investigated with 5 wt.-% MBAAm crosslinking agent and Tol/TCE ratios of 10/58–48/20 $g \cdot g^{-1}$ (Table 2, Runs 5 and 17–19). At a low Tol/TCE ratio (10/58 $g \cdot g^{-1}$), the density of the swollen polymer approximately corresponds to the density of the medium, and the resulting particles are thus well dispersed without sedimenting. However, the solubility of CAB improves with higher Tol contents in the mixture. The P(DMAAm-*co*-MBAAm) microsphere size thus decreases with increasing proportion of Tol in its mixture with TCE as a consequence of the better solubility of CAB (Figure 3a,b). At the same time, the particle polydispersity increases (Table 2), presumably because of the difference in the density of the dispersed (monomer) and continuous (oil) phases.

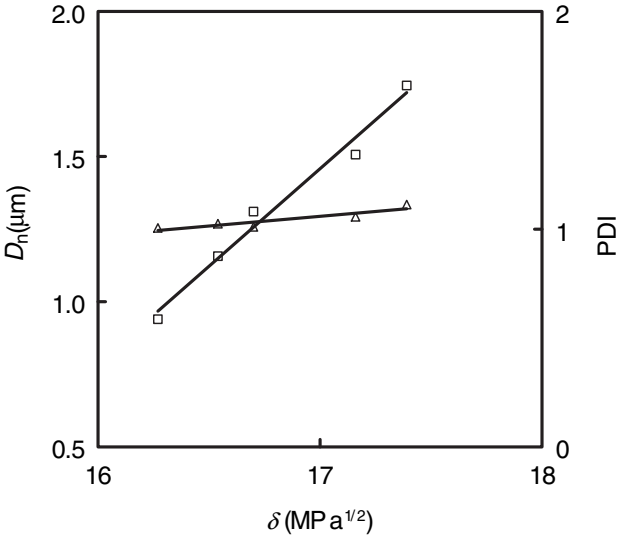

Figure 4. Dependence of PDMAAm microsphere size D_n and polydispersity PDI on the solubility parameter δ of the system (effect of the Tol/heptane solvent). Polymerization conditions of dispersion polymerization: 3.6 wt.-% monomer, 1 wt.-% Kraton G 1650, 1 wt.-% AIBN (relative to the monomer) in the feed.

Dispersion Polymerization of DMAAm

The advantage of the dispersion polymerization consists in the capability of producing monosized microspheres in the size range that is difficult to produce by suspension or emulsion polymerization. Its mechanism is different from that of suspension or emulsion polymerization and is described elsewhere.[18] Unlike emulsion and suspension polymerizations, all polymerization ingredients, including the monomer, initiator, and stabilizer, are initially dissolved in the polymerization medium. The particles are developed at the beginning of the polymerization by the precipitation of growing oligomeric chains from solution upon reaching a critical length. The precipitated precursor particles (nuclei) capture newly formed oligomers and/or aggregate, adsorb the polymer stabilizer, and become sterically stabilized. The anchor segment of the stabilizer must possess a good affinity to the formed polymer particles and the solvent-soluble segment provides a good dispersion of the stabilizer in the media.

Here, DMAAm is dispersion polymerized in a Tol/heptane medium. Kraton G 1650 and AIBN are the stabilizer and initiator, respectively.

Effect of Tol/Heptane Ratio

Apparently, Tol/heptane mixtures meet the solvency conditions required for narrow size or monodisperse particle formation: it dissolves the monomer but precipitates the forming polymer. According to theories of particle formation, the solvency of the reaction medium for growing polymer chains controls the critical molecular weight above which the polymer precipitates during the nucleation stage in the dispersion polymerization. This in turn regulates the size of the particles.[15] In the dispersion polymerization of DMAAm, the solvency of the polymerization mixture could be finely tuned by the Tol/heptane ratio. Solvency is expressed in terms of liquid polarity as defined by the solubility parameter. The solubility parameter of the reaction mixture δ is calculated from those of components δ_i according to the equation $\delta = (\Sigma v_i \cdot \delta_i^2)^{1/2}$, where v_i is the volume fraction of the i-th component, δ (DMAAm) = 21.48 MPa$^{1/2}$, δ (MBAAm) = 26.35 MPa$^{1/2}$, δ (TCE) = 17.96 MPa$^{1/2}$, δ (Tol) = 18.2 MPa$^{1/2}$, and δ (heptane) = 15.1 MPa$^{1/2}$. While the first two solubility parameters have been calculated according to Fedors,[19] the other values are taken from tables.[20] Figure 4 and 5 show that the PDMAAm microsphere size is proportional to the solubility parameter of the medium. This is typical of a dispersion polymerization of hydrophilic monomers, e.g., of 2-hydroxyethyl methacrylate,[21] acrylamide,[22] or *N*-vinylformamide.[23] On the contrary, an inverse correlation between the polystyrene or poly(methyl methacrylate) particle size and the dispersion medium polarity has been found.[24] This distinction results from poor solubility of non-polar polystyrene or poly(methyl methacrylate) in polar solvents, in contrast to polar polymers. Because heptane is a thermodynamically poorer solvent for PDMAAm than Tol, the critical chain length of precipitated oligomers decreases with increasing heptane content in the polymerization mixture, i.e., with decreasing solubility parameter. This results in an increase in the number of nuclei and, correspondingly, in a smaller size of the particles. The monodispersity of the resulting PDMAAm

microspheres is documented in Figure 5. The figure reflects a short particle nucleation stage and a particle growth stage free from both the formation of new particles and the coalescence of existing particles.

Effect of Stabilizer Concentration

Selection of a suitable stabilizer for the dispersion polymerization is always determined by its ability to be dissolved in the polymerization medium. The steric stabilizer has to prevent particles from approaching each other closely. Here, Kraton G 1650 is the stabilizer of choice for the dispersion polymerization of DMAAm in Tol/heptane medium. As expected, the PDMAAm particle size decreases with increasing stabilizer concentration (Figure 6) because more stabilizer stabilizes more particles and, in return, their size is smaller. Monodisperse microspheres are formed in the presence of 1–4 wt.-% of Kraton G 1650 in the feed. Concentrations higher than 4 wt.-% are impractical from an application point of view.

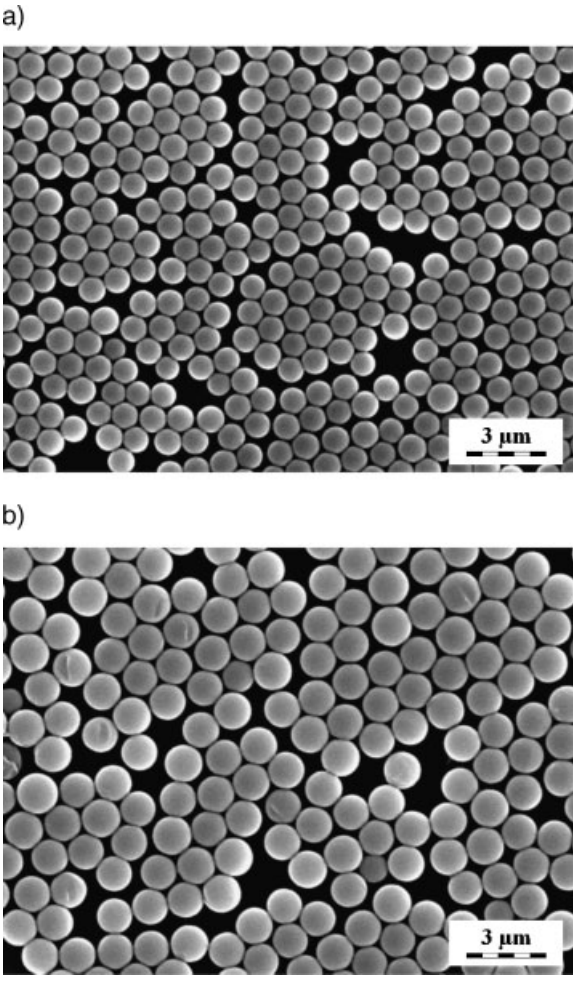

Figure 5. SEM micrograph of PDMAAm microspheres obtained by dispersion polymerization. Polymerization conditions (weight ratios are given): Tol/heptane a) 9.5/17.5 and b) 13.5/13.5; 3.6% monomer and 1% Kraton G 1650 in the feed, 1% AIBN relative to the monomer.

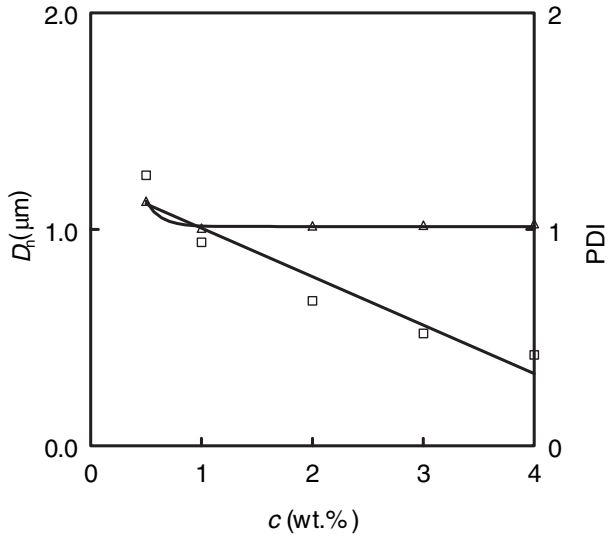

Figure 6. Dependence of (□) PDMAAm microsphere size D_n and (△) polydispersity PDI on the concentration c of Kraton G 1650 in the polymerization mixture. Polymerization conditions of dispersion polymerization: Tol/heptane 9.5/17.5 (g/g) and 3.6 wt.-% monomer in the feed, 1 wt.-% AIBN relative to monomer.

Effect of AIBN Initiator Concentration

The concentration of initiator also partially affects the size of the PDMAAm microspheres as shown in Figure 7. As the initiator concentration increases from 0.5 to 8 wt.-%, the diameter of the microspheres decreases from 0.9 to 0.7 μm. The formation of smaller microspheres at a higher initiator

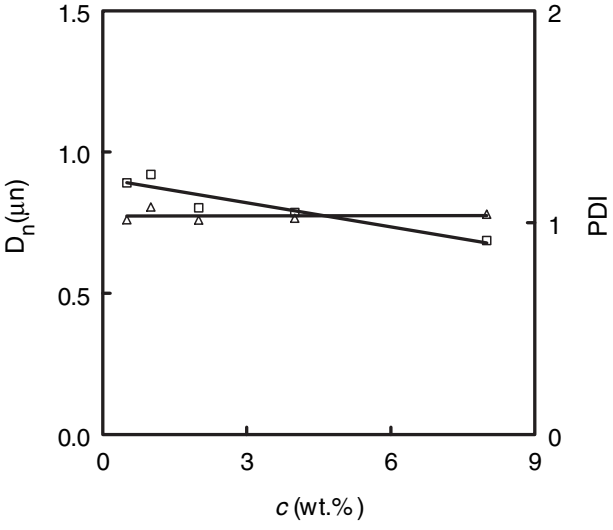

Figure 7. Dependence of (□) PDMAAm microsphere size D_n and (△) polydispersity PDI on the concentration of AIBN initiator c. Polymerization conditions of dispersion polymerization: 3.6 wt.-% monomer, 1 wt.-% Kraton G 1650, and Tol/heptane 9.5/17.5 (g/g) in the feed.

Macromol. React. Eng. **2007**, *1*, 86–94

Macromolecular Journals
DOI: 10.1002/mren.200600008

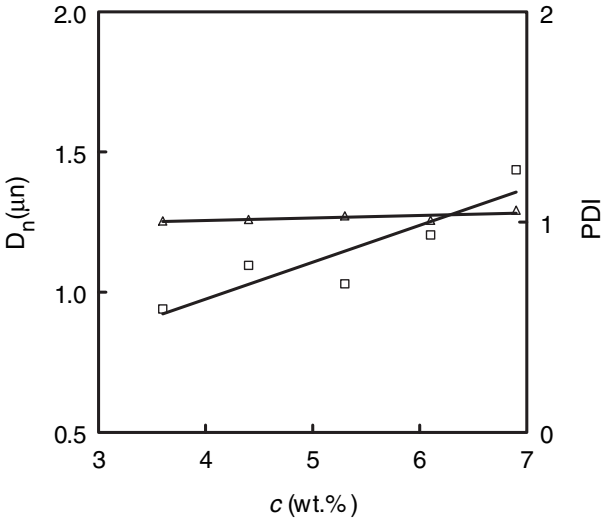

Figure 8. Dependence of (□) PDMAAm microsphere size D_n and (△) polydispersity PDI on the concentration of monomer *c* in the feed. Polymerization conditions of dispersion polymerization: Tol/heptane ratio 9.5/17.5 (g/g), 1 wt.-% of Kraton G 1650 in the feed, and 1 wt.-% of AIBN relative to the monomer.

concentration has also been observed by Kawaguchi et al.[25] and Wang et al.[26] and can be in favor of a homogeneous nucleation mechanism similar to emulsion polymerization. Increasing the initiator concentration causes an increase in the oligomeric radical concentration and thus an increase in the numbers of particles if sufficient particle stabilizer is available. This would lead to a smaller particle size.

Effect of Monomer Concentration

Variations in the monomer concentration can also have an effect on the nucleation process in a dispersion polymerization and, therefore, on the particle size and distribution. Stable and monodisperse particles are generated without coagulation with up to 7 wt.-% of DMAAm in the Tol/heptane medium. Significant coagulation is observed above 7 wt.-% of monomer. The effect of the monomer concentration on the size and uniformity of the microspheres is shown in Figure 8. The observed increase in PDMAAm microsphere size with the monomer concentration is usually explained by increased polymer solubility in the system as the monomer is a good solvent for the polymer, and this leads to an increase in the critical chain length of the oligomers before precipitation.[27,28]

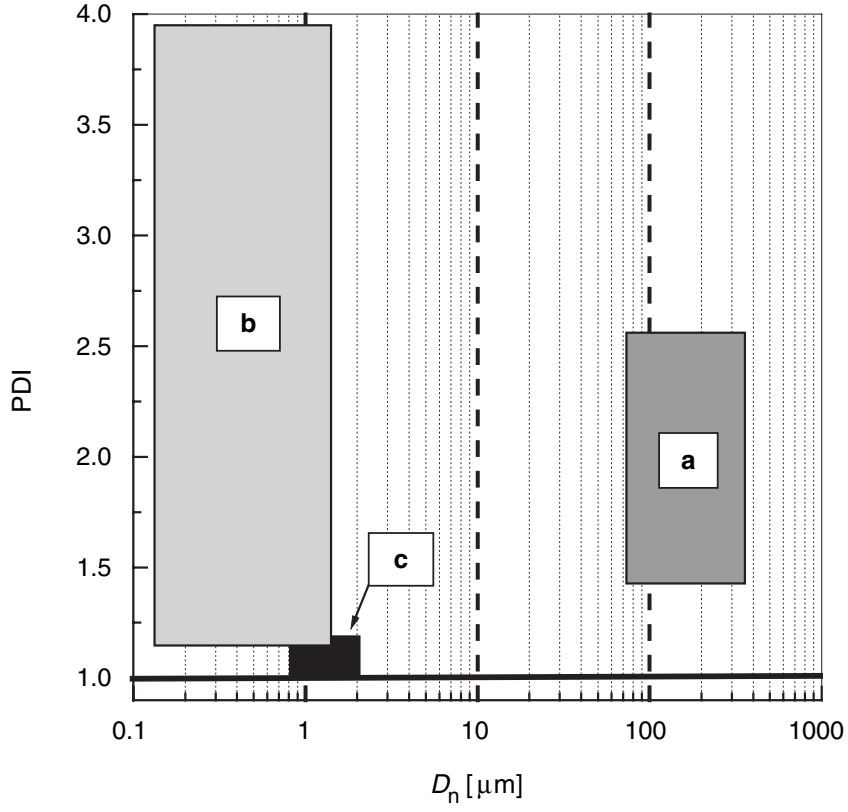

Figure 9. Schematic comparison of a) inverse suspension, b) inverse emulsion, and c) dispersion polymerization of PDMAAm in terms of microsphere size D_n and polydispersity PDI.

The delayed precipitation of polymer nuclei reduces the number of resulting particles and increases their size. In addition, an increase in the monomer concentration decreases the stabilizer-to-monomer ratio and enhances the extent of aggregation, which leads to larger particles.

Conclusion

PDMAAm microspheres have been prepared by inverse suspension, inverse emulsion, and dispersion polymerization. Figure 9 compares the methods in terms of their applicability to the preparation of particles of various sizes and polydispersities. The results demonstrate the feasibility of the suspension copolymerization of DMAAm and MBAAm in inverse mode to afford highly hydrophilic polydisperse beads of around 100 μm in diameter. The inverse emulsion copolymerization of DMAAm and MBAAm produces highly polydisperse microspheres, typically in the size range of 130 nm to 1 μm. The formation of microspheres is investigated using different emulsifier and initiator concentrations, crosslinker contents, and medium polarity. An advantage of inversion emulsion polymerization consists in the possibility of modification of the process to enable, e.g., the introduction of a functional monomer or incorporation of a magnetic core. Dispersion polymerization of DMAAm is unique in that it produces microspheres of uniform size of 1–2 μm. The method is simple, however, the system is sensitive to any changes in reaction parameters and, therefore, it is not very versatile. The microsphere size is controlled by the composition of mixed solvents (Tol/heptane). Hydrophilic PDMAAm microspheres can find applications, especially in biomedicine.

Acknowledgements: Financial support from the *Grant Agency of the Czech Republic* (203/05/2256) is gratefully acknowledged.

Received: June 19, 2006; Revised: August 11, 2006; Accepted: August 11, 2006; DOI: 10.1002/mren.200600008

Keywords: dispersion polymerization; hydrogels; inverse emulsion polymerization; inverse suspension polymerization; microspheres; particle size distribution; poly(*N,N*-dimethylacrylamide)

[1] S. Katayama, Y. Hirokawa, T. Tanaka, *Macromolecules* **1984**, *17,* 2641.
[2] T. Shibanuma, T. Aoki, K. Sanui, N. Ogata, A. Kikuchi, Y. Sakurai, T. Okano, *Macromolecules* **2000**, *33,* 444.
[3] C. L. McCormick, D. L. Elliott, *Macromolecules* **1986**, *19,* 542.
[4] Y. Aoki, M. Kawashima, H. Katono, K. Sanui, N. Igata, T. Okano, Y. Sakurai, *Macromolecules* **1994**, *27,* 947.
[5] S.-I. Yamamoto, S. Hayashi, H. Morita, O. Moriya, *J. Polym. Sci., Part A: Polym. Chem.* **2004**, *42,* 5021.
[6] M. Kralik, M. Hronec, S. Lora, G. Palma, M. Zecca, A. Biffis, B. Corain, *J. Mol. Catal., A* **1995**, *97,* 145.
[7] L. Šprincl, *J. Biomed. Mater. Res.* **1971**, *5,* 197.
[8] J. Kopeček, L. Šprincl, H. Bažilová, J. Vacík, *J. Biomed. Mater. Res.* **1975**, *7,* 111.
[9] C. S. Chaw, K. W. Chooi, M. Liu, D. Tan, L. Wang, Y. Y. Yang, *Biomaterials* **2004**, *25,* 4297.
[10] K. S. Soppimath, D. C.-W. Tan, Y.-Y. Yang, *Adv. Mater.* **2005**, *17,* 318.
[11] X. Yin, H. D. H. Stöver, *J. Polym. Sci., Part A: Polym. Chem.* **2005**, *43,* 1641.
[12] J. Štamberg, S. Ševčík, *Collect. Czech. Chem. Commun.* **1966**, *31,* 1009.
[13] F. J. Schork, Y. Luo, W. Smulders, J. P. Russum, A. Bulté, K. Fontesot, *Adv. Polym. Sci.* **2005**, *175,* 129.
[14] L. Boguslavsky, S. Baruch, S. Margel, *J. Colloid Interface Sci.* **2005**, *289,* 71.
[15] J. Ugelstad, A. Berge, T. Ellinsen, R. Schmid, T.-N. Nilsen, P. C. Mork, P. Stenstad, E. Hornes, O. Olsvik, *Prog. Polym. Sci.* **1992**, *17,* 87.
[16] H. Ni, H. Kawaguchi, *J. Polym. Sci., Part A: Polym. Chem.* **2004**, *42,* 2833.
[17] Y. Ma, W. Yang, *J. Polym. Sci., Part A: Polym. Chem.* **2004**, *42,* 2678.
[18] S. Kawaguchi, K. Ito, *Adv. Polym. Sci.* **2005**, *175,* 299.
[19] R. F. Fedors, *Polym. Eng. Sci.* **1973**, *14,* 147.
[20] J. Brandrup, E. H. Immergut, E. A. Grulke, "*Polymer Handbook*", 4th Ed., Wiley, New York 1999, pp. VII/684–686.
[21] D. Horák, *J. Polym. Sci., Part A: Polym. Chem.* **1999**, *37,* 3785.
[22] B. Ray, B. M. Mandal, *J. Polym. Sci., Part A: Polym. Chem.* **1999**, *37,* 493.
[23] H. Uyama, H. Kato, S. Kobayashi, *Polym. J.* **1994**, *26,* 858.
[24] C. K. Ober, K. P. Lok, *Macromolecules* **1987**, *20,* 268.
[25] S. Kawaguchi, M. A. Winnik, K. Ito, *Macromolecules* **1995**, *28,* 1159.
[26] D. Wang, V. L. Dimonie, E. D. Sudol, M. S. El-Aasser, *J. Appl. Polym. Sci.* **2002**, *84,* 2692.
[27] M.-Q. Chen, T. Serizawa, M. Akashi, *Polym. Adv. Technol.* **1999**, *10,* 120.
[28] S. Shen, E. D. Sudol, M. S. El-Aasser, *J. Polym. Sci., Part A: Polym. Chem.* **1994**, *32,* 1087.

Macromol. React. Eng. **2007**, *1*, 86–94

Macromolecular Journals

DOI: 10.1002/mren.200600008

Příloha č. 7

(19) Europäisches Patentamt
European Patent Office
Office européen des brevets

(11) EP 1 991 503 B1

(12) **EUROPEAN PATENT SPECIFICATION**

(45) Date of publication and mention of the grant of the patent:
08.09.2010 Bulletin 2010/36

(21) Application number: **07711106.0**

(22) Date of filing: **23.02.2007**

(51) Int Cl.:
C01G 49/08 *(2006.01)* ***C01G 49/06*** *(2006.01)*
A61K 49/18 *(2006.01)* ***C09C 1/24*** *(2006.01)*

(86) International application number:
PCT/CZ2007/000012

(87) International publication number:
WO 2007/095871 (30.08.2007 Gazette 2007/35)

(54) **METHOD OF PREPARATION OF SUPERPARAMAGNETIC NANOPARTICLES BASED ON IRON OXIDES WITH MODIFIED SURFACE AND SUPERPARAMAGNETIC NANOPARTICLES OBTAINED BY SUCH A METHOD**

VERFAHREN ZUR HERSTELLUNG VON SUPERPARAMAGNETISCHEN NANOPARTIKELN AUF BASIS VON EISENOXIDEN MIT MODIFIZIERTER OBERFLÄCHE UND NACH DIESEM VERFAHREN HERGESTELLTE SUPERPARAMAGNETISCHE NANOPARTIKEL

PROCÉDÉ DE PRÉPARATION DE NANOPARTICULES SUPERPARAMAGNÉTIQUES À BASE D'OXYDES DE FER AYANT UNE SURFACE MODIFIÉE ET NANOPARTICULES SUPERPARAMAGNÉTIQUES OBTENUES PAR LEDIT PROCÉDÉ

(84) Designated Contracting States:
DE FR GB IT SK

(30) Priority: **24.02.2006 CZ 20060120**

(43) Date of publication of application:
19.11.2008 Bulletin 2008/47

(73) Proprietors:
- **Ustav Makromolekularni Chemie Akademie Ved Ceske Republiky, v.v.i**
  16206 Praha 6 (CZ)
- **Ustav Experimentalni Mediciny Akademie Ved Ceske Republiky, v.v.i.**
  142 20 Praha 4 (CZ)

(72) Inventors:
- **HORAK, Daniel**
  [redacted]
- **SYKOVA, Eva**
  [redacted]
- **BABIC, Michal**
  [redacted]
- **JENDELOVA, Pavla**
  [redacted]
- **HAJEK, Milan**
  [redacted]

(74) Representative: **Beetz & Partner Patentanwälte**
Steinsdorfstrasse 10
80538 München (DE)

(56) References cited:
EP-A2- 0 516 252
WO-A-91/02811
WO-A-97/35200
DE-A1- 2 642 383
US-A- 4 101 435
US-A- 4 452 773
US-A- 4 827 945
US-A- 5 492 814
US-A1- 2005 271 593

EP 1 991 503 B1

Description

Technical field

[0001] The invention concerns a method of preparation of superparamagnetic nanoparticle probes based on iron oxides with modified surface and superparamagnetic nanoparticles obtained by such a method.

Background art

[0002] The development of medical diagnostics in recent years aims more and more at earlier diagnosis of frequently very serious diseases. A part of the new techniques is cell labelling or cell imaging by magnetic resonance. Magnetic resonance imaging (MRI) makes it possible to visualize internal organs of humans and hence is a great contribution not only in diagnostics but also in therapy and surgery. Medical diagnostics requires the use of nanometre particles. MRI makes use of the fact that magnetic nanoparticles create a magnetic field and influence the environment (Shinkai M., Functional magnetic particles for medical application, J. Biosci Bioeng 94, 606-613, 2002). The range of particle sizes can be divided, depending on application, into "large" (diameter > 50 nm) and "small" (diameter < 50 nm) particles. MR diagnostics of liver and spleen is their main application field as the particles of this size are readily and almost completely taken up by the macrophages of these organs (Kresse M., Pfefferer D., Lawaczeck R., EP 516,252 A2; Groman E.V., Josephson L., U.S. Pat. 4,770,183). The particles find applications also in clinical hyperthermia (Hasegawa M., Nagae H., Ito Y., Mizutani A., Hirose K., Ohgai M., Yamashita Y., Tozawa N., Yamada K, Kito K, Hokukoku S., WO 92/22586 A1; Gordon R.T., U.S. Pat. 4,731,239).

[0003] For labelling of cells it is of key importance to prepare monocrystalline nanoparticles of an iron oxide dispersible in water, which are also biocompatible, superparamagnetic, surface functionalizable and which are, at the same time, completely taken up by the cells.

[0004] At present, superparamagnetic iron oxides (without magnetic memory) are the class of materials with the strongest contrast in MR (Gromann E.V., Josephson L., Lewis J. M., US 4 827 945 A; Stark D.D., Weissleder R., Elizondo G., Hahn P.F., Saini S., Todd L.E., Wittenberg J., Ferrucci J.T., Superparamagnetic iron oxide: clinical application as a contrast agent for MR imaging of the liver, Radiology 168, 297-301, 1988), hence they are in low concentrations especially suitable for tissue-specific applications. A critical size namely exists, below which the particles can have only a single magnetic domain even in zero magnetic field. The condition for superparamagnetism is $KV \sim kT$, where KV is the anisotropy energy (K is the anisotropy constant, V is the particle volume) and $k\,T$ is the thermal energy of motion (k is the Boltzmann constant, T is absolute temperature). If this condition is fulfilled, particle magnetization can be caused by thermal energy kT provided that it exceeds the potential barrier of anisotropic energy. The critical size of superparamagnetic particles of magnetite is ca. 25 nm. Superparamagnetic iron oxides make it possible to enhance the tissue contrast by increasing the relaxation rates of water. Varying the size, coating, thickness, surface chemical reactions and targeting ligands, the nanoparticle probes can be targeted on specific organs and cells or can even become *in vivo* molecular markers for various diseases. However, the size of crystal core of iron oxides, which causes a specific character to the materials, is problematic because it shows an essential influence on biological behavior. A small size of the particles improves their precise targeting but the efficiency of the material decreases due to interdependence of the particle size and magnetic moment. As a consequence, it is necessary to seek a compromise between good contrast effect of the material and precise targetability (Kresse M., Pfefferer D., Lawaczeck R., Wagner S. Ebert W., Elste V., Semmler W., Taupitz M. Gaida J., Herrmann A., Ebert M., Swiderski U., U.S. Pat. Appl. 2003,0185757). As a rule, the iron-containing core should be as large as possible to obtain a high imaging effect (contrast), but the overall diameter should be small.

[0005] Examples of MRI contrast agents include injectable nuclei, radionuclides, diamagnetic, paramagnetic, ferromagnetic, superparamagnetic materials, contrast materials containing iron (e:g., iron oxide, iron(III) ions, ammonium iron(III) citrate), gadolinnium agents (e.g. gadolinium diethylenetriaminepentaacetate) and manganese paramagnetic materials. Typical commercial MRI contrast agents are, e.g., Magnevist® and Resovist® (both Schering); Omniscan®; Feridex®, and Combidex® (all three Advanced Magnetics), Endorem® and Sinerem® (Guerbet), and Clariscan® (Nycomed). A number of various methods of preparation of crystals containing iron (iron oxides) with superparamagnetic properties have been described. These can be classified according to many aspects. Two basic methods of manufacture of superparamagnetic crystals are based on sintering at high temperature and subsequent mechanical disintegration or chemical synthesis in aqueous solution. For applications in medicine, effective particles were produced by wet synthetic techniques; in contrast, sintering is described for production of iron oxides for technological (audio/video media, pigments for dyes, toners) and biotechnological applications such as magnetic separations (Schostek S., Beer A., DE 3,729,697 A1; Borelli N.F., Luderer A.A., Panzarino J.N., U.S. Pat. 4,323,056; Osamu I., Takeshi H., Toshihiro M., Kouji N., JP 60,260,463 A2). The wet chemical synthesis can be divided into a "two-step" synthesis, which first prepares iron oxide-containing nuclei by increasing pH, to which is subsequently added a stabilizer providing physical and other required properties (Kresse M., Pfefferer D., Lawaczeck R., Wagner S., Ebert W., Elste V., Semmler W., Taupitz M. Gaida J.,

Herrmann A., Ebert M., Swiderski U., U.S. Pat. Appl. 20030185757). In a "one-step" synthesis, iron oxides are prepared by precipitation of iron salts in the presence of a stabilizer, which coats the nuclei in the course of nucleation and thus hinders aggregation and sedimentation of nanocrystals. In addition to classification into "two-step" and "one-step" methods, there exists another differentiation, according to the type of the used solvent, into the methods using water (Hasegawa M., Hokukoku S., U.S. Pat. 4,101,435; Fuji Rebio K.K, JP 59,195,161) or organic solvents (Porath J., Mats L., EP 179,039 A2; Aoyama S., Kishimoto M., Manabe T., Interaction between polymers and magnetic particles - effect on the properties of particulate magnetic recording media, J. Mater. Chem. 2, 277-280, 1992; Norio H., Saturo O., JP 05,026,879 A2). Various order of iron (II) and iron (III) mixing with base influences the amount of produced iron oxide (Kunda W. Rudyk B. DE 2 642 383 A1). The crude product must be always carefully purified and excess admixtures and impurities thus removed. The method of choice is then thermal sterilization. The iron oxides used at present are characterized by particle polydispersity expressed by the polydispersity index, PDI > 1.3. (PDI = D_w/D_n, where $D_n = \Sigma\, Di/N_a$ $D_w = \Sigma\, D_i^4/\Sigma\, D_i^3$; where N is the number of particles, Di is the diameter of an individual particle). Polydisperse particles have different physical and chemical properties, in contrast to monodisperse ones, the properties of which, including magnetic, are uniform. A drawback of classical magnetite particles also is that they change their properties in air. Their chemical instability causes uncontrolled oxidation with air oxygen, magnetic susceptibility decreases, the colloid loses stability and the nanoparticles aggregate, which is unacceptable for applications in medicine. Therefore, it is better to subject the freshly prepared magnetite particles, immediately after synthesis, to controlled oxidation to maghmite (γ-Fe_2O_3), which is stable in air and does not change its properties.

[0006] Generally, the surface of magnetic particles for imaging in medicine is covered by polymers. Almost all nanoparticles commonly used in medicine at present are iron oxides prepared in the presence of polysaccharide dextran as stabilizer (Weissleder R. US 5 492 814 A; Hasegawa M., Hokukoku S., US 4 101 435, Bacic G., Niesman M.R, Bennett H.F., Magin R.L., Schwarz H.M., Modulation of water proton relaxation rates by liposomes containing paramagnetic materials, Magn. Reson. Med. 6, 445-58, 1988; Ohgushi M., Nagayama K., Wada A., Dextran-magnetite: a new relaxation agent and its application to T2 measurements in gel systems, J. Magn. Reson. 29, 599-601, 1978; Pouliquen D., Le Jeune J.J., Perdrisot R., Ermias A., Jallet P., Iron oxide nanoparticles for use as an MRI contrast agent pharmacokinetics and metabolism, Magn. Reson. Imaging 9, 275-283, 1991; Ferrucci J.T., Stark D.D., Iron oxide-enhanced MR imaging of the liver and spleen: review of the first 5 years, Am. J. Roentgenol. 155, 943-950, 1990). Synthesis of such particles is usually performed according to the Molday procedure (Molday R.S. US 4 452 773 A), (Molday R.S., MacKenzie D., Immunospecific ferromagnetic iron-dextran agents for the labelling and magnetic separation of cells, J. Immunol. Methods 52, 353-367, 1982) requiring laborious and costly purification procedures. Dextran, however, is chemically instable, for example it depolymerizes in acid medium and various other reactions may lead to its complete destruction in alkaline medium. Moreover, cells take up the dextran-covered nanoparticles insufficiently, which does not facilitate perfect MR monitoring of cells, probably due to relatively inefficient endocytosis. In addition to dextran, the use of other polysaccharides is described such as arabinogalactan (Josephson L., Groman E.V., Menz E., Lewis J.M., Bengele H., A functionalized superparamagnetic iron oxide colloid as a receptor directed MR contrast agent, Magn. Reson. Imaging 8, 637-646, 1990), starch (Fahlvik A.K., Holtz E., Schroder U., Klaveness J., Magnetic starch microspheres, biodistribution and biotransformation. A new organ-specific contrast agent for magnetic resonance imaging, Invest. Radiol. 25, 793-797, 1990), glycosaminoglycans (Kresse M. EP 0 516 252 A2), (Kresse M., Wagner S., Pfefferer D., Lawaczeck R., Elste V., Semmler W., Targeting of ultrasmall superparamagnetic iron oxide (USPIO) particles to tumor cells in vivo by using transferrin receptor pathways, Magn. Reson. Med. 40, 236-42, 1998) or proteins (Widder D.J., Greif W.L., Widder K.J., Edelman R.R., Brady T.J., Magnetite albumin microspheres: a new MR contrast material, Am. J. Roentgenol. 148, 399-404, 1987) such as albumin, even antibodies (Liberti P.A. ,WO 91/02811) or synthetic polymers such as polymethacrylates and polysilanes. Also transfection agents are described including also poly(amino acid)s (polyalanines, poly (L-arginine)s, DNA of salmon eggs, poly(L-omithine)s), dendrimers, polynucleotides (Frank J.A., Bulte J.W.M., Pat. WO 02100269 A1), polyglutamate, polyimines (Van Zijk P., Goffeney N., Duyn J.H., Bulte J.W.M., Pat. WO 03049604 A3).

[0007] Polymer coating considerably increases the particle size, which can affect their penetration and the rate of their metabolic removal in the body. Recently, also dispersions of bare superparamagnetic nanoparticles (polymer-uncoated) for MR imaging were described (Cheng F.-Y., Su C.-H., Yang Y.-S., Yeh C.-S., Tsai C.-Y., Wu C.-L., Wu M.-T., Shieh D.-B., Characterization of aqueous dispersions of Fe3O4 nanoparticles and their biomedical applications, Biomaterials 26, 729-738, 2005). They were prepared in water and stabilized with, e.g., a citrate monomer (Taupitz M., Schnorr J., Wagner S.A., Abramjuk C., Pilgrimm H., Kivelitz D., Schink T., Hansel J., Laub G., Humogen H., Hamm B., Coronary MR angiography: experimental results with a monomer-stabilized blood pool contrast medium, Radiology 222, 120-126, 2002) or tetramethylammonium hydroxide (Cheng F.-Y., Su C.-H., Yang Y.-S., Yeh C.-S., Tsai C.-Y., Wu C.-L., Wu M.-T., Shieh D.-B., Characterization of aqueous dispersions of Fe3O4 nanoparticles and their biomedical applications, Biomaterials 26, 729-738, 2005). The nanoparticles allegedly bring some advantages over those that require a polymer addition to be protected against aggregation.

[0008] Stem cells show the ability to differentiate into any specialized cell of the organism and that is why they are in the centre of interest of human medicine, in particular regenerative medicine and cell therapy, where their utilization can

be assumed. (Park H.C., Shims Y.S., Ha Y., Yoon S.H., Park S.R., Choi B.H., Park H.S., Treatment of complete spinal cord injury patients by autologous bone marrow cell transplantation and administration of granulocyte-macrophage colony stimulating factor, Tissue Eng. 11, 913-922, 2005; Akiyama Y., Radtke C., Honmou O., Kocsis J.D., Remyelination of the spinal cord following intravenous delivery of bone marrow cells, Glia 39, 229-236, 2002; Akiyama Y., Radtke C., Kocsis J.D., Remyelination of the rat spinal cord by transplantation of identified bone marrow stromal cells, J. Neurosci. 22, 6623-6630, 2002; Hofstetter C.P., Schwarz E.J., Hess D., Widenfalk J., El Manira A., Prockop J.D., Olson, L., Marrow stromal cells form guiding strands in the injured spinal cord and promote recovery, Proc. Natl. Acad. Sci. USA 96, 2199-2204, 2002; Chen J., Li Y., Katakowski M., Chen X., Wang L., Lu D., Intravenous administration of human bone marrow stromal cells induces angiogenesis in the ischemic boundary zone after stroke in rats, Circ. Res 92, 692, 2003; Chen J., Zhang Z.G., Li Y., Wang L., Xu Y.X., Gautam S.C., Intraarterial administration of marrow stromal cells in a rat model of traumatic brain injury, J.Neurosci.Res. 73, 778-786, 2003; Chopp M., Li Y., Treatment of neural injury with marrow stromal cells, Lancet Neurol. 1, 92-100, 2002; Chopp M., Zhang X.H., Li Y., Wang L., Chen J., Lu D., Spinal cord injury in rat: treatment with bone marrow stromal cell transplantation, Neuroreport 11, 3001-3005, 2000; Ramon-Cueto A., Plant G.W., Avila J., Bunge M.B., Long-distance axonal regeneration in the transected adult rat spinal cord is promoted by olfactory ensheathing glia transplants, J. Neurosci. 18, 3803-3815, 1998; Syková E., Urdziková L., Jendelová P., Burian M., Glogarová K., Hájek M., Bone marrow cells - a tool for spinal cord injury repair, Exp. Neurol. 193, 261-262, 2005).

Disclosure of invention

[0009] The subject of the invention is surface-modified superparamagnetic nanoparticle probes based on iron oxides for diagnostic and therapeutical applications. Superparamagnetic nanoparticle probes based on iron oxides, to advantage magnetite or maghemite, with modified surface are formed by a colloid consisting of particles, the size of which ranges from 10 to 30 nm, and their polydispersity index is smaller than 1.3. Their surface is coated with mono-, di- or polysaccharides, amino acids or poly(amino acid)s or synthetic polymers based on (meth)acrylic acid and their derivatives. The saccharides are selected from the group formed by D-arabinose, D-glucose, D-galactose, D-mannose, lactose, maltose, dextrans, dextrins. The amino acid or poly(amino acid) is selected from the group formed by polyalanine, polyglycine, polyglutamine, polyasparagine; polyhistidine, polyarginine, poly(L-lysine), poly(aspartic acid) and poly(glutamic acid). Polymers of derivatives of (meth)acrylic acid are selected from the group containing poly(*N,N* dimethylacrylamide), poly (*N,N*-dimethylmethacrylamide), poly(*N,N*-diethylacrylamide), poly(*N,N*-diethylmethacrylamide), poly(*N*-isopropylacrylamide), poly(N-isopropylmethacrylamide). The surface layer of a modification agent amounts to 0.1-30 wt.%, to advantage 10 wt.%, and the iron oxide content to 70-99.9 wt.%, to advantage 90 wt.%. The agents on the surface of particles enable their penetration into cells.

[0010] Superparamagnetic nanoparticle probes according to the invention are prepared by preprecipitation of colloidal $Fc(OH)_3$ by the treatment of aqueous 0.1-0.2M solution of Fe(III) salt, to advantage $FeCl_3$, with less than an equimolar amount of NH_4OH, at 21 °C, under 2-min sonication at 350 W. To the hydroxide, 0.1-0.2 M solution of a Fe(II) salt, to advantage $FeCl_2$, is added in the mole ratio Fe(III)/Fe(II) = 2 under 2-min sonicadon and the mixture is poured into five- to tenfold, to advantage eightfold, molar excess of 0.5 M NH_4OH. The mixture is left aging for 0-30 min, to advantage 15 min, and then the precipitate is repeatedly, to advantage 7-10 time, magnetically separated and washed with deionized water of resistivity 18 $M\Omega \cdot cm^{-1}$. In contrast to the present state-of-the-art, 1-3 fold amount, to advantage 1.5 fold amount relative to the amount of magnetite, of 0.1 M aqueous solution of sodium citrate is added and then, dropwise, 1-3 fold amount, to advantage 1.5 fold amount relative to the amount of magnetite, of 0.7 M aqueous solution of sodium hypochlorite. The precipitate is repeatedly, to advantage 7-10 times, washed with deionized water of resistivity 18 $M\Omega \cdot cm^{-1}$, under the formation of colloidal maghemite to which, after dilution, is added dropwise, possibly under 5-min sonication, an aqueous solution of a modification agent in the weight ratio modification agent/iron oxide 0.1-10, to advantage 0.2 for amino acids and poly(amino acid)s and 5 for saccharides.

[0011] The thus prepared nanoparticles reach the size around 10 nm, according to transmission electron microscopy (TEM), with comparatively narrow size distribution characterized by PDI < 1.3. The colloidal stability of the particles in water is a consequence of the presence of the charges originating from Fe(III) and citrate ions.

[0012] An essential feature of the preparation of superparamagnetic nanoparticle probes with modified surface according to the invention consists in the fact that slow addition of a solution of modification agent follows precipitation. At that, the modification agent nonspecifically adsorbs on the iron oxide surface. The interaction is a consequence of hydrogen bonds between the polar OH groups of the modification agent and hydroxylated and protonated sites on the oxide surface, or of the agent charge interacting with the citrate complexed on the iron oxide surface. The particles coated with the modification agent do not aggregate as was confirmed by TEM micrographs, according to which the size of surface-modified particles was the same as that of starting iron oxide particles.

[0013] Nanoparticles are modified with the agents based on poly(amino acid)s such as polyalanine, polyglycine, polyglutamine, polyasparagine, polyarginine, polyhistidine or polylysine, poly(aspartic acid) and poly(glutamic acid),

monosaccharides (e.g. arabinose, glucose, mannose, galactose), disaccharides (e.g. lactose, maltose) and polysaccharides including starch, dextrans and dextrins, and polymers of derivatives of (meth)acrylic acid (e.g. poly(*N*,*N*-dimethylacrylamide), poly(*N*,*N*-dimethylmethacrylamide), poly(*N*,*N*-diethylacrylamide), poly(*N*,*N*-diethylmethacrylamide), poly (*N*-isopropylacrylamide), poly(*N*-isopropylmethacrylamide)).

[0014] Superparamagnetic nanoparticle probes with modified surface according to the invention are designed for labelling of living cells, in particular stem cells. The method will find broad applications in monitoring cells suitable for cell therapy (e.g., stem cells of bone marrow, olfactory glial cells, fat tissue cells). After administration of cells, their fate can be monitored in the recipient body by a noninvasive method, magnetic resonance.

[0015] It was found experimentally that the capability of targeting superparamagnetic nanoparticle probes according to the invention in cells is significantly better than with iron oxide particles according to the hitherto used methods. The uptake of poly(amino acid)-modified iron oxide nanoparticles by cells is made possible by their interaction with negatively charged cell surface and subsequent endosomolytic absorption. The nanoparticles are in this way transferred into endosomes, fused with lysosomes under simultaneous destruction of vesicular membrane. Another mechanism of transport of nanoparticle probes into cells may consist in the mannose transporter present on the surface of many types of mammalian cells. Compared with Endorem® (0.11 mg Fe_3O_4, per ml of medium), considerably lower concentrations of iron oxide nanoparticles modified according to the invention were sufficient for complete labelling of cells. An additional advantage is that the patient organism is considerably less loaded with applied particles than it is necessary when using currently commercially available agents.

[0016] The invention provides a tool for monitoring the history and fate of cells transplanted into organism including their *in vivo* migration. Nanoparticle probes according to the invention are suitable for determination of diagnoses of pathologies associated with cellular dysfunction. First, the stem cells of the patient are labelled *ex vivo*. In cell labelling, 5-20 μl, to advantage 10 μl, of a colloid containing 0.05-45 mg iron oxide per ml, to advantage 1-5 mg iron oxide per ml of the medium, is added to complete the culture medium and the cells are cultured for 1-7 days, to advantage for 1-3 days, at 37 °C and 5 % of CO_2. During the culturing, the cells fagocytize nanoparticles from the medium to cytoplasm. The thus labelled cells are introduced
into the patient organism, which, when using magnetic field, makes it possible to monitor the movement, localization and survival of exogenous cells by MRI imaging and thus to reveal pathologies associated with cellular dysfunctions.

Examples

Example 1

Preparation of starting (uncoated) superparamagnetic iron oxide nanoparticles

[0017] 12 ml of aqueous 0.2 M $FeCl_3$ was mixed with 12 ml of aqueous 0.5 M NH_4OH under sonication (Sonicator W-385; Heat Systems-Ultrasonics, Inc., Farmingdale, NY, USA) at laboratory temperature for 2 min. Then 6 ml of aqueous 0.2 M $FeCl_2$ was added under sonication and the mixture was poured into 36 ml of aqueous 0.5 M NH_4OH. The resulting magnetite precipitate was left aging for 15 min, magnetically separated and repeatedly (7-10 times) washed with deionized water of resistivity 18 $M\Omega \cdot cm^{-1}$ to remove all residual impurities (including NH_4Cl). Finally, 1.5 ml of aqueous 0.1 M sodium citrate was added under sonication and magnetite was oxidized by slow addition of 1 ml of 5 % aqueous solution of sodium hypochlorite. The above procedure of repeated washing afforded the starting primary colloid.

[0018] For determination of the nanoparticle size, dynamic light scattering (DLS) was used, which gave the average hydrodynamic diameter of particles amounting to 90 ± 3 nm, suggesting a narrow size distribution. From TEM micrograph, then D_n = 6.5 nm a PDI = 1.26. PDI is the polydispersity index characterizing the size distribution width, PDI = D_w/D_n, where D_w and D_n are the weight- and number-average particle diameter.

Example 2

Treatment of superparamagnetic iron oxide nanoparticles with poly(amino acid)s - "two-step synthesis"

[0019] To 10 ml of the starting colloid solution containing iron oxide nanoparticles prepared according to Example 1 and diluted to the concentration 2.2 mg iron oxide/ml, 0.01-2 ml (typically 0.2 ml) of aqueous solution of a poly(amino acid) of concentration 0.5-10 mg/ml (typically 1 mg/ml) was added dropwise under stirring and the mixture was sonicated for 5 min.

[0020] The poly(amino acid) can be polyalanine, polyglycine, olyglutamine, polyasparagine, polyarginine, polyhistidine or poly(L-lysine), poly(aspartic acid) and poly(glutamic acid).

Example 3

Treatment of superparamagnetic iron oxide nanoparticles with saccharides - "two-step synthesis"

[0021] Various volumes (0.1-5 ml) of 4 wt.% aqueous solution of a saccharide were added dropwise under stirring to 10 ml of the starting colloid solution containing iron oxide nanoparticles prepared according to Example 1, diluted to the concentration 2.2 mg iron oxide/ml and the mixture was sonicated for 5 min. The particles were repeatedly washed.

[0022] The saccharide can be D-arabinose, D-glucose, D-galactose, D-mannose, lactose, maltose, dextrans, dextrins.

Example 4

Treatment of superparamagnetic iron oxide nanoparticles with (meth)acrylic acid derivatives - "two-step synthesis"

[0023] To an 0.003-0.07 wt.% (typically 0.03 wt.%) solution of 4,4'-azobis(4-cyanopentanoic acid) was added a corresponding amount of the colloid containing 0.1-2 g (typically 0.5 g) of particles prepared according to Example 1 so that the total volume of the mixture was 30 ml. To the solution was added 0.1-2 (typically 1) g of a (meth)acrylic acid derivative, the solution was bubbled with nitrogen for 10 min and heated at 70 °C for 8 h under stirring (400 rpm). The resulting product was repeatedly (3-5 times) magnetically separated or centrifuged (14 000 rpm), washed with water or isotonic 0.15 M sodium chloride and sonicated until the formation of a colloidal solution.

[0024] The (meth)acrylic acid derivative can be poly(*N,N*-dimethylacrylamide), poly(*N,N*-dimethylmethacrylamide), poly(*N,N*-diethylacrylamide), poly(*N,N*-diethylmethacrylamide), poly(*N*-isopropylacrylamide), poly(*N*-isopropylmethacrylamide).

Example 5

Example 5

Optical microscopy of labelled cells

[0025] Stromal cells of bone marrow (MSC) of rat labelled by both starting uncoated and surface-modified superparamagnetic iron oxide nanoparticles were observed in optical microscope. The cells labelled with Endorem® (0.11 mg Fe_3O_4/ml) served as control (Fig. 1a). A drawback of Endorem® was its tendency to adhere to the cell surface; moreover, it sticked also to the bottom of vessel.

[0026] The cells in contact with starting (uncoated) nanoparticles prepared according to Example 1 proliferated and approximately one of every ten cells endocytized iron oxide nanoparticles of iron oxide (Fig. 1 b).

[0027] From observation of the cells in contact with superparamagnetic nanoparticles modified with D-mannose by the "two-step method" (after the synthesis) according to Example 3, the
optimum concentration of D-mannose added to the colloid was assessed amounting to 12.8 mg D-mannose per ml of the colloid, which ensures labelling of ca. 50 % of cell population (Fig. 1c)

[0028] Maximum labelling of cells (almost 100 %) was achieved with poly(L-lysine)-modified nanoparticles (0.02 mg poly(L-lysine) per ml colloid (Fig. 1d)).

Example 6

Transmission electron microscopy of cells labelled with superparamagnetic iron oxide nanoparticles

[0029] Transmission electron micrograph of MSC cells labelled with superparamagnetic nanoparticles of iron oxide modified with D-mannose according to Example 3 and with poly(L-lysine) (PLL) according to Example 2 is shown in Fig. 3. Numerous aggregates of both types of superparamagnetic nanoparticles inside cells labelled with nanoparticles modified with both D-mannose and poly(L-lysine) are visible. The nanoparticle aggregates were evenly distributed in cell cytoplasm; their accumulation on cell membranes was not perceptible.

Example 7

Quantitative determination of cells labelled with superparamagnetic iron oxide nanoparticles

[0030] Superparamagnetic iron oxide nanoparticles modified with both poly(L-lysine) according to Example 2 and with

D-mannose according to Example 3 were successfully endocytized by MSC cells (as follows from Figs. 1 and 2). MSC cells were cultivated in duplicate on uncoated six-well culture plates at the density 10^5 cells per mm^2. Endorem® and the nanoparticles modified with poly(L-lysine) or D-mannose were added to culture medium (10 μl/ml) and the cells incubated for 72 h. After washing out excess contrast substance with the culture medium, the cells were fixed with 4 % solution of paraformaldehyde in 0.1 M phosphate buffer (PBS) and tested for iron under the formation of iron(III) ferrocyanide (Prussian Blue). The number of labelled and unlabelled cells was determined in an inverted light microscope (Axiovert 200, Zeiss) by counting randomly selected five fields per well and two wells per each run (Table 1). The cells in each image were manually labelled as Prussian Blue-positive or negative; the number of labelled cells was then counted using the image analysis toolbox in program Matlab 6.1 (The MathWorks, Natick, MA, USA). The best labelling of cells was obtained with nanoparticles containing 0.02 mg poly(L-lysine) per ml of colloid.

Table 1. Percentage of stromal cells of bone marrow (MSC) labelled *in vitro* with superparamagnetic nanoparticles

	Uncoated iron oxide	PLL-modifid iron oxide (0.02 mg PLL/ml)	D-Mannose-modified iron oxide	Endorem®
MSC (rat)	27.9	92.2	50.8	60.0
MSC (human)	not tested	87.5	not tested	65.2

Example 8

Relaxivity of cells labelled with superparamagnetic iron oxide nanoparticles modified with poly(L-lysine)

[0031] To further verify the presence of poly(L-lysine)-modified superparamagnetic iron oxide nanoparticles prepared according to Example 2 in bone marrow cells (MSCs), samples with suspension of Endorem® and poly(L-lysine)-modified superparamagnetic nanoparticles in a 4% gelatin solution and samples with suspensions of Endorem®-labelled cells and poly(L-lysine)-modified superparamagnetic nanoparticles with various amounts of cells in gelatin solution were prepared. Subsequently, relaxation times of samples were measured and their MR images were obtained.

[0032] For determination of relaxation times T_1 a T_2, a relaxometer Bruker Minispec 0.5 T was used. The values were recalculated to proton relaxivities $R_1=1/T_1$, $R_2 = 1/T_1$ and related to real concentrations $r_1= R_1/c$ (s^{-1}/mmol), $r_2 = R_2/c$ (s^{-1}/mmol), or they were related to the number of cells in 1 ml, where R_2 and R_1 are corrected for gelatin. The relaxivity values are given in Tables 2 and 3. From Table 3 follows that the r_2 value of poly(L-lysine)-modified superparamagnetic iron oxide nanoparticles according to Example 2 is considerably higher than with Endorem®.

Table 2. η values of poly(L-lysine)-modiried superparamagnetic iron oxide nanoparticles (PLL) and Endorem®

	Relaxivity r_1 of suspension of contrast agent in gelatin (s^{-1}/mmol Fe)	Relaxivity r_1 of suspension of labelled cell in gelatin ($s^{-1}/10^6$ cells per ml)
PLL-modified iron oxide	17.4	0.32
Endorem	19.6	0.18

Table 3. r_2 values of poly(L-lysine)-modified superparamagnetic iron oxide nanoparticles (PLL) and Endorem®

	Relaxivity r_2 of contrast material suspension in gelatin (l^{-1}/mmol Fe)	Relaxivity r_2 of labelled cell suspension in gelatin ($s^{-1}/10^6$ cells per ml)
PLL-modified iron oxide	213	4.29
Endorem®	126	1.24

The average iron content determined spectrophotometrically after mineralization amounted to 35.9 pg Fe per cell in poly (L-lysine)-modified superparamagnetic iron oxide nanoparticles and 14.6 pg Fe per cell in Endorem®-labelled cells

Example 9

[0033] ***In vitro*** **MR imaging of cells labelled with superparamagnetic nanoparticle probes** Imaging of labelled cells *in vitro* is advantageous for proof of MRI sensitivity and, at the same time, for imitating the course of the signal in brain tissue. Rat MSC cells were labelled with poly(L-lysine)-modified superparamagnetic iron oxide nanoparticles according to Example 2 and a cell suspension in a 4 % gelatin solution of concentration 4,000, 2,000, 1,600, 1,200, 800, 400 and 200 cells per μl was prepared. The unlabelled MSC rat cells were suspended in a 4 % gelatin solution of concentration 4,000, 1,200 and 200 cells per μl.

[0034] The cell samples were subsequently imaged with a 4.7 T Bruker spectrometer using standard turbospin sequence (sequence parameters: repetition time TR = 2 000 ms, effective echo-time TE = 42.5 ms, turbo factor = 4, number of acquisitions AC = 16, image field FOV = 64 x 64 mm, matrix MTX = 512 x 512, layer thickness 0.75 mm; the set geometry affords a comparable size of voxel as in *in vivo* measurement) and the gradient echo sequence (TR = 180 ms, TE = 12 ms, the same geometry of imaging).

[0035] When using both sequences, the cells labelled with poly(L-lysine)- or D-mannose-modified superparamagnetic iron oxide nanoparticles modified with poly(L-lysine) (Fig. 3 A, B) or D-mannose afford an excellent contrast compared with unlabelled cells. A visible contrast in MR image was observed also in a sample, each image voxel of which contained mere 2.3 cells on average. A similar series of experiments were given in the preceding work (Jendelová. P., Herynek V., DeCroos J., Glogarová K, Andersson B., Hájek M., Syková E., Imaging the fate of implanted bone marrow stromal cells labeled with superparamagnetic nanoparticles, Magn. Reson. Med. 50, 767-776, 2003), where MR imaging of gelatin phantoms showed a hypointensive signal at concentrations above 625 cells per μl.

Example 10

In vivo **MR imaging of cells labelled with superparamagnetic nanoparticle probes**

[0036] Wistar rats were in the course of measurement. The rats were monitored for 3 days after transplantation in a Broker 4.7 T spectrometer equipped with a surface coil of domestic production. Simple sagital, coronal and transverse scans were obtained by a fast gradient echo sequence for localization of subsequent T_2- and T_2*-weighted images measured by standard turbospin sequence (TR = 2 000 ms, TE = 42.5 ms, turbo factor = 4, AC = 16, FOV = 30 x 30 mm, matrix MTX 256 x 256, layer thickness 0.75 mm) and gradient echo sequence (TR = 180 ms, TE = 12 ms, the same geometry of imaging). Figure 3C proves that cells labelled with poly(L-lysine)-modified superparamagnetic iron oxide nanoparticles according to Example 2 were clearly discernible also *in vivo.* Unlabelled cell implants were visible in MR images as a tissue inhomogeneity without a hypotensive signal (Fig. 3C).

Industrial applicability

[0037] The invention can be exploited in human and veterinary medicine, biology and microbiology.

Claims

1. Method of preparation of superparamagnetic nanoparticle probes **characterized in that** colloidal $Fe(OH)_3$ is pre-precipitated by the treatment of aqueous 0.1-0.2 M solution of Fe(III) salt, to advantage $FeCl_3$, under sonication, with less than an equimolar amount of NH_4OH, at 21 °C, to which 0.1-0.2 M solution of a Fe(II) salt, to advantage $FeCl_2$, is added in the mole ratio Fe(III)/Fe(II) = 2 and the mixture is poured into five- to tenfold, to advantage eightfold, molar excess of 0.5 M NH_4OH, the mixture is left aging for 0-30 min, to advantage for 15 min, then the precipitate is repeatedly, to advantage 7-10 times, magnetically separated and washed with deionized water of resistivity 18 $M\Omega\,cm^{-1}$, then a 1-3 fold amount, to advantage 1.5 fold amount relative to the amount of magnetite, of 0.1 M aqueous solution of sodium citrate is added under sonication and then, dropwise, 1-3 fold amount, to advantage 1.5 fold amount relative to the amount of magnetite, of 0.7 M aqueous solution of sodium hypochlorite. The precipitate is repeatedly, to advantage 7-10 times, washed with deionized water of resistivity 18 $M\Omega\,cm^{-1}$, under the formation of colloidal maghemite to which, after dilution, is added dropwise, possibly under 5-min sonication, an aqueous solution of a modification agent in the weight ratio modification agent/iron oxide 0.1-10, to advantage 0.2 for poly (amino acid)s and 5 for saccharides.

2. Superparamagnetic nanoparticle probes based on iron oxides, to advantage magnetite or maghemite, with modified surface obtained with the method according to claim 1, **characterized in that** they are coated with mono-, di- or polysaccharides from the group including D-arabinose, D-glucose, D-galactose, D-mannose, lactose, maltose or

poly(amino acid)s from the group including polyalanine, polyglycine, polyglutamine, polyasparagine, polyhistidine, polyarginine, poly(L-lysine), poly(aspartic acid) and poly(glutamic acid) or polymers of (meth)acrylic acid derivatives from the group containing poly(*N,N*-dimethylacrylamide), poly(*N,N*-dimethylmethacrylamide), poly(*N,N*-diethylacrylamide), poly(*N,N*-diethylmethacrylamide), poly(*N*-isopropylacrylamide), poly(*N*-isopropylmethacrylamide) and form a colloid consisting of particles with narrow size distribution with polydispersity index lower than 1.3, the average size of which ranges from 10 to 30 nm, iron oxide content amounts to 70-99.9 wt.%, to advantage 90 wt.%, the modification agent content makes 0.1-30 wt.%, to advantage 10 wt.%.

Patentansprüche

1. Verfahren zur Herstellung superparamagnetischer Nanopartikelsonden, **dadurch gekennzeichnet, dass** kolloidales $Fe(OH)_3$ durch die Behandlung von 0,1 - 0,2 M wässeriger Lösung eines Fe(III)-Salzes, vorzugsweise von $FeCl_3$, unter Ultraschallbehandlung mit weniger als einer äquimolaren Menge an NH_4OH bei einer Temperatur von 21 °C ausgefällt wird, zu der eine 0,1 -0,2 M Lösung eines Fe(II)-Salzes, vorzugsweise $FaCl_2$, in einem Molverhältnis Fe (III)/Fe(II) = 2 hinzugefügt wird, das Gemisch in einen 5- bis 10-fachen, vorzugsweise 8-fachen, molaren Überschuss von 0,5 M NH_4OH gegeben wird, das Gemisch für 0 - 30 min, vorzugsweise 15 min, ruhen gelassen wird, worauf der Niederschlag mehrfach, vorzugsweise 7- bis 10-mal magnetisch getrennt und mit entionisiertem Wasser mit einem Widerstand von 18 $M\Omega cm^{-1}$ gewaschen wird, dann eine 1- bis 3-fache Menge, vorzugsweise eine 1,5-fache Menge, bezogen auf die Magnetitmenge, einer 0,1 M wässerigen Lösung von Natriumcitrat unter Ultraschallbehandlung hinzugefügt wird und dann tropfenweise eine 1- bis 3-fache Menge, vorzugsweise eine 1,5-fache Menge, bezogen auf die Magnetitmenge, einer 0,7 M wässerigen Lösung von Natriumhypochlorit hinzugefügt wird, und der Niederschlag wiederholt, vorzugsweise 7- bis 10-mal, mit entionisiertem Wasser mit einem Widerstand von 18 $M\Omega cm^{-1}$ unter Bildung von kolloidalem Maghemit gewaschen wird, zu dem nach Verdünnung tropfenweise, gegebenenfalls unter einer 5-minütigen Ultraschallbehandlung, eine wässerige Lösung eines Modifikators in einem Gewichtsverhältnis Modifikator/Eisenoxid von 0,1-10, vorzugsweise 0,2 für Polyaminosäuren und vorzugsweise 5 für Saccharide, hinzugefügt wird.

2. Superparamagnetische Nanopartikelsonden auf der Basis von Eisenoxiden, vorzugsweise Magnetit oder Maghemit, mit einer durch das Verfahren gemäß Anspruch 1 modifizierten Oberfläche, **dadurch gekennzeichnet, dass** die Nanopartikel mit Mono-, Di- oder Polysacchariden aus der Gruppe umfassend D-Arabinose, D-Glucose, D-Galactose, D-Mannose, Lactose und Maltose, oder Polyaminosäuren aus der Gruppe umfassend Polyalanin, Polyglycin, Polyglutamin, Polyasparagin, Polyhistidin, Polyarginin, Poly-L-lysin), Polyasparaginsäure und Polyglutaminsäure, oder Polymeren von (Meth)acrylsäurederivaten aus der Gruppe Poly(N,N-dimethylacrylamid), Poly(N,N-dimethylmethacrylamid), Poly(N,N-diethylacrylamid), Poly(N,N-diethylmethacrylamid), Poly(N-isopropylacrylamid), Poly(N-isopropylmethacrylamid) beschichtet sind, und die Nanopartikel ein Kolloid bilden, bestehend aus Partikeln mit einer engen Größenverteilung mit einem Polydispersitätsindex kleiner als 1,3, wobei die mittlere Größe im Bereich von 10 bis 30 nm liegt, und der Eisenoxidgehalt 70 bis 99,9 Gew.-%, vorzugsweise 90 Gew.-%, beträgt, und der Modifikatorgehalt 0,1 -30 Gew.-%, vorzugsweise 10 Gew.-%, ausmacht.

Revendications

1. Méthode de préparation de sondes à nanoparticules super paramagnétiques **caractérisée en ce que** du $Fe(OH)_3$ colloïdal est préprécipité par le traitement d'une solution aqueuse de 0.1 à 0.2M de sel de Fe(III), de préférence de $FeCl_3$, sous ultrasons, avec une quantité inférieure à une quantité équimolaire de NH_4OH, à 21°C, puis on ajoute une solution de 0.1 à 0.2 M de sel de Fe(II), de préférence de $FeCl_2$, dans un rapport molaire de Fe(III)/Fe(II) égal à 2, et le mélange est versé dans un excédent molaire d'un facteur 5 à 10, de préférence d'un facteur 8, de NH_4OH 0.5 M, on laisse agir le mélange pendant 0 à 30 min, de préférence pendant 15 min, et ensuite, à plusieurs reprises, de préférence 7 à 10 fois, le précipité est séparé magnétiquement et est lavé avec de l'eau déminéralisée ayant une résistivité de 18 $M\Omega\,cm^{-1}$. Ensuite une quantité d'une solution aqueuse 0.1M de citrate de sodium de 1 à 3 fois, de préférence de 1.5 fois, la quantité de magnétite est ajoutée en appliquant des ultrasons et ensuite, goutte à goutte, une quantité d'une solution aqueuse 0.7 M d'hypochlorite de sodium de 1 à 3 fois, de préférence 1.5 fois, la quantité de magnétite. Le précipité est lavé à plusieurs reprises, de préférence 7 à 10 fois, avec de l'eau déminéralisée ayant une résistivité de 18 $M\Omega\,cm^{-1}$, jusqu'à la formation de maghémite colloïdale à laquelle, après dilution, on ajoute goutte à goutte, éventuellement en appliquant des ultrasons pendant 5 min, une solution aqueuse d'un agent de modification, dans un rapport en poids de l'agent de modification/oxyde de fer compris entre 0.1 et 10, de préférence égal à 0.2 pour les poly(acides aminés) et à 5 pour les saccharides.

2. Sondes à nanoparticules super paramagnétiques à base d'oxydes de fer, de préférence de magnétite ou de maghémite, ayant une surface modifiée obtenue à l'aide de la méthode selon la revendication 1, **caractérisées en ce qu'**elles sont recouvertes de monosaccharides, de disaccharides ou de polysaccharides provenant du groupe comprenant le D-arabinose, le D-glucose, le D-galactose, le D-mannose, le lactose et le maltose, ou recouvertes de poly(acides aminés) provenant du groupe comprenant la polyalanine, la polyglycine, la polyglutamine, la polyasparagine, la polyhistidine, la polyarginine, la poly(L-lysine), le poly(acide aspartique) et le poly(acide glutamique) ou recouvertes de polymères de dérivés d'acide (méth)acrylique provenant du groupe contenant le poly(*N,N*-diméthylacrylamide), le poly(*N,N*-diméthylméthacrylamide), le poly(*N,N*-diéthylacrylamide), le poly(*N,N*-diéthylméthacrylamide), le poly(*N*-isopropylacrylamide), le poly(*N*-isopropylméthacrylamide), et forment un colloïde constitué de particules ayant une répartition granulométrique étroite avec un indice de polydispersité inférieur à 1.3, dont la taille moyenne est comprise entre 10 et 30 nm, dont la teneur en oxyde de fer est de 70 à 99,9 % en poids, de préférence de 90 % en poids, et dont la teneur en agent de modification est de 0.1 à 30 % en poids, de préférence de 10 % en poids.

Figures

Fig. 1. Microscopic observation of stromal marrow bone cells labelled with (a) Endorem® (control experiment, concentration 0.11 mg Fe_3O_4/ml), (b) starting uncoated superparamagnetic iron oxide nanoparticles, (c) superparamagnetic iron oxide nanoparticles modified with D-mannose according to the "two-step method" (concentration 0.022 mg iron oxide/ml) and (d) superparamagnetic iron oxide nanoparticles modified with poly(L-lysine) (concentration 0.022 mg iron oxide/ml). Scale (a-c) 100 μm, (d) 50 μm.

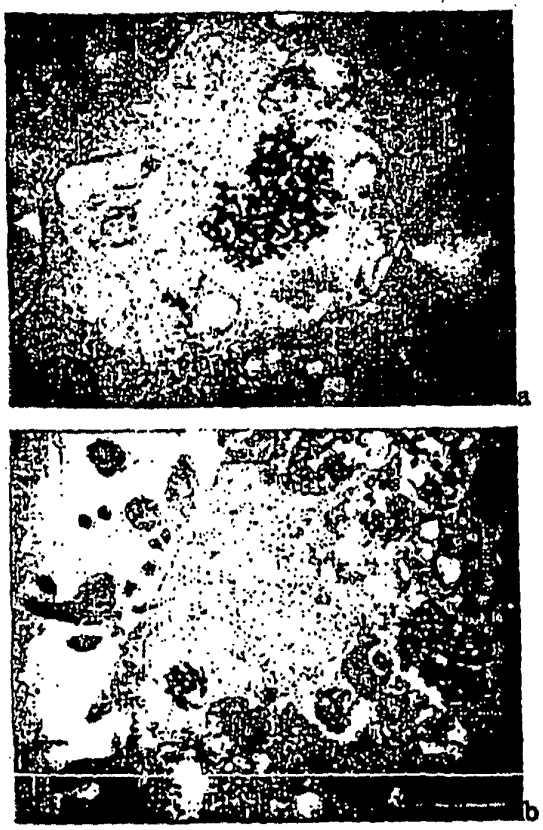

Fig. 2 TEM micrographs cells labelled with superparamagnetic iron oxide nanoparticles modified with (a) D-mannose and (b) poly(L-lysine).

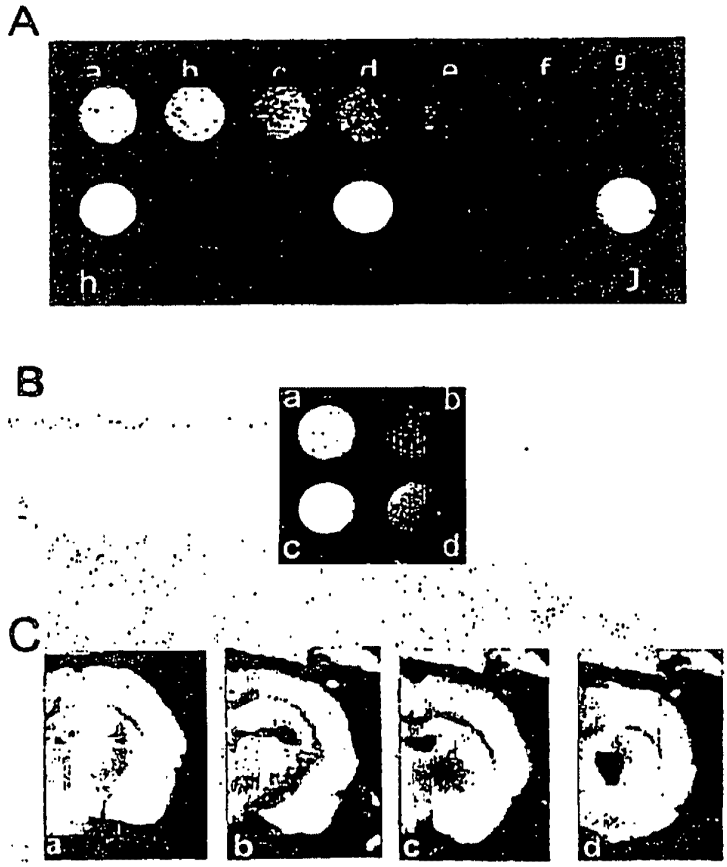

Fig. 3. A: Gelatin phantoms containing (a) 100,000, (b) 200,000, (c) 400,000, (d) 600,000, (e) 800,000, (f) 1,000,000 and (g) 2,000,000 cells labelled with superparamagnetic iron oxide nanoparticles modified with poly(L-lysine) and controls with (h) 100,000, (i) 600,000, (j) 2,000,000 unlabelled cells.

B: Gelatin phantoms containing (a, b) 100,000 cells labelled with superparamagnetic iron oxide particles modified with poly(L-lysine) and (c, d) unlabelled cells in 0.5 µl. Scans (a, c) were obtained in standard turbospin echo sequence, (b, d) by gradient echo sequence. Even though gradient echo sequence gives a worse signal/noise ratio, the higher sensitivity of poly(L-lysine)-modified iron oxide nanoparticles markedly enhances the signal/noise ratio.

C: Rat hemispheres with (a) 90,000 implanted unlabelled cells and (b) 22,000, (c) 45,000, (d) 90,000 cells labelled with superparamagnetic iron oxide nanoparticles modified with poly(L-lysine). MR imaging was scanned for 3 days after implantation.

REFERENCES CITED IN THE DESCRIPTION

This list of references cited by the applicant is for the reader's convenience only. It does not form part of the European patent document. Even though great care has been taken in compiling the references, errors or omissions cannot be excluded and the EPO disclaims all liability in this regard.

Patent documents cited in the description

- EP 516252 A2, Kresse M., Pfefferer D., Lawaczeck R. **[0002]**
- US 4770183 A, Groman E.V., Josephson L. **[0002]**
- WO 9222586 A1 **[0002]**
- US 4731239 A, Gordon R.T. **[0002]**
- US 4827945 A, Gromann E.V., Josephson L., Lewis J. M. **[0004]**
- US 20030185757 A **[0004] [0005]**
- DE 3729697 A1, Schostek S., Beer A. **[0005]**
- US 4323056 A, Borelli N.F., Luderer A.A., Panzarino J.N. **[0005]**
- JP 60260463 A, Osamu I., Takeshi H., Toshihiro M., Kouji N. **[0005]**
- US 4101435 A, Hasegawa M., Hokukoku S. **[0005] [0006]**
- JP 59195161 B, Fuji Rebio K.K **[0005]**
- EP 179039 A2, Porath J., Mats L. **[0005]**
- JP 05026879 A, Norio H., Saturo O. **[0005]**
- DE 2642383 A1, Kunda W. Rudyk B. **[0005]**
- US 5492814 A, Weissleder R. **[0006]**
- US 4452773 A, Molday R.S. **[0006]**
- EP 0516252 A2 **[0006]**
- WO 9102811 A, Liberti P.A. **[0006]**
- WO 02100269 A1, Frank J.A., Bulte J.W.M. **[0006]**
- WO 03049604 A3, Van Zijk P., Goffeney N., Duyn J.H., Bulte J.W.M. **[0006]**

Non-patent literature cited in the description

- **Shinkai M.** Functional magnetic particles for medical application. *J. Biosci Bioeng,* 2002, vol. 94, 606-613 **[0002]**
- **Stark D.D. ; Weissleder R. ; Elizondo G. ; Hahn P.F. ; Saini S. ; Todd L.E. ; Wittenberg J. ; Ferrucci J.T.** Superparamagnetic iron oxide: clinical application as a contrast agent for MR imaging of the liver. *Radiology,* 1988, vol. 168, 297-301 **[0004]**
- **Aoyama S. ; Kishimoto M. ; Manabe T.** Interaction between polymers and magnetic particles - effect on the properties of particulate magnetic recording media. *J. Mater. Chem.,* 1992, vol. 2, 277-280 **[0005]**
- **Bacic G. ; Niesman M.R ; Bennett H.F. ; Magin R.L. ; Schwarz H.M.** Modulation of water proton relaxation rates by liposomes containing paramagnetic materials. *Magn. Reson. Med.,* 1988, vol. 6, 445-58 **[0006]**
- **Ohgushi M. ; Nagayama K. ; Wada A.** Dextran-magnetite: a new relaxation agent and its application to T2 measurements in gel systems. *J. Magn. Reson.,* 1978, vol. 29, 599-601 **[0006]**
- **Pouliquen D. ; Le Jeune J.J. ; Perdrisot R. ; Ermias A. ; Jallet P.** Iron oxide nanoparticles for use as an MRI contrast agent pharmacokinetics and metabolism. *Magn. Reson. Imaging,* 1991, vol. 9, 275-283 **[0006]**
- **Ferrucci J.T. ; Stark D.D.** Iron oxide-enhanced MR imaging of the liver and spleen: review of the first 5 years. *Am. J. Roentgenol.,* 1990, vol. 155, 943-950 **[0006]**
- **Molday R.S. ; MacKenzie D.** Immunospecific ferromagnetic iron-dextran agents for the labelling and magnetic separation of cells. *J. Immunol. Methods,* 1982, vol. 52, 353-367 **[0006]**
- **Josephson L. ; Groman E.V. ; Menz E. ; Lewis J.M. ; Bengele H.** A functionalized superparamagnetic iron oxide colloid as a receptor directed MR contrast agent. *Magn. Reson. Imaging,* 1990, vol. 8, 637-646 **[0006]**
- **Fahlvik A.K. ; Holtz E. ; Schroder U. ; Klaveness J.** Magnetic starch microspheres, biodistribution and biotransformation. A new organ-specific contrast agent for magnetic resonance imaging. *Invest. Radiol.,* 1990, vol. 25, 793-797 **[0006]**
- **Kresse M. ; Wagner S. ; Pfefferer D. ; Lawaczeck R. ; Elste V. ; Semmler W.** Targeting of ultrasmall superparamagnetic iron oxide (USPIO) particles to tumor cells in vivo by using transferrin receptor pathways. *Magn. Reson. Med.,* 1998, vol. 40, 236-42 **[0006]**
- **Widder D.J. ; Greif W.L. ; Widder K.J. ; Edelman R.R. ; Brady T.J.** Magnetite albumin microspheres: a new MR contrast material. *Am. J. Roentgenol.,* 1987, vol. 148, 399-404 **[0006]**
- **Cheng F.-Y. ; Su C.-H. ; Yang Y.-S. ; Yeh C.-S. ; Tsai C.-Y. ; Wu C.-L. ; Wu M.-T. ; Shieh D.-B.** Characterization of aqueous dispersions of Fe3O4 nanoparticles and their biomedical applications. *Biomaterials,* 2005, vol. 26, 729-738 **[0007]**

- **Taupitz M. ; Schnorr J. ; Wagner S.A. ; Abramjuk C. ; Pilgrimm H. ; Kivelitz D. ; Schink T. ; Hansel J. ; Laub G. ; Humogen H.** Coronary MR angiography: experimental results with a monomer-stabilized blood pool contrast medium. *Radiology,* 2002, vol. 222, 120-126 **[0007]**
- **Park H.C. ; Shims Y.S. ; Ha Y. ; Yoon S.H. ; Park S.R. ; Choi B.H. ; Park H.S.** Treatment of complete spinal cord injury patients by autologous bone marrow cell transplantation and administration of granulocyte-macrophage colony stimulating factor. *Tissue Eng.,* 2005, vol. 11, 913-922 **[0008]**
- **Akiyama Y. ; Radtke C. ; Honmou O. ; Kocsis J.D.** Remyelination of the spinal cord following intravenous delivery of bone marrow cells. *Glia,* 2002, vol. 39, 229-236 **[0008]**
- **Akiyama Y. ; Radtke C. ; Kocsis J.D.** Remyelination of the rat spinal cord by transplantation of identified bone marrow stromal cells. *J. Neurosci.,* 2002, vol. 22, 6623-6630 **[0008]**
- **Hofstetter C.P. ; Schwarz E.J. ; Hess D. ; Widenfalk J. ; El Manira A. ; Prockop J.D. ; Olson, L.** Marrow stromal cells form guiding strands in the injured spinal cord and promote recovery. *Proc. Natl. Acad. Sci. USA,* 2002, vol. 96, 2199-2204 **[0008]**
- **Chen J. ; Li Y. ; Katakowski M. ; Chen X. ; Wang L. ; Lu D.** Intravenous administration of human bone marrow stromal cells induces angiogenesis in the ischemic boundary zone after stroke in rats. *Circ. Res,* 2003, vol. 92, 692 **[0008]**
- **Chen J. ; Zhang Z.G. ; Li Y. ; Wang L. ; Xu Y.X. ; Gautam S.C.** Intraarterial administration of marrow stromal cells in a rat model of traumatic brain injury. *J.Neurosci.Res.,* 2003, vol. 73, 778-786 **[0008]**
- **Chopp M. ; Li Y.** Treatment of neural injury with marrow stromal cells. *Lancet Neurol.,* 2002, vol. 1, 92-100 **[0008]**
- **Chopp M. ; Zhang X.H. ; Li Y. ; Wang L. ; Chen J. ; Lu D.** Spinal cord injury in rat: treatment with bone marrow stromal cell transplantation. *Neuroreport,* 2000, vol. 11, 3001-3005 **[0008]**
- **Ramon-Cueto A. ; Plant G.W. ; Avila J. ; Bunge M.B.** Long-distance axonal regeneration in the transected adult rat spinal cord is promoted by olfactory ensheathing glia transplants. *J. Neurosci.,* 1998, vol. 18, 3803-3815 **[0008]**
- **Syková E. ; Urdziková L. ; Jendelová P. ; Burian M. ; Glogarová K. ; Hájek M.** Bone marrow cells - a tool for spinal cord injury repair. *Exp. Neurol.,* 2005, vol. 193, 261-262 **[0008]**
- **Jendelová. P. ; Herynek V. ; DeCroos J. ; Glogarová K ; Andersson B. ; Hájek M. ; Syková E.** Imaging the fate of implanted bone marrow stromal cells labeled with superparamagnetic nanoparticles. *Magn. Reson. Med.,* 2003, vol. 50, 767-776 **[0035]**